

MODULATION OF NEUTROPHIL FUNCTIONS BY GOLD NANOPARTICLES

DOCTORAL THESIS

In partial fulfillment of the requirements for the degree
“Doctor rerum naturalium (Dr. rer. nat.)”

To the
Faculty of Biology

At the
University of Duisburg-Essen

Submitted by
Ronja Larissa Schirrmann
(née Weller)

Born in Esslingen am Neckar

July 2022

The experiments underlying the present work were conducted at the research department of the clinic for otorhinolaryngology of the University Hospital Essen as part of the University of Duisburg-Essen.

1. Examiner: Prof. Dr. Sven Brandau

2. Examiner: Prof. Dr. Daniel R. Engel

3. Examiner:

Chair of the Board of Examiners: Prof. Dr. Matthias Gunzer

Date of the Oral Examination: 16.12.2022

“Nanoparticles don't make your life any easier...”

Ronja Schirrmann, 2019

TABLE OF CONTENTS

ABBREVIATIONS	VIII
LIST OF FIGURES	XIII
SUPPLEMENTARY FIGURES	XIV
LIST OF TABLES	XV
LIST OF SUPPLEMENTARY TABLES	XV
1 INTRODUCTION	1
1.1 Polymorphonuclear Neutrophils	1
1.1.1 <i>The Life of a Neutrophil: From Bone Marrow to Peripheral Release</i>	3
1.1.2 <i>PMN Effector Functions</i>	4
1.1.3 <i>Attraction and Migration Towards Infection Sites</i>	8
1.2 Cancer Immunology	9
1.2.1 <i>MDSC</i>	10
1.2.2 <i>Tumor Microenvironment</i>	10
1.2.3 <i>TAN</i>	11
1.3 Hyperthermia: Treatment Against Cancer	11
1.4 Hyperthermia Mediated by Photosensitizers	12
1.4.1 <i>Photodynamic Therapy</i>	12
1.4.2 <i>Photothermal Therapy</i>	13
1.5 Nanoparticles	13
1.5.1 <i>Noble Metal Nanoparticles as Photosensitizers</i>	14
1.5.2 <i>Gold Nanoparticles in PTT</i>	14
1.5.3 <i>Gold Nanoparticles - Cell Interaction</i>	15
1.6 Antibody Targeted Therapy	17
1.7 Immunotargeting of Gold Nanoparticles	17
AIM OF THE STUDY	19
2 MATERIAL	21
2.1 Consumable Supplies	21
2.2 Equipment	22

2.3	Chemicals	24
2.4	Ready to Use Reaction Systems	25
2.5	Primers	26
2.6	Inhibitors	28
2.7	Antibodies	30
2.7.1	<i>Antibodies for Flow Cytometry</i>	30
2.7.2	<i>Antibodies for Immunofluorescence</i>	31
2.7.3	<i>Antibodies for Western Blot</i>	32
2.7.4	<i>Antibodies for AuNP Coupling</i>	32
2.7.5	<i>Antibodies for the Identification of PMN, T cells and Monocytes</i>	32
2.8	Buffers, Solutions and Media	33
2.9	Software	34
3	METHODS	36
3.1	Primary Cell Isolation	36
3.1.1	<i>Isolation of Human PMN</i>	36
3.1.2	<i>Isolation of Human T cells</i>	36
3.1.3	<i>Medium Preparation with Autologous Serum</i>	36
3.2	AuNR treatment	37
3.3	Sample Preparation for Microscopy	37
3.3.1	<i>Transmission Electron Microscopy – Uptake of AuNR</i>	37
3.3.2	<i>Confocal Microscopy - Uptake of AuNR-RITC</i>	37
3.3.3	<i>Confocal Microscopy - Uptake of AuNR-RITC and E.coli</i>	38
3.3.4	<i>Confocal Microscopy - Uptake of Antibody-Coated AuNR by Immune Cells</i>	38
3.3.5	<i>Structured Illumination Microscopy</i>	38
3.3.6	<i>Fluorescence Microscopy</i>	40
3.4	Molecular Biology	40
3.4.1	<i>RNA Isolation</i>	40
3.4.2	<i>PCR and Real-Time qPCR</i>	41
3.4.3	<i>Data Analysis of qPCR</i>	41
3.4.4	<i>Human Cellular Stress Response Array</i>	42
3.5	Protein Biochemistry	42
3.5.1	<i>Sample Preparation for Western Blot</i>	42

3.5.2	<i>Sample Preparation for Fractionated Western Blot</i>	43
3.5.3	<i>Western Blot</i>	43
3.6	Ca²⁺ Imaging	44
3.7	Analysis of PMN Secretion	44
3.7.1	<i>Luminex assay</i>	44
3.7.2	<i>Zymography</i>	44
3.7.3	<i>ELISA from Whole Blood Samples</i>	44
3.8	Flow Cytometry	45
3.8.1	<i>Inhibition of AuNR Uptake</i>	45
3.8.2	<i>Detection of Apoptosis</i>	45
3.8.3	<i>Detection of Caspase Activation</i>	46
3.8.4	<i>Migration Assay</i>	46
3.8.5	<i>Transendothelial Migration Assay (TEM)</i>	46
3.8.6	<i>Whole blood AuNR treatment</i>	47
3.8.7	<i>Low-Density Neutrophil Detection</i>	47
3.8.8	<i>Inhibition of Protein Transcription or Translation</i>	47
3.8.9	<i>Endoplasmic Reticulum Stress Inhibition</i>	47
3.8.10	<i>Reactive Oxygen Species (ROS)</i>	47
3.8.11	<i>Cell Surface Staining on Isolated PMN</i>	48
3.8.12	<i>Whole Blood Staining</i>	48
3.8.13	<i>T cell Suppression Assay</i>	49
3.8.14	<i>Antibody-Mediated AuNR Targeting of Isolated Immune Cells</i>	49
3.8.15	<i>Targeting Immune Cells by Antibody-Conjugated AuNP of Different Sizes</i> ..	50
3.9	Killing of Isolated Immune Cells by Photothermal Therapy	50
3.9.1	<i>PTT of Multicellular Immune Cell Cultures</i>	50
3.9.2	<i>PTT of T cells</i>	50
3.9.3	<i>Laser Irradiation</i>	50
3.9.4	<i>Data Analysis of FACS Data</i>	51
3.10	Statistics	51
4	RESULTS	52
4.1	The Role of PMN in the Interaction with Theranostic Agents	52
4.1.1	<i>PMN are Taking up AuNR</i>	53

4.1.2	<i>Phagocytosis as Major AuNR Uptake Mechanism in PMN</i>	54
4.1.3	<i>AuNR Enter the Endocytic Pathway of PMN</i>	57
4.2	AuNR Uptake Activates PMN ex vivo	59
4.2.1	<i>AuNR Uptake Induces the Expression of Activation Markers on PMN</i>	59
4.2.2	<i>AuNR Uptake Induces Degranulation</i>	62
4.2.3	<i>AuNR Induce Stronger Migration Towards Tumor Supernatant</i>	64
4.2.4	<i>AuNR Uptake is not Affecting the Viability of PMN ex vivo</i>	65
4.3	AuNR Treatment Induces Cellular Stress	67
4.3.1	<i>AuNR Uptake Activates the Xenobiotic Metabolism</i>	67
4.3.2	<i>AuNR Uptake Affects the Protein Folding Machinery</i>	73
4.3.3	<i>PMN Show Higher Ubiquitination Status after AuNR Treatment</i>	74
4.3.4	<i>AuNR Uptake Impedes Protein Folding</i>	75
4.3.5	<i>AuNR Uptake Affects Ca²⁺ and ROS Homeostasis</i>	76
4.3.6	<i>AuNR Uptake Activates UPR</i>	78
4.3.7	<i>AuNR Uptake Induces Expression of LOX1 on PMN</i>	78
4.3.8	<i>LOX1 is not Synthesized de novo at Short Time Points</i>	80
4.3.9	<i>ER Stress Mediates IL8 Secretion and LOX1 Expression</i>	80
4.4	AuNR Activated an Autocrine Activation Loop	81
4.4.1	<i>LOX1 Mediated Activation Loop</i>	81
4.4.2	<i>IL8-CD182 Mediated Activation Loop</i>	84
4.5	AuNR Uptake did not Affect T cell Suppressive Capacity of PMN	86
4.6	PMN Primed with AuNR Still Phagocytose Pathogens	87
4.7	AuNR Induce Functional Changes in PMN of Cancer Patients	88
4.8	AuNR as Photosensitizers for Specific PTT	90
4.8.1	<i>Targeting Immune Cells with Antibody coated AuNR</i>	90
4.8.2	<i>Binding of Antibody-Coupled AuNR to Non-Phagocytic T cells</i>	92
4.8.3	<i>Uptake of Antibody-Coupled AuNR by Phagocytes</i>	93
4.8.4	<i>Phagocytosis of AuNR Depends on the Isolation Method of Target Cells</i>	95
4.9	Killing of immune cells by Photothermal Therapy (PTT)	96
4.9.1	<i>PTT of Multi-Immune Cell Cultures</i>	96
4.9.2	<i>PTT of Non-Phagocytic T cells</i>	98
5	DISCUSSION	100

5.1	Gold Nanoparticle Modification and their Biomedical Application	101
5.2	AuNR Size as the Major Cause of AuNR Clearance by Phagocytes?	103
5.3	AuNP Delivery Systems	104
5.3.1	<i>Passive Delivery of Nanoparticles</i>	104
5.3.2	<i>Camouflaging Techniques to Avoid Nanoparticle Phagocytosis.....</i>	105
5.4	Interaction of AuNP with Immune Cells	107
5.4.1	<i>Interaction of AuNR with PMN.....</i>	107
5.4.2	<i>ER Stress in PMN.....</i>	108
5.5	Therapeutic Implications.....	109
5.6	Conclusions	110
6	SUMMARY	111
7	ZUSAMMENFASSUNG	113
	REFERENCES	115
	APPENDIX	131
8	PUBLICATIONS AND PRESENTATIONS	140
8.1	Publications	140
8.1.1	<i>First Author</i>	140
8.1.2	<i>Shared First Author.....</i>	140
8.1.3	<i>Co-Author</i>	140
8.2	Oral presentations	140
8.3	Poster presentations	140
	ACKNOWLEDGMENTS.....	142
	CURRICULUM VITAE.....	144
	AFFIDAVIT	146

ABBREVIATIONS

Table 1: List of abbreviations

Abbreviation	Denotation
3HNA	3-Hydroxy-2-naphthoic acid
A549	Human Lung cancer cell line
APC	Allophycocyanin
AS	Autologous serum
ATP	Adenosine triphosphate
AuNP	Gold nanoparticle
AuNR	Gold nanorods
AuNSPH	Gold nanospheres
BSA	Bovine Serum Albumin
BV421	Brilliant Violet 421™
Ca ²⁺	Calcium
C/EBP	CCAAT/enhancer-binding protein
C17.2	Mouse retrovirally immortalized neuronal cell line
CD	Cluster of differentiation
CF-31	human dermal fibroblast cell line
CH	Chlorpromazine hydrochloride
CPDye	Cell proliferation dye
CTL	Cytotoxic lymphocytes
CYP	Cytochrome P450
CytD	Cytochalasin D
DAMPs	Damage-associated molecular patterns
DARC	Duffy antigen receptor for chemokines
DC	Dendritic cells
DMSO	Dimethylsulfoxid

DNA	Deoxyribonucleic acid
dNTP	Deoxy nucleoside triphosphate
<i>E.coli</i>	<i>Escherichia coli</i>
e.g.	exempli gratia
ECM	Extra cellular matrix
EGFR	Epidermal growth factor
ELISA	Enzyme linked immunosorbent assay
EPR	Enhanced permeability and retention effect
ER	Endoplasmic reticulum
Et al.	lat.: ET ALTERI
FACS	Fluorescence activated cell sorting
FITC	Fluorescein isothiocyanate
fMLP	N-Formylmethionyl-leucyl-phenylalanine
FSC	Forward Scatter
GAG	Glycosaminoglycans
G-CSF	Granulocyte-colony stimulating factor
Gro α	Growth-Regulated α Protein
Gt	Goat
HD	Healthy Donor
HSPGs	heparan sulfate proteoglycans
HeLa	Human Cervical cancer cell line
Ho	horse
HR	Hydrodynamic radius
HSC	Hematopoietic Stem Cells
HSPG	Heperan Sulfate Proteoglycans
HUVEC	Human umbilical vein endothelial cell line
IL17A	Interleukin 17A

IL1 β	Interleukin 1 β
IL23	Interleukin 23
IL6	Interleukin 6
IL8	Interleukin 8
IMCES	Imaging Center Essen
J774-A1	Mouse monocyte macrophage cell line
K562	Human caucasian chronic myelogenous leukaemia cell line
kDA	kilo-Dalton
Kira	Kinase Inhibiting RNase Attenuator 6
LAMP1	Lysosomal-associated membrane protein 1
Laser	Light Amplification by the Stimulated Emission of Radiation
LDN	Low-Density Neutrophils
LFA-1	Lymphocyte function-associated antigen 1 is an integrin
LOX1	Lectin-type oxidized LDL receptor 1
LPS	Lipopolysaccharide
LSM	Laser Scanning Microscope
LSPR	Localized Surface Plasmon Resonance
LTB4	Leukotriene B(4)
M	Mouse
mAB	Monoclonal Antibody
MAC-1	Macrophage 1 antigen (CD11b/CD18)
MACS	Magnetic Activated Cell Sorting
MCF-7	Human breast cancer cell line
MDSC	Myeloid Derived Suppressor Cells
MHC I	Major Histocompatibility Complex class I molecules
MIF	Macrophage Migration Inhibitory Factor
Min	Minutes

MIP1 β	Macrophage Inflammatory Protein 1 β
MMP	Matrix metalloprotease
MPO	Myeloperoxidase
M β CD	Methyl- β -Cyclodextrin
NAC	N-acetyl cysteine
NDN	Normal-density neutrophils
NADPH	Nicotinamide Adenine Dinucleotide Phosphate
NE	Neutrophil Elastase
NET	Neutrophil Extracellular Traps
NIR	Near-Infrared Region
NLR	Neutrophil-Lymphocyte Ratio
Nm	Nanometer
PAD4	Peptidyl-Arginine Deaminase 4
PAF	Platelet-Activating Factors
PAGE	Polyacrylamide Gelelectrophoresis
PBMC	Peripheral Blood Mononuclear Cells
PBS	Phosphate Buffered Saline
PC12	Transplantable rat pheochromocytoma
PDT	Photodynamic Therapy
PE	Phycoerythrin
PKC	Phosphokinase C
PMN	Polymorphonuclear Neutrophil
PS	Phosphatidylserine
PTT	Photothermal Therapy
PVDF	Polyvinylidene Difluoride
R	Rat
Rab	Ras-related protein

Raw264.7	Mouse monocyte macrophage cell line
Rb	Rabbit
RIPA	Radioimmunoprecipitation assay buffer
RNA	Ribonucleic acid
ROS	Reactive oxygen species
SDS	Sodium-Dodecyl-Sulfate
SIM	Structured illumination microscopy
Sk-Mel-28	Human malignant melanoma cell line
SSC	Side Scatter
TAN	Tumor Associated Neutrophils
TBS	Tris Buffered Saline
TEM	Transendothelial Migration
TEMED	N,N,N',N'-Tetramethylethylenediamin
TIL	tumor infiltrating T cells
TLR	Toll-like receptors
TMB	3,3',5,5'-Tetramethylbenzidine
TNF α	Tumor necrosis factor α
TRiC	T-complex protein Ring Complex
TWEEN	Polyoxyethylensorbitanmonolaurat
UA	Uracil acid
US FDA	United States Food and Drug Administration
VLA4	integrin dimer, composed of CD49d (alpha 4) and CD29 (beta 1)
α	anti

LIST OF FIGURES

Figure 1: Schematic overview of the classical hematopoietic hierarchy in the human immune system.....	2
Figure 2: Schematic overview of the granulopoiesis in the bone marrow.....	4
Figure 3: Schematic overview of phagocytosis by PMN.....	6
Figure 4: Schematic overview of the split LSPR of gold nanorods.....	15
Figure 5: AuNR uptake by PMN.....	53
Figure 6: Specific inhibition of PMN's actin-, clathrin- and caveolin-dependent uptake mechanisms.....	55
Figure 7: PMN engulf AuNR actin-dependently.....	56
Figure 8: AuNR enter the endolysosomal system of PMN.....	58
Figure 9: AuNR uptake does not affect PMNs' surface expression of CD16, CD35, CD54, CD64, CD95 and CD274.....	60
Figure 10: AuNR uptake regulates the surface expression of CD62L, CD11b, CD182 and CD181 on PMN.....	61
Figure 11: PMN secrete IL8 upon AuNR treatment.....	63
Figure 12: AuNR treatment induces MMP9 secretion and generates mature low density PMN...64	64
Figure 13: PMN migrate faster to tumor-conditioned medium after AuNR priming.....	65
Figure 14: AuNR uptake induces pan-caspase activation in PMN after 4h.....	66
Figure 15: AuNR uptake induces cellular stress.....	69
Figure 16: AuNR uptake activates SHP and AhR transcription, further repressing NFκB and inducing the transcription of CYPs.....	70
Figure 17: AuNR uptake activates AhR signaling in PMN.....	71
Figure 18: AuNR uptake induces transcription of FMO1.....	72
Figure 19: AuNR uptake accelerates the transcription of HOPX, HSPB1 and CCT3.....	74
Figure 20: AuNR uptake induces higher ubiquitination in PMN after 5 and 15 min.....	75
Figure 21: AuNR uptake induces upregulation of Ero1Lα and PDI after 30 min.....	75
Figure 22: AuNR uptake increases cytosolic Ca ²⁺ level.....	77
Figure 23: AuNR uptake upregulates BiP.....	78
Figure 24: ER stress induces LOX1 expression via XBP1 splicing.....	79
Figure 25: AuNR-induced LOX1 is not produced de novo at early time points.....	80
Figure 26: AuNR-induced IL8 secretion and LOX1 expression is ER stress dependent.....	81

Figure 27: AuNR-induced LOX1 expression correlates with IL8 secretion and ROS production.	82
Figure 28: AuNR-induced LOX1 mediates ROS production and IL8 secretion.	83
Figure 29: IL8 signaling blockade reduces AuNR-induced activation.	85
Figure 30: AuNR uptake does not affect PMNs' ability to suppress T cell proliferation.	87
Figure 31: AuNR do not impede phagocytosis of E.coli by PMN.	88
Figure 32: PMN of cancer patients react comparable to AuNR as healthy donor PMN.	89
Figure 33: Phagocytic immune cells impede antibody-mediated binding of AuNR.	91
Figure 34: AuNR size and shape does not affect AuNP- α CD3 targeting of T cells.	93
Figure 35: AuNR size and shape massively affect antibody-mediated targeting of PMN in whole blood assays.	94
Figure 36: Targeting of AuNR- α CD11b depends on AuNR size and on culture conditions.	96
Figure 37: Phagocytosis impedes AuNR targeting resulting in unspecific PTT.	98
Figure 38: T cells can be specifically killed in PTT using AuNR- α CD3.	99
Figure 39: Graphical Abstract	112

SUPPLEMENTARY FIGURES

Supplementary Figure 1: Gating strategy for isolated PMN in flow cytometry.	131
Supplementary Figure 2: Whole blood flow cytometry gating strategy for PMN.	132
Supplementary Figure 3: Gating of PMN, T cells and Monocytes from mixed PBMC / PMN cultures.	133
Supplementary Figure 4: Gating of PMN, T cells and Monocytes from whole blood.	133
Supplementary Figure 5: AuNR pretreatment reduced PMN spontaneous migration and accelerated directed migration towards tumor supernatant.	134
Supplementary Figure 6: Negatively charged AuNR are non-toxic.	134
Supplementary Figure 7: ER stress inhibition did not change expression of CD182, CD11b or ROS production.	135
Supplementary Figure 8: IgG antibody does not affect IL8 secretion and ROS production.	136
Supplementary Figure 9: LOX1 neutralizing does not affect AuNR-induced CD11b expression.	136
Supplementary Figure 10: Exemplary histograms of cell associated AuNR fluorescence.	137

LIST OF TABLES

Table 1: List of abbreviations.....	VIII
Table 2: Consumables used in this work.....	21
Table 3: Equipment used in the laboratory.	22
Table 4: Chemicals used in this work.	24
Table 5: Kits used in this work.....	25
Table 6: Primers used in this work.....	26
Table 7: Inhibitors used in this work.....	28
Table 8: Specific antibodies used in flow cytometry.	30
Table 9: Isotype and secondary antibodies used for flow cytometry.....	31
Table 10: Antibodies used for immunocytochemistry.	31
Table 11: Antibodies used for Western Blot.....	32
Table 12: Antibodies used for coupling of AuNP.....	32
Table 13: Antibodies used for phenotypic identification of PMN, T cells and monocytes.....	32
Table 14: Buffers used in this work.	33
Table 15: Software used in this work.....	34

LIST OF SUPPLEMENTARY TABLES

Supplementary Table 1: Detailed description of patients used in this thesis.....	138
Supplementary Table 2: Dynamic light scattering analysis of AuNR size during protein coupling. Analysis was performed by Oliver Sritharan and Michael Erkelenz (Department of Chemistry, University of Duisburg-Essen).....	139

1 INTRODUCTION

1.1 POLYMORPHONUCLEAR NEUTROPHILS

The human immune system is designed to protect the host from everything that is foreign. This depends on distinguishing non-self molecules as for example viruses, bacteria and parasites as well as abnormal host cells like cancer from healthy host-cells. In order to deal with these various tasks, the human immune system comprises a multi-layered defense starting with mechanical barriers as the skin or mucosa, followed by the fast, rather unspecific, innate immune system and finally the specialized, but slower, adaptive immune system (Figure 1). Furthermore, the complement system, consisting of proteins and glycoproteins, supports several functions of the innate and adaptive immune system by stimulating the binding of antibodies or promoting the clearance of non-self molecules *via* phagocytosis.

Upon infection, after a pathogen circumvented the mechanical barrier of the skin, tissue-resident macrophages phagocytose the pathogen and secrete pro-inflammatory signal molecules, so-called cytokines. These stimulate polymorphonuclear neutrophils (PMN) to migrate from the blood into the tissue to support macrophages. The interplay of humoral and cellular immune mediators with the pathogen marks the transition from infection to acute or, when long-lasting, chronic inflammation. Additionally, to PMN, natural killer cells support phagocytes by secretion of cytotoxic compounds, so-called granules, which further promote the killing of pathogens. Dendritic cells account for the transition from innate to adaptive immune system. They process pathogen-derived antigens, present them to naïve T cells to activate them. The activation of T cells promotes a subsequent activation of lymph node resident B cells to produce antigen-specific antibodies (Neumann 2008). Though the adaptive immune system stands out with its' specific antigen response and the memory immunity, one major drawback is the time needed in order to function. In case of a previously encountered infection, the adaptive immune system acts within 4 to 96 h post infection (memory immunity) (Murphy 2012). However, during primary infection, when the immune system is still naïve to the pathogen, specific T and B cells need 96 h to get activated by the cooperative activity of the innate immune system and antigen-presenting cells. This emphasizes the importance of the innate immune system, mediating the immune response especially during the first 4 h of infection. PMN are typically the first and major players during acute inflammation (Kolaczowska *et al.* 2013). They represent the most abundant white blood cells, accounting for up to 70 % of human peripheral blood leukocytes (Summers *et al.* 2010). Their name origins from

their staining characteristics in hematoxylin and eosin staining additional to their nuclear morphology (Dale *et al.* 2008). Experimental and clinical data showed that PMN recruitment to the site of inflammation is crucial for the clearance of infections. By phagocytosing the pathogens, PMN reduce the infectious burden due to reduction and containment of the infectious dose. Accordingly, the reduction of PMN count within the blood results in severe immunodeficiency in humans (Zeidler *et al.* 2009).

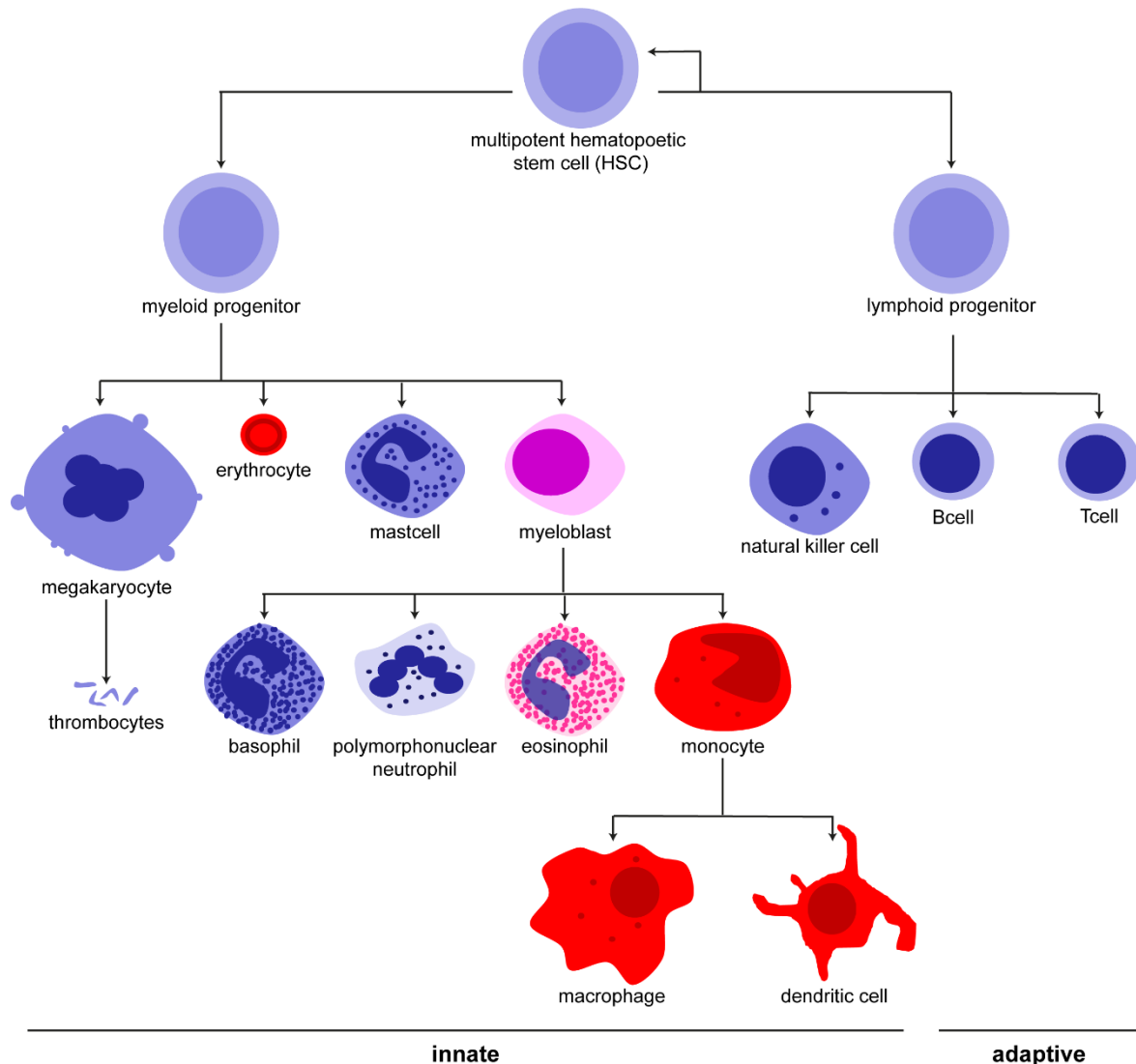


Figure 1: Schematic overview of the classical hematopoietic hierarchy in the human immune system.

Hematopoiesis describes the formation of the blood cellular components and takes place in the bone marrow. It starts with multipotent hematopoietic stem cells (HSC) localized in niches provided by osteoblasts and endothelial cells within the bone marrow (Borregaard 2010). HSC differentiate into pluripotent progenitors, which further proliferate into lineage-committed myeloblasts (Cheng *et al.* 2020). Basophil, neutrophil and eosinophil granulocytes, as well as monocytes, macrophages, dendritic cells and natural

killer cells are part of the innate immune system, whereas B and T cells are part of the adaptive immune system.

1.1.1 THE LIFE OF A NEUTROPHIL: FROM BONE MARROW TO PERIPHERAL RELEASE

When released from the bone marrow to the peripheral circulation, PMN have a short life span. Depending on the way of estimation in the respective studies, life time measurements range between a few hours and several days (Pillay *et al.* 2010). Due to this, PMN are continuously generated in the bone marrow resulting in the release of about $1-2 \times 10^{11}$ cells per day, depending on the rate of apoptosis of tissue-resident PMN (Borregaard 2010). Apoptotic PMN are phagocytosed by macrophages and dendritic cells which subsequently produce less of the cytokine interleukin 23 (IL23). IL23 promotes the release of Interleukin 17A (IL17A) by neutrophil regulating T cells (mostly $\gamma\delta$ -T cells or natural killer cells (NK)-like T cells). IL17A in turn stimulates the production of granulocyte-colony stimulating factor (G-CSF) and promotes granulopoiesis (Stark *et al.* 2005). Interestingly, G-CSF is necessary for tuning PMN production during inflammation, but is not required for granulopoiesis (Stanley *et al.* 1994). Granulopoiesis starts with multipotent hematopoietic stem cells (HSC) localized in niches provided by osteoblasts and endothelial cells within the bone marrow (Borregaard 2010). HSC differentiate into pluripotent progenitors, which further proliferate into lineage-committed myeloblasts (Figure 1). Besides extrinsic cytokines, hematopoietic differentiation is driven by intrinsic transcription factors (Cheng *et al.* 2020). The development and lineage commitment is strongly regulated by the transcription factors PU.1 and CCAAT/enhancer-binding protein α (C/EBP α) among others (Rosmarin *et al.* 2005). While high expression of PU.1 drives monocytic differentiation, C/EBP α promotes granulopoiesis (transition from myeloblast to promyelocyte) with contribution of C/EBP β , especially during infections (Radomska *et al.* 1998, Hirai *et al.* 2006) (Figure 2). In a later phase, C/EBP ϵ promotes the exit from the cell cycle during the transition from promyelocyte to myelocyte stage (Gery *et al.* 2004). During the last step of granulopoiesis, the myelocyte stage, C/EBP ϵ is expressed and mediates the transcription of granule proteins (Gombart *et al.* 2001, Bjerregaard *et al.* 2003). The role of C/EBP δ , C/EBP γ , is not entirely clear, but their expression level increases dramatically during cell cycle arrest (metamyelocytes) (Bjerregaard *et al.* 2003, Kardosova *et al.* 2018) and endoplasmic reticulum (ER) stress induction (Xia *et al.* 2012). However, these proteins might also play a role in transcriptional initiation of mature PMN markers such as gelatinase, N-formylmethionyl-leucyl-phenylalanine (fMLP) -receptor, CD35, and Toll-like receptor 4 (TLR4). Finally, mature PMN leave the bone marrow. The retention and release of PMN from the bone

marrow is determined by the downregulation of C-X-C chemokine receptor type 4 (CXCR4), favoring retention, and upregulation of CXCR2, favoring release, and their respective ligands CXCL12, Gro α (CXCL1) and Gro β (CXCL2) (Martin *et al.* 2003, Eash *et al.* 2010). G-CSF further stimulates PMN release directly or indirectly by reducing the CXCL12 expression on endothelial cells and enhancing their expression of Gro β (Wengner *et al.* 2008, Mukaida *et al.* 2020).

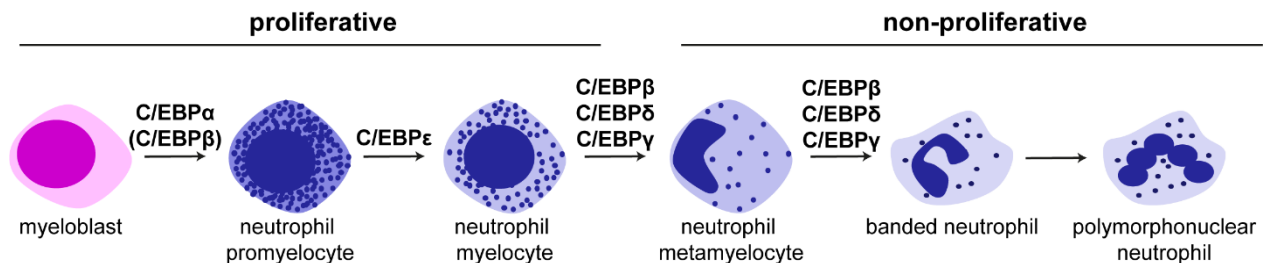


Figure 2: Schematic overview of the granulopoiesis in the bone marrow.

HSC differentiate into pluripotent progenitors, which further proliferate into lineage-committed myeloblasts. By the expression of the transcription factor C/EBP α , or during emergency granulopoiesis C/EBP β , myeloblasts differentiate into neutrophil promyelocytes. C/EBP ϵ mediates the exit from the cell cycle and formation of granules during the myelocyte stage. C/EBP δ , C/EBP γ further mediate the exit from the cell cycle and are highly expressed during the neutrophilic myelocyte and metamyelocytes stage as well as during the maturation to a banded neutrophil. Finally the mature PMN gets released from the bone marrow towards the periphery by their expression of CXCR2 and CXCR4 and the secretion of their ligands by endothelial cells.

1.1.2 PMN EFFECTOR FUNCTIONS

PMN are a heterogeneous population of cells possessing various effector functions upon stimulation. Their heterogeneity is defined by local activation at the site of infection, their age and the disease context. Whether this heterogeneity is reflected by different functional properties remains unclear to date (Hedrick *et al.* 2021). The following sections point out PMNs' key effector functions.

1.1.2.1 PMN Granules and Secretory Vesicles

PMN contain granules densely packed with antimicrobial proteins. As described in the aforementioned section, granules build during granulopoiesis and mark the transition from myeloblasts to promyelocytes, developing until the final, segmented stage of maturation (Figure 2). Their content is a heterogeneous mixture of proteins synthesized from PMN precursor to mature PMN. They can be classified into four subtypes according to their formation during maturation. (1) Primary (azurophilic) granules, contain mostly myeloperoxidase (MPO) and are formed before and during the promyelocyte phase, (2) secondary (specific) granules are formed during the myelocyte phase and mostly contain lactoferrin, followed by (3) tertiary (gelatinase) granules that are formed during the metamyelocyte and banded cell stage. Finally, (4) secretory vesicles are formed via

endocytosis during banded and segmented stage of late maturation. They contain a mixture of cell surface receptors and integrins, resulting, upon merging with the membrane, in a higher affinity to ligands and therefore to additional activation and transmigration from blood to tissue (Faurischou *et al.* 2003, Borregaard *et al.* 2007, Yin *et al.* 2018). Secretory vesicles are mobilized via several stimuli, relevant for the interaction of PMN with activated endothelial cells (signaling of selectins, chemokines like interleukin 8 (IL8) or fMLP) (Borregaard 2010). Interestingly, granules are exocytosed in reverse order of development. Secretory vesicles are released first, equipping the membrane with effector molecules and receptors, allowing the migration to the site of infection (for more details see 1.1.3). Subsequently, specific and gelatinase granules are released, facilitating PMN migration through tissue and containing some antimicrobial proteins. Finally, MPO-containing granules, providing potent antimicrobial effector molecules, get either released at the site of infection or into the pathogen-containing phagosome (Borregaard *et al.* 2007). Additionally to degranulation, PMN release cytokines to fight pathogens and attract further immune cells. Main cytokines released by PMN are tumor necrosis factor α (TNF α), IL1 β , IL8, macrophage inflammatory protein 1 β (MIP1 β), and MIP1 α (Lapinet *et al.* 2000). All of them potentially act on monocytes, macrophages and endothelial cells but mainly activate PMN themselves.

1.1.2.2 Phagocytosis

Phagocytosis is defined as the cellular uptake of particles around 500 nm and bigger. It is related to macropinocytosis, an endocytic uptake of soluble ligands and smaller particles by fluid-phase and receptor-mediated pathways (Gordon 2016). However, in contrast to macropinocytosis, phagocytosis involves recognition and binding, prior to engulfment. Phagocytosis fulfills several defense mechanisms, (1) clearance of bacteria and fungi from infectious sites, (2) initiating pro-inflammatory cytokine release, thereby attracting phagocytes and lymphoid cells and (3) antigen presentation to lymphoid cells. PMN express plasma-membrane receptors mediating phagocytic recognition of microbes (foreign) or senescent cells (altered self). Distinguishing both is crucial for the subsequent anti- or pro-inflammatory reactions upon phagocytosis. Pattern-recognition receptors recognize foreign particles like bacteria, fungi or parasites directly (TLRs, CD14 or CD36) (Flannagan *et al.* 2012). Furthermore, foreign particles can be opsonized with e.g. immunoglobulins within the blood. Fc γ receptors bind to the Fc-fragment of antibodies, activating phagocytosis of pathogens and the transport of C-type lectins, as well as complement receptors, to the cell surface. On the other hand, senescent cells release various molecules like adenosine triphosphate (ATP), lysophosphatidylcholine, or fractalkine, signaling their apoptosis (Chekeni *et*

al. 2011). Additionally, apoptotic cells express “eat me” signals like phosphatidylserine (PS) on their surface, binding to several receptors (T cell immunoglobulin mucin, BAI1, Stabilin-2) (Flannagan *et al.* 2012). Since activated T and B cells also express PS on their membrane, they additionally express so-called “don’t eat me “-signals in order to avoid unwanted phagocytosis. Examples of these are CD31 or CD47 (Simon Brown 2002, Tsai *et al.* 2008).

When foreign particles are phagocytosed, the engulfed material is preliminary sorted within early endosomes, expressing Ras-related protein (Rab) 5. Membrane receptors get recycled, whereas foreign material stays in endosomes. Rab5 gets exchanged by Rab7, a transport molecule mediating the merge with lysosomal-associated membrane protein 1 (LAMP1) positive lysosomes. NADPH oxidases transport electrons in the vacuole, producing superoxide radicals (O_2^-). These partially dismutate to O_2^{2-} and form HO and H_2O_2 , increasing the pH by H^+ consumption, resulting in an accumulation of antimicrobial reactive oxygen species (ROS). Due to the combination of depolarization of the vacuole membrane, induced by NADPH, and elevated levels of cytosolic Ca^{2+} , Ca^{2+} -activated K^+ channels open and K^+ enters the vacuole. Moreover, primary and secondary granules fuse with the pathogen containing vacuole within 20 seconds after vacuole formation, buffering the pH and enabling neutral proteases, mainly neutrophil elastase (NE), to enter and kill the phagocytosed pathogen (Segal 2005) (Figure 3). Finally chloride enters the phagosome and forms, together with MPO and H_2O_2 , antimicrobial agents like hypochlorous acid (HOCl), followed by chlorines, chloramines, hydroxyl radicals and more (Klebanoff 2005). In summary, PMN kill pathogens during phagocytosis by the combination of antimicrobial granule proteins, activated by the phagosomal environment of fine-tuned pH, charges, ROS and oxidized halides.

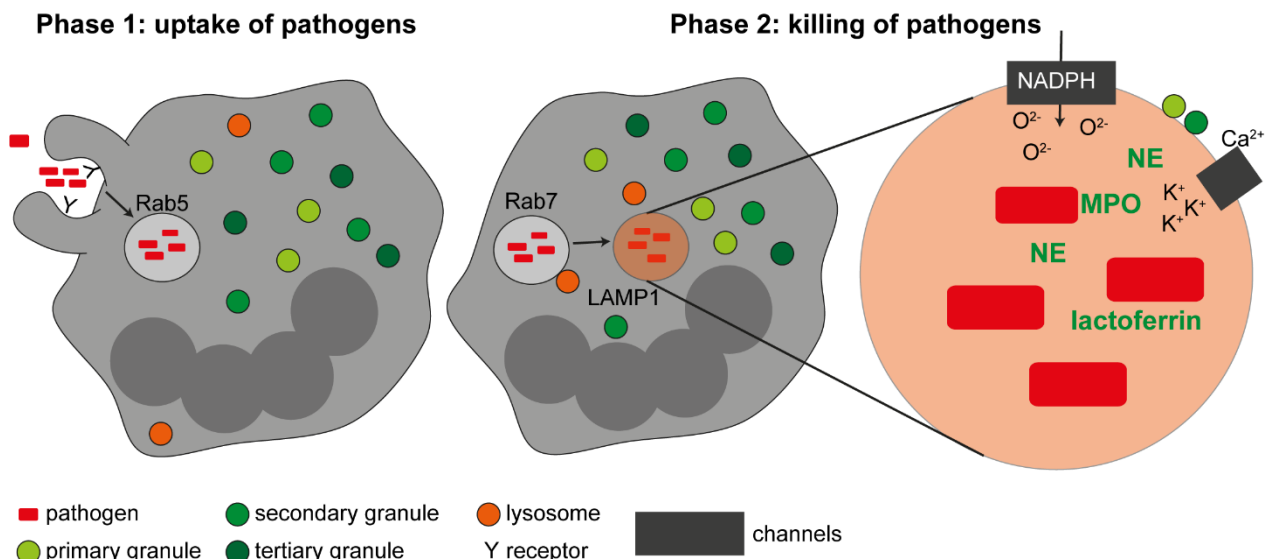


Figure 3: Schematic overview of phagocytosis by PMN.

Pathogens are phagocytosed in a receptor-mediated manner. They enter PMN *via* early endosomes expressing Rab5. Here, the engulfed material is preliminary sorted into recycling and killing (Phase 1). Rab5 gets exchanged by Rab7, a transport molecule mediating the merge with LAMP1⁺ lysosomes. NADPH oxidases pump reactive oxygen into the lysosomes, inducing a depolarization of the vacuole membrane and Ca²⁺ release into the cytosol. This activates potassium channels, to pump potassium into the lysosome creating a perfect environment for elastases to work. Furthermore, primary and secondary granules merge with the lysosome and neutrophil elastase, MPO and lactoferrin enter and kill the pathogen.

1.1.2.3 Neutrophil Extracellular Traps (NETosis)

Besides degranulation and phagocytosis, PMN possess a final ace up their sleeves when it comes to pathogen clearance: suicide. This special kind of cell death was first described in 1996. Contrary to other cell death mechanisms, like necrosis and apoptosis, PMN undergo a decondensation of chromatin during NETosis. It was first described in 2004 by Brinkmann and colleagues. They defined this process as novel host defense mechanism and named it neutrophil extracellular traps (NET) formation (Brinkmann *et al.* 2004). NET formation can be induced either by pathogens like bacteria, bacterial products (LPS), fungi, protozoa, viruses or by antibodies, immune complexes, cytokines and chemokines like IL8 (Vorobjeva *et al.* 2020). Depending on the stimulus, NADPH oxidase is activated via c-RAF-MEK-ERK signaling cascade and phosphorylation by phosphokinase C (PKC). Similar to phagosomal killing of bacteria, NADPH promotes the formation of H₂O₂ and ROS. Both pathways, c-RAF-MEK-ERK and PKC, stimulate the expression of induced myeloid leukemia cell differentiation protein (Mcl-1), an anti-apoptotic protein. A key point during NETosis is the release of granules to the cytosol, especially of MPO and NE, induced by ROS (Metzler *et al.* 2014). MPO and NE first break down the cytoskeleton, followed by disruption of lamin and histones and induce decondensation of the nuclear envelope. Moreover, peptidyl-arginine deaminase 4 (PAD4) translocates to the nucleus promoting citrullination of histones in a hydrogen peroxidase dependent manner (Li *et al.* 2010). Finally, the nuclear envelope is released to the cytosol, pores are formed in the plasma membrane and granule-decorated chromatin is released into the environment to capture and kill extracellular pathogens. It has been shown that PMN are able to release chromatin without dying. Although some investigators tried to refer to it as “vital NETosis”, the Cell death nomenclature committee disagreed 2018 and rather accepted vital NET release (Galluzzi *et al.* 2018). Vital NET release was observed *in vivo* after infecting skin with gram-positive bacteria. Surprisingly, nuclear-free PMN were still able to phagocytose bacteria and migrate towards a stimulus (Yipp *et al.* 2012).

1.1.3 ATTRACTION AND MIGRATION TOWARDS INFECTION SITES

Due to the fact that PMN are the most common leukocytes within the human immune system and among the first cells recruited towards infectious sites, rapid recruitment is crucial for their function. Indeed, PMN are equipped with finely tuned sensors for stimuli of various kinds. Classically, the guided migration along a gradient of a chemical signal is called chemotaxis. Within the vasculature, chemoattractants, such as chemokines, are immobilized by glycosaminoglycans (GAGs) or heparan sulfate, in particular on the luminal membrane of endothelial cells (Middleton *et al.* 2002, Handel *et al.* 2005). Outside the blood stream, extracellular matrix (ECM) binds chemoattractants, guiding PMN towards the infectious site (chemokinesis or haptotaxis) (Petri *et al.* 2018). Chemoattractants can be divided in four families: (1) chemotactic lipids, like leukotriene B(4), released by myeloid cells, or platelet-activating factors (PAF), expressed by activated endothelium. (2) Formyl peptides (e.g. N-formyl-Met-Leu-Phe (fMLP)) released by bacteria, (3) complement anaphylotoxins (e.g. C3a, C5a) and (4) chemokines (cytokines with chemotactic activity, e.g. CXCL1-3, CXCL5-8, MIP1 α and 1 β) (McDonald *et al.* 2011, Metzemaekers *et al.* 2020). The latter derive from tissue resident cells like macrophages, dendritic cells (DCs) or fibroblasts sensing the pathogen invasion (Takeuchi *et al.* 2010). At first glance, all this chemoattractants fulfill the same function, attraction and subsequent migration of PMN to infection. Nevertheless, PMN further distinguish chemoattractants in a hierarchical manner with lipid mediators and chemokines mediated by the host, representing “intermediate targets” and pathogen-derived fMLP and C5a being markers for the “end-target”. This is due to the higher constitutive activity of “end-target” chemoattractant receptors on the PMN surface as well as a differential signal transduction after receptor activation induced by “intermediate” or “end-target” chemoattractants (Heit *et al.* 2008, McDonald *et al.* 2010, Metzemaekers *et al.* 2020).

During PMN migration, pathogen-activated endothelium expresses selectins, enabling initial tethering and rolling of PMN upon binding to their ligands. Thus, decelerated PMN detect chemokines, derived from tissue damage or infection, by glycosaminoglycans (GAG)-, heptaspanning membrane receptors (duffy antigen receptor for chemokines (DARC))-, or heparan sulfate proteoglycans (HSPGs)-immobilized chemoattractants on the endothelial layer. Binding of chemoattractants by G-protein coupled receptors (GPCRs) facilitates gradient sensing, polarization and cell motility in PMN, resulting in integrin activation (LFA-1, MAC-1, VLA4) and adhesion to the endothelium (Iglesias *et al.* 2008, Dixit *et al.* 2011). Afterwards, PMN crawl *via* binding of CD11b/CD18 along the chemoattractants gradient. Simultaneously, PMN secrete matrix

metalloproteinases from tertiary granules to modulate the ECM structure and enhance the surface expression of CD11b/CD18, which in turn releases further ECM bound molecules such as cytokines, enhancing the immune activation (Mollinedo *et al.* 1997, Parks *et al.* 2004). This results in a firm adhesion of PMN, so that they arrest on the endothelial surface at the site of infection. Following the arrest, PMN polarize and flatten on the endothelial lumen surface in order to find an unrestricted site for transmigration (diapedes). Depending on the intensity of tissue inflammation, diapedes either occurs between two endothelial cells (paracellular route) or directly through an endothelial cell (transcellular route). Finally, PMN cross the pericyte layer and pass the venular basal membrane before arriving at the inflamed tissue (Filippi 2019). There, pathogen-associated molecular patterns (PAMPs) and endogenous damage-associated molecular patterns (DAMPs) promote the complete activation of PMN, resulting in granule secretion, phagocytosis and NET formation as described in earlier sections.

1.2 CANCER IMMUNOLOGY

Malignant progression includes dysregulation of metabolic energy pathways, genomic instability and evasion of the immune attack as well as tumor promoting inflammation (Hanahan *et al.* 2011). During effective immunosurveillance, tumor cells are initially recognized and killed by the innate immune system, followed by DC-mediated T cell priming and the generation of tumor-antigen specific T cells homing to the tumor origin and effectively inducing an antitumor response (elimination phase). In the equilibrium phase, tumor cells are exposed to a higher selection pressure, due to the activated host immune system or a therapeutic treatment. This leads to the development of less immunogenic cell clones and consequently to a reduced tumor recognition by reduced antigen presentation *via* major histocompatibility complex class I molecules (MHC I). Finally, selected tumor cell variants escape the immune system and potentially grow in an immunological intact environment (Dunn *et al.* 2004). In addition to classical immune escape mechanisms in the context of immunoediting (see above), cancer cells further reprogram tumor-infiltrating immune cells. Hence, myeloid cells are polarized from an anti- towards a pro-tumoral and / or immunosuppressive phenotype, thereby driving the tumor progression, the formation of metastases and resistance against cancer therapy (Lecot *et al.* 2019, Galli *et al.* 2020). In this study we particularly focused on tumor-associated neutrophils (TAN) and myeloid-derived suppressor cells (MDSC) that are described in more detail below.

1.2.1 MDSC

Additionally to the development of less immunogenic cells clones, tumors modulate the immune system by secretion of cytokines (e.g. TNF α) and the production of MDSC. MDSC are pathologically expanded cells that suppress other immune cells, dependent on host-derived factors (Dumitru *et al.* 2012). High frequencies of circulating MDSC have been correlated with poor survival of cancer patients suggesting a clinical relevance for these cells (Lang *et al.* 2018). In humans, several subsets of MDSC were identified by their expression of surface markers: granulocytic MDSC (PMN-MDSC, CD15⁺, CD66b⁺, CD33⁺, CD14⁻), monocytic MDSC (M-MDSC, CD66b⁻, CD15⁻, CD33⁺, CD14⁺, HLA-DR⁻) and early stage MDSC (e-MDSC, CD33⁺, CD11b⁺, HLA-DR^{low}, CD14⁻, CD15⁻, CD66b⁻) (Fujimoto *et al.* 2000, Brandau *et al.* 2011, Dumitru *et al.* 2012, Mandruzzato *et al.* 2016). Since these surface markers are not exclusively expressed on MDSC, phenotyping in combination with suppressive function assessment has been established as method to identify MDSC (Bronte *et al.* 2016). Furthermore, recent studies suggested the high expression of lectin-type oxidized LDL receptor 1 (LOX1) as specific marker for PMN-MDSC, distinguishing these from mature PMN (Condamine *et al.* 2016, Nan *et al.* 2018). LOX-1 is a class E scavenger receptor that is expressed on macrophages, platelets and chondrocytes, as well as on endothelial and smooth muscle cells. It has been implicated to play an important role in different diseases, e.g. atherosclerosis and metabolic diseases activity (Taye *et al.* 2013). Until now it remains unclear, whether human MDSC remain in the blood circulation or migrate from circulation into tumors.

1.2.2 TUMOR MICROENVIRONMENT

Besides tumor cells, the tumor consists of a mixture of fibroblast, mesenchymal cells and immune cells. Additional to this complexity of cells their spatial organization is of special importance, particularly for tumor-associated immune cells with pro-tumoral properties as TAN (Si *et al.* 2019). Immune cells are distributed within the tumor along vascular or lymphatic vessels and the fibroblastic stromal support in the tumor margin (Rocquelin *et al.* 1981). In general, functional populations of immune cells tend to organize in different regions within the tumor. The tumor microenvironment can be classified according to their infiltration into (1) infiltrated-excluded, characterized by exclusion of cytotoxic lymphocytes (CTL) in the core of the tumor and an accumulation of CTL around the tumor periphery; (2) infiltrated-inflamed, showing high expression of PD-L1 on tumor and myeloid cells as well as high counts of activated CTL and (3)

infiltrated-tertiary lymphoid structure (TLS), with lymphoid aggregates whose cellular composition resemble lymph nodes (Binnewies *et al.* 2018).

1.2.3 TAN

As described in the prior section, tumors are usually highly infiltrated by various immune cells including PMN, macrophages and lymphocytes (Greten *et al.* 2019). Until 1992, PMNs' role in tumor formation and progression was rather neglected, due to their short life span and their low amount of mRNA expressing bioactive molecules (Lloyd *et al.* 1992). However, evidence is growing that not only PMN frequency in the peripheral blood correlates with poor prognosis of cancer patients (Templeton *et al.* 2014) but also their ratio to lymphocytes (neutrophil-lymphocyte ratio = NLR) has been shown to play a crucial role in tumorigenesis. High NLR marks high risk patients with more advanced disease (Guthrie *et al.* 2013). Furthermore, it has been shown that high densities of PMN within the tumor, so-called TAN, correlate with poor prognosis in various cancer types (Gentles *et al.* 2015). Pioneering work has been performed in order to unravel TANs functional mechanism, but, until now, it is not entirely clear how TAN affect tumor progression. TAN have been shown to act actively anti- or pro-tumoral or passively *via* antigen-presentation to CD4⁺ T cells or T cell suppression, depending on further stimuli (Shaul *et al.* 2021). Furthermore, the crosstalk between TAN and tumor infiltrating T cells (TIL) has been demonstrated to act *via* cell-cell contact or *via* mediators, such as proteases, cytokines, and ROS. Moreover, TAN have been shown to play a crucial role in epithelial-to mesenchymal-transition by secretion of NE, MMP9, TGFβ and NETosis, promoting the formation of metastasis (Albregues *et al.* 2018, Mukaida *et al.* 2020). This initiated the development of several strategies to reduce PMN frequency (inhibition of IL23, IL17, G-CSF) or their migration into the tumor (inhibition of CXCR1/2) showing promising results in cancer therapy (Ocana *et al.* 2017).

1.3 HYPERTHERMIA: TREATMENT AGAINST CANCER

Heat has become a treatment modality against cancer, since its ancient implementation in 1700 BC when a glowing tip of a torch was used for breast cancer therapy (Breasted 1930). Rather modern techniques including radiofrequency (Gazelle *et al.* 2000), microwaves (Seegenschmiedt *et al.* 1990), or ultrasound waves (Wu *et al.* 2001) were invented, mediating moderate heat in a specific target region, which is termed hyperthermia. Hyperthermia is commonly defined as heating of tissue to a temperature in the range of 41–47°C for 20 to 30 min and results in cell damage by loosening of cell membranes and denaturizing proteins. The application time is exponential dependent on temperature. Different reports described halving of time for every 1 to 2 °C rise in

applied temperatures (Svaasand *et al.* 1990). Clinical studies showed that additional hyperthermic therapy substantially enhanced the effectiveness of radio- and chemotherapy, showing improved tumor control and prolonged disease-free survival (Datta *et al.* 2015). To date, one major obstacle is the damage of surrounding tissue due to the unspecific application of hyperthermia in cancer therapy. The development of lasers (**L**ight **A**mplification by the **S**timulated **E**mission of **R**adiation) was a revolutionary step. Laser light has the characteristics of monochromaticity, coherence, and collimation providing a narrow beam of high intensity (Bogdan Allemann *et al.* 2011). Lasers were invented in 1960 by T.H. Maiman (Maiman 1960) and first reported in medical application by ophthalmologists in 1963 (Kapany *et al.* 1963), followed by wide interest in the late 1960s (Goldmann 1967, Tuffin *et al.* 1980). The laser light was either transmitted from an optical fiber tip to exposed tumors or by insertion of the fiber into the center of the targeted tumor, termed interstitial laser hyperthermia (Steger *et al.* 1989, Masters *et al.* 1992). Nevertheless, a disadvantage of laser therapy, the non-selectivity, remained, since both, normal and tumor cells in the path of the laser light get damaged. Furthermore, this therapy required high power density up to tens to hundreds of watts to induce the tumor killing (Sultan 1990).

1.4 HYPERTHERMIA MEDIATED BY PHOTSENSITIZERS

In order to overcome this obstacle, locally applied photosensitizers mediating the phototherapy were invented (Abrahamse *et al.* 2016). Here, two different therapies were developed, the photodynamic and the photothermal therapy, further described in the following sections.

1.4.1 PHOTODYNAMIC THERAPY

Photodynamic therapy (PDT) involves cell destruction caused by means of toxic singlet oxygen and / or other free radicals produced by a sequence of photochemical and photobiological processes (Gold 2007). A photosensitizer, exposed to a specific wavelength of light in the visible (380-700nm) or near-infrared (NIR, 800-2500nm) region, induces a reaction with tissue oxygen. A major advantage of NIR light, compared to visible light, is its' significantly higher penetration depth for biological tissue ("water window"). This penetration depth reaches up to 10 cm, for example in breast tissue (Smith *et al.* 2009, Abadeer *et al.* 2016). The earliest sensitizer used was acridine, killing paramecia in 1900, followed by eosin for skin cancer treatment in 1903. To date, many chemicals have been reported for photodynamic therapy, but porphyrin-based sensitizers are mostly used in cancer treatment due to their preferential retention in cancer tissues and their efficient production of reactive oxygen (Huang *et al.* 2008). Nonetheless, porphyrin-based therapy is limited to tumors on, or just underneath the skin, or on the lining of internal organs or cavities,

because it absorbs light shorter than 640 nm in wavelength. For deep-seated tumors, second generation sensitizers, absorbing in the NIR region, such as hematoporphyrin derivatives, chlorins (like Temporfin, Foscan and Bremachlorin), bacteriochlorins (like TOOKAD and LUZ11), or synthetic dyes (like phthalocyanines (RLP068) and phenothiazinium salts (EtNBS), Rose Bengal) have been developed and clinically approved in cancer treatment (Abrahamse *et al.* 2016). A major drawback of PDT is that the photosensitizing drug stays in the body for a long time, resulting in severe light sensitivity in patients (Huang *et al.* 2008).

1.4.2 PHOTOTHERMAL THERAPY

Alternatively, photothermal therapy (PTT) emerged. Instead of inducing the production of free radicals, photothermal agents are introduced into the cancer tissue to selectively induce heat in their local environment. Mechanistically, surface-electrons of photothermal agents transition from ground to the excited state. This excitation energy subsequently relaxes through non-radiative decay, resulting in an increase in kinetic energy, leading to the overheating of the local environment around the light absorbing agent and thereby inducing tissue damage (Camerin *et al.* 2005, Camerin *et al.* 2009). Different photoabsorbing agents, like natural chromophores with very low absorption rates, or dye molecules (indocyanine green, naphthalocyanines, and porphyrins) bound to transition metals, have been developed (Huang *et al.* 2008). Dye-molecules showed strong absorption and highly efficient light-to-heat conversion. However, dye molecules fade under laser irradiation due to photobleaching. To circumvent this disadvantage, a vast variety of nanostructures with unique optical properties that are useful in biology and biomedical applications were developed (Link *et al.* 1999, Xia *et al.* 2005, Ali *et al.* 2017).

1.5 NANOPARTICLES

“Nano” origins from the ancient Greek word *nános* meaning dwarf. Nanostructures are objects between 1 and 100 nm. The term “nanotechnology” defines the manipulation of material down to atomic scale and was firstly mentioned by Richard Feynman in 1959. He discussed, how downsizing of machines could offer opportunities of physical manipulation of single atoms to nanoscale (Feynman 1960). To date, nanotechnology finds its application in various fields, ranging from semiconductor physics, supramolecular chemistry, energy storage, as well as molecular biology and biomedicine. It is commercially used for catalysts in cars, titanium dioxide nanoparticles in sunscreens, or bandages imprinted with nanoparticles for a better wound healing (Khlebtsov *et al.* 2011, Dykman *et al.* 2014, Abadeer *et al.* 2016).

1.5.1 NOBLE METAL NANOPARTICLES AS PHOTSENSITIZERS

Noble metal nanoparticles are promising tools for PTT because of their enhanced absorption, being four to five times larger than those of conventional photoabsorbing dyes mentioned above (Huang *et al.* 2008). This strong absorption is beneficial for laser therapy, since it allows lower laser energies, thereby reducing side effects enabling minimally invasive therapy. Furthermore, metal nanostructures have higher photostability, thus do not bleach during therapy. Currently, gold nanospheres (Khlebtsov *et al.* 2006), gold nanorods (Huang *et al.* 2006, Li *et al.* 2016), gold nanoshells (Baek *et al.* 2011), gold nanocages (Skrabalak *et al.* 2007), and carbon nanotubes (Kam *et al.* 2005) are the main nanostructures demonstrating successful PTT due to their strongly enhanced absorption in the visible and NIR regions. Especially gold nanoparticles are promising agents due to their ease of preparation, their efficient absorption and heat conversion, high photostability, low cytotoxicity, ready multi-functionalization, and tunable optical properties (Hwang *et al.* 2014).

1.5.2 GOLD NANOPARTICLES IN PTT

Faraday was the first investigator producing colloidal gold nanoparticles in 1857 by reducing gold chloride with phosphors (Faraday 1887). In 1951, Turkevich and colleagues (Turkevich *et al.* 1951) developed a more advanced method that allowed multiple studies on the interaction of gold nanoparticles and light (Link *et al.* 2000). From 2000, the rising interest for gold nanoparticles in biomedical applications, ranging from bioimaging to cancer treatment (Storhoff *et al.* 1998, Sokolov *et al.* 2003, El-Sayed *et al.* 2005, Skrabalak *et al.* 2007) led to new approaches, especially in the preparation of gold nanorods (AuNR) (Jana *et al.* 2001, Jana *et al.* 2001). Upon excitation with light, the gold nanoparticles delocalized conduction band electrons coherently oscillate under resonant conditions leading to the appearance of a characteristic absorption band. Since this excitation is not spreading further than the particle itself, it is a local phenomenon, called localized surface plasmon resonance (LSPR). AuNR are especially promising for PTT, as they exhibit two LSPR modes, a transversal mode located at ~520 nm and a red-shifted longitudinal LSPR mode (~5-600 nm, Figure 4A). The location of the longitudinal plasmon mode depends on the aspect ratio of the AuNR and can be located in the near infrared (NIR ~650-950 nm, Figure 4A) (Link *et al.* 1999). The application of AuNR for PTT has shown promising results in multiple murine tumor models (Huang *et al.* 2006, Almeida *et al.* 2014, Ali *et al.* 2016, Yin *et al.* 2017, Zhang *et al.* 2019).

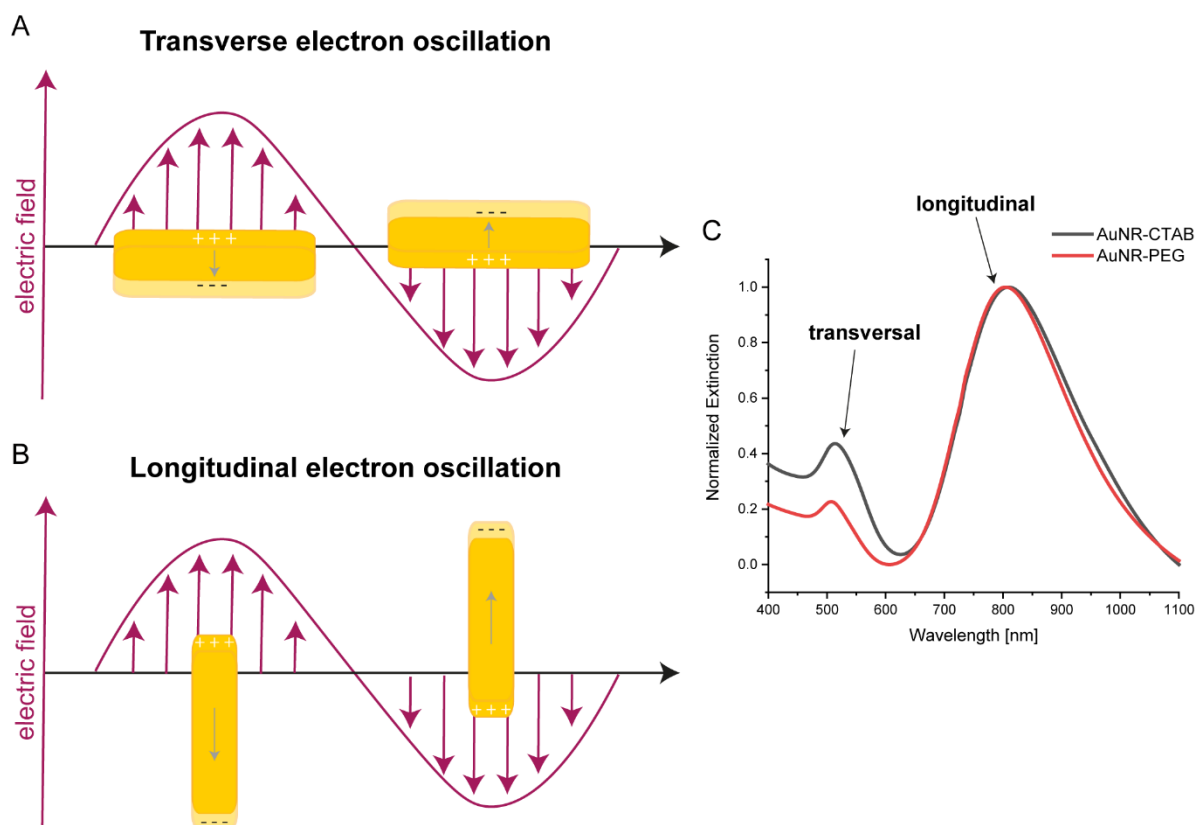


Figure 4: Schematic overview of the split LSPR of gold nanorods.

The interaction of the electric field of light with free electrons on the nanoparticle surface induces a charge separation of free electrons and the ionic gold core. Due to Coulomb repulsion, the free electrons move to in the opposite direction, resulting in a collective oscillation of electrons. AuNR show two kinds of oscillation, **(A)** transversal and **(B)** longitudinal. This is visible in normalized UV-Vis extinction spectra. Surface functionalization (cetrimonium bromide (CTAB) or polyethylene glycol (PEG)) can affect the extinction spectra. **(C)** UV-Vis extinction spectra of AuNR used in this thesis. These measurements were conducted by our cooperation partner AG Schlücker. The longitudinal plasmon mode associated with the AuNR length is located at 809 nm wavelength. Upon functionalization with heterobifunctional PEG it blue-shifts to 804 nm.

1.5.3 GOLD NANOPARTICLES - CELL INTERACTION

AuNP interaction with cells heavily depends on AuNP physicochemical properties as shape, size, aspect ratio and surface modifications which further affect the formation of a protein corona (Riveros *et al.* 2013). The protein corona consists of a dynamic and multi-layered protein structure which is formed instantly when nanoparticles get in contact with biological material as blood or cell culture medium. All this might have an effect on the internalization pathway, although the properties of cells, as phagocytosis for phagocytes, play a major role. Nevertheless, most studies investigating AuNP uptake used cancer cell lines. AuNP have been shown to be internalized either by receptor-mediated endocytosis or *via* phagocytosis (Oh *et al.* 2011). Especially the size of AuNP determines the accumulation at different sites inside cells, ranging from cytoplasmic and nuclear

accumulation (2 and 6 nm AuNP) to accumulation in vesicular structures within the cytoplasm (\geq 15 nm AuNP) (Huang *et al.* 2012). Considering cytotoxicity, the surface coating has been shown to be of major importance. During the production of AuNP the detergent cetyltrimonium bromide (CTAB) is necessary to stabilize AuNP. CTAB has been shown to be especially cytotoxic to CF-31, MCF-7, A549 cell lines and human adipose-derived stromal cells (Mironava *et al.* 2010, Qiu *et al.* 2010, Wang *et al.* 2011, Mironava *et al.* 2014). In order to overcome this toxicity, methods to exchange the CTAB after stabilization with less toxic polymers, for example polyethylene glycol (PEG), have been developed (Kinnear *et al.* 2013). Considering the size of AuNP, small AuNP (1-2 nm) have been shown to be extremely toxic compared to 15 nm AuNP in a time and concentration dependent manner (HeLa, SK-Mel-28, L929, J774A1 cell lines) (Pan *et al.* 2007). Furthermore, it has been demonstrated that shorter, round AuNP are engulfed more easily than rod-shaped AuNP resulting in higher cytotoxicity in MCF-7 cells (Qiu *et al.* 2010). Cytotoxic effects of AuNP potentially root in induced cell cycle arrest and DNA damage as shown with HeLa cells (Jeyaraj *et al.* 2014) and in the inhibition of proliferation due to damaged chromosomes, shown in studies using Raw264.7 mouse macrophages (Di Bucchianico *et al.* 2014). Furthermore, AuNP have been shown to induce aggregation of microtubules resulting in cell cycle arrest and apoptosis of A549 cells (Choudhury *et al.* 2013). Furthermore, Soenen and colleagues described that AuNP decrease mitochondrial membrane potentials, induce the generation of ROS, elevate intracellular Ca^{2+} levels, and cause DNA damage in PC12, C17.2, HUVEC cell lines (Soenen *et al.* 2014). This was supported by Tsai and colleagues showing an induction of oxidative and endoplasmic reticulum (ER) stress as well as autophagy in K562 cells due to AuNP treatment (Tsai *et al.* 2011). With respect to immune cells it has been shown that AuNP modulated the cell morphology and enhanced the transcription of pro-inflammatory genes in J774A1 mouse monocytes (IL1, IL6, TNF α) (Yen *et al.* 2009). Additionally, AuNP promoted IgG secretion in murine B cells *in vivo* via regulation of B-lymphocyte-induced maturation protein 1 (blimp1) and downregulated paired box 5 (pax5) in a size dependent manner (Lee, C. H. *et al.* 2014). All these studies provide preliminary insights in AuNP-cell interaction, but lack the translational relevance. Studies on AuNP interaction with primary immune cells are rare, although these cells, especially the phagocytosing immune cells, like PMN, monocytes, macrophages and dendritic cells, constitute the first contact points upon AuNP administration.

1.6 ANTIBODY TARGETED THERAPY

Paul Ehrlich envisioned a “magic bullet”, enabling targeted therapy of a specific diseases without harming the body itself, already in the beginning of the 20th century (Nobel Prize in Physiology or Medicine 1908). In 1975, Milstein and Köhler invented the production of monoclonal antibodies (Nobel Prize in Physiology or Medicine 1984) by developing the hybridoma technology. This technology allows the production of chemically identical antibodies by injection of antigens into mammals. After B cells start to produce antibodies against the injected antigen, they are harvested and fused with an immortal myeloma cell line and form so-called hybridomas owing the ability to produce antibodies, while being durable and reproducible (Kohler *et al.* 1975). Monoclonal antibodies (mAB) specifically targeting epitopes of e.g. malignant cells, may deliver therapeutic agents to targets or can be used for imaging *in vivo*. Their main benefit is specific targeting with low adverse effects, resulting in massive investigation and production of therapeutic mAB. Until 2019, at least 570 mAB were investigated in clinical trials and 79 got approved by United States Food and Drug Administration (US FDA), 30 of them for cancer therapy (Lu *et al.* 2020).

1.7 IMMUNOTARGETING OF GOLD NANOPARTICLES

In chapter 1.5.2., the efficiency of gold nanoparticles was emphasized. In order to develop efficient PTT, the photosensitizer (e.g. gold nanorods) has to specifically accumulate at the site of the tumor. This can be accomplished by intratumoral injection, bearing the disadvantage of low distribution within the tumor and clearance by intratumoral phagocytic immune cells (Smilowitz *et al.* 2018). Alternatively, immunotargeting strategies by bio-functionalization of AuNP, in order to deliver photosensitizers selectively to diseased cells, offers efficient killing of tumor cells without harming healthy cells in PTT. Polymers are widely used to stabilize and functionalize AuNP. The most abundantly used polymer for AuNP stabilization is PEG, which is available in various modifications like thiol-, carboxyl- amino- and hydroxyl groups as well as different chain lengths ranging from less than 0.5 kDa to more than 20 kDa. It further reduces the formation of protein corona, due to the formation of a hydrate shell around the hydrophilic polyether backbone (Dreaden *et al.* 2012, Dykman *et al.* 2017). *In vivo*, PEGylated nanoparticles passively accumulate in the tumor due to the enhanced permeability and retention effect (EPR) (Maeda 2001), although the relevance of such an effect is controversially discussed (Dai *et al.* 2018). Furthermore, PEGylation allows the conjugation of AuNP to targeting agents like antibodies, aptamers or DNA (Takahashi *et al.* 2006). This allows a selective targeting and active accumulation in the region of interest. Especially nanoparticles conjugated to anti-epidermal growth factor receptor (EGFR) antibodies,

targeting overexpressed EGFR on tumor cells (Sokolov *et al.* 2003, El-Sayed *et al.* 2005, El-Sayed *et al.* 2006, Huang *et al.* 2006, Patra *et al.* 2008), as well as anti-Her2 targeting overexpressed Her2, or seprase on breast cancer cells showed promising results (Loo *et al.* 2005, Zharov *et al.* 2005). Even Fab fragments or aptamers demonstrated successful therapeutic targeting of AuNP in cancer drug delivery or as biosensors (Cortez-Retamozo *et al.* 2002, Han *et al.* 2013). All these functionalizations offer exciting possibilities in the biomedical field. Nevertheless, the limitations of AuNP targeting due to unspecific phagocytic clearance is insufficiently investigated. Therefore, this study aims to unravel the interaction of AuNP with phagocytic immune cells in order to further enhance the development of safe and efficient cancer therapies.

AIM OF THE STUDY

Gold nanoparticles (AuNP) are promising agents for diverse biomedical applications such as drug and gene delivery, bioimaging and cancer treatment. They are considered to be bioinert and can be coated with DNA, proteins and polymers, which allows the combination of diagnostics and therapy (Theranostic). Understanding the interaction of AuNP with immune cells is a key point for developing safe and efficient therapeutic applications. Therefore, this project aims to analyze how different types of AuNP interact with neutrophil granulocytes (PMN), a subset of leukocytes with professional phagocytic activity.

In humans, neutrophils are the most abundant immune cell population, representing 50–70% of all leukocytes in the circulation. More than 10^{11} neutrophils may be produced per day. They are key player cells in inflammation. Due to their high phagocytic activity and abundance, PMN are prototypic target cells for AuNP in the peripheral blood.

In order to investigate the molecular interaction of AuNP and PMN, the following questions will be answered:

- Do PMN take up AuNP *ex vivo*?
- Does the uptake of AuNP have an impact on the survival of PMN *ex vivo*?
- How (molecular mechanism) are AuNP taken up by PMN *ex vivo*?
- Does the uptake of AuNP affect the activation level of PMN *ex vivo*?
- What are the molecular mechanisms behind a potential activation of PMN *ex vivo*?
- Can immune cells be targeted by AuNP, functionalized with cell-type specific antibodies?

Methods and experimental plan:

Used methods will include flow cytometry (8-colour) for surface phenotyping, fluorescence microscopy (2D and 3D), ELISA, transmission electron microscopy (TEM), bioassays (Luminex), Western Blot and quantitative PCR.

PMN will be isolated from peripheral blood of healthy donors. AuNP with different shapes (spherical-, rod-shaped) will be tested on PMN in a time and dose-dependent manner. Transmission electron microscopy and fluorescence microscopy via fluorescently labelled AuNP will validate the uptake of AuNP. Major focus will be the analysis of the morphology and survival of PMN as

well as the quantification of the uptake efficiency in a time dependent manner. In the following, it is planned to analyze the uptake mechanisms of AuNP in PMN. For this, chemical inhibitors will be used in combination with fluorescently labelled AuNP. Furthermore, the route of AuNP inside PMN shall be analyzed. To investigate the effects of AuNP treatment on PMN, different techniques will be used, including flow cytometry measurements and 3D image analysis. Additionally, we want to know whether the uptake of AuNP has an impact on the activation level of PMN. Published data on other immune cells, like macrophages and dendritic cells, are pointing towards an activation of cells by AuNP treatment. Therefore, we are planning to perform surface phenotyping *via* flow cytometry and investigate the production of ROS and several typical neutrophil effector molecules. Furthermore, the molecular signal transduction pathways, induced by uptake of AuNP, will be investigated. Analysis shall combine the uptake mechanisms (point 2) with the investigated activation level of PMN in point 3. To investigate these pathways, different techniques, like flow cytometry measurements, Western Blot and ELISA will be used. Finally, antibody-mediated targeting shall be combined with AuNP in order to develop a specific photothermal therapy. Of special interest shall be PMN, representing phagocytic immune cells. The project will yield new information on the interaction of AuNP and the immune system. We hope to gain new insights on how AuNP are taken up and processed by circulating human PMN. Based on this information we perform initial steps directed towards cell-type specific therapeutic targeting of immune cells by antibody-AuNP conjugates and PTT.

2 MATERIAL

2.1 CONSUMABLE SUPPLIES

Table 2: Consumables used in this work

consumables	manufacturer	location
24 well Cell Culture plate	Sarstedt	Nümbrecht Germany
96 well cell culture plate round bottom	Greiner bio-one	Frickenhausen Germany
Biosphere®pipette tips 10 µL	Sarstedt	Nümbrecht Germany
Biosphere®pipette tips 100 µL	Sarstedt	Nümbrecht Germany
Biosphere®pipette tips 1000 µL	Sarstedt	Nümbrecht Germany
Biosphere®pipette tips 20 µL	Sarstedt	Nümbrecht Germany
Biosphere®pipette tips 200 µL	Sarstedt	Nümbrecht Germany
Casy Cups	Omni life Science	Bremen Germany
Cover slips round 12mm	Carl Roth	Karlsruhe Germany
Filtropur BT 50, Bottle top filter	Sarstedt	Nümbrecht Germany
Immuno PlatesMaxisorp F96 Nunc	VWR	Darmstadt Germany
LS Columns	Miltenyi	Bergisch Gladbach Germany
Multiply-&Strip pro 4 tubes chain with lid	Sarstedt	Nümbrecht Germany
Pipette tips clear (300 &L)	Sarstedt	Nümbrecht Germany
PP sealing foil	Kisker-Biotech	Steinfurt Germany
Protein low-binding 1.5 mL reaction tubes	Eppendorf AG	Germany
Protein low-binding 1.5 mL reaction tubes	Thermo Fisher Scientific	Germany
PVDF Western Blotting Membranes	Roche Applied Science	Wiesbaden Germany
Reaction tubes 0.5 mL	PP Sarstedt	Nümbrecht Germany
Reaction tubes 1.5 mL without cap	Sarstedt	Nümbrecht Germany

Reagent and centrifuge tubes 15 mL	Sarstedt	Nümbrecht Germany
S-Monovette®10 mL 9NC (Citrat)	Carl Rot	Nümbrecht Germany
SuperFrost® plus glass slides	Langenbrinck	Karlsruhe Germany
TC 24 well insert 3 µm Falcon	Sarstedt	Nümbrecht Germany
Tissue culture plate 24 well	Sarstedt	Nümbrecht Germany
Transfer pipette 3.5 mL sterile	Sarstedt	Nümbrecht Germany

2.2 EQUIPMENT

Table 3: Equipment used in the laboratory.

consumables	manufacturer	location
Amersham Imager 600 (used in the Cardio Science Lab, West German Heart- and Vascular Center, Clinic for Cardiology and Angiology, University Hospital Essen)	cytiva	Freiburg Germany
Analytical balance AE260	Mettler-Toledo	Giessen Germany
Applied Biosystems StepOne plus	ThermoScientific	Karlsruhe Germany
Autoclave VX75	Systec	Linden Germany
BD FACSCANTO II	BD Biosciences	Heidelberg Germany
Casy Cell Counter + Analyzer System version TT	Omni life Science	Bremen Germany
Centrifuge Micro 200R	Hettich Zentrifugen	Tuttlingen Germany
Centrifuge Universal 320	Hettich Zentrifugen	Tuttlingen Germany
Centrifuge Universal 420R	Hettich Zentrifugen	Tuttlingen Germany
CO ₂ Incubator HERAcell 240 und 240i	Thermo Scientific	Langenselbold Germany
ELISA-Washer ELx50	Fisher scientific	Schwerte Germany
Eppendorf Research pipette 0.5-10 &L	Eppendorf	Hamburg Germany

Eppendorf Research pipette 20-200 &L	Eppendorf	Hamburg Germany
GFL Water bath	Lauda	Lauda-Königshofen Germany
Heating block Neoblock 1	Neolab	Heidelberg Germany
Ice box 2.5 L	Carl Roth	Karlsruhe Germany
Incubator & shaker TH30	Edmund Bühler	Hamburg Germany
InLab Routine Pro pH electrode	Mettler-Toledo	Giessen Germany
Laminar flow hood MSC-Advance 1.8	Thermo scientific	Langenselbold Germany
Liquid nitrogen tank LD25	Taylor-Wharton	Wiesbaden Germany
MACSmix™ Tube Rotator	Miltenyi	Bergisch Gladbach Germany
Minishaker 3D	Kisker-Biotech	Steinfurt Germany
MyCycler PCR machine	BioRad	Munich Germany
Optris Xi 80	Optris	Berlin Germany
Pipetman-Pipette P10	Gilson	Limburg-Offheim Germany
Pipetman-Pipette P100	Gilson	Limburg-Offheim Germany
Pipetman-Pipette P1000	Gilson	Limburg-Offheim Germany
Pipetman-Pipette P20	Gilson	Limburg-Offheim Germany
Pipetman-Pipette P200	Gilson	Limburg-Offheim Germany
Precision analytical balance AZ612	Sartorius	Göttingen Germany
QuadroMACSTM Separator	Miltenyi	Vernon Hills USA
Scotsman AF80 ice flaker	Scotsman	Vernon hills Illinois USA
Screw Top Bottles clear 2000 mL	Carl Roth	Karlsruhe Germany
Screw Top Bottles clear 250 mL	Carl Roth	Karlsruhe Germany
Screw Top Bottles clear 500 mL	Carl Roth	Karlsruhe Germany
Seven Easy pH-Meter	Mettler-Toledo	Giessen Germany
Staining boxes acc. to Schiefferdecker	Carl Roth	Karlsruhe Germany
Synergy 2Multi-Mode Reader	Fisher scientific	Schwerte Germany
UVP ChemiDoc-It®Imager	Analytik Jena	Jena Germany

Variomag Powertherm (magnetic stirrer & heat plate)	HP Medizintechnik GmbH	Oberschleissheim Germany
VortexMixer VTX-300L	Kisker-Biotech	Steinfurt Germany
Western blot transfer Wet/Tank Blotting Systems	Bio-Rad	München Germany
ZEISS Elyra (IMCES)	ZEISS	Jena Germany

2.3 CHEMICALS

Table 4: Chemicals used in this work.

Chemicals and reagents	manufacturer	location
0.9 % Sodium chloride solution	Fresenius Kabi	Bad Homburg Germany
123counting beads	Thermo Fisher Scientific	Darmstadt Germany
40 % Acrylamide/Bis solution	Bio-Rad	München Germany
7AAD Staining Solution	BD Bioscience	Heidelberg Germany
Ammoniumpersulfate	Serva Electrophoresis	Heidelberg Germany
Aqua B. Braun	B.Braun	Melsungen Germany
BD CST Beads	BD Bioscience	Heidelberg Germany
BD Cytotfix Cytoperm	BS Bioscience	Heidelberg Germany
BD FACS Flow Sheat Fluid	BD Bioscience	Heidelberg Germany
BD FACSRinse Solution	BD Bioscience	Heidelberg Germany
BD Pharmingen 10x Lysis Buffer	BD Bioscience	Heidelberg Germany
BD Shutdown Solution	BD Bioscience	Heidelberg Germany
Biocoll separating solution 1.077 g/ml	Merck	Berlin Germany
CASYton	Omni life science Bremen	Bremen Germany
Cell culture medium RPMI 1640	Thermo Fisher scientific	Darmstadt Germany
Cell proliferation Dye eFlour 405	Thermo Fisher Scientific	Darmstadt Germany

Cholera toxin subunit-B Alexa Fluor 488	Thermo Fisher Scientific	Darmstadt Germany
Collagen V	Sigma-Aldrich	Taufkirchen Germany
DAPI	BioLegend	Fell Germany
DihydroRhodamin 123	Thermo Fisher Scientific	Darmstadt Germany
eBioscience Fixable Viability Dye eFluor780	Thermo Fisher Scientific	Darmstadt Germany
Fluoromount G	Thermo Fisher Scientific	Darmstadt Germany
L-Arginin	Sigma-Aldrich	Taufkirchen Germany
L-Lysin	Sigma-Aldrich	Taufkirchen Germany
Penicillin/Streptomycin	Thermo Fisher Scientific	Darmstadt Germany
PhosphoSTOP	Sigma-Aldrich	Taufkirchen Germany
Poly(vinyl alcohol)	Sigma-Aldrich	Taufkirchen Germany
Protease inhibitor I	Merck Millipore	Darmstadt Germany
Protease inhibitor III	Merck Millipore	Darmstadt Germany
SILAC RPMI 1640	Thermo Fisher scientific	Darmstadt Germany
TEMED	Bio-Rad	München Germany
Transferrin Alexa Fluor 488	Thermo Fisher Scientific	Darmstadt Germany

2.4 READY TO USE REACTION SYSTEMS

Table 5: Kits used in this work.

Kit	manufacturer	location
10x PermWash buffer	BD Bioscience	Heidelberg Germany
Annexin V:PE Apoptosis Detection Kit	BD Bioscience	Heidelberg Germany
ApoStat Intracellular Caspase Detection Kit (FITC-VAD-FMK)	BioTechne	Wiesbaden Germany
BD Cytotfix/Cytoperm	BD Bioscience	Heidelberg Germany
Cholesterol assay kit (cell based)	abcam	Cambridge UK

Clarity Max Western ECL Substrate	Bio-Rad	München Germany
dNTP-Mix, 10mM each 1ml	Thermo Fisher Scientific	Darmstadt Germany
IL8/CXCL8 DuoSet ELISA	BioTechne	Wiesbaden Germany
Luna® Universal qPCR Master Mix	New England Biolabs	Frankfurt Germany
MACS Buffer	Miltenyi	Bergisch Gladbach Germany
Pierce NE-PER Nuclear and Cytoplasmic Extraction Reagent	Thermo Fisher Scientific	Darmstadt Germany
RNeasy ® Mini Kit	Qiagen	Hilden Germany
RT ² First Strand Kit	Qiagen	Hilden Germany
RT ² Profiler PCR Array: human cellular stress response (PAHS-019ZC-6)	Qiagen	Hilden Germany
RT ² SYBR® Green Mastermix	Qiagen	Hilden Germany
SignalBoost™ Immunoreaction Enhancer Kit	Merck Millipore	Darmstadt Germany
SuperScript II RT	Thermo Fisher Scientific	Darmstadt Germany
Fluo Calcium Indicators Fluo-4AM	Thermo Fisher Scientific	Darmstadt Germany

2.5 PRIMERS

Table 6: Primers used in this work.

Primer	Sequence (5' - 3')	
hu_CCT3	forward	GCACAGAACCAGCAGAGTCTC
	reverse	ATCATCGGAAGCAAACCTAAATGGA
Hu_β2-microglobulin	forward	GCTGTGCTCGCGCTACTCTC
	reverse	GCGGCATCTTCAAACCTCCAT
hu_AHR	forward	GAAGCCGGTGCAGAAAACAG
	reverse	TCCTGGCCTCCGTTTCTTTC
hu_FMO1	forward	ACCTGTTCTCTATGCTCCTAACG

	reverse	CCTTGAATGTTCCGGTCCCCT
hu_LOX1	forward	GACTGGATCTGGCATGGAGAAA
	reverse	AGTGGGGCATCAAAGGAGAAC
hu_FMO4	forward	CACTGTGTGCAGCATAACGAAG
	reverse	CAGGAAAGGCTTCCAAAGGTAAAT
hu_CYP2F1	forward	CTTTCTGTACCTCACCGCCA
	reverse	CCAAGACCTGAGCTGAGTGG
hu_CYP1A1	forward	AAGCGGAAGTGTATCGGTGAG
	reverse	GTTGCAGCAGGATAGCCAGG
hu_CLU	forward	CTTCTTTCCCAAGTCCCGCA
	reverse	CCTGCTGAGCCTCGTGTATC
hu_HOPX	forward	GTACAACTTCAACAAGGTGACAA
	reverse	CATTTCTGGGTCTCCTCCTCG
hu_CYP2D6	forward	GAACGACTCATCACCAACCT
	reverse	GCTTCACAAAGTGGCCCTG
hu_HSPB1	forward	ATAGCCGCCTCTTCGACCA
	reverse	GCCTAACCACTGCGACCA
hu_CYP7A1	forward	CCGATGGATGGAAATACCACTGA
	reverse	AGGCAGCGGTCTTTGAGTTAG
hu_FMO5	forward	CCAGGGAGGATGACATTGATGC
	reverse	CAAGAGTTGGCCTTTCCAGGT
hu_CCT3	forward	GCACAGAACCAGCAGAGTCTC
	reverse	ATCATCGGAAGCAAATAAATGGA
hu_AHRnew	forward	GAAGCCGGTGCAGAAAACAG
	reverse	TCCTGGCCTCCGTTTCTTTC
hu_FMO1	forward	ACCTGTTCTCTATGCTCCTAACG
	reverse	CCTTGAATGTTCCGGTCCCAC8T

hu_LOX1new	forward	GACTGGATCTGGCATGGAGAAA
	reverse	AGTGGGGCATCAAAGGAGAAC
hu_FMO4	forward	CACTGTGTGCAGCATAACGAAG
	reverse	CAGGAAAGGCTTCCAAAGGTAAAT
hu_CYP2F1	forward	CTTCTGTACCTCACCGCCA
	reverse	CCAAGACCTGAGCTGAGTGG
hu_CYP1A1	forward	AAGCGGAAGTGTATCGGTGAG
	reverse	GTTGCAGCAGGATAGCCAGG
hu_CLU	forward	CTTCTTTCCCAAGTCCCGCA
	reverse	CCTGCTGAGCCTCGTGTATC
hu_HOPXnew	forward	GTACAACTTCAACAAGGTGACAA
	reverse	CATTTCTGGGTCTCCTCCTCG
hu_CYP2D6	forward	GAACGACACTCATCACCAACCT
	reverse	GCTTCACAAAGTGGCCCTG
hu_HSPB1new	forward	ATAGCCGCCTCTTCGACCA
	reverse	GCCTAACCACTGCGACCA
hu_CYP7A1	forward	CCGATGGATGGAAATACCACTGA
	reverse	AGGCAGCGGTCTTTGAGTTAG
hu_FMO5	forward	CCAGGGAGGATGACATTGATGC
	reverse	CAAGAGTTGGCCTTTCCAGGT
hu_CXCL8	forward	GAGAGTGATTGAGAGTGGACCAC
	reverse	CACAACCCTCTGCACCCAGTTT

2.6 INHIBITORS

Table 7: Inhibitors used in this work.

inhibitor	concentration	function	company	CAS number
-----------	---------------	----------	---------	------------

3-Hydroxy-2-naphthoic acid (3HNA)	1 mM	XBP1 inhibitor	Sigma-Aldrich	92-70-6
Actinomycin D	1 μ M	Blocking transcription	Sigma-Aldrich	50-76-0
AZD 5069 (AZD)	10 μ M	Blocking CXCR2	AstraZeneca	878385-84-3
Chlorpromazine hydrochloride (CH)	10 μ M	Blocking clathrin mediated endocytosis via loss of clathrin and adaptor protein 2	Sigma-Aldrich	69-09-0
Cycloheximide	0.5 μ M	Blocking translation	Merck Millipore	
Cytochalasin D (CytD)	400 μ M	Actin polymerisation inhibitor	Cayman	22144-77-0
IL8 neutralizing antibody (mIgG1)	1 μ g/mL	IL8 neutralizing (clone 6217)	BioTechne	
Kinase Inhibiting RNase Attenuator 6 (Kira)	1 μ M	IRE α inhibitor	Cayman	1589527-65-0
LOX1 neutralizing antibody (mIgG1)	1 μ g/mL	LOX1 inhibitor (clone 331219)	BioTechne	128446-36-6
Methyl- β -cyclodextrin (M β CD)	100 mM	blocking caveolin dependent endocytosis via depletion of cholesterol from the membrane	Sigma-Aldrich	128446-36-6
mIgG1 LEAF	1 μ g/mL	Isotype control for IL8 and LOX1 neutralizing antibody(clone MOPC-21)	BioLegend	

N-acetyl-L-cysteine NAC	1 mM	ROS and ER stress inhibitor	Cayman	616-91-1
Ursolic Acid (UA)	10 μ M	PERK inhibitor	Cayman	77-52-1

2.7 ANTIBODIES

2.7.1 ANTIBODIES FOR FLOW CYTOMETRY

Table 8: Specific antibodies used in flow cytometry.

antigen	isotype	fluorochrome	clone	concentration [μ g/mL]	company
CD10	mIgG1	APC	HI10a	10	BioLegend
CD11b	mIgG1	APC-Cy7	ICRF44	1	BD Bioscience
CD11b	mIgG1	V450	ICRF44	1	BD Bioscience
CD16	mIgG1	PE-Cy7	3G8	0.05	BD Bioscience
CD181	mIgG2b	BV510	5A12	4	BD Bioscience
CD182	mIgG1	PerCP eFluor 710	5E8-C7-F10	1	eBioscience
CD274	mIgG1	PerCP eFluor 710	MIH1	4	eBioscience
CD35	mIgG1	PE	E11	0.08	BioLegend
CD4	mIgG1	FITC	RPA-T4	1:50	BD Bioscience
CD45	mIgG2a	VioGreen	5B1	0.5	Miltenyi
CD54	mIgG1	APC	HA58	2	eBioscience
CD62L	mIgG1	V450	DREG-56	2.5	BD Bioscience
CD64	mIgG1	BV421	10.1	2	BioLegend
CD66b	mIgG1	FITC	80H3	1	Beckmann coulter
CD8	mIgG1	V500	RPA-T8	1:50	BD Bioscience
CD95	mIgG1	APC	DX2	2	BioLegend
LOX1	mIgG2a	APC	15C4	0.5	BioLegend

LOX1	mIgG1	APC	REA1188	1	Miltenyi
LOX1	mIgG2a	PE	15C4	0.5	BioLegend

Table 9: Isotype and secondary antibodies used for flow cytometry.

antibody	fluorochrome	clone	company
mIgG1	V450	MOPC-21	BD Bioscience
mIgG1	PE-Cy7	MOPC-21	BioLegend
mIgG1	APC-Cy7	MOPC-21	BD Bioscience
mIgG1	BV421	MOPC-21	BioLegend
mIgG1	PE	MOPC-21	BD Bioscience
mIgG1	PerCP eFluor 710	MOPC-21	eBioscience
mIgG1	APC	MOPC-21	BioLegend
mIgG1	APC	REA293	Miltenyi
mIgG2a	APC	G155-178	BioLegend
mIgG2a	PE	MOPC-173	BioLegend
mIgG2b	BV510	27-35	BD Bioscience
Gt α m	PE		Beckman coulter
dk α r	Alexa 488		Dianova

2.7.2 ANTIBODIES FOR IMMUNOFLUORESCENCE

Table 10: Antibodies used for immunocytochemistry.

antigen	isotype	clone	concentration [μ g/mL]	company
LAMP1	mIgG1	H4A3	1	abcam
NFkB	mIgG2b	L8F6	0.5	cell signaling
Rab5	rbIgG	C8B1	0.23	cell signaling
RAB7	rbIgG	D95F2	0.5	cell signaling
Donkey α mouse Alexa Fluor 647	IgG (H+L)		10	Thermofisher Scientific

Donkey α rabbit Alexa Fluor 488	IgG (H+L)	5	Thermofisher Scientific
---	-----------	---	-------------------------

2.7.3 ANTIBODIES FOR WESTERN BLOT

Table 11: Antibodies used for Western Blot.

antigen	isotype	clone	concentration [$\mu\text{g/mL}$]	company
AHR	rbIgG	EPR7119(N)(2)	1:1000	cell signaling
Anti-Mouse IgG	hoIgG HRP-linked		1:2500	cell signaling
Anti-rabbit IgG	gtIgG HRP-linked		1:2500	cell signaling
BiP	rbIgG	C50B12	1:1000	cell signaling
Ero1L α	rbIgG		0.0214	cell signaling
PDI	rbIgG	C81H6	0.113	cell signaling
Vinculin	rbIgG		1:1000	cell signaling
XBP1s	rbIgG	D2C1F	1:1000	cell signaling

2.7.4 ANTIBODIES FOR AUNP COUPLING

Table 12: Antibodies used for coupling of AuNP.

antigen	isotype	clone	company
CD3	mIgG2a	OKT-3	BioXcell
	mIgG2a	Cl.18.4	BioXcell
CD11b	rIgG2a	M1/70	BioXcell
	rIgG2a	LTF-2	BioXcell

2.7.5 ANTIBODIES FOR THE IDENTIFICATION OF PMN, T CELLS AND MONOCYTES

Table 13: Antibodies used for phenotypic identification of PMN, T cells and monocytes.

antigen	isotype	fluorochrome	clone	company
CD14	mIgG2a	PE-Cy7	M5E2	BD Bioscience

CD3	mIgG1	BV421	UCHT1	BD Bioscience
CD66b	mIgG1	FITC	80H3	Beckmann coulter

2.8 BUFFERS, SOLUTIONS AND MEDIA

Table 14: Buffers used in this work.

Buffer	Recipe
10x phosphate buffer saline, PBS	150 mM sodium chloride 2.7 mM potassium chloride 8.1 mM sodium dihydrogen phosphate 1.5 mM potassium dihydrogen phosphate pH 7.3
10x Tris buffered saline, TBS	20 mM Tris 1.5 M sodium chloride pH 7.2-7.4
5x SDS sample buffer	50 mM Tris-HCl pH 6.8, 2% SDS) 10% glycerol 1% β -mercaptoethanol 12.5 mM EDTA 0.02 % bromophenol blue
Arginin-low medium	SILAC RPMI 1640 100 mM L-Lysin 100 mM Arginin
blocking buffer (R&D ELISA)	1 % BSA 0.2 M Saccharose 7.7 mM Sodium azide 1x PBS
Cell culture medium	RPMI 1640 10 % fetal calf serum 1 % Penicillin/Streptomycin
ELISA washing buffer	0.05 % Tween 20 in PBS

IL8 Reagent Diluent (R&D ELISA)	1 % BSA in PBS pH 7.3 0.05 % Tween 20
Laemmli running buffer	1918.2 mM Glycine 34.7 mM SDS 247.1 mM Tris
Reagent Diluent (R&D ELISA)	1 % BSA in PBS pH 7.3
RIPA lysis buffer	150 mM sodium chloride 5 mM EDTA 50 mM Tris-buffer 1 % NP-40 0.5 % sodium deoxycholate 0.1 % SDS
SDS lysis buffer 25 mM Hepes (pH 7.3 PAN Biotech)	0.1 % [w/v] SDS 1 % [v/v] Triton X-100 10 mM EDTA 10 mM Sodium pyrophosphate 10 mM Sodium fluoride 125 mM Sodium chloride
TMB Substrate Buffer 32.8mM citric acid (Merck Chemicals)	0.02 % [v/v] Kathon pH 4.1
Zymography buffer	50 mM Tris pH 7.5 200 mM sodium chloride 5 mM calcium chloride 1% Triton-X-100

2.9 SOFTWARE

Table 15: Software used in this work.

software	company	location
Adobe Illustrator 2020	Adobe System GmbH	München Germany

BD FACSDiva 8 and 10	BD Bioscience	Heidelberg Germany
Fiji ImageJ 1.52i	Wayne Rasband, National Institute of Health	Bethesda USA
FlowJo 10	BD Bioscience	New Jersey USA
Gen5	Fisher scientific	Schwerte Germany
GraphPad Prism V 7+8	GraphPad Software, Inc.	La Jolla USA
LightCycler 3	Roche Applied Science	Wiesbaden Germany
Microsoft Office 2010	Microsoft GmbH	Unterschleißheim Germany
Optris Pix connect	Optris	Berlin Germany
Stepone Software V2.3	Thermo Fisher Scientific	Darmstadt Germany
ZEN (black, blue edition)	Zeiss	Jena Germany

3 METHODS

3.1 PRIMARY CELL ISOLATION

3.1.1 ISOLATION OF HUMAN PMN

Human PMN were isolated from healthy donor blood using density gradient centrifugation. Due to their granularity PMN can be separated from mononuclear cells in a gradient with a 1.077 g / mL polysucrose solution. Blood should be proceeded within one hour after donation and all steps are performed at room temperature unless indicated otherwise. Venous blood was taken in 10 mL 9NC blood collection tubes containing 3.2 % trisodium citrate solution (S-Monovette®) and diluted 1:1 with PBS. Afterwards, the diluted blood was carefully pipetted on 15 mL separation solution and centrifuged at 300 g for 30 min with minimal acceleration and without break. Mononuclear cells were removed and the pellet containing PMN and erythrocytes was collected. Next, erythrocytes were sedimented by addition of the same volume of freshly filtered 1 % polyvinyl alcohol for 30 min. The PMN-containing upper phase was collected and pelleted by centrifugation for 5 min at 300 g. Remaining erythrocytes were removed by hypotonic lysis in 0.2 % NaCl for 60 seconds with subsequent readjustment of osmolarity. Cells were counted and adjusted to a 1×10^6 cells / mL concentration in filtered RPMI Medium 1640 supplemented with 10% autologous Serum (10% AS Medium, described in 3.1.3). Before performing the subsequent experiments, cells were rested in the incubator for 1 h at 37 °C and 5 % CO₂.

3.1.2 ISOLATION OF HUMAN T CELLS

Peripheral blood mononuclear cells (PBMC) were isolated from healthy donors by density gradient centrifugation as described above. After washing with PBS for three times, T cells were isolated using magnetically labelled anti- (α) CD3 MicroBeads from Miltenyi Biotec according to manufacturer's instructions.

3.1.3 MEDIUM PREPARATION WITH AUTOLOGOUS SERUM

Venous Blood was taken in a 7.5 mL blood collection tube S-Monovette® and rested for 30 min to allow the cruor to build. Afterwards, the tube was centrifuged at 2000 g for 10 min to separate the serum from the cellular component. The serum was harvested and added to RPMI Medium 1640 1:10 (e.g. 3 mL serum + 27 mL RPMI), followed by filtering through a 0.2 μ m filter to exclude cells that have been remained.

3.2 AUNR TREATMENT

The synthesis of the AuNR is based on a modified seeded growth method (Jia *et al.* 2015). AuNR were coated with 3.5 kDa polyethylene glycol and size, charge, monodispersity were characterized. The concentration of AuNR colloids was determined using UV / Vis absorption spectroscopy as described before (Hendel *et al.* 2014). Synthesis and characterization were performed by our cooperation partner (AG Schlücker, Department of Chemistry University Duisburg-Essen). AuNR (OD ~1) were used in a 1:10 dilution corresponding to 5000 AuNR / cell in isolated PMN experiments. Due to a higher concentration of PMN in whole blood, we used AuNR 1:5 corresponding 5000 AuNR / PMN. Inductively coupled plasma-mass spectrometry (ICP-MS, performed by AG Schlücker) revealed a concentration of 0.04875 $\mu\text{g Au} / \text{mL} \pm 15.7\%$ (0.078 nM or 0.04875 pg / cell) for isolated PMN experiments and a final concentration of 0.0929 $\mu\text{g Au} / \text{mL} \pm 15.7\%$ (0.149 nM AuNR or a maximum concentration of 0.04875 pg / PMN) for whole blood experiments. For Photothermal therapy a higher concentration of AuNR was necessary. Here, AuNR (OD ~1) were diluted 1:5, corresponding 10 000 AuNR / cell equalling 0.0975 $\mu\text{g Au} / \text{mL} \pm 15.7\%$ (0.156 nM or 0.0975 pg / cell). Since AuNR were added in an aqueous solution and a dilution of culture medium by water could affect the activation status of immune cells, we performed all experiments with an unstimulating water control (water), meaning we added the same volume water as AuNR to isolated cells or whole blood.

3.3 SAMPLE PREPARATION FOR MICROSCOPY

3.3.1 TRANSMISSION ELECTRON MICROSCOPY – UPTAKE OF AUNR

PMN were isolated as described in 3.1.1. 3×10^6 cells / 3 mL were incubated with 5000 AuNR / PMN in protein low-binding reaction tubes for 1 h at 37°C in rotation. Subsequently, cells were washed with PBS and fixed in 2.5 % glutaraldehyde and 4 % formaldehyde in 1x PHEM buffer (60 mM PIPES, 25 mM HEPES, 10 mM EGTA, and 4 mM $\text{MgSO}_4 \cdot 7\text{H}_2\text{O}$ provided by electron microscopy unit) for 1 h. Afterwards, the samples were embedded in EPON, sliced in ~ 55 nm slices and imaged by the electron microscopy unit of the Imaging Center Essen (IMCES).

3.3.2 CONFOCAL MICROSCOPY - UPTAKE OF AUNR-RITC

Isolated PMN were treated with 5000 AuNR-RITC / PMN over 5, 15, 30, 60, 120 or 240 min at 37 °C in protein low-binding reaction tubes in rotation. Afterwards, samples were washed with PBS, resuspended in fetal calf serum and cytopins onto 24 x 48mm thick coverslips were prepared. Cells were fixed using BD Cytofix/Cytoperm and a nuclear counter staining with DAPI was performed. Cover slips were mounted on slides with Fluoromount G and images were done using

a Laser Scanning Microscope (LSM). LSM are suitable for high resolution imaging of biological or material samples in 3D. In contrast to wide field microscopy, the specimen is illuminated in a raster-fashion with a focused laser beam. The optical arrangement prevents light from out-of-focus regions of the specimen contributing to the image formation. Confocal microscopy was performed using a 63x magnification oil objective and ZEISS Elyra PS.1 LSM710 with ZEN system 2012 black edition of the imaging center Essen (IMCES). Single cell fluorescence intensity of AuNR within PMN was analyzed using Fiji ImageJ 1.53c. For each time point and blood donor (n = 6) 100 cells were analyzed. Afterwards, the median of these 100 cells was determined.

3.3.3 CONFOCAL MICROSCOPY - UPTAKE OF AUNR-RITC AND *E. COLI*

Isolated PMN were treated with 5000 AuNR-RITC / PMN, or *E. coli* (50:1 *E. coli*: PMN) for 30 min, as well as AuNR in combination with *E. coli* for 30 min (AuNR + *E. coli*), or AuNR for 30 min, followed by *E. coli* treatment (AuNR - *E. coli*) at 37 °C in protein low-binding reaction tubes in rotation. Afterwards, samples were washed with PBS, resuspended in fetal calf serum and cytopins onto 24 x 48mm thick coverslips were prepared. Cells were fixed using BD Cytotfix/Cytoperm and a nuclear counter staining with DAPI was performed. Cover slips were mounted on slides with Fluoromount G and images were done using a LSM. Confocal microscopy was performed using a 63x magnification oil objective and ZEISS Elyra PS.1 LSM710 with ZEN system 2012 black edition of the imaging center Essen (IMCES). Single cell fluorescence intensity of AuNR within PMN was analyzed using Fiji ImageJ 1.53c. For each time point and blood donor (n = 4) 100 cells were analyzed. Afterwards, the median of these 100 cells was determined.

3.3.4 CONFOCAL MICROSCOPY - UPTAKE OF ANTIBODY-COATED AUNR BY IMMUNE CELLS

PMN and PBMC were isolated from healthy blood donors as described in 3.1.1. PMN and PBMC were mixed in a 1:1 ratio and treated with 5000 fluorescently labelled AuNR with additional antibody coating (α mIgG2a-, α CD-3-, α rIgG2a-, or α CD11b-AuNR) for 30 min at 37 °C in protein low-binding reaction tubes in rotation. Cytospins and images were made as described in 3.3.2.

3.3.5 STRUCTURED ILLUMINATION MICROSCOPY

PMN were isolated from healthy blood donors as described in 3.1.1. Isolated PMN were treated with 5000 AuNR-RITC / PMN for 5, 15 and 30 min at 37 °C in protein low-binding reaction tubes in rotation, to investigate the intracellular transport of AuNR. For later time points, PMN were incubated for 30 min with AuNR, followed by a washing step with PBS to remove excess nanoparticles. Afterwards, PMN were cultured for additional 1 h, 2 h and 4 h. After the indicated

time points, cells were fixed with BD Cytofix/Cytoperm. Early endosomes in combination with lysosomes, as well as late endosomes were stained in PermWash (antibodies are listed in Table 10). Nuclear counter staining with DAPI and cytopins were performed as described above. Structured illumination microscopy was conducted using a 63x magnification oil objective and ZEISS Elyra PS.1 Super resolution Pal-M/STORM; SIM with ZEN system 2012 black edition of the IMCES. Co-localization of AuNR-RITC with endosomes and lysosomes was analyzed using Fiji ImageJ 1.53c. Light microscope resolution is restricted by the diffraction of light at the object level that creates a diffraction barrier at a maximum resolution of ~200 nm in the lateral (x,y) and 500 nm in the axial (z) dimension. To overcome this diffraction limitations, structured illumination microscopy (SIM) uses the Moiré-effect, where detected images are interpreted as overlay of a known excitation pattern (grating phase) and an unknown object frequency. In the instrument the laser beam is polarized and a phase grating is applied to generate a structured illumination which superimposes on the specimen while capturing the image. The grid pattern is shifted or rotated in steps between the capture of each image set. Following processing with a specialized algorithm, high-frequency information can be extracted from the raw data to produce a reconstructed image having a lateral resolution approximately twice that of diffraction-limited instruments and an axial resolution ranging between 150 and 300 nanometers. All images were captured with the same settings, generating 16-Bit, 17 images per stack, 70.58nm x 70.58nm x 318.4 nm per pixel and 956 x 956 pixel per image. Stacks of AuNR-treated PMN stained for different endosomal markers were loaded into Image J. The channels were split and the background subtracted with a rolling ball radius of 50. Channels of endosomal markers (green and red) were converted into a binary picture using “Moments” with default setting. The AuNR channel was transformed to an 8-bit image. To evaluate the co-localized areas of AuNR and endosomal markers, the “AND” function of the image calculator was used. The mean integrated density (sum of the values of the pixels in the image or selection) of five pictures per treatment and staining was analyzed. The distribution was analyzed by summarizing all co-localized areas and calculating the percentage for AuNR co-localized with Rab5⁺, Rab7⁺ or LAMP1⁺ vesicles. Exemplary images were generated by using only 1 image of a stack and cropping this to the area of interest, an AuNR-positive cell. To visualize the co-localization of AuNR with endosomes and lysosomes, the profile tool of ZEN blue was used to draw a histogram of a line through that image.

3.3.6 FLUORESCENCE MICROSCOPY

3.3.6.1 Cholesterol Depletion by Methyl- β -cyclodextrin (M β CD)

M β CD forms aggregates with cholesterol, separating cholesterol from membranes. This blocks cholesterol dependent uptake pathways as caveolin-dependent endocytosis and lipid raft internalization but also clathrin-dependent endocytosis (Kuhn *et al.* 2014). To evaluate M β CD ability to remove cholesterol from the membrane, we performed a filipinIII staining (cholesterol assay kit). PMN were isolated from healthy blood donors as described in 3.1.1. Isolated PMN were incubated in protein low-binding 1.5 mL reaction tubes with 10, 50 or 100 mM M β CD for 30 min at 37 °C. Subsequently, PMN were fixed with fixative solution of the kit for 10 min and washed three times with 100 μ L of the cholesterol detection wash buffer. FilipinIII was added 1:100 and stained for 45 min at room temperature. PMN were washed twice with cholesterol detection wash buffer and cytopspins were performed as described in 3.3.2. Fluorescence images were taken with using a 40x magnification objective and the AxioObserver.Z1 (ZEISS) of the IMCES, followed by a single cell analysis using Fiji ImageJ 1.53c.

3.3.6.2 Translocation of NF κ B

PMN were isolated from healthy blood donors as described in 3.1.1 and treated with water or 5000 AuNR / PMN for 30 min, 1 h, 2h, 3h, or 5 h. Subsequently, PMN were washed with PBS and cytopspins were performed as described in 3.3.2. PMN were fixed with Cytofix/Cytoperm and stained for NF κ B over night at 4 °C. Secondary antibody staining in combination with a counterstaining for nuclei using DAPI was performed on the next day for 30 min (antibodies are listed in Table 10). Fluorescence images were taken with using a 40x magnification objective and the AxioObserver.Z1 (ZEISS) of the IMCES, followed by a single cell analysis using Fiji ImageJ 1.53c.

3.4 MOLECULAR BIOLOGY

3.4.1 RNA ISOLATION

PMN were isolated as described in 3.1.1. 4×10^6 PMN per sample were added to a 6 well plate. After 1 h resting under culture conditions, cells were treated with water or 5000 AuNR / PMN over 5, 15 or 60 min followed by 3 times washing with 1 mL PBS on ice. Then, RNA was isolated using the RNeasy Mini Kit (Table 5). First, cells were disrupted with 350 μ L RLT buffer supplemented with 35 μ L β -mercaptoethanol. Subsequently, the lysate was pipetted in a QiaShredder and centrifuged for 2 min at 14 000 g. To homogenize the lysate, 350 μ L of 70% ethanol were added to the flow through, followed by a transfer onto RNeasy spin column and another centrifugation

for a minute at 8000 g. The flow through was discarded and the membrane was washed with 350 μ L RW1 and centrifuged for a minute at 8 000 g. The DNA was digested with DNase, for which 10 μ L DNase were mixed with 70 μ L RDD buffer. Then 80 μ L of DNase mixture was added to the membrane of the spin column and incubated for 15 min at room temperature. Afterwards, the membrane was washed again with RW1, followed by 500 μ L RPE and centrifugation for 1 min. Subsequently, 500 μ L RPE were added and centrifuged for 2 min at 8 000 g. Then, the spin column was placed on a fresh collection tube and centrifuged for another minute at 14 000 g, to ensure that the membrane was completely dry. Afterwards, the RNEasy spin column was placed in a 1.5 mL collection tube and 30 μ L RNase free water was added and centrifuged for 1 min at 8 000 g to elute the RNA. This step was repeated with the flow-through to increase the RNA concentration. PCR was performed immediately, since RNA isolated from PMN is not stable.

3.4.2 PCR AND REAL-TIME QPCR

For reverse transcription, 10 μ L RNA was added into a nuclease-free microcentrifuge tube, together with 50 ng / μ L random primer and 5 mM dNTP Mix. This mixture was incubated for 5 min at 65 °C and cooled on ice immediately after. Then, 4 μ L of 5x First Strand and 2 μ L of 0.1 M DTT were added and incubated for 2 min at 25°C. Finally, 1 μ L of 200 U / μ L SuperScript™ II Reverse Transcriptase was added and incubated for 10 min at 25 °C, 50 min on 42 °C and 15 min on 70 °C. Resulting cDNA was frozen at -20 °C until further qPCR. cDNA was transcribed using Luna® Universal qPCR Master Mix (Table 5) and StepOnePlus Real-Time PCR System and Stepone Software V2.3 software. Afterwards, all bubbles were removed by carefully tapping the plate on the desk, after the plate was sealed, it was placed into the StepOne plate holder. qPCR started with a first cycle of 10 min, 95 °C to activate the *Taq* polymerase followed by 40 cycles with 15 seconds at 95 °C and 1 min at 60 °C to perform the fluorescence data collection. AuNR induced transcription of genes was normalized to housekeeping to house-keeping gene (β 2-microglobulin) and water. The sequence for each primer is listed in Table 6.

3.4.3 DATA ANALYSIS OF QPCR

Differential expression was analyzed by the $2^{-\Delta\Delta C_T}$ method (Livak *et al.* 2001). Expression was normalized to the internal standard, β 2-microglobulin, and the difference between water and AuNR treatment was assessed over all analyzed time points using the equation shown in this section. Due to the exponential relation of the DNA amount to the respective cycle, the normalized difference of mRNA which was present in the original samples is described logarithmically. The resulting value represents the fold difference in expression in the analyzed samples.

$$\Delta C_T = \Delta C_T(\text{target}) - \Delta C_T(\text{internalstandard})$$

$$\Delta\Delta C_T = \Delta C_T(\text{sample}) - \Delta C_T(\text{negativecontrol})$$

$$\text{relative expression} = 2^{-\Delta\Delta C_T}$$

3.4.4 HUMAN CELLULAR STRESS RESPONSE ARRAY

PMN were isolated as described in 3.1.1. 4×10^6 PMN per sample were added to a 6 well plate. After 1 h resting under culture conditions, cells were treated with water or 5000 AuNR / PMN over 5, 15 or 60 min followed by 3 times washing with 1 mL PBS on ice. Then, RNA was isolated using the RNeasy Mini Kit, described in 3.4.1. RNA concentration was measured using a plate reader (Synergy 2). 50 ng total RNA of four donors per sample was pooled to get 200 ng RNA for reverse transcription using RT2 First Strand Kit (Table 5). cDNA synthesis reaction was mixed with RT² SYBR[®] Green Mastermix and 25 μ L / well of the resulting PCR components mix was added to the RT² Profiler PCR array (PAHS-019ZA) using an 8-channel pipette. Afterwards, all bubbles were removed by carefully tapping the plate on the desk, after the plate was sealed, it was placed into the StepOne plate holder. qPCR started with a first cycle of 10 min, 95 °C to activate the *Taq* polymerase followed by 40 cycles with 15 seconds at 95 °C and 1 min at 60 °C to perform the fluorescence data collection. AuNR induced transcription of genes was normalized to housekeeping genes provided by the array and to unstimulated water control. The resulting value represents the fold difference in expression in the analyzed samples (equation is shown in 3.4.3). Clustering and heat maps were generated using Graphpad Prism.

3.5 PROTEIN BIOCHEMISTRY

3.5.1 SAMPLE PREPARATION FOR WESTERN BLOT

PMN were isolated as described in 3.1.1. 2×10^6 PMN were pipetted into a 6 well plate and rested for 1 h under culture conditions. Cells were treated with water or 5000 AuNR / PMN for 5, 15, 30 or 60 min. After the indicated time points, cells were harvested and washed three times with cold PBS. After the last washing step, the supernatant was discarded and the samples were resuspended in 100 μ L RIPA Lysis buffer or SDS Lysis buffer (recipe in Table 14) supplemented 1:10 with phosphostop and 1:25 with Protease Inhibitor I and III and mixed vigorously for 15 seconds. Lysis buffer were incubated for 30 min, with 15 seconds mix every ten minutes (RIPA), or 5 min (SDS). Afterwards, samples were centrifuged for 10 min 4 °C 14 000 g. The supernatant was harvested

and incubated with 5x SDS sample buffer (recipe in Table 14) cooking for 10 min at 95 °C and frozen (-20 °C) until further usage.

3.5.2 SAMPLE PREPARATION FOR FRACTIONATED WESTERN BLOT

To measure translocation of transcription factors from cytoplasm to nucleus, fractionated samples for western blot were produced using the Pierce NE-PER Nuclear and Cytoplasmic Extraction Reagent. PMN were isolated as described in 3.1.1. 3×10^6 PMN were pipetted into a 6 well plate and rested for 1 h under culture conditions. PMN were treated with water or 5000 AuNR / PMN for 5, 15, 30 or 60 min. After the indicated time points, cells were harvested and washed three times with cold PBS to stop any further translocation. After the last washing step, the supernatant was discarded and the samples were resuspended in 100 μ L ice-cold CER I supplemented 1:10 with phosphostop and 1:25 with Protease Inhibitor I and III. After vigorous mixing for 15 seconds, samples were incubated on ice for 10 min. In the following, 5.5 μ L CER II was added per sample and mixed for another 5 seconds, followed by another minute incubation on ice and another five seconds of mixing. To extract the cytoplasmic protein content, the samples were centrifuged for 5 min at 4 °C and 14 000 g and the supernatant was transferred to pre-chilled 1.5 mL reaction tubes. To extract the nuclear protein content, the remaining pellet was resuspended in 50 μ L NER supplemented 1:10 with phosphostop and 1:25 with Protease Inhibitor I and III and mixed vigorously for 15''. NER was incubated for 40 min with a 15 second mix every 10 min. Afterwards, samples were centrifuged for 10 min at 4 °C and 14000 g. The nuclear extract was harvested and both, the cytoplasmic and the nuclear extract were incubated with 5x SDS sample buffer and cooked for 10 min at 95 °C and frozen for further usage.

3.5.3 WESTERN BLOT

Further analysis was performed by 10 % Sodium Dodecyl Sulfate-Polyacrylamide Gel Electrophoresis (SDS-PAGE), followed by a transfer to a PVDF membranes. Incubation with primary antibodies was performed over night at 4 °C, secondary antibody incubation for 1 h at room temperature. Antibodies were diluted using the SignalBoost™ Immunoreaction Enhancer Kit. Chemiluminescent detection was performed with an Amersham imager 600. Used antibodies are listed in Table 11. Expression levels were analyzed using Fiji ImageJ 1.53c and normalized to GAPDH (normal Western Blot) or Vinculin (Fractionated Western Blot).

3.6 Ca^{2+} IMAGING

PMN were isolated as described in 3.1.1. 0.2×10^6 PMN per sample were incubated with $4 \mu\text{M}$ Fluo-4AM for 20 min at 37°C . Fluo-4AM was removed and cells were treated with water or 5000 AuNR / PMN. Additionally a positive control for phagocytosis and activation, 10:1 (bacteria: PMN) *Escherichia coli* (*E.coli*), was analyzed. Fluorescence of cytosolic Ca^{2+} was measured every minute using Synergy 2 and Gen5 software. Fluorescence was normalized to water control.

3.7 ANALYSIS OF PMN SECRETION

3.7.1 LUMINEXASSAY

PMN were isolated as described in 3.1.1. 0.2×10^6 PMN were treated with water or 5000 AuNR / PMN for 2, 4, 8, or 24 h. Additionally, a positive control for PMN activation, 10 ng / mL LPS, was analyzed. Secretion of IL1 β , IL6, MIP1 β , TNF α , MIF or Gro α by PMN was determined by Luminexassay performed by Kirsten Bruderek.

3.7.2 ZYMOGRAPHY

PMN were isolated as described in 3.1.1. 0.2×10^6 PMN were treated with water or 5000 AuNR / PMN for 2, 4 or 8 h at 37°C . Additionally, a positive control for PMN activation, 10 ng / mL LPS, was analyzed. Supernatants were collected and incubated with Zymogram sample buffer at a final concentration of 80 mM Tris pH 6.8, 1 % sodium dodecylsulfate (SDS), 4% glycerol and 0.006% bromphenol blue. This technique allows the detection of hydrolytic enzymes, in this case the gelatinase MMP9, by addition of the substrate, gelatine, in the separation gel. Using 10 % Sodium Dodecyl Sulfate-Polyacrylamide Gel Electrophoresis (SDS-PAGE) containing 0.2 % gelatine, the proteins were separated. Samples were renatured in 2.5 % Triton-X-100 for 1 h at room temperature. In order to let the enzymatic reaction proceed, samples were incubated in zymography buffer (recipe in Table 14) for 16 h at 37°C . To visualize digested bands, the gel was stained with 0.5 % Coomassie blue, 30 % methanol and 10 % acetic acid for 2 h at room temperature, followed by multiple destaining steps in a solution containing methanol and 10 % acetic acid. Gels were scanned and area of digested bands was analyzed using Fiji ImageJ 1.53c.

3.7.3 ELISA FROM WHOLE BLOOD SAMPLES

3.8 % sodium citrate anticoagulated blood of healthy donors was always used freshly. All experiments were performed in protein low-binding 1.5 mL reaction tubes. Whole blood was treated with water or 5000 AuNR / PMN over as indicated in 3.3. Afterwards, blood plasma was

isolated via centrifugation for 10 min at 9 000 rpm and IL8 ELISA was performed according to manufacturers' instructions.

3.8 FLOW CYTOMETRY

Flow cytometry can be used to detect, measure and analyze physical and chemical characteristics of cells or particles. In general, a cell suspension is led through a fluidic system to create a single cell suspension. The focused sample is then led through a laser beam. In line (forward scatter, FSC) and vertical (side scatter, SSC) with the laser stream detectors provide information on cell size and volume as well as the cells granularity and inner complexity. Furthermore, flow cytometry offers the opportunity to measure fluorescence via special filters and detectors. Measurements were carried out on a BD FACSCanto II machine with 3 fixed-wavelength lasers (488, 633 and 405 nm) providing detection on 8 photomultiplier tubes (PMT). All experiments were conducted using BD FACSDiva 8 and 10 and analyzed with FlowJo 10.

3.8.1 INHIBITION OF AUNR UPTAKE

To study the uptake mechanism of AuNR by PMN, inhibitors were chosen as described by Kuhn and colleagues (Kuhn *et al.* 2014). PMN were isolated as described in 3.1.1. 0.2×10^6 PMN per sample were pre-treated for 30 min at 37 °C, with 400 μ M Cytochalasin D (CytD), 10 μ M chlorpromazine hydrochloride (CH), or 100 mM methyl- β -cyclodextrin (M β CD), followed by incubation for additional 30 min with 5000 AuNR-RITC / PMN of different sizes (~ 20/ 50/ 100 nm) as described in 3.3. To evaluate the specificity of the inhibitors, pLVX-ZsGreen1 transformed TOP10 *E.coli* (50 x PMN concentration, CytD, generated by Kirsten Bruderek) and Alexa Flour 488 coupled human Transferrin (100 μ g / mL, CH), or Alexa Flour 488 coupled cholera toxin subunit-B (10 μ g / mL, M β CD) were used as positive controls. Afterwards, PMN were washed with PBS and resuspended in PBS supplemented with 3 % human serum. Uptake of positive controls or AuNR was measured by flow cytometry.

3.8.2 DETECTION OF APOPTOSIS

For the determination of apoptosis, cells were stained for the presence of phosphatidylserine on the cell surface by AnnexinV membrane binding, which resembles an early apoptotic phase, and for 7AAD incorporation, which is taking place upon membrane dysfunction by dead, necrotic and late apoptotic cells. PMN were isolated as described in 3.1.1. 0.2×10^6 PMN were treated with water or 5000 AuNR / PMN over for 2, 4 or 8, or 24 h at 37 °C. Additionally, a positive control for PMN activation, 10 ng / mL LPS, was analyzed. Treated cells were washed with PBS and resuspended

in 50 μL 1 x Annexin binding buffer (provided by the AnnexinV:PE Kit, BD) containing AnnexinV-PE and 7AAD in a 1:100 dilution each. Staining was carried out for 15 min at room temperature and was followed by addition of 200 μL PBS and a centrifugation at 460 g for 5 min. In order to analyze in flow cytometry, samples were resuspended in 200 μL PBS supplemented with 3 % humane serum. Surviving cells were identified by being AnnexinV and 7AAD double negative. To ensure the correct adjustment of gates, unstained cells were measured as a control. Annexin and 7AAD-positive PMN were detected by flow cytometry.

3.8.3 DETECTION OF CASPASE ACTIVATION

Cystein proteases with aspartate specificity (caspases) play a role in inflammatory and apoptotic processes, including heat shock. The activation of caspases leads to a signaling cascade, resulting in cell death. By using FITC-conjugated caspase inhibitors, intracellular caspase activity can be detected and measured in flow cytometry. In order to analyze the activation of caspases, PMN were isolated as described in 3.1.1. 0.2×10^6 PMN were treated with water or 5000 AuNR / PMN for 2, 4 or 6 h at 37 °C. Additionally, a positive control for PMN activation, 10 ng / mL LPS, was analyzed. 30 min prior to the end of incubation 0.5 μg / mL ApoStat Intracellular Caspase Detection Kit was added to the culture. To ensure the correct adjustment of gates, unstained cells were measured as a control. Caspase-positive PMN were detected by flow cytometry.

3.8.4 MIGRATION ASSAY

PMN were isolated as described in 3.1.1. 0.5×10^6 PMN per sample were treated with water or 5000 AuNR / PMN or 10 ng / ml LPS for 4 h at 37 °C. Afterwards, PMN were harvested, counted and seeded on 3 μm transwells in same concentrations. PMN were allowed to migrate towards medium (spontaneous migration) or tumor supernatant (directed migration) for 3 h, followed by washing with PBS and resuspension in PBS supplemented with 3 % human serum. Cell count was measured by the addition of 123counting beads and analyzed by flow cytometry. Migration index was calculated by normalization of directed to spontaneous migration.

3.8.5 TRANSENDOTHELIAL MIGRATION ASSAY (TEM)

3 μm transwells were coated with 2.5 μg / cm^2 collagen V for 2 h at 37 °C. Afterwards, transwells were washed with PBS and dried at room temperature. The immortalized microvascular endothelial cell line cdc.HMEC-1 was seeded in transwells and allowed to build a monolayer for 2 days at 37 °C. For transendothelial migration, culture medium was removed, transwells were washed and used as for migration towards supernatant as described in 3.8.4.

3.8.6 WHOLE BLOOD AUNR TREATMENT

3.8 % sodium citrate anticoagulated blood of healthy donors was always used freshly. All experiments were performed in protein low binding 1.5 mL reaction tubes. Whole blood was incubated as described in 3.3 at 37 °C in rotation over various time points indicated in figures and legends.

3.8.7 LOW-DENSITY NEUTROPHIL DETECTION

500 µL whole blood was treated with water or 5000 AuNR / PMN as described in 3.8.6 for 2 h. Afterwards, samples were diluted 1:1 with PBS and applied on 1 mL 1.077 g / mL polysucrose solution (Biocoll Separating Solution (Biochrom/Merck, Berlin, Germany)). PBMC fraction was isolated and washed 3 times with PBS. Subsequently PBMC were stained for CD45 and CD66b and the frequency of CD66b⁺ cells within the CD45 fraction was analyzed by flow cytometry.

3.8.8 INHIBITION OF PROTEIN TRANSCRIPTION OR TRANSLATION

Whole blood was pre-treated with 0.5 µM cycloheximide, or 1 µM actinomycin D followed by the treatment with water or 5000 AuNR / PMN as described in 3.8.6 for 2 h, 4 h, or 6 h. Surface staining was performed as described in 3.9.7 and LOX1 expression was analyzed in flow cytometry.

3.8.9 ENDOPLASMIC RETICULUM STRESS INHIBITION

Whole blood was pre-treated with inhibitors (see Table 7) for 30 min followed by the treatment with water or 5000 AuNR / PMN as described in 3.8.6 for 2 h. Afterwards, samples were divided for surface staining (see 3.8.12), ROS staining (see 3.8.10) and IL8 ELISA (see 3.7.3).

3.8.10 REACTIVE OXYGEN SPECIES (ROS)

ROS are highly reactive chemical molecules, formed by electron acceptability of O₂. They occur as a natural byproduct of the normal aerobic metabolism of oxygen and have important roles in cell signaling and homeostasis (Devasagayam *et al.* 2004). During times of environmental stress (e.g., UV or heat exposure), ROS levels can increase dramatically, inducing significant damage to cell structures (oxidative stress). Myeloid cells, including macrophages and PMN, are especially implicated in the respiratory burst (Herb *et al.* 2021). As they are phagocytic, the respiratory burst is vital for the subsequent degradation of internalized bacteria or other pathogens. This is an important aspect of the innate immunity. Respiratory burst requires a 10 to 20-fold increase in oxygen consumption through NADPH oxidase (NOX2 in humans) activity. The NOX2 enzyme is

bound in the phagolysosome membrane. Post bacterial phagocytosis, it is activated, producing superoxide via its redox center, which transfers electrons from cytosolic NADPH to O₂ in the phagosome (Leto *et al.* 2006). ROS can be detected using DihydroRhodamin 123. It penetrates the cells and is oxidized by ROS to Rhodamin which is not able to leave the cell again, but can be detected by its fluorescence (ex/em 508/529 nm). Whole blood samples were prepared as described in 3.8.6 or 3.8.9. Afterwards, 50 µL of whole blood were transferred in a fresh low-binding 1.5 mL reaction tube and 31.25 µL of a 1.25 µg / mL final concentration of DihydroRhodamin 123 was added for 10 min under culture conditions, followed by a lysis with 900 µL 1x BD lysis buffer for 7 min. After lysis, samples were centrifuged at 3500 rpm, at 4° for 5 min. Supernatant was removed and samples were washed with 1 mL PBS followed by another centrifugation (3500 rpm, 4 °C, 5 min). Last, samples were resuspended in 200 µL PBS supplemented with 3 % HS and Rhodamin fluorescence was directly acquired using flow cytometry. PMN were depicted according to their granular morphology. Unstained cells were recorded to subtract autofluorescence from Rhodamin staining (Δ Median).

3.8.11 CELL SURFACE STAINING ON ISOLATED PMN

PMN were isolated as described in 3.1.1. 0.5×10^6 PMN per sample were treated with water or 5000 AuNR / PMN or 10 ng / ml LPS for 2 h, 4 h, 8 h or 24 h at 37 °C. Staining of cell surface epitopes was generally carried out using fluorochrome coupled antibodies in a 96 well round bottom plate. Cells were washed with PBS and split in two wells prior to staining for specific antibody staining or unspecific isotype control. Primary antibodies were diluted in PBS 3 % human serum, which was used to block unspecific binding and incubated with the cells for 30 min at 4°C. After another wash with PBS, a viability staining was performed for 30 min at 4 °C. In the following, cells were resuspended in PBS 3 % human serum and directly analyzed in the flow cytometer. PMN were identified by expression of CD66b, CD45 and CD16 (Supplementary Figure 1). Antibodies used for flow cytometry and applied concentrations are listed in Table 8. Unspecific autofluorescence was removed by subtracting the median fluorescence of the isotype staining from the median fluorescence of the specific staining (Δ Median). Isotype antibodies are listed in Table 9.

3.8.12 WHOLE BLOOD STAINING

Whole blood samples were prepared as described in 3.8.6 or 3.8.9. Afterwards, samples were split, and 30 µL for both, specific and isotype staining were transferred in a fresh 1.5 mL reaction tube. Antibodies were added in the titrated dilutions that were also used for normal surface staining (see Table 8 and Table 9) and incubated for 25 min at room temperature. Erythrocytes were lysed

directly after staining using 1 mL of 1xBD Pharm Lysis Buffer per sample for 7 min. After lysis, cells were sedimented at 3500 rpm for 5 min, washed with 1 mL PBS and resuspended in PBS 3 % HS for analysis using flow cytometer. PMN were depicted as shown in Supplementary Figure 2. Unspecific autofluorescence was removed by subtracting the median fluorescence of the isotype staining from the median fluorescence of the specific staining (Δ Median). Isotype antibodies are listed in Table 9.

3.8.13 T CELL SUPPRESSION ASSAY

300 μ L whole blood was treated with water or 5000 AuNR / PMN as described in 3.8.6 for 90 min followed by staining of PMN with CD66b-FITC for 25 min at 37 °C in rotation. Afterwards, samples were diluted by addition of 14.7 mL RPMI supplemented with 10 % FCS and 1 % Penicillin. Samples were kept in rotation at room temperature. PMN were sorted by Kirsten Bruderek in the IMCES using the BD FACS Aria II Flow Cytometry Cell Sorter (BD). The 96-well round bottom plate (Sarstedt) was coated with 1 μ g / mL CD3 (OKT3) and 2 μ g / mL CD28 (CD28.2) in PBS for at least 2 h at 37 °C. T cells were isolated like described in 3.1.2 and labelled with 5 μ M Cell proliferation Dye (CPDye) for 10 min at room temperature. T cells were washed with culture medium. T cells and PMN (with or without AuNR priming) were combined in wells in a 2:1 (T cell : PMN) ratio. Upon cell division, the CPDye load of the parental cell is equally distributed to the daughter cells resulting in a reduction of emitted fluorescence intensity by 50 %. Proliferation can be analyzed in flow cytometry. For negative control (no proliferation) T cells were not activated by CD3 / CD28, for positive control T cells were activated without further addition of PMN. After 4 days at 37 °C CD4 and CD8 T cells were stained, in order to distinguish cytotoxic from T helper cells using CD4 and CD8. The percentage of proliferating and the division index of CD4⁺ and CD8⁺ T cells was analyzed with the “Proliferation Modelling” tool in FlowJo 10.

3.8.14 ANTIBODY-MEDIATED AUNR TARGETING OF ISOLATED IMMUNE CELLS

PMN were isolated as described in 3.1.1. Peripheral blood mononuclear cells (PBMCs) were isolated from healthy donors by density gradient centrifugation as described above. After washing with PBS for three times, 0.1x10⁶ PMN and 0.1x10⁶ PBMC per sample were mixed in a 1:1 ratio. Samples were either treated with single antibodies or with 5000 AuNR, coated with respective antibodies / cell for 30 min. Antibodies are listed in Table 12. After washing with PBS, cells were stained with a secondary antibody (Table 9) and analyzed *via* flow cytometry. Gating strategy to

identify PMN, T cells and monocytes is shown in Supplementary Figure 3. These experiments were performed by Kim Lamers as part of her Bachelor thesis.

3.8.15 TARGETING IMMUNE CELLS BY ANTIBODY-CONJUGATED AUNP OF DIFFERENT SIZES

Whole blood was treated with 5000 AuNR or gold nanospheres (AuNSPH) / PMN of three different sizes (15nm (AuNR = 0.449 $\mu\text{g} / \text{mL}$, 0.449 pg / cell , AuNSPH = 1.67 $\mu\text{g} / \text{mL}$, 1.67 pg / cell), 30nm (AuNR = 4.08 $\mu\text{g} / \text{mL}$, 4.08 pg / cell , AuNSPH = 13.2 $\mu\text{g} / \text{mL}$, 13.2 pg / cell) and 60nm (AuNR = 33.31 $\mu\text{g} / \text{mL}$, 33.31 pg / cell , AuNSPH = 106.23 $\mu\text{g} / \text{mL}$, 106.23 pg / cell)) with fluorescently labelled BSA or antibodies (listed in Table 12) for 30 min in rotation at 37 °C. Afterwards, T cells, PMN and monocytes were stained for 25 min at 4°C using population markers (listed in Table 13) and fluorescence was analyzed in flow cytometry. Gating strategy to identify PMN, T cells and monocytes is shown in Supplementary Figure 4.

3.9 KILLING OF ISOLATED IMMUNE CELLS BY PHOTOTHERMAL THERAPY

3.9.1 PTT OF MULTICELLULAR IMMUNE CELL CULTURES

PMN and PBMC were isolated from healthy human blood donors as described in 3.1. Cells were treated with PBS or 10 000 AuNR with different surface modifications (BSA-, $\alpha\text{rIgG2b-}$, $\alpha\text{CD11b-}$, $\alpha\text{mIgG2a-}$, or $\alpha\text{CD3-}$) / PMN for 30 min at 37 °C. Excess of unbound AuNR was removed by washing with PBS. Afterwards cells were re-suspended in 10 % AS medium, before undergoing laser irradiation (chapter 3.9.3.).

3.9.2 PTT OF T CELLS

T cells were isolated as described in 3.1.2. T cells were treated with PBS or 10 000 AuNR with different surface modifications (BSA-, $\alpha\text{mIgG2a-}$, or $\alpha\text{CD3-}$) / T cell for 30 min at 37 °C. Excess of unbound AuNR was removed by washing with PBS. Afterwards, cells were re-suspended in 10 % AS medium, before undergoing laser irradiation (chapter 3.9.3.).

3.9.3 LASER IRRADIATION

The samples were irradiated one by one in a 96-well plate format, with one single laser beam of 5 W with a beam diameter of 0.64 cm (15.5 W / cm^2) at 808 nm wavelength for 5 min. Afterwards, cells were rested either for 1 h (multi-cellular cultures) or 24 h (T cells only) at 37 °C. Staining of apoptotic cells was performed as described in 3.8.2. Percentage of apoptotic cells was analyzed in flow cytometry. This experiment was performed by Kim Lamers as part of her Bachelor thesis.

3.9.4 DATA ANALYSIS OF FACS DATA

FACSDiva 8 and 10 Software was used for the acquisition of flow cytometry data. The data analysis was performed in FlowJo V10. Cells were always gated on singlets according to FSC-A and FSC-H, then according their SSC versus FSC-A followed by distinct staining of population markers. Expression markers were analyzed with the help of isotype staining. Expression of cell surface receptors was assessed via median fluorescence intensities.

3.10 STATISTICS

Statistical analysis was performed with GraphPad Prism 8 software. Tests used in the study are indicated within the legends. Tests comprised paired t-test, unpaired t-test, one-way ANOVA, two-way ANOVA, Pearson-correlation and ROC Analysis. Data are depicted as mean value with standard deviation (+/-SD). N indicates the number of experimental repetitions, each performed with individual, independent blood donors.

4 RESULTS

4.1 THE ROLE OF PMN IN THE INTERACTION WITH THERANOSTIC AGENTS

Theranostic agents either simultaneously or sequentially combine **therapy** and **diagnostics**. They have become a popular field in biomedical therapy, since their application allows targeted therapy, thereby improving the local accumulation of drugs and reducing undesirable side effects of current therapies, especially in malignant diseases. Nanoparticles offer a lot of opportunities, due to their modifiable surface functionalization allowing targeted delivery of chemotherapeutics or hyperthermia-mediated cell killing and even allow personalized medicine. However, most of these outstanding therapeutics did not reach clinical application until now, since it lacks the transition from murine to human studies. To overcome this translational barrier a comprehensive understanding of the interaction of gold nanoparticles (AuNP) with potential target cells is required. An important potential target cell for AuNP are professional phagocytic immune cells (Gref *et al.* 1994). Equipped with efficient uptake mechanisms to engulf foreign material like bacteria and fungi but also nanoparticles, these phagocytes potentially clear AuNP from the circulation and from tissues upon injection. Thus, the efficiency of theranostic therapeutics is strongly influenced by the interaction of phagocytes with those theranostic agent. To date, most studies investigating this interaction, focused on macrophages (Dykman *et al.* 2017). However, in contrast to mice, in humans, polymorphonuclear neutrophils (PMN) represent the most abundant white blood cells with professional phagocytic activity (Summers *et al.* 2010). Despite its' clear translational relevance, only few studies investigated the consequences of AuNP and PMN interaction. PMN have been shown to clear AuNP *via* neutrophil extracellular traps (NETs) rather than phagocytosing those (Bartneck *et al.* 2010). Another study showed that phagocytosis of AuNP induced endoplasmic reticulum (ER) stress, followed by caspase-mediated cell death of PMN (Noël *et al.* 2016). There is limited information about how PMN engulf, transport and process AuNP and about the effects of AuNP uptake on PMN function *ex vivo*. Therefore, the first part of this work aimed to characterize the molecular interaction of gold nanorods (AuNR), as part of AuNP, with PMN, giving insights in the uptake, intracellular transport and functional activation of human PMN. In the context of the first part of this doctoral work, the following article was accepted for publication in ACS Nano (Schirrmann *et al.* 2022).

4.1.1 PMN ARE TAKING UP AuNR

To evaluate the uptake of AuNR by PMN, we performed transmission electron microscopy. Gold has a higher electron density than biological material, which increases electron scattering resulting in dark spots. PMN were isolated as described in 3.1.1 and treated with AuNR for 1 h prior to fixation. AuNR accumulated in multivesicular structures within PMN (Figure 5A+B). To evaluate the uptake efficiency, we used fluorescently labelled AuNR and confocal microscopy (Figure 5C-H). We found AuNR uptake by PMN already after 5 min of co-incubation, showing a significant shift in fluorescence intensity (Figure 5I). Furthermore, we found 60 % of PMN positive for AuNR with donor dependent variabilities. AuNR uptake by PMN plateaued after 15 min with around 80 % of positive cells (Figure 5J). To ensure that AuNR were not exocytosed over time, we analyzed the fluorescence intensity of PMN over longer time periods up to 4 h. Confocal microscopy showed no reduction over 4 h of incubation with fluorescently labeled AuNR (Figure 5K).

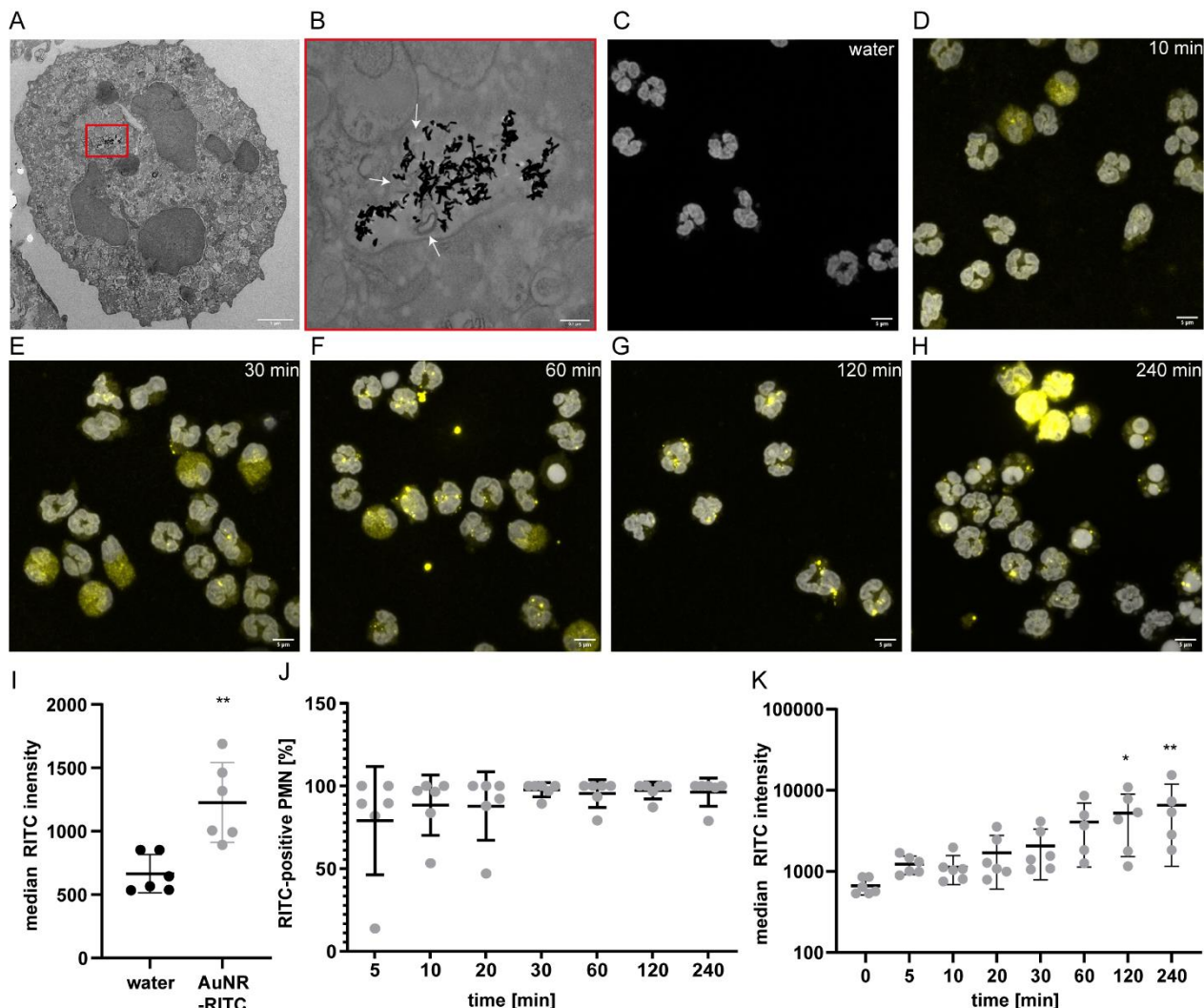


Figure 5: AuNR uptake by PMN.

Uptake by isolated PMN was investigated using transmission electron microscopy. All experiments were performed using isolated PMN treated with water or 5000 AuNR / PMN. **(A)** AuNR accumulated within multivesicular structures, indicated by red rectangle (scale bar = 1 μm) **(B)** and higher magnification (scale bar = 100 nm). Multivesicular structures are marked by white arrows. **(C)** For uptake efficiency analysis, isolated PMN were treated with water or 5000 fluorescently labelled AuNR-RITC / PMN over various time points. Fluorescence was visualized using confocal microscopy for PMN treated over **(D)** 10 min, **(E)** 30 min, **(F)** 60 min, **(G)** 120 min and **(H)** 240 min (scale bar = 5 μm). **(I-K)** Maximum intensity per cell was analyzed in Fiji ImageJ 1.53c. For each time point and blood donor (n=6), 100 cells were analyzed. Afterwards, the maximum intensity of 100 cells was determined. **(I)** Median fluorescence intensity of n = 6 donors after 5 min incubation with water or AuNR-RITC (n=6, unpaired t-test). **(J)** Percentage of AuNR-RITC positive cells was analyzed by using the Δ Median of water as cutoff. **(K)** Quantification of the median RITC intensity for up to 240 min (n=6, ordinary one-way ANOVA). The statistical significance was defined as ****p \leq 0.0001; ***p \leq 0.001; **p \leq 0.01; *p \leq 0.05N indicates the number of experimental repetitions, each performed with independent blood donors.

4.1.2 PHAGOCYTOSIS AS MAJOR AUNR UPTAKE MECHANISM IN PMN

Knowing the uptake mechanism of AuNR and PMN is crucial for determining nanoparticles function and intracellular fate after application (Clift *et al.* 2011, Panariti *et al.* 2012). Cellular uptake of particles by PMN is mainly driven by phagocytosis as well as clathrin-dependent and caveolin-dependent endocytosis. To evaluate, which uptake mechanism is most important for AuNR ingestion by PMN, we blocked these specific uptake mechanisms prior to AuNR treatment (Kuhn *et al.* 2014). All experiments in this section were performed with Kim Lamers as part of her “Orientierungspraktikum” during her Bachelor of Biology studies. PMN are phagocytic cell, so the phagocytic mechanism was considered to be most relevant. Phagocytosis as well as macropinocytosis are dependent on actin. Cytochalasin D (CytD) depolymerizes actin filaments, leaving actin in globular state and thereby inhibiting phagocytosis and macropinocytosis as well as further transport of vesicles from the membrane to inner compartments. To evaluate CytD inhibitor efficiency we tested PMNs’ ability to phagocytose pLVX-ZsGreen1 transformed TOP10 *Escherichia coli* (*E.coli*). CytD blocked the uptake of *E.coli* by PMN significantly, whereas other inhibitors, of which the function is elucidated below, did not affect *E.coli* uptake. This indicates a specific blocking of actin-dependent uptake (Figure 6A). Clathrin-mediated endocytosis was blocked using chlorpromazine hydrochloride (CH) which removes clathrin and the adaptor protein complex 2 on the cell surface. Furthermore, it specifically blocks the uptake of the serum protein transferrin. CH blocked the uptake of transferrin, indicating a specific blockade of clathrin-dependent uptake (Figure 6B). To inhibit caveolin-dependent endocytosis and lipid raft internalizations, we used methyl- β -cyclodextrin (M β CD). M β CD depletes cholesterol from the plasma membrane by forming inclusion complexes with cholesterol. Cholera toxin subunit-B has been shown to enter cells via caveolin-mediated endocytosis, so we implemented alexa-488-conjugated cholera toxin subunit-B as positive control. M β CD did not inhibit cholera toxin subunit-

B uptake (Figure 6C). To evaluate the capacity of M β CD functionality, we stained cholesterol on the surface of PMN. M β CD removed cholesterol from the cell surface at 100 mM concentration (Figure 6D). This data suggests that the inhibitor worked as supposed to, but caveolin-dependent endocytosis, or lipid raft internalizations were not the major uptake mechanism of cholera toxin subunit-B in PMN.

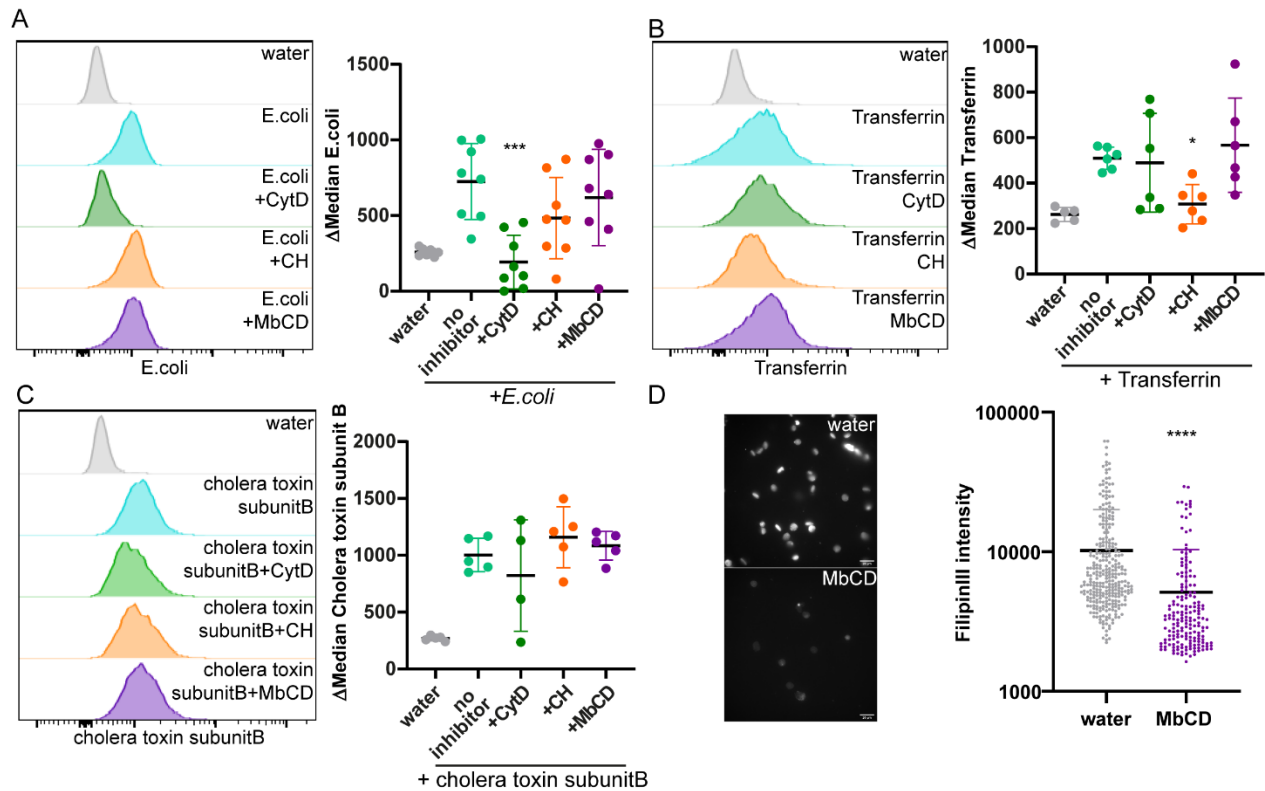


Figure 6: Specific inhibition of PMN's actin-, clathrin- and caveolin-dependent uptake mechanisms.

These experiments were performed with Kim Lamers. Isolated PMN were pre-treated with 400 μ M Cytochalasin D (CytD), 10 μ M chlorpromazine hydrochloride (CH) or 100 mM methyl- β -cyclodextrin (M β CD) for 30 min, followed by addition of pLVX-ZsGreen1 transformed TOP10 *E. coli* (50:1 *E. coli*: PMN, transformed by Kirsten Bruderek), alexa-488-conjugated Transferrin (100 μ g / mL) or alexa-488-conjugated cholera toxin subunit-B (10 μ g / mL) for 30 min. Fluorescence intensity of *E. coli*, transferrin and cholera toxin subunit-B was analyzed in flow cytometry. **(A)** CytD inhibition, left panel shows exemplary histogram, right panel quantification of fluorescence intensity of transformed *E. coli* (n=8, ordinary one-way ANOVA, Dunnett's multiple comparisons test). **(B)** CH inhibition, left panel shows exemplary histogram, right panel quantification of fluorescence intensity of alexa-488-conjugated Transferrin (n=6, mixed effects analysis, Dunnett's multiple comparisons test). **(C)** M β CD inhibition, left panel shows exemplary histogram, right panel quantification of fluorescence intensity of alexa-488-conjugated cholera toxin subunit-B **(D)** M β CD depletion of cholesterol on the plasma membrane. Cholesterol was stained by filipin III and images were performed using a 40x magnification objective and the AxioObserver.Z1 (ZEISS). Upper picture shows no addition of M β CD, lower picture shows 30 min M β CD treatment. Scale bar = 25 μ m. Maximum intensity per cell (NC= 296 cells; M β CD = 180 cells) was analyzed in Fiji ImageJ 1.53c. Data of 3 donors was pooled (one-way ANOVA, Dunnett's multiple comparisons test). The statistical significance was defined as ****p \leq 0.0001; ***p \leq 0.001; **p \leq 0.01; *p \leq 0.05. N indicates the number of experimental repetitions, each performed with independent donors.

To evaluate the uptake dependency on AuNR size, we tested three different sizes of fluorescently labelled AuNR (20 nm, 50 nm and 100 nm). PMN were pretreated with inhibitors for 30 min prior to addition of AuNR. After 30 min AuNR treatment, the fluorescence intensity of PMN was measured in flow cytometry. CytD was most efficient in blocking the uptake of all kinds of AuNR, showing a reduction in fluorescence intensity by around 25 % (Figure 7A+B). CH, on the other hand, reduced the uptake of 20 nm AuNR by 24 %, indicating a contribution of clathrin-mediated uptake with smaller AuNR (Figure 7A+C). Blocking of caveolin-dependent endocytosis did not affect PMN ability to take up AuNR of any size (Figure 7A+D).

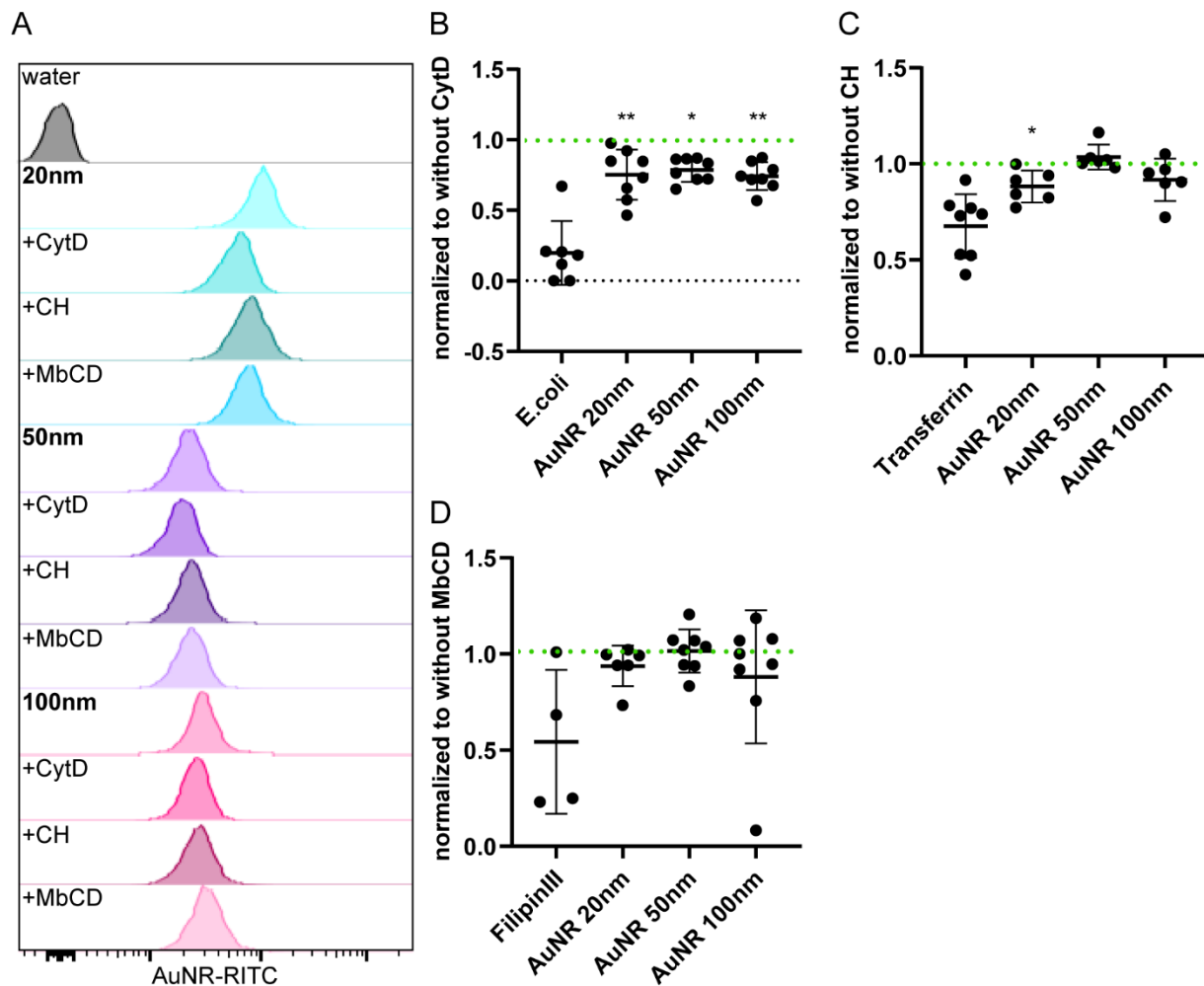


Figure 7: PMN engulf AuNR actin-dependently.

These experiments were performed with Kim Lamers. Isolated PMN were pre-treated with 400 μ M Cytochalasin D (CytD), 10 μ M chlorpromazine hydrochloride (CH) or 100 mM methyl- β -cyclodextrin (M β CD) for 30 min, followed by addition of 5000 AuNR-RITC of three different sizes (20, 50, 100 nm) / PMN. AuNR were incubated for 30 min. **(A)** Exemplary histograms show the PMN-associated fluorescence intensity of AuNR. **(B)** CytD inhibition normalized to respective positive control without inhibitor (= 1, represented by green dashed line) (n=8, ordinary one-way ANOVA). **(C)** CH inhibition normalized to respective positive control without inhibitor (= 1 indicated by green line) (n=6 ordinary one-way ANOVA). **(D)** M β CD inhibition normalized to respective positive control without inhibitor (= 1 indicated by green line) (n=6 ordinary one-

way ANOVA). The statistical significance was defined as **** $p \leq 0.0001$; *** $p \leq 0.001$; ** $p \leq 0.01$; * $p \leq 0.05$. N indicates the number of experimental repetitions, each performed with independent donors.

4.1.3 AUNR ENTER THE ENDOCYTIC PATHWAY OF PMN

We further investigated the fate of AuNR within PMN, in order to mechanistically understand AuNR uptake by PMN. By staining early (Rab5) and late (Rab7) endosomes as well as lysosomes (LAMP1) and performing high resolution structured illumination microscopy (SIM), we determined the intracellular localization of AuNR over time. Exemplary images represent 0.32 μm thick images of single cells as well as representative histograms of the fluorescence intensity along the red arrow drawn over the merged image. Within the first 5 min we found an equal distribution of AuNR within early and late endosomes as well as lysosomes (Figure 8A+B+G). We did not observe any accumulation of AuNR in LAMP1⁺Rab7⁻lysosomes until 4 h post application, hinting towards an arrest of AuNR within the endosomal compartment. Interestingly, we found an accumulation of AuNR within Rab5⁺ endosomes after 10 to 20 min post application compared to relatively low AuNR amount within the Rab7⁺ vesicles (Figure 8C+D+G). Rab5 is normally part of the early endocytosis whereas Rab7 acts in later stages, mediating the transport from early endosomes to lysosomes (Deinhardt *et al.* 2006). We found a large proportion of AuNR (48 % of total AuNR) localized in Rab7⁺ late endosomes already after 30 min post AuNR treatment, supporting the hypothesis of sequential co-localization of AuNR with Rab5 and Rab7 endosomes (Figure 8E+F+G). Since we could not show AuNR accumulating in Rab5⁺ endosomes at 5 min of AuNR treatment, it is not entirely clear whether this is due to extremely rapid “classic” endocytic transport, slowing down around 10 and 20 min, thereby showing an accumulation in Rab5⁺ endosomes with later accumulation in Rab7⁺ endosomes (30 min). Another possibility could be a “non-classical” mechanism of early intracellular transport circumventing Rab5⁺ early endosomes.

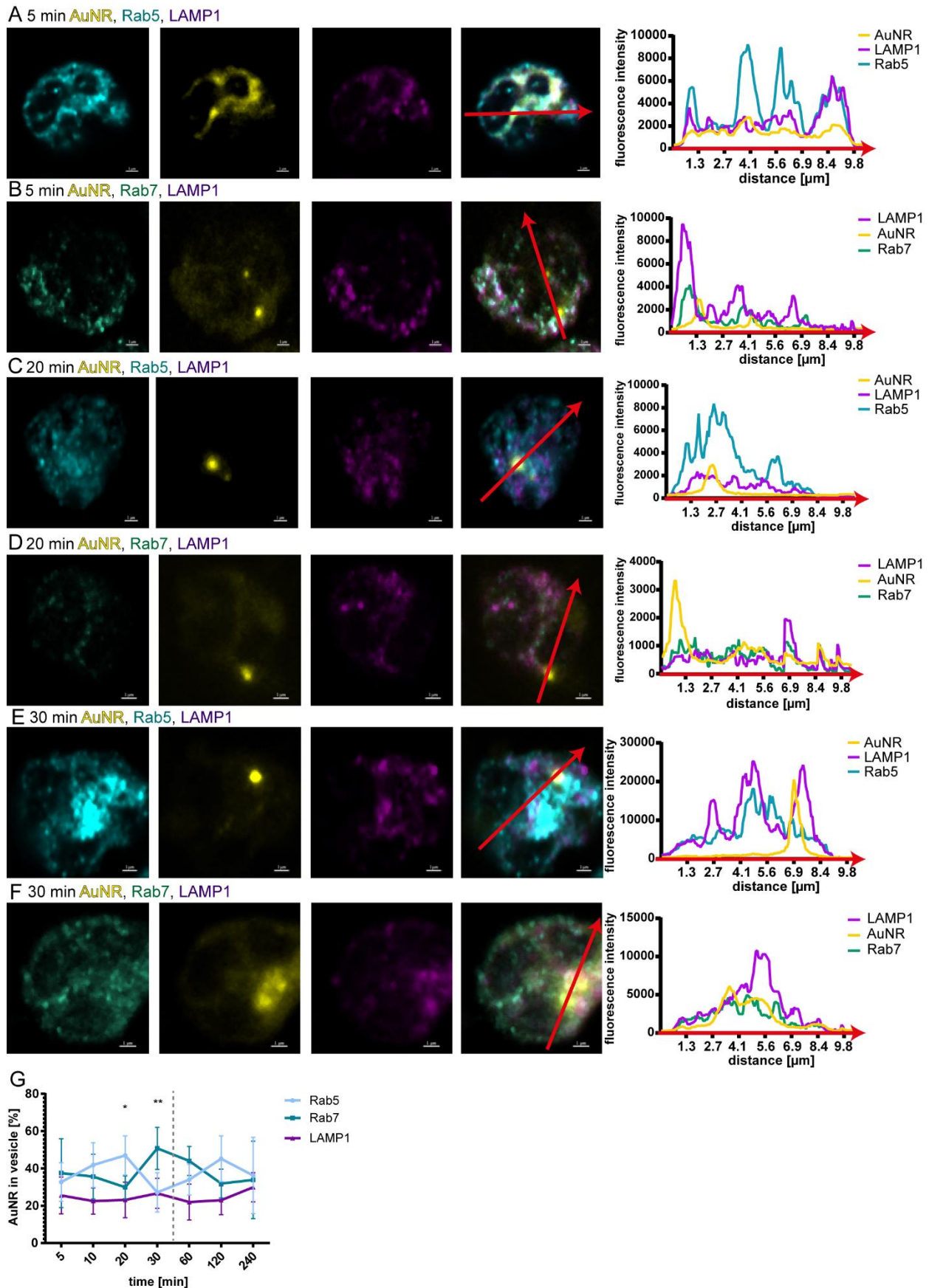


Figure 8: AuNR enter the endolysosomal system of PMN

Isolated PMN were treated with 5000 AuNR-RITC / PMN (yellow) for up to 4 h. Early (Rab5⁺, light blue in A+C+E), late (Rab7⁺, green in B+D+F) endosomes as well as lysosomes (LAMP1, purple in A-F) were stained. Structured illumination microscopy was performed to show co-localization of AuNR with Rab5, Rab7 or LAMP1 over time. Exemplary pictures shown in this graph represent a single picture of a stack (0.32 μm depth). All images are shown as single channel and merged pictures. Exemplary histograms show the fluorescence intensity of all channels along the red arrow marked in the merged picture. Exemplary picture of **(A)** AuNR co-localized with early endosomes and lysosomes and **(B)** late endosomes and lysosomes after 5 min of AuNR treatment. **(C)** Exemplary picture of AuNR co-localized with early endosomes and lysosomes and **(D)** late endosomes and lysosomes after 20 min of AuNR treatment. **(E)** Exemplary picture of AuNR co-localized with early endosomes and lysosomes and **(F)** late endosomes and lysosomes after 30 min of AuNR treatment. Scale bar = 1 μm . **(G)** Co-localization analysis was performed for up to 30 min of AuNR treatment. For later time points, AuNR were incubated for 30 min followed by additional incubation for 60, 120, 240 min. The dashed line separates the different experimental setups (n=7, two-way ANOVA, Tukey's multiple comparisons test). The statistical significance was defined as ****p \leq 0.0001; ***p \leq 0.001; **p \leq 0.01; *p \leq 0.05. N indicates the number of experimental repetitions, each performed with independent donors.

4.2 AUNR UPTAKE ACTIVATES PMN *EX VIVO*

PMN represent the first line of defense and are the most prominent phagocytes in human circulation and tumor microenvironment. Their activation status contributes to many immunologic changes within our body. To evaluate the state of activation in PMN, we performed flow cytometry to screen for changes in the expression of cell surface markers, PMNs ability to migrate to tumor conditioned medium, their viability as well as morphology and a luminex assay to measure the secretion of cytokines and chemokines.

4.2.1 AUNR UPTAKE INDUCES THE EXPRESSION OF ACTIVATION MARKERS ON PMN

Upon activation, PMN can change their expression of surface molecules, of which most of them are associated with a cluster of differentiation (CD) identifier. CD16 is constitutively expressed on mature PMN and can be downregulated during aging and activation. It is a low-affinity receptor for IgG, preferentially IgG1 and IgG3 isotypes and a little less pronounced IgG2 and IgG4. We did not observe any change in CD16 expression on PMN upon AuNR treatment over various time points compared to water control, indicating no accelerated aging of PMN upon AuNR treatment (Figure 9A). We further analyzed the expression of CD35, the complement receptor type 1. CD35 binds particles and immune complexes that have been activated by the complement system. We did not observe a changed expression of CD35 upon AuNR treatment, but stimulation of PMN by LPS positive control induced higher expression of CD35 (Figure 9B). This indicates that AuNR are not covered with proteins of the complement system upon contact with human blood serum within the culture medium. Furthermore, we did not observe a changed expression of CD54 (Figure 9C), which binds integrins. Its' expression can be induced by Interleukin 1 (IL1) and tumor necrosis factor (TNF) stimulation and mediates binding to endothelial cells promoting the transmigration

into tissue. AuNR treatment did not alter CD64 expression on PMN (Figure 9D). CD64 binds monomeric IgG-type antibodies and can be induced by Interferon γ (INF γ) and granulocytic colony stimulating factor (G-CSF). We further analyzed the expression of CD95, a receptor that induces programmed cell death. We did not observe any changes in CD95 expression upon AuNR treatment (Figure 9E). The same applied for CD274 (programmed death-ligand 1, PD-L1), a marker often associated with enhanced T cell suppressive capacity (Figure 9F). In conclusion, AuNR uptake did not induce aging of PMN or comparable activation as LPS, hinting towards no severe endotoxin load of AuNR.

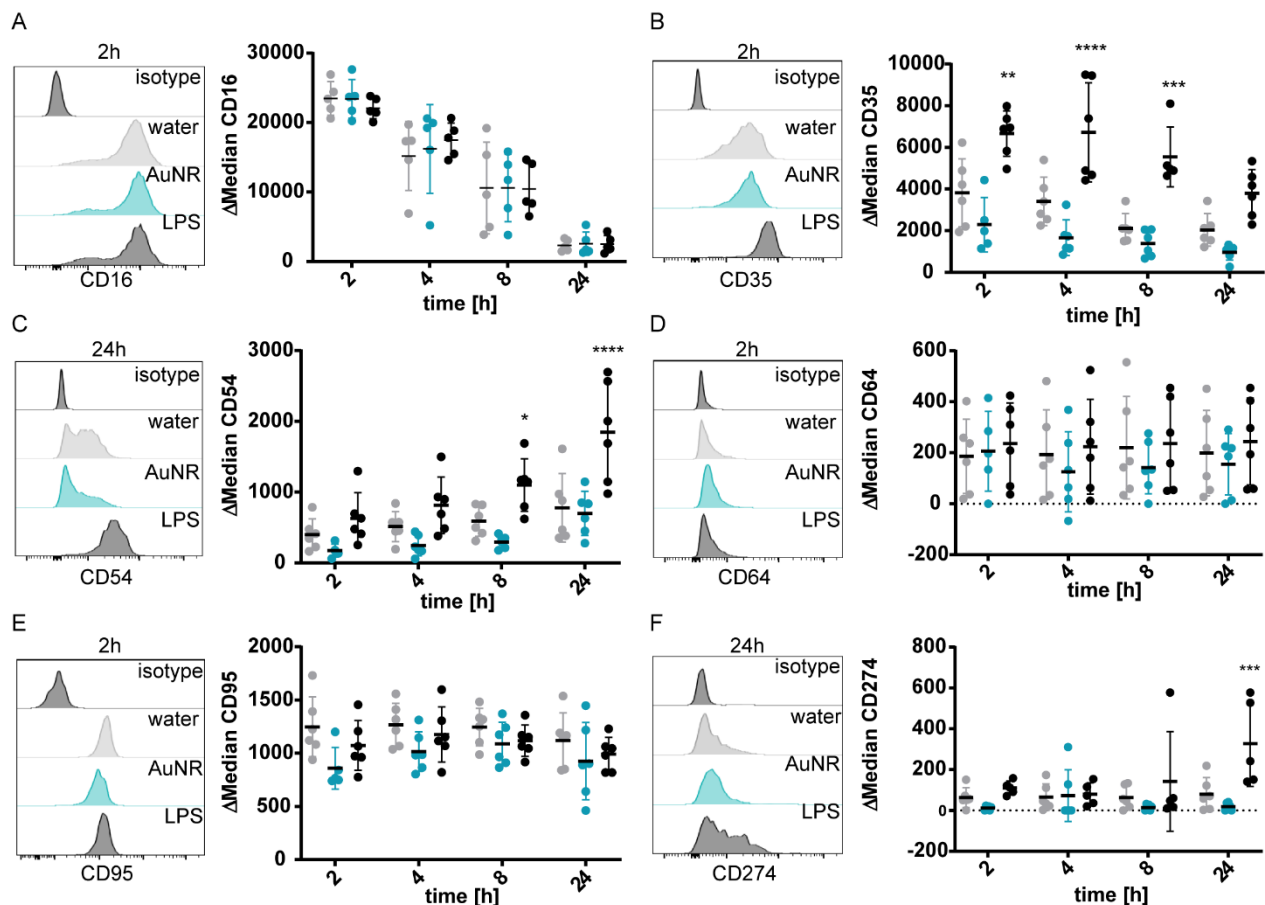


Figure 9: AuNR uptake does not affect PMNs' surface expression of CD16, CD35, CD54, CD64, CD95 and CD274.

Isolated PMN were treated with water (grey), 5000 AuNR / PMN (blue), or 10 ng / mL LPS (black) over 2 h, 4 h, 8 h and 24 h. Surface expression of CD16, CD35, CD54, CD64, CD95 and CD274 was stained with fluorescently labelled antibodies and normalized to the respective isotype control. (A-F) PMN were identified by expression of CD66b, CD45 and CD16 (Supplementary Figure 1). Fluorescence was analyzed in flow cytometry. Exemplary histograms after indicated time points and quantifications of (A) CD16, (B) CD35, (C) CD54, (D) CD64, (E) CD95 (F) and CD274 are shown (n=5, two-way ANOVA with Bontferroni's multiple comparisons test). The statistical significance was defined as ****p \leq 0.0001; ***p \leq 0.001; **p \leq 0.01; *p \leq 0.05. N indicates the number of experimental repetitions, each performed with independent donors.

However, a key feature of PMN is the homing to inflammation in tissue, so we further investigated the surface expression of CD62L and found a significant downregulation after two hours of AuNR treatment (Figure 10A). CD62L acts as a homing receptor and is constitutively expressed on PMN mediating the migration to inflamed tissue (Solovjov *et al.* 2005). CD62L shedding is classically considered the first step, “priming”, during migration and goes along with an upregulation of CD11b (Kishimoto *et al.* 1989). We further analyzed CD11b expression and found a significant upregulation at all investigated time points (Figure 10B). CD11b is an integrin mediating inflammation by regulating the adhesion and migration, as well as phagocytosis, chemotaxis and cellular activation (Solovjov *et al.* 2005). Among chemotaxis receptors, we found a strong reduction in CD182 (CXCR2) expression after 2 h and 4 h of AuNR treatment (Figure 10C). CD182 is the receptor for interleukin 8 (IL8). Another receptor of IL8 is CD181 (CXCR1). We found a significant downregulation of CD181 after 4 h (Figure 10D). The downregulation of both markers hints towards an activation of PMN and a potential oversaturation of IL8 (Samanta *et al.* 1990). The regulation of CD62L, CD11b, CD182 and CD181 but not CD16, CD35, CD54, CD64, CD95 and CD274 further shows that the uptake of AuNR results in a very specific activation of PMN.

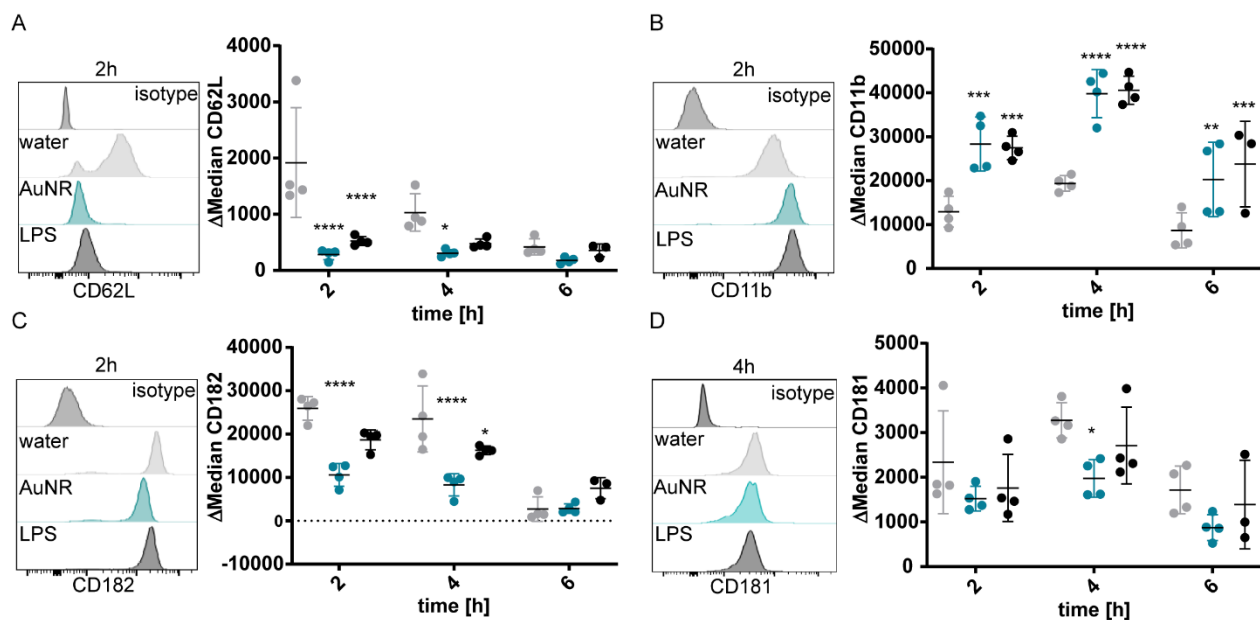


Figure 10: AuNR uptake regulates the surface expression of CD62L, CD11b, CD182 and CD181 on PMN.

Whole blood was treated with water (grey), 5000 AuNR / PMN (blue), or 10 ng / mL LPS (black) for 2 h, 4 h and 6 h. **(A-D)** PMN were identified by expression of CD66b, CD45 and CD16 (Supplementary Figure 1). The expression of **(A)** CD62L, **(B)** CD11b, **(C)** CD182 and **(D)** CD181 was determined by flow cytometry. Histograms show exemplary experiments from 2 h or 4 h time points (n=4, two-way ANOVA, Dunnett's multiple comparisons test). The statistical significance was defined as ****p ≤ 0.0001; ***p ≤ 0.001; **p ≤ 0.01; *p ≤ 0.05.

0.01; * $p \leq 0.05$. N indicates the number of experimental repetitions, each performed with independent donors.

4.2.2 AUNR UPTAKE INDUCES DEGRANULATION

In the next series of experiments we screened for the secretion of cytokines by PMN after AuNR treatment using first a luminex assay. We analyzed various cytokines involved in the activation of PMN. Macrophage migration inhibitory factor (MIF) is released upon endotoxin activation e.g. *via* Toll like receptor 4 (TLR4) and mediates pro-inflammatory activation of the innate immune system (Calandra *et al.* 2003). Gro α (CXCL1) is produced by macrophages, PMN and epithelial cells, it binds to CD182 and induces migration of PMN, thereby regulating inflammation. Interleukin 1 β (IL1 β) is a pyrogen inducing systemic fever via prostaglandin E2 and peripheral rushes as well as production of Interleukin 6 (IL6). Furthermore, together with IL23 and IL17A it promotes the mobilization of granulocyte progenitors and mature neutrophils from the bone marrow (Dinarello 2005). IL6 is another pro-inflammatory cytokine involved in many diseases like multiple sclerosis, cancer and arteriosclerosis. Macrophage inflammatory protein 1 β (MIP1 β , CCL4) activates human PMN, leading to acute neutrophilic inflammation by inducing further synthesis and release of other pro-inflammatory cytokines such as IL1, IL6 and tumor necrosis factor α (TNF α). TNF α , like IL1 β , is a pyrogen inducing a pro-inflammatory activation via the activation of nuclear factor kappa-light-chain-enhancer of activated B cells (NF κ B). We found no change in secretion of IL1 β , IL6, MIP1 β , TNF α , MIF and Gro α (Figure 11A-F). However, we found a massive secretion of IL8 (Figure 11G). IL8 induces different physiological responses required for migration and phagocytosis like increased intracellular Ca²⁺, exocytosis and respiratory burst (Dixit *et al.* 2012). Furthermore, oxidative stress promotes IL8 secretion thereby causing the recruitment of inflammatory cells. By a positive feedback loop, IL8 secretion increases oxidative stress mediators, thus playing a key role in local inflammation (Harada *et al.* 1994).

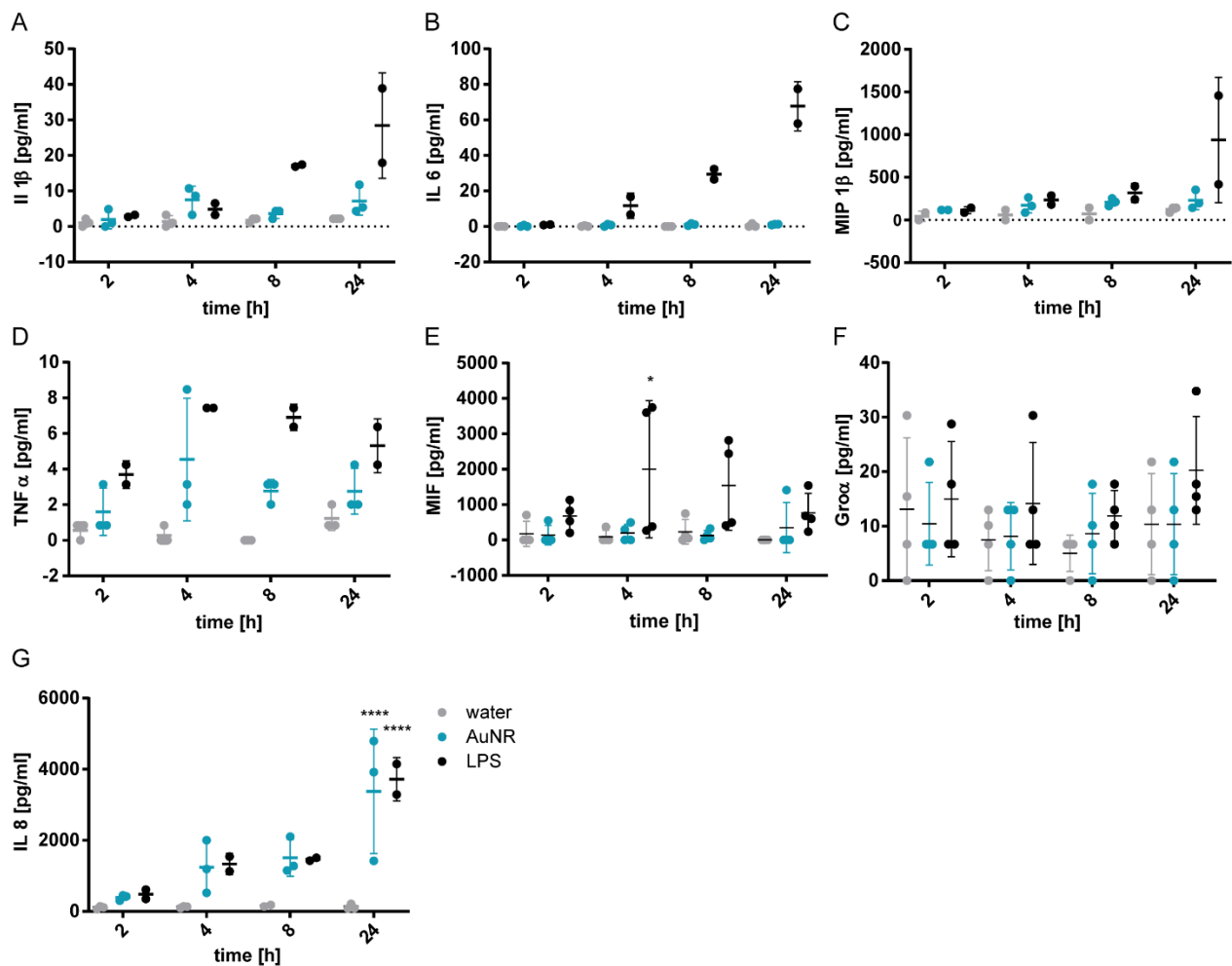


Figure 11: PMN secrete IL8 upon AuNR treatment.

Samples were measured by Kirsten Bruderek using a luminex assay. Isolated PMN were treated with water (grey), 5000 AuNR / PMN (blue), or 10 ng / mL LPS (black) over 2 h, 4 h, 8 h and 24 h. Cell supernatant was harvested. Secretion of **(A)** IL1 β , **(B)** IL6, **(C)** MIP1 β , **(D)** TNF α , **(E)** MIF, **(F)** Gro α and **(G)** IL8 was analyzed in luminex assay (n=3, two-way ANOVA, Bonferroni's multiple comparisons test). The statistical significance was defined as ****p \leq 0.0001; ***p \leq 0.001; **p \leq 0.01; *p \leq 0.05. N indicates the number of experimental repetitions, each performed with independent donors.

Besides the downregulation via internalization upon ligand binding, CD182 can be regulated by metalloproteinase activity (Mishra *et al.* 2015). Therefore, we further investigated the PMN activation status by analyzing the secretion of matrix metalloproteinase 9 (MMP9). MMP9 is located in tertiary granules and classically secreted upon activation of PMN during degranulation. We found significantly higher secretion of active MMP9 after 2 h of AuNR stimulation compared to the unstimulated water control. This was not the case for 4 h and 8 h incubation, indicating this is just a transient induction (Figure 12A). Furthermore, we evaluated the amount of degranulated neutrophils by analyzing the frequency of PMN in the peripheral blood mononuclear cell (PBMC)

fraction after 2 h of AuNR treatment in whole blood. AuNR treatment resulted in a higher frequency of CD66b⁺ neutrophils within the PBMC fraction compared to water control (Figure 12B). This indicates that uptake of AuNR promotes the release of granules and vesicles resulting in a less dense PMN morphology.

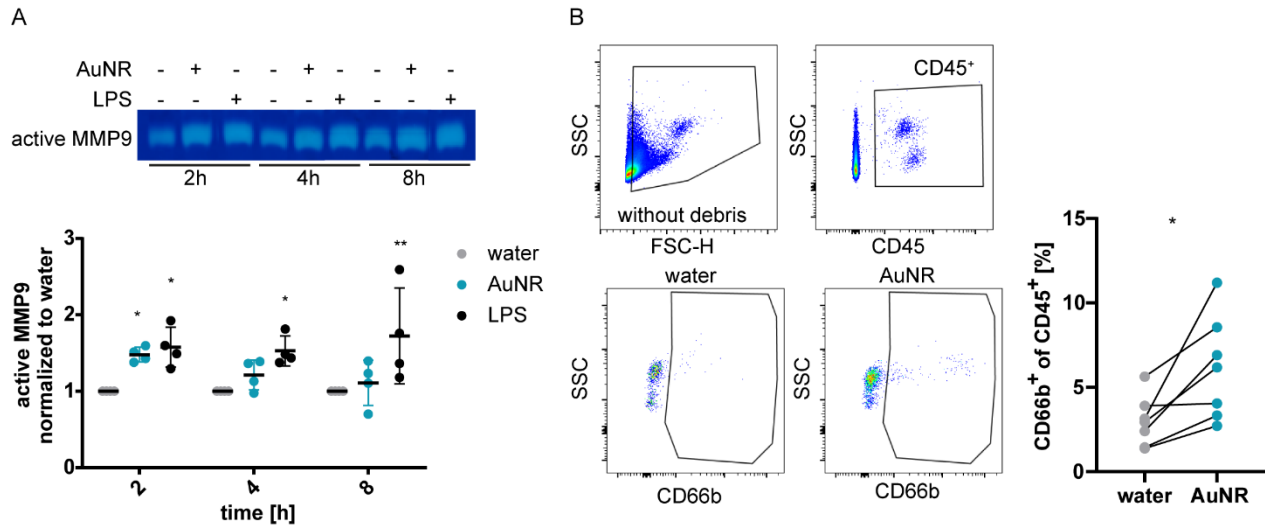


Figure 12: AuNR treatment induces MMP9 secretion and generates mature low density PMN.

(A) Isolated PMN were incubated with water (grey), 5000 AuNR / PMN (blue), or 10 ng / mL LPS (black) for 2 h, 4 h or 8 h. Secreted MMP9 within supernatant was analyzed by zymography. All data was normalized to unstimulated water control (n=4, two-way ANOVA, Dunnett's multiple comparisons test). (B) Whole blood was treated with water (grey), or 5000 AuNR / PMN (blue) for 2 h. Neutrophils were depicted according to their expression of CD45 and CD66b (left panel) using flow cytometry. Quantification is shown in the right panel (n=7, paired-t-test). The statistical significance was defined as ****p ≤ 0.0001; ***p ≤ 0.001; **p ≤ 0.01; *p ≤ 0.05. N indicates number of experimental repetitions, each performed with independent donors.

4.2.3 AUNR INDUCE STRONGER MIGRATION TOWARDS TUMOR SUPERNATANT

Keeping in mind that the treatment with AuNR induced a strong secretion of IL8 after 2 h and regulated CD182, both important mediators of PMN migration, we analyzed the migration ability of PMN *ex vivo* after AuNR treatment. To test this, PMN were pre-treated with AuNR for 4 h prior to addition to a previously established system of PMN migration towards tumor cell conditioned media (Brandau *et al.* 2011). Indeed, more PMN were migrating towards tumor supernatant after 4 h priming with AuNR compared to water-primed PMN (Figure 13A). PMN are highly active and one of their key features is the homing from circulation to inflamed tissue (Faurischou *et al.* 2003). In order to evaluate PMNs ability to migrate from circulation to tissue, we generated a system with an endothelial layer. Surprisingly, AuNR pre-treatment did not alter PMN ability to migrate through endothelial layer significantly. Nevertheless, we observed a slight trend towards a stronger migration after AuNR-priming (Figure 13B).

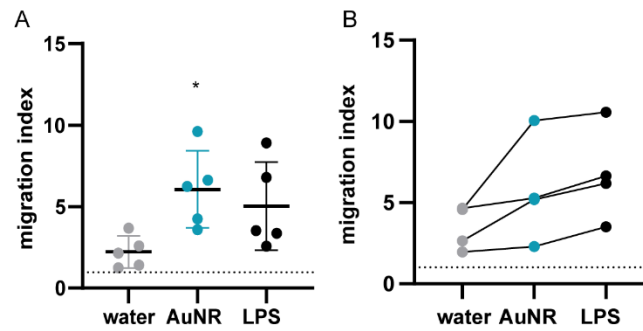


Figure 13: PMN migrate faster to tumor-conditioned medium after AuNR priming.

Isolated PMN were incubated with water (grey), 5000 AuNR / PMN (blue), or 10 ng / mL LPS (black) for 4 h. **(A)** PMN were transferred to 3 μm transwells. After 3 h, migrated PMN were counted. (n=5, one-way ANOVA, Dunnett's multiple comparisons test). The dashed line indicates migration index of "1" representing the level of random, non-directed spontaneous migration. Both, spontaneous migration and directed migration are shown in Supplementary Figure 5. **(B)** Migration of PMN through a monolayer of HMEC-1 on transwells. (n=4, ordinary one-way ANOVA, Dunnett's multiple comparisons test). The dashed line indicates migration index of "1" representing the level of random, non-directed spontaneous migration. The statistical significance was defined as **** $p \leq 0.0001$; *** $p \leq 0.001$; ** $p \leq 0.01$; * $p \leq 0.05$. N indicates the number of experimental repetitions, each performed with independent donors.

4.2.4 AUNR UPTAKE IS NOT AFFECTING THE VIABILITY OF PMN EX VIVO

Noël and colleagues showed that AuNR uptake induces ER stress and activates caspases in PMN *ex vivo* (Noël *et al.* 2016). Therefore we evaluated the cytotoxicity of AuNR over time. AuNR treatment did not induce Annexin V dependent apoptosis even at long incubation times like 24 h (Figure 14A). The same applied for higher doses of AuNR per PMN as well as different surface charges of AuNR, except positively charged AuNR at higher dosages (2.4 times higher than normally used in this study (Supplementary Figure 6). Nevertheless, we found a higher pan-caspase activity after four hours of AuNR incubation compared to the unstimulated water control, indicating that the accumulation of AuNR is inducing caspase activation but is not resulting in a higher amount of apoptotic or necrotic cells (Figure 14B).

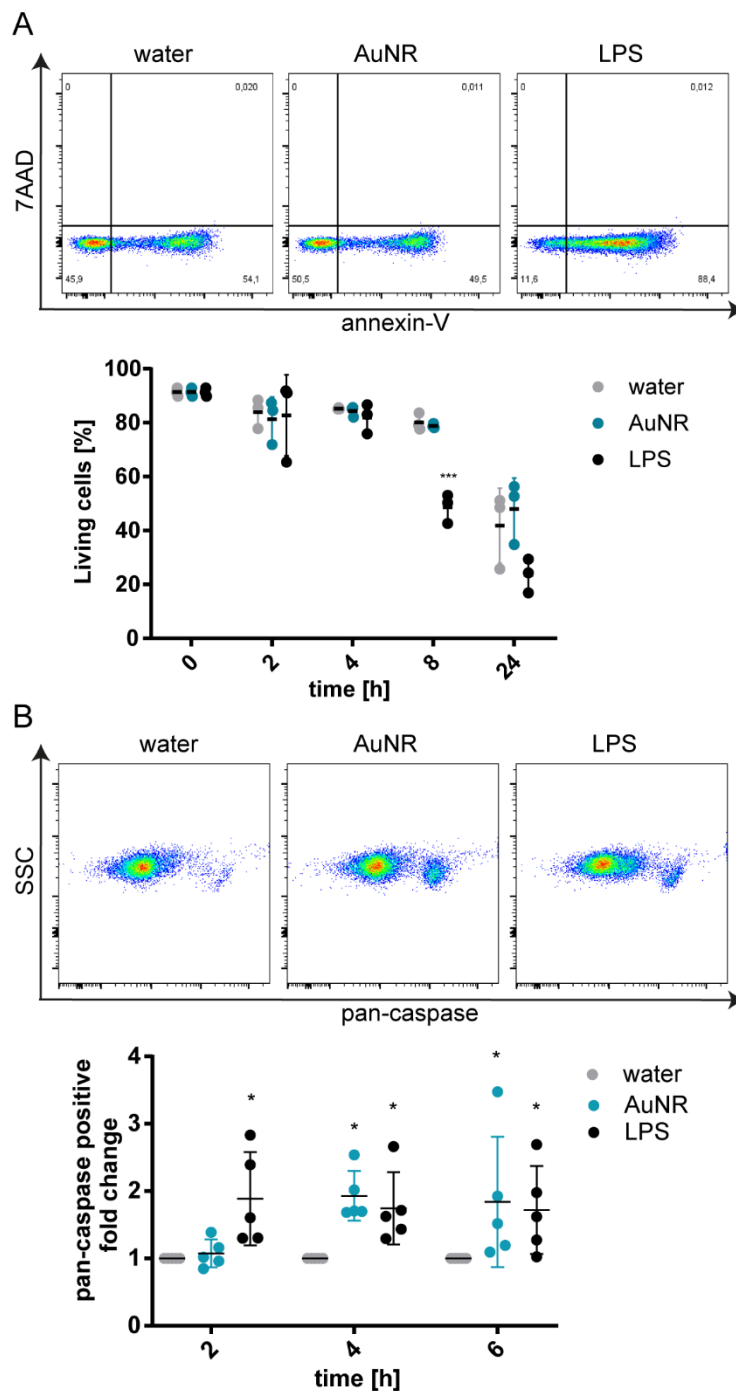


Figure 14: AuNR uptake induces pan-caspase activation in PMN after 4h.

(A) Isolated PMN were incubated with water (grey), 5000 AuNR / PMN (blue), or 10 ng / mL LPS (black) over 2 h, 4 h, 8 h and 24 h and apoptosis-related changes in cell membrane topology were assessed by Annexin V Apoptosis Detection Kit in flow cytometry. The upper panel shows exemplary dot plots of the Annexin-V after water, AuNR and LPS treatment, lower panel the quantification of Annexin V and 7AAD double negative cells ($n=3$, two-way ANOVA Bonferroni's multiple comparisons test). **(B)** PMN were exposed to water (grey), 5000 AuNR / PMN (blue), or 10 ng / mL LPS for 2 h, 4 h, 6 h and the percentage of pan-caspase positive cells was determined by ApoStat Intracellular Caspase Detection Kit in flow cytometry. Upper panel shows exemplary dot plots of water, AuNR and LPS, lower panel the quantification of pan-caspase positive cells ($n=5$, two-way ANOVA, Dunnett's multiple comparisons test). The statistical significance was defined as **** $p \leq 0.0001$; *** $p \leq 0.001$; ** $p \leq 0.01$; * $p \leq 0.05$. N indicates the number of experimental repetitions, each performed with independent donors.

4.3 AUNR TREATMENT INDUCES CELLULAR STRESS

Caspases are a family of cytosolic cysteine proteases and crucial mediators of apoptosis. Three major apoptotic pathways have been identified, namely cytokine activation (caspase-1, -4, -5, and -13), apoptosis initiation (caspase-2, -8, -9, -and -10), and apoptosis execution (caspase-3, -6, and -7). In general, caspase activity is connected to cellular stress (Momoi 2004). Furthermore, it has been shown that nanoparticles, independent of size or conformation (e.g. silica, metal), induce endoplasmic reticulum (ER) stress in e.g. endothelial cells (Cao *et al.* 2017) revealing a potential mechanism of nanoparticle-induced toxicity. The ER is the largest organelle within the cell and represents a major site of protein synthesis, folding and transport, and is further involved in the lipid and steroid synthesis, carbohydrate metabolism and Ca^{2+} storage. However, the most prominent function of the ER is the protein synthesis. Even though several chaperones and folding enzymes mediate the proper folding of proteins, an accumulation of unfolded or misfolded proteins in the lumen of the ER, defining the so-called ER stress, can occur. In order to restore normal function of the ER and the cell, unfolded or misfolded proteins need to be degraded and chaperones need to be produced. This process is called unfolded protein response (UPR). If the ER fails to circumvent the ER stress, apoptosis via caspases is initiated (Schwarz *et al.* 2016).

4.3.1 AUNR UPTAKE ACTIVATES THE XENOBIOTIC METABOLISM

To investigate a potential stress induction by AuNR uptake in PMN on a transcriptional level, we first performed a cellular stress array. Surprisingly, we found most of the transcriptional differences between water and AuNR already after five minutes of treatment. Most of the regulated genes belonged to the cytochrome P450 (CYP) family, suggesting an activation of the xenobiotic metabolism. This metabolism comprises the chemical transformation of foreign compounds, e.g. drugs, by a biological system, and normally converts relatively lipophilic compounds into more easily excretable hydrophilic metabolites. The xenobiotic metabolism is conventionally divided into four phases. First, xenobiotics are taken up (phase 0), then enzymes of the CYP family or flavin-containing monooxygenases (FMO) introduce reactive groups in the xenobiotic (phase 1). After turning the xenobiotic to a reactive intermediate, e.g. glutathione-S-transferases (GST) form a hydrophilic product by transferring polar groups to the intermediate (phase 2) and the water-soluble end product is excreted (phase 3) (Stanley 2017). We found significantly higher transcription levels of CYP1A1 (Relative Quantification = RQ = 9.44) and CYP2F1 (RQ = 2.22) after 5 min of AuNR treatment compared to the unstimulated water control. Furthermore, genes from FMO family were upregulated (FMO1 (RQ = 19.02) and FMO5 (RQ = 2.07). This was

accompanied by a reduced transcription of glutathione redox system (GSR (RQ = 0.43)) after 5 min and GPX2 (RQ = 0.47) as well as SOD3, an antioxidant, after 15 min (RQ = 0.45). Additionally, CES1, an important player in the detoxification of xenobiotics, was upregulated (RQ = 3.12) after 15 min, strengthening the hypothesis that AuNR uptake is activating the xenobiotic metabolism via oxidation of the foreign material (Brzezinski *et al.* 1994). We did not observe higher transcription of members of the GST family, on the contrary, GSTA1, GSTA5 and GSTM5 were downregulated (RQ = 0.45 – 0.47) after 15 min of AuNR treatment compared to water. Interestingly, we also found a downregulation of genes coding for proteins important for the proper folding of proteins (CCT3 (RQ = 0.28), CCT4 (RQ = 0.26), HOPX (RQ = 0.1) and HSPB1 (RQ = 0.03)) after 5 min of AuNR treatment followed by an upregulation after 15 min (HSPB1 (RQ = 5.66)) implying an impairment in protein folding upon AuNR treatment and a higher need of chaperones within the ER. Furthermore, we found a higher transcription of genes important for the prevention of aggregation of proteins intra- and extracellular (CRYAB (RQ = 1.65), CLU (RQ = 2.89)) (Figure 15).

We further validated the activation of CYP family by qPCR. We confirmed the downregulation of CYP2D6 (RQ = 0.4). CYP2D6 is a major drug metabolizing enzyme mediating the hepatic metabolism of around 20 % of drugs (e.g., codeine, amitriptyline, fluvoxamine, risperidone, fluoxetine, aripiprazole, paroxetine, and dextromethorphan) (Zanger *et al.* 2004). CYP2D6 is repressed by small heterodimer partner (SHP), so we analyzed the transcription of SHP and found significant upregulation after 5 min (RQ = 10), that reversed after 60 min (RQ = 0.28) (Figure 16A). In unstimulated cells, SHP is associated with the NFκB p65 subunit in the cytoplasm and inhibits its nuclear translocation, resulting in the attenuation of pro-inflammatory transcriptional activity (Yuk *et al.* 2016). In order to validate whether SHP was functionally active we performed fluorescence microscopy, validating the inhibition of NFκB p65 translocation after AuNR treatment. We did not observe a change in the translocation of NFκB p65 during the first 3 h of AuNR treatment. After 3 h, less NFκB p65 was located within the nucleus after AuNR treatment compared to water (Figure 16B-D). The activation of the xenobiotic metabolism, especially via CYP1A1, is regulated by the transcription factor aryl hydrocarbon receptor (AhR) (Ramadoss *et al.* 2005). The activation of AhR is not only resulting in a higher transcription rate of itself but also of other CYP enzymes, especially of CYP1A1 and CYP2F1. Therefore, we analyzed the transcription of AhR and found a significant upregulation after 15 min (RQ = 3.66) and further confirmed the upregulation of CYP1A1 and CYP2F1 (Figure 16E).

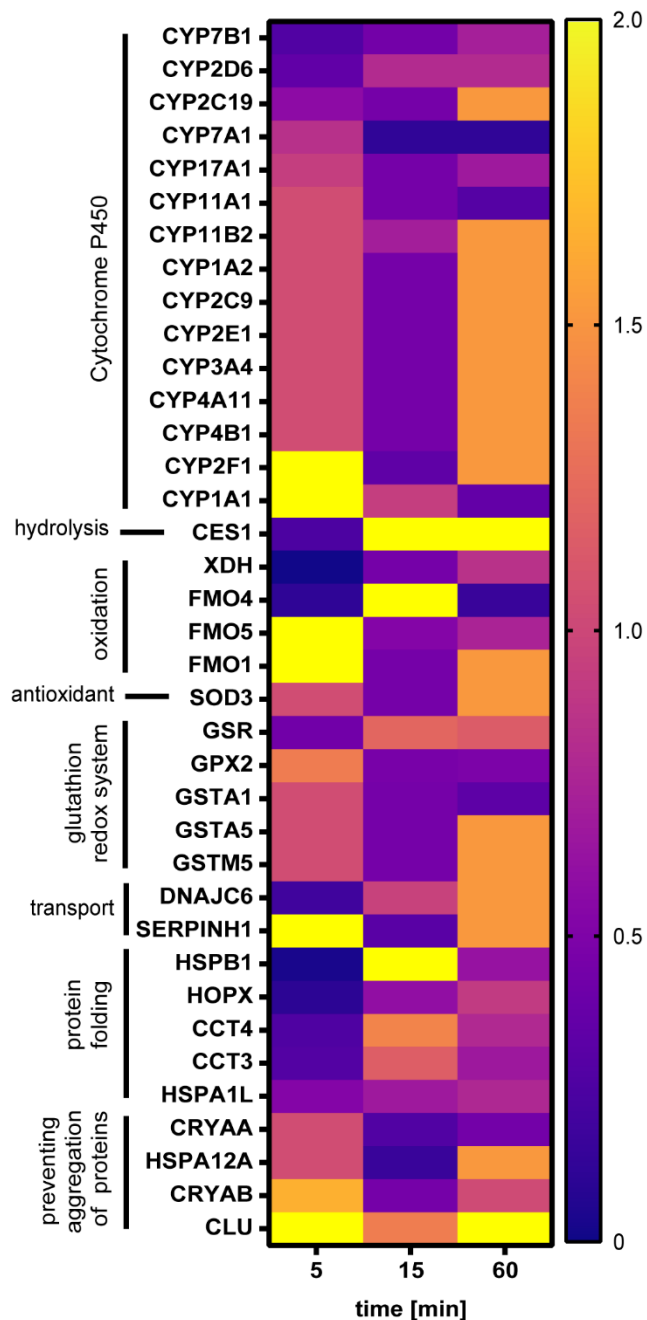


Figure 15: AuNR uptake induces cellular stress.

Isolated PMN were incubated with water, or 5000 AuNR / PMN for 5 min, 15 min, or 60 min. RNA of 4 donors was pooled in equal amounts. We performed a cellular stress array (Qiagen). All data was normalized to housekeeping genes included in the cellular stress array and to the unstimulated water control (set as RQ = 1 reference). RQ = relative quantification of gene expression, significant change is below 0.5 (downregulation, purple) and above 2 (upregulation, yellow).

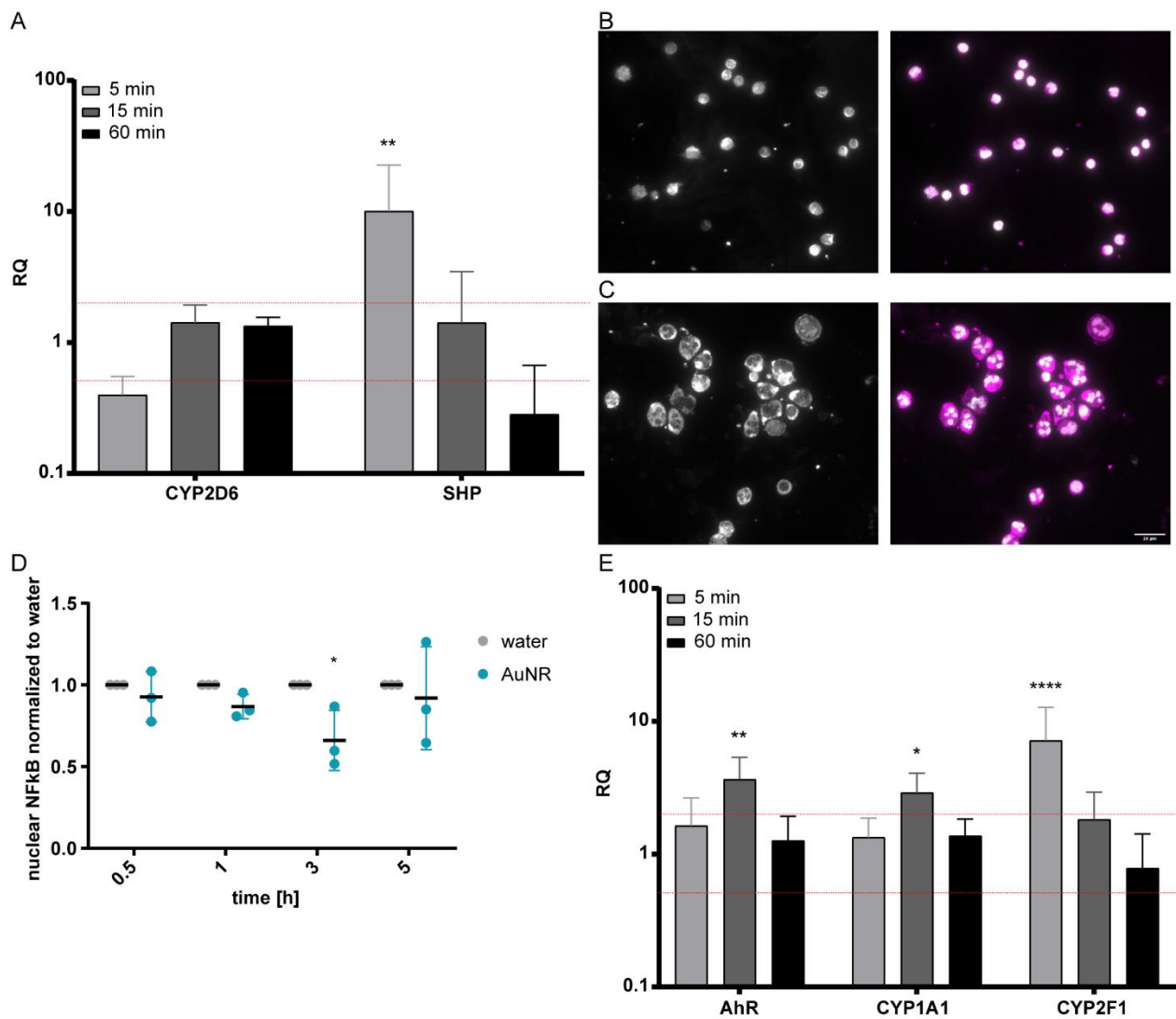


Figure 16: AuNR uptake activates SHP and AhR transcription, further repressing NFκB and inducing the transcription of CYPs.

(A) Isolated PMN were incubated with water, or 5000 AuNR / PMN for 5 min, 15 min, or 60 min. CYP2D6 and SHP transcription was normalized to housekeeping gene (β 2-microglobulin) and unstimulated water control (set as RQ = 1 reference). RQ = relative quantification of gene expression, significant regulation of lower than 0.5 and above 2 is indicated with red dashed lines ($n=6$ two-way ANOVA, Dunnett's multiple comparisons test). (B-D) Isolated PMN were incubated with water or 5000 AuNR / PMN for 0.5 up to 5h. Subsequently, PMN were fixed and NFκB p65 was stained. Images were performed using a 40x magnification objective and the AxioObserver.Z1 (ZEISS). Exemplary pictures show the NFκB p65 staining (left panel, white) and composite picture with DAPI (right panel, NFκB = pink, DAPI = white) of (B) water- and (C) AuNR-treated PMN after 3 h. Scale Bar = 20 μ m. (D) Co-localization of NFκB p65 with DAPI was quantified using Fiji ImageJ 1.52i and normalized to unstimulated water control (grey, AuNR (blue)) ($n = 3$, paired t-test). (E) Isolated PMN were incubated with water, or 5000 AuNR / PMN for 5 min, 15 min, or 60 min. AhR, CYP1A1 and CYP2D1 transcription was normalized to housekeeping gene (β 2-microglobulin) unstimulated water control (set as RQ = 1 reference). RQ = relative quantification of gene expression, significant regulation of lower than 0.5 and above 2 is indicated with red dashed lines ($n=6$ two-way ANOVA, Dunnett's multiple comparisons test). The statistical significance was defined as **** $p \leq 0.0001$; *** $p \leq 0.001$; ** $p \leq 0.01$; * $p \leq 0.05$. N indicates the number of experimental repetitions, each performed with independent donors.

AhR is a transcription factor, located in the cytosol, translocating to the nucleus upon activation (Ramadoss *et al.* 2005). To further evaluate the biological relevance of AhR activation, we examined the translocation of AhR protein from cytosol to nucleus using fractionated Western Blotting. We found a significant nuclear accumulation after 5 min of AuNR treatment (Figure 17). This is of special interest, since a recent study connected AhR activation with ER stress (Kunitomi *et al.* 2021).

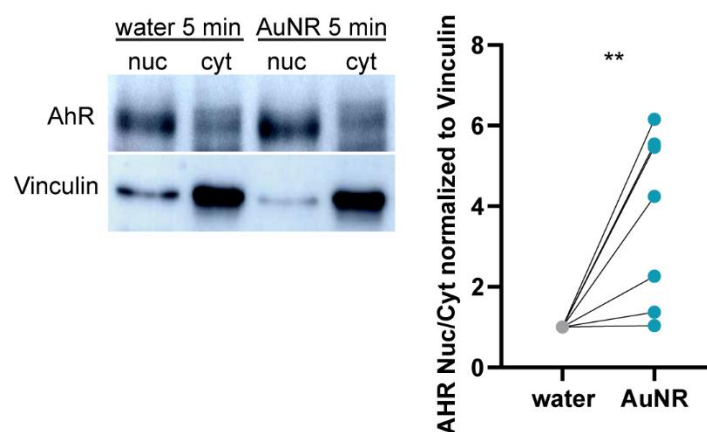


Figure 17: AuNR uptake activates AhR signaling in PMN.

Isolated PMN were incubated with water (grey), or 5000 AuNR / PMN (blue) for 5 min. Using fractionated Western blotting, proteins of the cytosol and nuclei were isolated separately. Left panel shows an exemplary SDS-PAGE, right panel the accompanying quantification (n=7, unpaired t-test). The statistical significance was defined as ****p ≤ 0.0001; ***p ≤ 0.001; **p ≤ 0.01; *p ≤ 0.05. N indicates the number of experimental repetitions, each performed with independent donors.

Besides CYP family activation (Figure 15 and Figure 16), we confirmed a higher transcription of FMO1 (Figure 18). This protein is involved in the oxidative metabolism of a variety of xenobiotics such as drugs and pesticides. Form I catalyzes the N-oxygenation of secondary and tertiary amines (Cashman 2000). We did not observe an upregulation of FMO5 like in the cellular stress array.

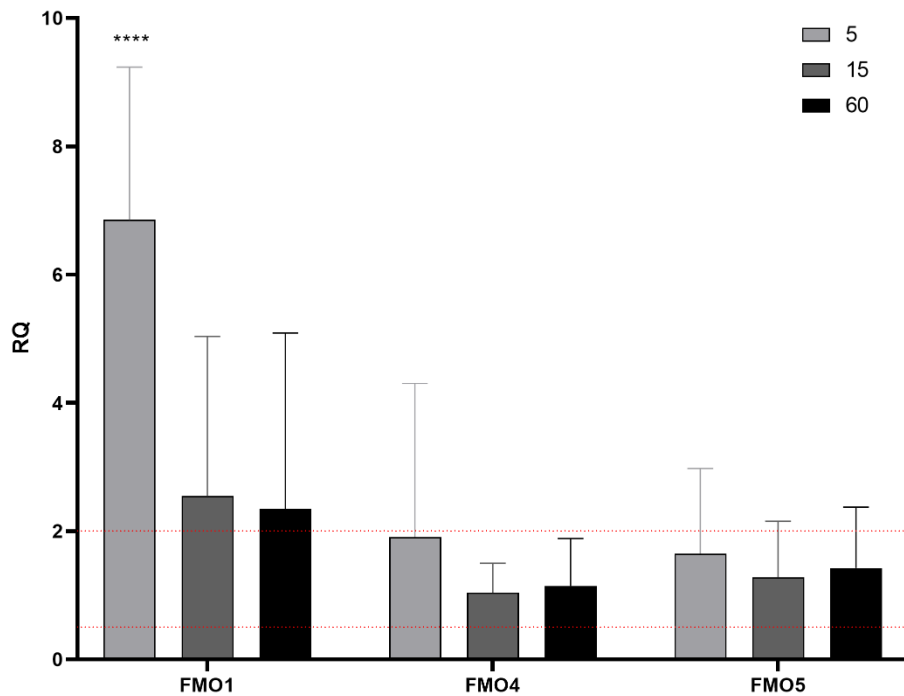


Figure 18: AuNR uptake induces transcription of FMO1.

Isolated PMN were incubated with water, or 5000 AuNR / PMN for 5 min, 15 min, or 60 min. All data was normalized to housekeeping gene (β 2-microglobulin) and unstimulated water control (set as RQ = 1 reference). RQ = relative quantification of gene expression, significant regulation of lower than 0.5 and above 2 is indicated with red dashed lines (n=6, two-way ANOVA, Dunnett's multiple comparisons test). The statistical significance was defined as ****p \leq 0.0001; ***p \leq 0.001; **p \leq 0.01; *p \leq 0.05. N indicates the number of experimental repetitions, each performed with independent donors.

In summary, these data suggest that AuNR uptake induced the activation of the xenobiotic metabolism *via* AhR, regulating the transcription of chaperones important for protein folding. Furthermore, we found a differential expression of SHP, potentially regulating the translocation of NF κ B, a pro-inflammatory transcription factor. Since the nuclear NF κ B reduction happened after 3 h it was not considered to be an inducer of the aforementioned changes in CD11b, CD62L and CD182 surface expression and IL8 secretion already occurring after 2 h of AuNR treatment (Figure 10).

4.3.2 AUNR UPTAKE AFFECTS THE PROTEIN FOLDING MACHINERY

Despite the activation of xenobiotic metabolism, we found massive changes in the transcription of genes relevant for protein folding and prevention of protein aggregation, especially at early time points (Figure 15). Therefore we wondered, whether the regulation of the protein folding capacity could induce the functional changes described in earlier sections. We further analyzed their transcription and confirmed the upregulation of HOPX, HSPB1 and CCT3 (Figure 19). The protein coded by CCT3 is a molecular chaperone and part of the chaperonin containing TCP1 complex (CCT), also known as the TCP1 ring complex (TRiC). This complex is built up of two identical stacked rings, each containing eight different proteins. Unfolded polypeptides enter the TRiC, which in turn folds proteins in an ATP-dependent manner (Seo *et al.* 2010). HOPX is a homeodomain protein, acting *via* interaction with Hsp70 (HSPA1A) and Hsp90 (HSPA1B) assisting in chaperone-mediated protein refolding (Seo *et al.* 2016). Similar to HOPX, HSPB1 plays an important role as molecular chaperone. It maintains denatured proteins in a folding competent state, thereby contributing to stress resistance and the organization of actin (Rogalla *et al.* 1999). In conclusion, AuNR uptake accelerated the need of protein folding, resulting in the transcription of TRiC components and chaperones maintaining protein refolding. This further hints towards an accumulation of misfolded proteins that need to be kept in a denatured state until further processing.

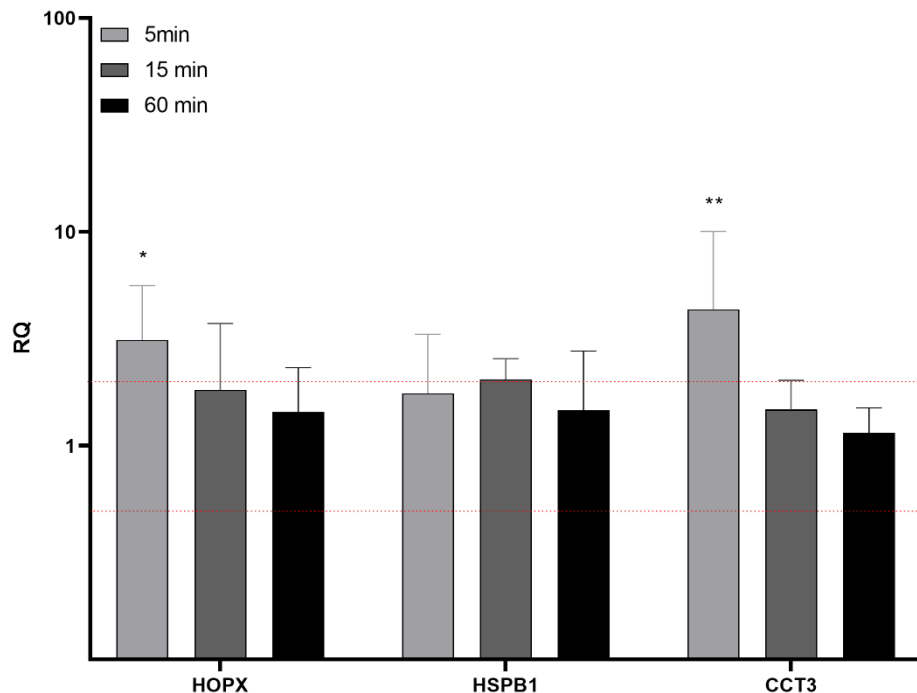


Figure 19: AuNR uptake accelerates the transcription of HOPX, HSPB1 and CCT3.

Isolated PMN were incubated with water, or 5000 AuNR / PMN for 5 min, 15 min, or 60 min. All data was normalized to housekeeping gene (β 2-microglobulin) and unstimulated water control (set as RQ = 1 reference). RQ = relative quantification of gene expression, significant regulation of lower than 0.5 and above 2 is indicated with red dashed lines (n=6 two-way ANOVA, Dunnett's multiple comparisons test). The statistical significance was defined as **** $p \leq 0.0001$; *** $p \leq 0.001$; ** $p \leq 0.01$; * $p \leq 0.05$. N indicates the number of experimental repetitions, each performed with independent donors.

4.3.3 PMN SHOW HIGHER UBIQUITINATION STATUS AFTER AUNR TREATMENT

Post-translational modifications and folding of secretory proteins, as well as their trafficking and degradation takes place in the ER. Therefore, we hypothesized that AuNR uptake induces an accumulation of misfolded proteins in the ER, further promoting ER stress. To examine this, we analyzed the level of protein ubiquitination in PMN upon AuNR treatment using Western Blot (Figure 20A). AuNR uptake induced higher levels of ubiquitination in PMN after 5 and 15 min compared to water (Figure 20B). This induction was abolished after 60 min, suggesting a regulation of protein folding machinery and unfolded protein response (UPR) induction.

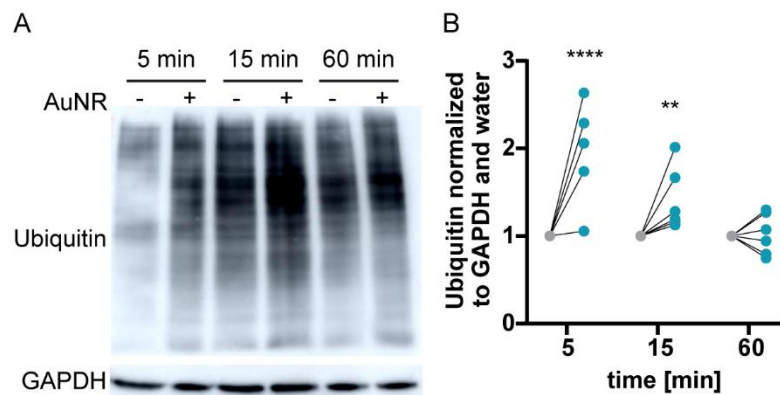


Figure 20: AuNR uptake induces higher ubiquitination in PMN after 5 and 15 min.

Isolated PMN were incubated with water (grey), or 5000 AuNR / PMN (blue) for 5, 15, or 60 min. **(A)** Exemplary SDS PAGE shows ubiquitin and GAPDH of full PMN cell lysates. **(B)** Quantification of ubiquitin normalized to GAPDH (n=7, two-way ANOVA with Sidak's multiple comparisons test). The statistical significance was defined as ****p \leq 0.0001; ***p \leq 0.001; **p \leq 0.01; *p \leq 0.05. N indicates the number of experimental repetitions, each performed with independent donors.

4.3.4 AUNR UPTAKE IMPEDES PROTEIN FOLDING

To evaluate whether AuNR uptake induced ubiquitination of not properly folded proteins, thereby activating an UPR, we further investigated mediators of protein folding. We found a significant upregulation of endoplasmic oxidoreductin-1 (Ero1 α), as well as a protein disulfide isomerase (PDI) after 30 min (Figure 21). Ero1 α is known to provide oxidizing potential in the ER enabling PDI to form intra- or inter-molecular disulfide bonds (oxidative protein folding) (Tu *et al.* 2004).

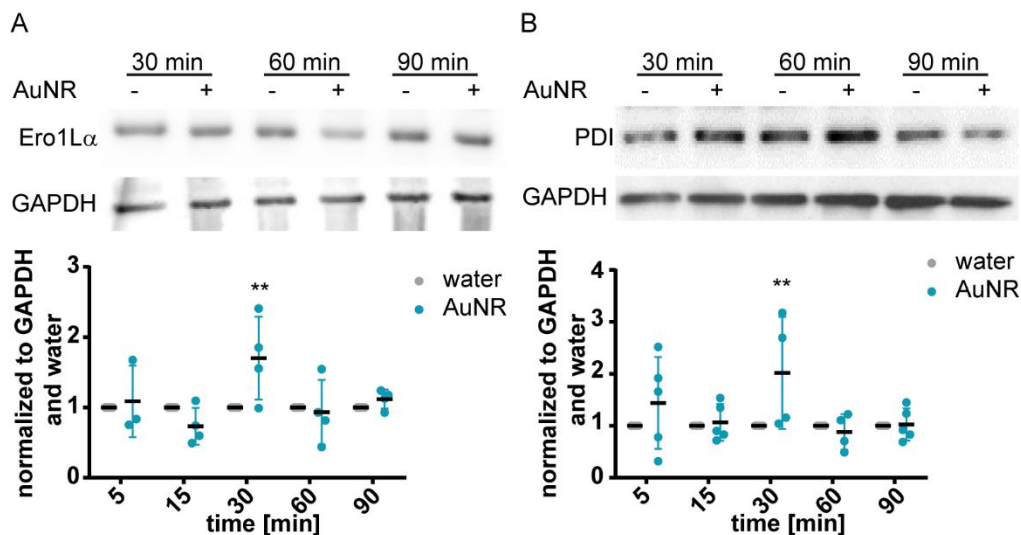


Figure 21: AuNR uptake induces upregulation of Ero1 α and PDI after 30 min.

Isolated PMN were incubated with water (grey), or 5000 AuNR / PMN (blue) for 30 min, 60 min and 90 min. Full PMN lysates were isolated after the indicated time points. **(A)** Western blot of Ero1 α . The upper panel shows an exemplary SDS PAGE from 30 min to 90 min, the lower panel shows its quantification. AuNR-induced (blue) Ero1 α was normalized to unstimulated water control (grey) (n=4, two-way ANOVA, Sidak's multiple comparisons test). **(B)** Western blot of PDI. The upper panel shows an exemplary SDS PAGE from 30 min to 90 min, the lower panel shows the quantification of 5 independent donors. AuNR-induced (blue)

PDI was normalized to unstimulated water control (grey) (n=5, two-way ANOVA, Sidak's multiple comparisons test). The statistical significance was defined as ****p ≤ 0.0001; ***p ≤ 0.001; **p ≤ 0.01; *p ≤ 0.05. N indicates the number of experimental repetitions, each performed with independent donors.

4.3.5 AUNR UPTAKE AFFECTS CA²⁺ AND ROS HOMEOSTASIS

Besides protein folding, one of the major tasks of the ER is Ca²⁺ homeostasis (Krebs *et al.* 2011). ER stress induction *via* altered oxidative protein folding and ROS is closely related to altered intracellular Ca²⁺ levels. ROS potentially targets ER-based Ca²⁺ channels, which open and release Ca²⁺ from the ER into the cytosol, thereby activating ER stress signaling (Zhang *et al.* 2008). To examine, whether AuNR uptake induces a misbalance in Ca²⁺ homeostasis, we primed PMN with a fluorescent labelling reagent to detect cytosolic Ca²⁺ over time. AuNR treatment elevated the cytosolic Ca²⁺ level after 20 to 40 min of AuNR exposure, comparable to *E.coli* uptake, which served as a positive control (Figure 22A+B). The disruption of Ca²⁺ homeostasis and the accumulation of misfolded proteins are both known to induce ER stress (Rao *et al.* 2004). As already mentioned, oxidative protein folding via Ero1L α and PDI and Ca²⁺ homeostasis interplay with redox homeostasis (Enyedi *et al.* 2010). Therefore, we analyzed PMNs' ROS production and found significantly higher ROS after 2 h of AuNR incubation (Figure 22C). The high intracellular Ca²⁺ was a transient effect between 10 and 40 min after AuNR exposure, around the same time of Ero1L α and PDI regulation. Since ROS production was only slightly induced after 2 h of AuNR treatment we concluded this as a rather additive as inducing effect of aforementioned regulations. Nevertheless, all effects support the hypothesis of cellular stress induction on protein level upon AuNR exposure.

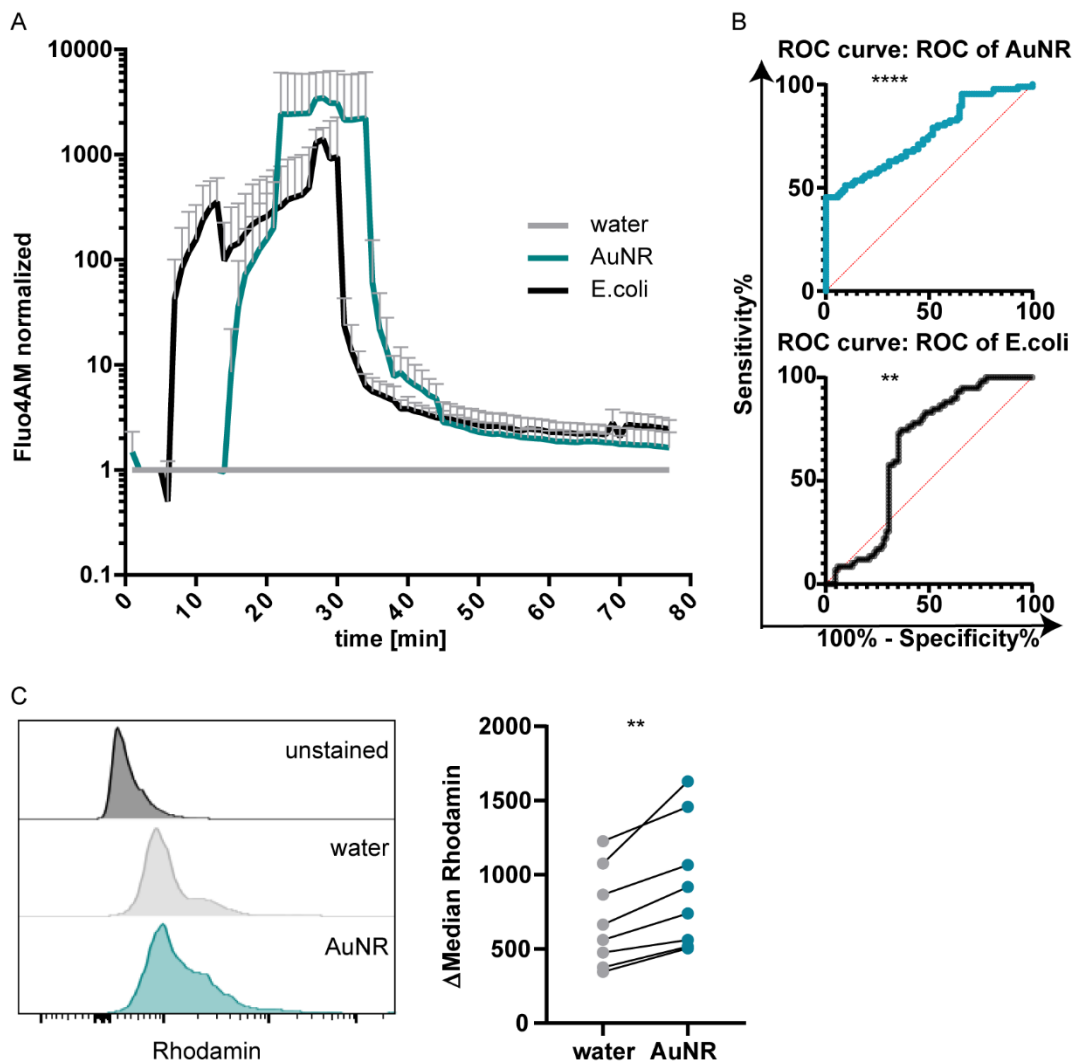


Figure 22: AuNR uptake increases cytosolic Ca^{2+} level.

(A) Isolated PMN were incubated with 4 μM Fluo4AM for 20 min at 37°C. After washing, water (grey), 5000 AuNR / PMN (blue), or *E.coli* (50:1 *E.coli*: PMN, black) were added and fluorescence of cytosolic Ca^{2+} was measured every minute using Synergy 2. Fluorescence intensity was normalized to time point 0 before addition of stimulants and unstimulated water control. (B) Calcium imaging revealed an increase of cytosolic calcium within 30 min comparable to *E.coli* treatment ($n=3$, ROC curve, Wilson/Brown). (C) Whole blood was treated with water (grey) or 5000 AuNR / PMN (blue) for 2 h. ROS production was analyzed using a DiRhodamin staining for 15 min, followed by flow cytometry. The left panel shows an exemplary histogram, the right panel the quantification of 8 independent donors ($n=8$, paired t-test). The statistical significance was defined as **** $p \leq 0.0001$; *** $p \leq 0.001$; ** $p \leq 0.01$; * $p \leq 0.05$. N indicates the number of experimental repetitions, each performed with independent donors.

4.3.6 AUNR UPTAKE ACTIVATES UPR

In order to proof the hypothesis of cellular activation due to ER stress induction upon AuNR uptake, we evaluated the regulation of important ER stress mediators. Using Western Blot, we found significantly increased expression of the chaperone binding immunoglobulin protein (BiP) after 60 min of AuNR treatment (Figure 23). BiP is a key player in UPR since it captures unfolded proteins in the ER preventing their aggregation and thereby activating the three main ER stress sensors, namely activating transcription factor 6 (ATF6), Protein Kinase RNA-like Endoplasmic Reticulum Kinase (PERK) and inositol-requiring enzyme 1 α (IRE α).

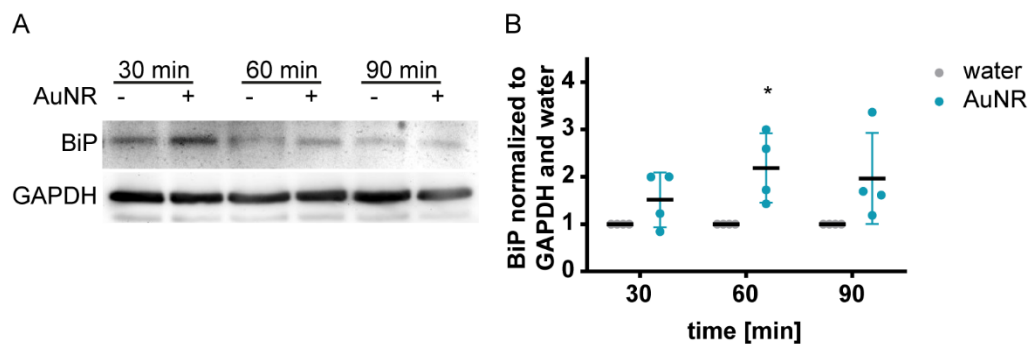


Figure 23: AuNR uptake upregulates BiP.

Isolated PMN were incubated with water (grey), or 5000 AuNR / PMN (blue) for 5 min, 15 min, 30 min, 60 min and 90 min. **(A)** Exemplary SDS PAGE of full PMN lysates of BiP. **(B)** Quantification of BiP expression normalized to GAPDH expression and unstimulated water control (n=4, two-way ANOVA, Bonferroni's multiple comparisons test). The statistical significance was defined as ****p \leq 0.0001; ***p \leq 0.001; **p \leq 0.01; *p \leq 0.05. N indicates the number of experimental repetitions, each performed with independent donors.

4.3.7 AUNR UPTAKE INDUCES EXPRESSION OF LOX1 ON PMN

Upon release of BiP, IRE α dimerizes and splices X-box binding protein 1 (XBP1u to XBP1s), which then translocates to the nucleus and acts as a transcription factor for various genes. It has been shown that BiP is also regulated by XBP1s, creating a positive feedback loop of ER stress induction (Chen *et al.* 2017). To evaluate downstream effects of AuNR-induced ER stress, we measured the level of XBP1s. Surprisingly, we found massive increase in XBP1s upon AuNR treatment compared to water already after 5 min (Figure 24A). We further evaluated XBP1s activity, by performing a fractionated Western Blot and found higher levels of nuclear XBP1s after AuNR treatment compared to unstimulated water control after 5 min (Figure 24B). In a recent study, XBP1s-mediated ER stress has been linked to the expression of lectin-type oxidized LDL receptor 1 (LOX1) in PMN and granulocytic myeloid-derived suppressor cells (PMN-MDSC) (Condamine *et al.* 2016, Nan *et al.* 2018). Considering our findings that AuNR treatment induces ER stress, we analyzed LOX1 expression on PMN and found a striking upregulation after AuNR

treatment at all investigated time points (Figure 24C). These data show that uptake of AuNR-induced impairment in oxidative protein folding and Ca^{2+} homeostasis. This ER stress induction resulted in higher LOX1 expression on PMN surface. Considering the higher ubiquitination status, the cytosolic release of Ca^{2+} , regulation of the protein folding machinery on the transcriptional and protein level, we identified ER stress as main mediator of AuNR-induced activation of PMN *ex vivo*.

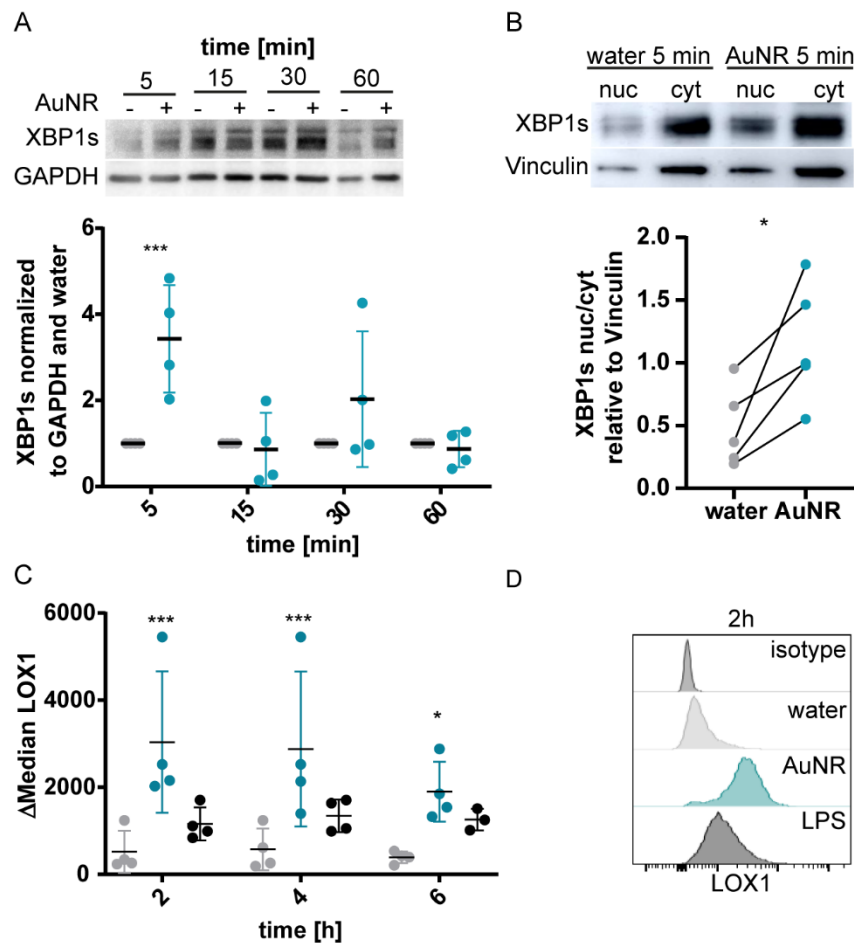


Figure 24: ER stress induces LOX1 expression via XBP1 splicing.

(A) Isolated PMN were incubated with water (grey), or 5000 AuNR / PMN (blue) for 5 min, 15 min, 30 min, or 60 min. Spliced XBP1 was analyzed in full lysates using Western Blot. The upper panel shows an exemplary SDS-PAGE, the lower panel shows the quantification normalized to unstimulated water control (n=4, two-way ANOVA with Sidak's multiple comparisons test). (B) Isolated PMN were exposed to water (grey) or 5000 AuNR / PMN (blue) for 5 min. Using fractionated Western blot, we separately isolated proteins of the cytosol and nuclei. The upper panel shows exemplary SDS-PAGE, the lower panel shows the quantification (n=5, paired t-test). (C) Whole blood was treated with water (grey), 5000 AuNR / PMN (blue) or 10 ng / mL LPS (black) for 2 h, 4 h or 6 h. Surface expression of LOX1 on PMN was analyzed using flow cytometry. The gating strategy is shown in Supplementary Figure 2 (n=4, two-way ANOVA, Dunnett's multiple comparisons test). (D) Exemplary histogram of LOX1 expression on PMN. The statistical significance was defined as ****p ≤ 0.0001; ***p ≤ 0.001; **p ≤ 0.01; *p ≤ 0.05. N indicates the number of experimental repetitions, each performed with independent donors.

4.3.8 LOX1 IS NOT SYNTHESIZED DE NOVO AT SHORT TIME POINTS

Since the AuNR-induced LOX1 induction was very fast, we wondered whether the LOX1 receptor was produced *de novo* or transported from the cytosol to the cell membrane. To test this, we blocked transcription or translation using cycloheximide or actinomycin D. Both compounds, but especially actinomycin D, blocking transcription, reduced the AuNR-induced LOX1 expression on PMN at 4 h but not 2 h (Figure 25). This indicates that there is indeed a higher transcription of LOX1 after AuNR treatment, but this is not the cause of a higher LOX1 expression at early time points up to 2 h.

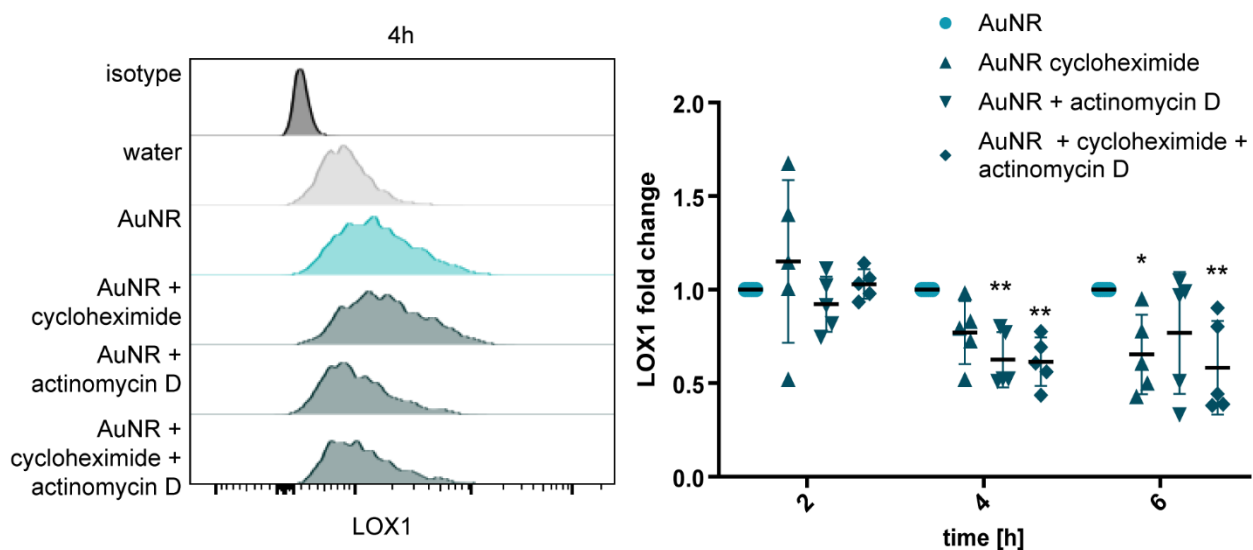


Figure 25: AuNR-induced LOX1 is not produced *de novo* at early time points.

Whole blood was treated with 0.5 μM cycloheximide, or 1 μM actinomycin D in combination with water (grey) or 5000 AuNR / PMN (blue) for 2 h, 4 h, or 6 h at 37 $^{\circ}\text{C}$ in rotation. LOX1 expression was analyzed in flow cytometry. The gating strategy is shown in Supplementary Figure 2. Exemplary histogram (left panel) shows LOX1 expression after 4 h of treatment, the right panel shows the quantification of LOX1 expression after inhibition (dark blue) normalized to AuNR treatment without inhibition (light blue) ($n=5$, two-way ANOVA, Dunnett's multiple comparisons test). The statistical significance was defined as **** $p \leq 0.0001$; *** $p \leq 0.001$; ** $p \leq 0.01$; * $p \leq 0.05$. N indicates the number of experimental repetitions, each performed with independent donors.

4.3.9 ER STRESS MEDIATES IL8 SECRETION AND LOX1 EXPRESSION

In order to understand the molecular interplay of AuNR-induced ER stress and pro-inflammatory activation of PMN, we utilized inhibitors of ER stress and examined their effect on AuNR-induced neutrophil activation. To this end, we used inhibitors blocking specific pathways of UPR, namely IRE α -, XBP1s- and PERK- as well as an overall inhibitor (N-acetylcysteine) blocking several mediators in ER stress, additionally to ROS production (inhibitors are listed in Table 7). We found significantly reduced secretion of IL8 after IRE α inhibition compared to AuNR treatment alone (Figure 26A). Furthermore, AuNR-induced LOX1 expression was reduced after pretreatment with

IRE α inhibitor and overall inhibitor (Figure 26B), but did not affect the AuNR-induced regulation of CD182 and CD11b expression, or ROS production (Supplementary Figure 7). Therefore, we concluded that AuNR-induced LOX1 expression and IL8 secretion were regulated directly *via* IRE α -mediated ER stress response, whereas CD182 and CD11b expression, or ROS production were not directly regulated *via* ER stress induction.

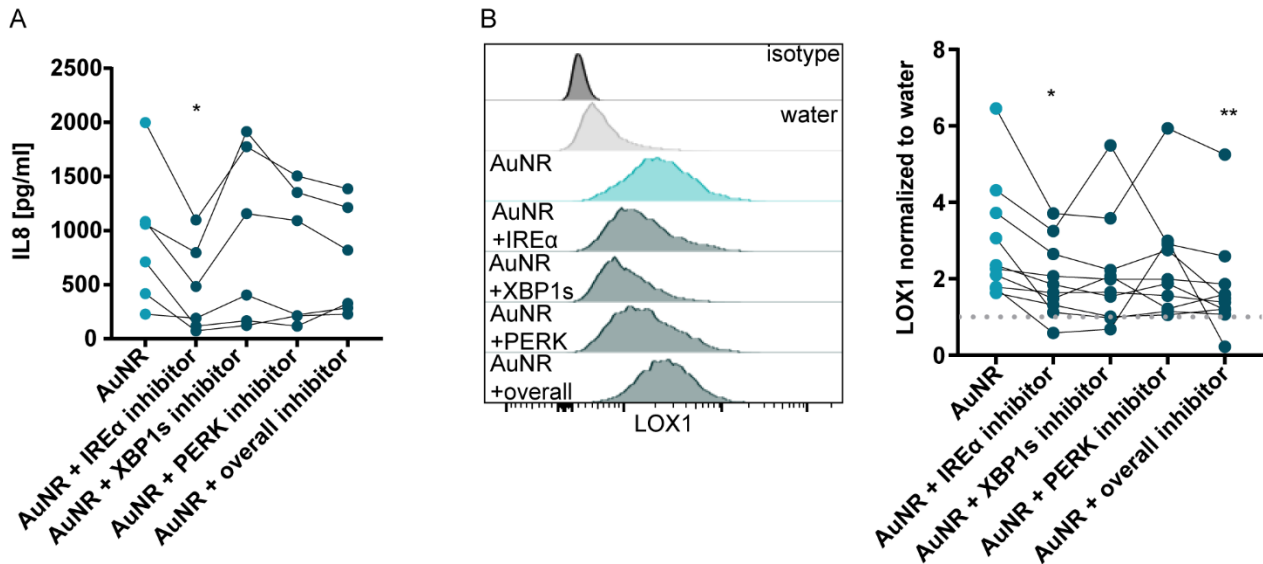


Figure 26: AuNR-induced IL8 secretion and LOX1 expression is ER stress dependent.

Whole blood was incubated with ER stress inhibitors (listed in Table 7) for 30 min at 37°C in rotation prior to addition of water (grey) or 5000 AuNR / PMN (blue). Whole blood was incubated for another 2 h. All samples were divided for **(A)** IL8 ELISA (of the serum) and **(B)** LOX1 surface marker analysis (antibodies are listed in Table 8) using flow cytometry. The gating strategy is shown in Supplementary Figure 2. The left panel shows an exemplary histogram of LOX1 expression after 2 h ER stress inhibition and AuNR treatment, the right panel shows LOX1 expression normalized to respective unstimulated water control or water with respective ER stress inhibitor (n=11, one-way ANOVA, Dunnett's multiple comparisons test). The statistical significance was defined as ****p \leq 0.0001; ***p \leq 0.001; **p \leq 0.01; *p \leq 0.05. N indicates the number of experimental repetitions, each performed with independent donors.

4.4 AUNR ACTIVATED AN AUTOCRINE ACTIVATION LOOP

4.4.1 LOX1 MEDIATED ACTIVATION LOOP

Since ER stress inhibitors reduced LOX1 and IL8, we wondered whether these regulations were occurring independent from, or conditioned each other. To evaluate this, we performed correlation and time course analyses. We found a positive correlation between LOX1 expression and IL8 secretion (Figure 27A), as well as LOX1 expression and ROS production (Figure 27B). Time course analysis identified LOX1 as first marker being regulated by AuNR uptake showing a 2-fold higher expression already after 30 min compared to unstimulated water control (Figure 27C+D). LOX1 expression peaked after 2 h around 15-fold higher expression compared to water. IL8

secretion started after 2 h of AuNR incubation (Figure 27E). Similarly, ROS production was upregulated by 1.33-fold after 2h of AuNR treatment compared to water (Figure 27F).

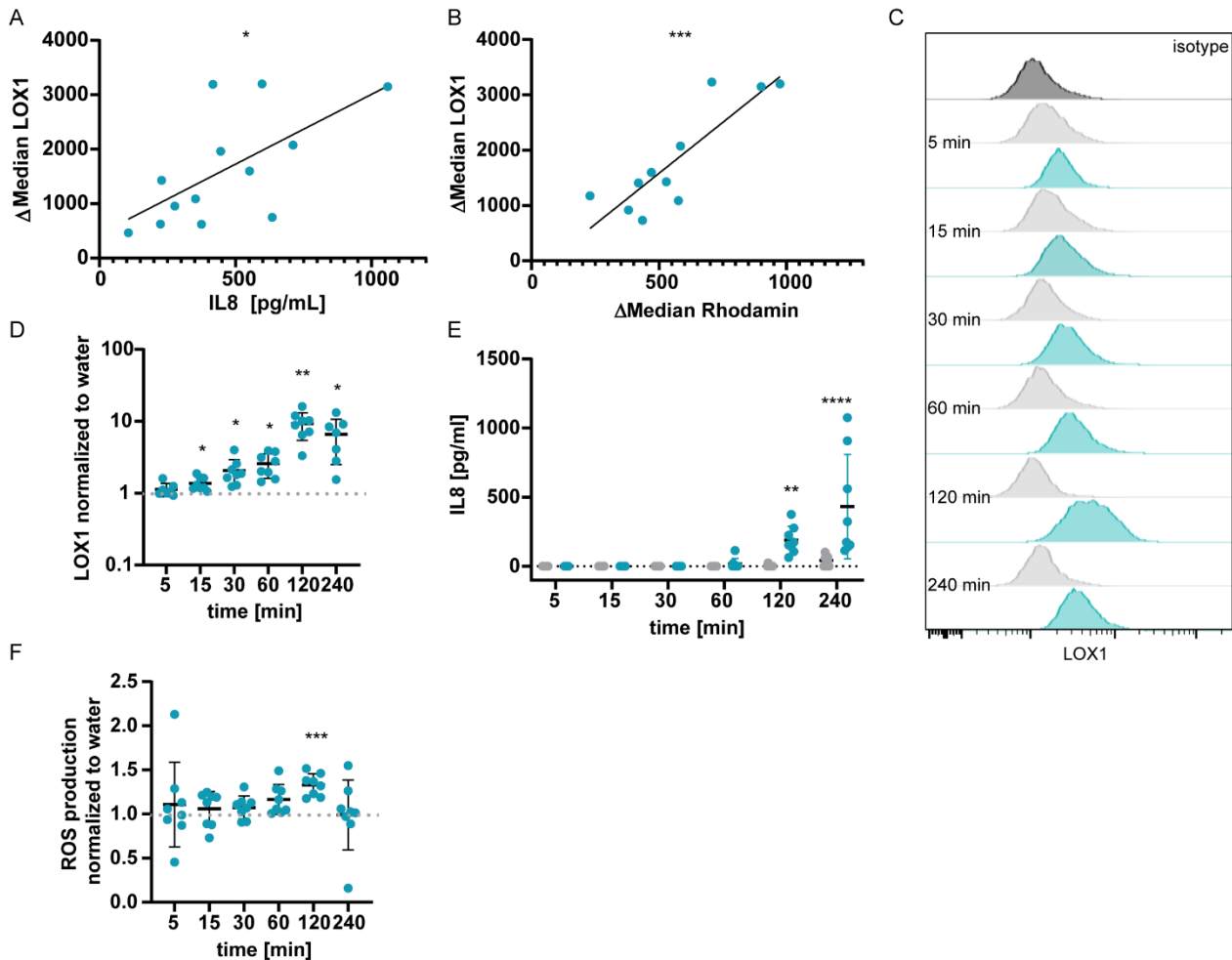


Figure 27: AuNR-induced LOX1 expression correlates with IL8 secretion and ROS production.

Whole blood was incubated with 5000 AuNR / PMN (blue) for 2 h at 37 °C in rotation. All samples were divided for serum isolation (IL8 ELISA), LOX1 expression measurement, or ROS production measurement by fluorescence intensity of Rhodamin using flow cytometry. **(A)** Correlation of LOX1 Median and IL8 secretion after 2 h AuNR treatment (n=13, Pearson correlation). **(B)** Correlation of LOX1 and Rhodamin Median after 2 h AuNR treatment (n=11, Pearson correlation). **(C-F)** Whole blood was incubated with water (grey) or 50000 AuNR / PMN (blue) for 5 min, 15 min, 30 min, 60 min, 120 min and 240 min at 37 °C in rotation and **(C+D)** LOX1 expression (n=8, one-way ANOVA with Dunnett's multiple comparisons test), **(E)** IL8 secretion (n=8, two-way ANOVA with Sidak's multiple comparisons test) and **(F)** ROS production (n=8, one-way ANOVA with Dunnett's multiple comparisons test) were analyzed as described above. The statistical significance was defined as ****p ≤ 0.0001; ***p ≤ 0.001; **p ≤ 0.01; *p ≤ 0.05. N indicates the number of experimental repetitions, each performed with independent donors.

Our data suggest LOX1 as being the first marker regulated upon AuNR treatment. Since ER stress inhibitors reduced LOX1 and IL8, we explored a potential positive autocrine activation mechanism. To evaluate the functional involvement of LOX1, we performed inhibition experiments using a LOX1-blocking antibody. LOX1 blocking reduced the AuNR-induced IL8 secretion and ROS

production significantly, showing that both, IL8 secretion and ROS production, partially depend on LOX1 (Figure 28A+B). IL8 and ROS were not altered by mIgG1 isotype control (Supplementary Figure 8). Concluding, AuNR uptake induced a higher LOX1 surface expression on PMN that further accelerated the pro-inflammatory IL8 secretion. To verify that LOX1 mediates this pro-inflammatory activation, we experimentally primed PMN with AuNR and subsequently stimulated the primed PMN with oxLDL DiL, a fluorescently labelled functional ligand for LOX1. AuNR priming resulted in a significantly higher uptake of oxLDL DiL (Figure 28C). Furthermore, accelerated oxLDL DiL uptake resulted in higher levels of ROS production and slightly higher IL8 secretion (Figure 28D+E).

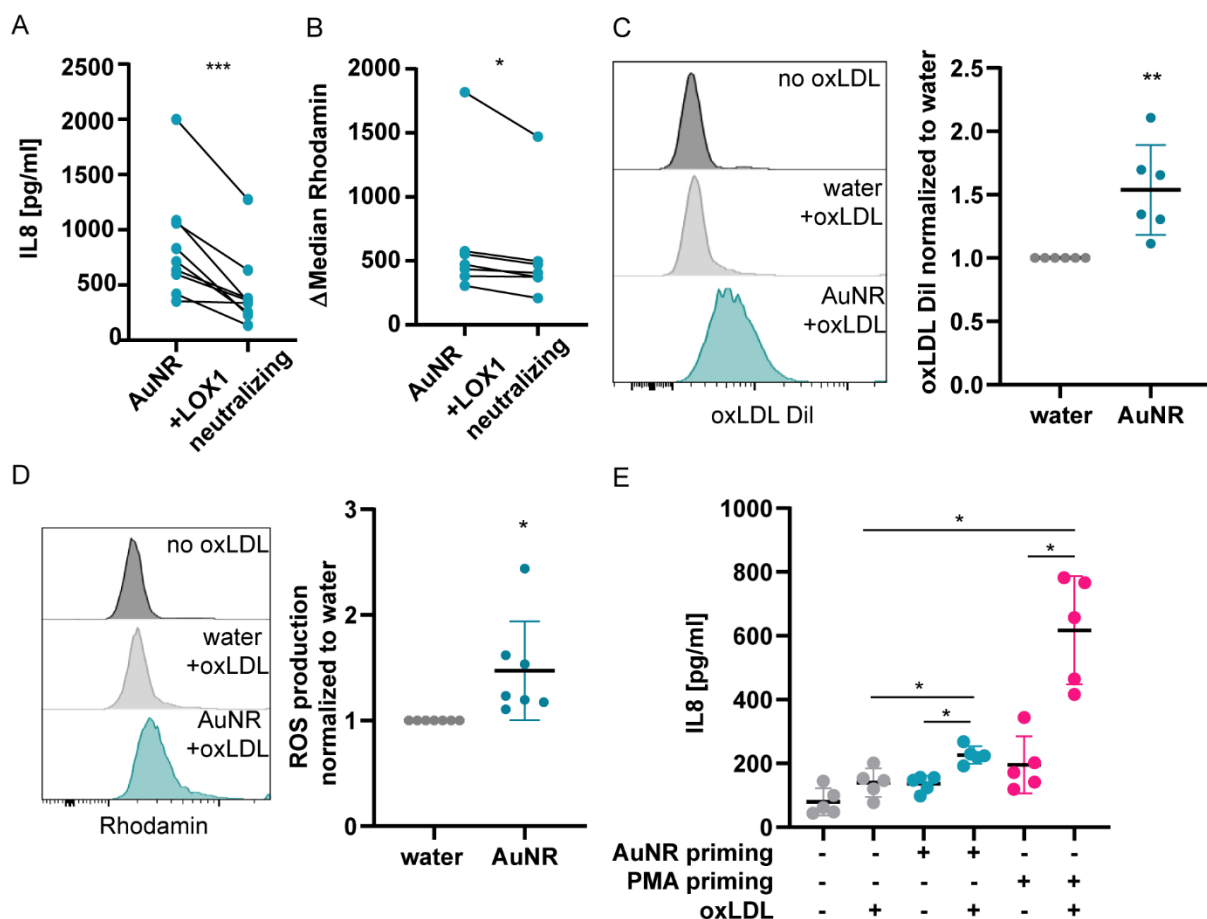


Figure 28: AuNR-induced LOX1 mediates ROS production and IL8 secretion.

Whole blood was incubated with a LOX1 neutralizing antibody (1 $\mu\text{g} / \text{mL}$) for 30 min prior to addition of water (grey), or 5000 AuNR / PMN (blue) and cultured for 2 h at 37 $^{\circ}\text{C}$ in rotation. **(A)** IL8 secretion was measured *via* ELISA and **(B)** ROS production measurement by fluorescence intensity of Rhodamin in flow cytometry (n=8, paired t-test). **(C)** Isolated PMN were primed with water (grey) or 5000 AuNR / PMN (blue) for 30 min. Subsequently, AuNR were removed by washing with PBS and PMN were treated with 50 $\mu\text{g} / \text{mL}$ oxLDL DiL for 90 min. Fluorescence intensity of oxLDL DiL was analyzed in flow cytometry. The left panel shows an exemplary histogram, the right panel the quantification of the median fluorescence intensity normalized to unstimulated water control (n=6, unpaired t-test). **(D)** Measurement of Rhodamin intensity using flow cytometry. The left panel shows an exemplary histogram, the right panel shows the quantification normalized to unstimulated water control (n=7, unpaired t-test). **(E)** Isolated PMN were primed for 30 min

with water (grey), 5000 AuNR / PMN (blue), or 20 nM PMA (pink). Subsequently, stimuli were removed by washing with PBS and PMN were treated with 50 µg / mL oxLDL for 90 min. IL8 secretion upon no, AuNR or PMA priming in combination with oxLDL was measured using an IL8 ELISA (n=5, one-way ANOVA, Dunnett's multiple comparisons test). The statistical significance was defined as ****p ≤ 0.0001; ***p ≤ 0.001; **p ≤ 0.01; *p ≤ 0.05. N indicates the number of experimental repetitions, each performed with independent donors.

4.4.2 IL8-CD182 MEDIATED ACTIVATION LOOP

AuNR priming with oxLDL treatment did not induce massive secretion of IL8 (Figure 28E). Additionally, we showed reduced secretion of IL8 upon ER stress inhibition (Figure 26A), so we wondered, whether IL8 is also secreted in an ER stress dependent manner, and sustains PMN activation via a feed-forward loop (2 h and later) after the initial activation (30 min) took place. In this loop, IL8 might act on ROS production and LOX1, creating a vicious cycle of activation between LOX1, IL8 and its receptor CD182. We blocked IL8 by using a neutralizing antibody and by pharmacologically blocking CD182 signaling. Both inhibitors reduced the AuNR-induced LOX1 expression after 2 h of incubation (Figure 29A). Additionally, IL8 neutralizing, as well as CD182 inhibition resulted in reduced AuNR-induced CD11b expression (Figure 29B). Interestingly, we could not observe this reduction in CD11b when neutralizing LOX1 or inhibiting ER stress suggesting that IL8 may induce autocrine activation effects that are independent of LOX1 (Supplementary Figure 7 and Supplementary Figure 9). We further analyzed ROS production and found no reduction in ROS production by IL8 neutralization or CD182 inhibition (Figure 29C). Concluding, IL8 signaling *via* CD182 promotes LOX1 and CD11b expression, creating a vicious cycle of surface expression and interleukin secretion. This results in a pro-inflammatory environment with potential immunopathological effects. Interestingly, blocking of CD182 turned out to be more efficient than blocking IL8 using a neutralizing antibody, although IL8 can also act *via* CD181. This further identifies CD182 as major mediator of AuNR-induced inflammatory activation (Figure 29D).

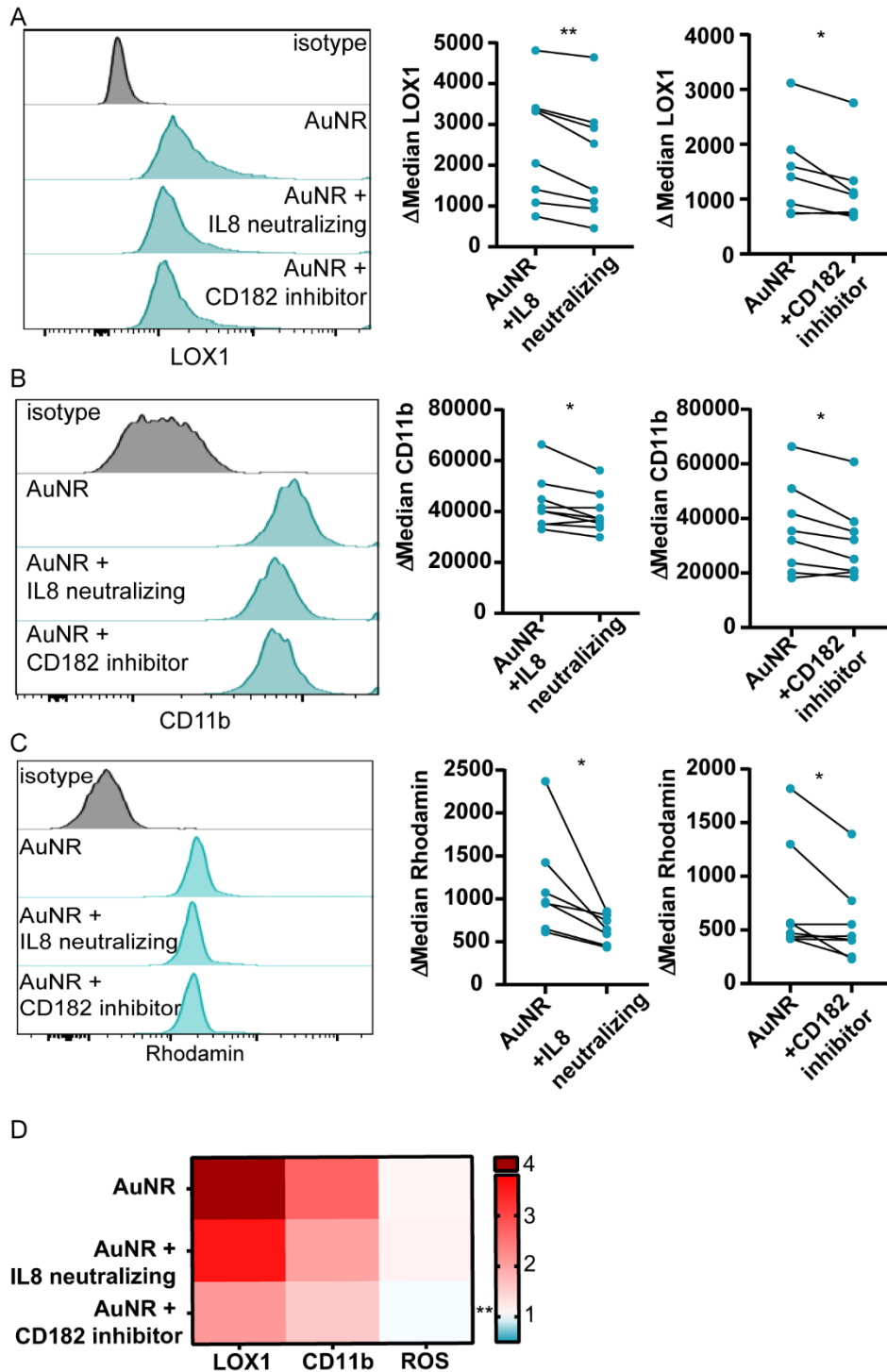


Figure 29: IL8 signaling blockade reduces AuNR-induced activation.

Whole blood was incubated with an IL8 neutralizing antibody (1 μ g / mL) or CD182 inhibitor (AZD, 10 μ M) for 30 min prior to addition of water (grey), or 5000 AuNR / PMN (blue) for 2 h at 37 $^{\circ}$ C in rotation. **(A)** The left panel shows an exemplary histogram of AuNR-induced LOX1 expression with additional IL8 neutralizing or CD182 inhibition, measured in flow cytometry. The gating strategy is shown in Supplementary Figure 2. The middle panel shows the quantification of IL8 neutralizing reduced LOX1 expression (n=8, paired t-test), the right panel shows the quantification of CD182 inhibition reduced LOX1 expression (n=7, paired t-test). **(B)** The left panel shows an exemplary histogram of AuNR-induced CD11b expression with additional IL8 neutralizing or CD182 inhibition (same concentrations as above) measured in flow cytometry. The middle panel shows the quantification of AuNR-induced CD11b expression with additional IL8 neutralizing (n=9,

paired t-test), whereas the right panel shows the quantification of AuNR-induced CD11b with additional CD182 inhibition (n=8, paired t-test) measured in flow cytometry. **(C)** The upper panel shows an exemplary histogram of AuNR-induced ROS production with additional IL8 neutralizing or CD182 inhibition measured by fluorescence intensity of Rhodamin in flow cytometry. Left bottom panel shows IL8 neutralizing of AuNR-induced ROS production (n=7, paired t-test), while the right bottom panel shows CD182 inhibition of AuNR-induced ROS production (n=8, paired t-test). **(D)** Combining LOX1 and CD11b expression with ROS production, we found a significant reduction of AuNR-induced effects after CD182 inhibition (n=11, two-way ANOVA, Dunnett's multiple comparisons test). The statistical significance was defined as ****p ≤ 0.0001; ***p ≤ 0.001; **p ≤ 0.01; *p ≤ 0.05. N indicates the number of experimental repetitions, each performed with independent donors.

4.5 AUNR UPTAKE DID NOT AFFECT T CELL SUPPRESSIVE CAPACITY OF PMN

Condamine and colleagues observed ER stress-induced LOX1 expression on PMN and PMN-MDSC *ex vivo* in 2016 (Condamine *et al.* 2016). They found LOX1 being expressed on PMN-MDSC and presented it as potential population marker for these pathological expanded cells. Nevertheless, they also showed that induction of ER stress results in LOX1 expression on healthy PMN. We found persisting LOX1 induction *via* XBP1 splicing by AuNR uptake (Figure 24C). The key feature of PMN-MDSC is the suppression of T cell proliferation (Bronte *et al.* 2016). To test a potential immunosuppressive capacity of PMN upon AuNR uptake, we performed a T cell suppression assay. For this, whole blood was primed with water or AuNR. We ensured LOX1 expression upon AuNR treatment by flow cytometry (Figure 30A) and PMN were sorted according to their CD66b expression. Autologous T cells were either used unstimulated (-stim), or activated using CD28 and CD3 antibodies (+stim). Stimulated T cells were exposed to water- or AuNR-primed PMN and proliferation of CD3⁺, CD4⁺ and CD8⁺ T cells was analyzed after four days of co-incubation. Subsets of T cells were divided according to their expression of population markers (Figure 30B). We did not observe any immunosuppressive capacity of PMN on T cells irrespective of PMN priming (Figure 30C-F). This further supports the hypothesis that LOX1 expression and ER stress are not necessarily turning PMN immunosuppressive. Furthermore, we show that LOX1 surface expression is not suitable as marker for PMN-MDSC, since LOX1 is inducible and not functionally involved in an immunosuppressive phenotype. Our data shows, that LOX1 expression is a rather independent feature of ER stress induction, especially when the IREα-mediated UPR is activated.

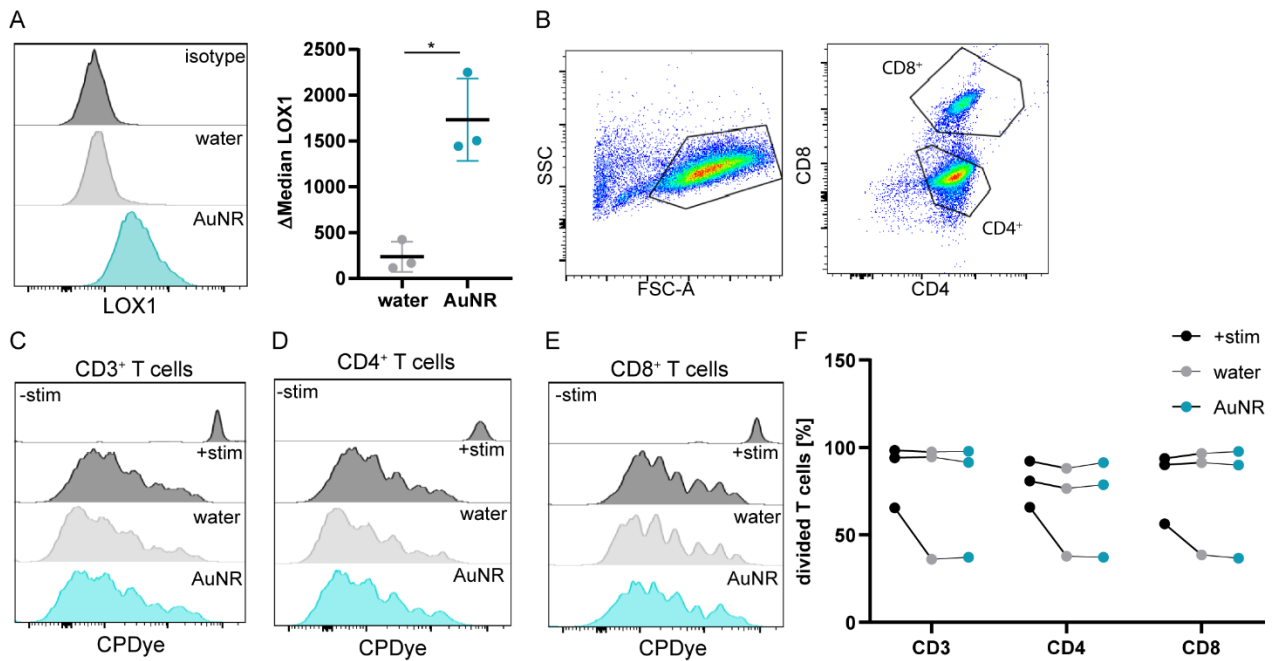


Figure 30: AuNR uptake does not affect PMNs' ability to suppress T cell proliferation.

Whole blood was treated with water (grey) or 5000 AuNR / PMN (blue) for 2 h. **(A)** Afterwards, 60 μ L of primed whole blood was removed for LOX1 staining, to ensure AuNR-induced a LOX1 surface expression ($n=3$, paired t-test). The rest of whole blood was treated with a fluorescently labelled CD66b antibody to stain PMN. PMN were sorted by Kirsten Bruderek using the BD FACS Aria II cell sorter of IMCES. Autologous T cells were isolated and stained using 5 μ M Cell proliferation dye (CPDye). Proliferation of T cells was induced by antibody coating of the culture plate with CD28 and CD3. T cells and PMN were cultured in a 2:1 ratio in arginine-low medium for 4 days. Then, CD4⁺ and CD8⁺ T cells were stained and proliferation of T cells was analyzed in flow cytometry. **(B)** Gating strategy of activated T cells. For negative control (-stim) T cells were not activated by CD3/CD28, for positive control T cells were activated without further addition of PMN (+stim). **(C-E)** Exemplary histogram of CD3⁺-, CD4⁺- and CD8⁺-T cells. **(F)** Quantification of percentage of divided T cells of all conditions. ($n=3$, two-way ANOVA, Dunnett's multiple comparisons test). The statistical significance was defined as **** $p \leq 0.0001$; *** $p \leq 0.001$; ** $p \leq 0.01$; * $p \leq 0.05$. N indicates the number of experimental repetitions, each performed with independent donors.

4.6 PMN PRIMED WITH AUNR STILL PHAGOCYTOSE PATHOGENS

In the last sections we took a detailed look on the molecular interaction of AuNR with PMN, elucidating the pathway of activation and showing potential immunopathological effects of PMN activation. PMN have a high intrinsic phagocytic capacity and contain granules densely packed with antimicrobial proteins (Faurischou *et al.* 2003). Their major function is the clearance of pathogens. Since PMN rapidly took up large quantities of AuNR, we investigated whether this uptake would compromise the phagocytosis of *E.coli*, and thus limit the anti-microbial capacity of PMN. We found that AuNR treatment, neither prior to *E.coli* nor simultaneously, compromised the phagocytosis of *E.coli* by PMN (Figure 31A+B). Furthermore, *E.coli* addition did not impede the amount of phagocytosed AuNR by PMN (Figure 31A+C). Correlation analysis revealed a positive correlation of the uptake of AuNR and *E.coli* when treated simultaneously (Figure 31D).

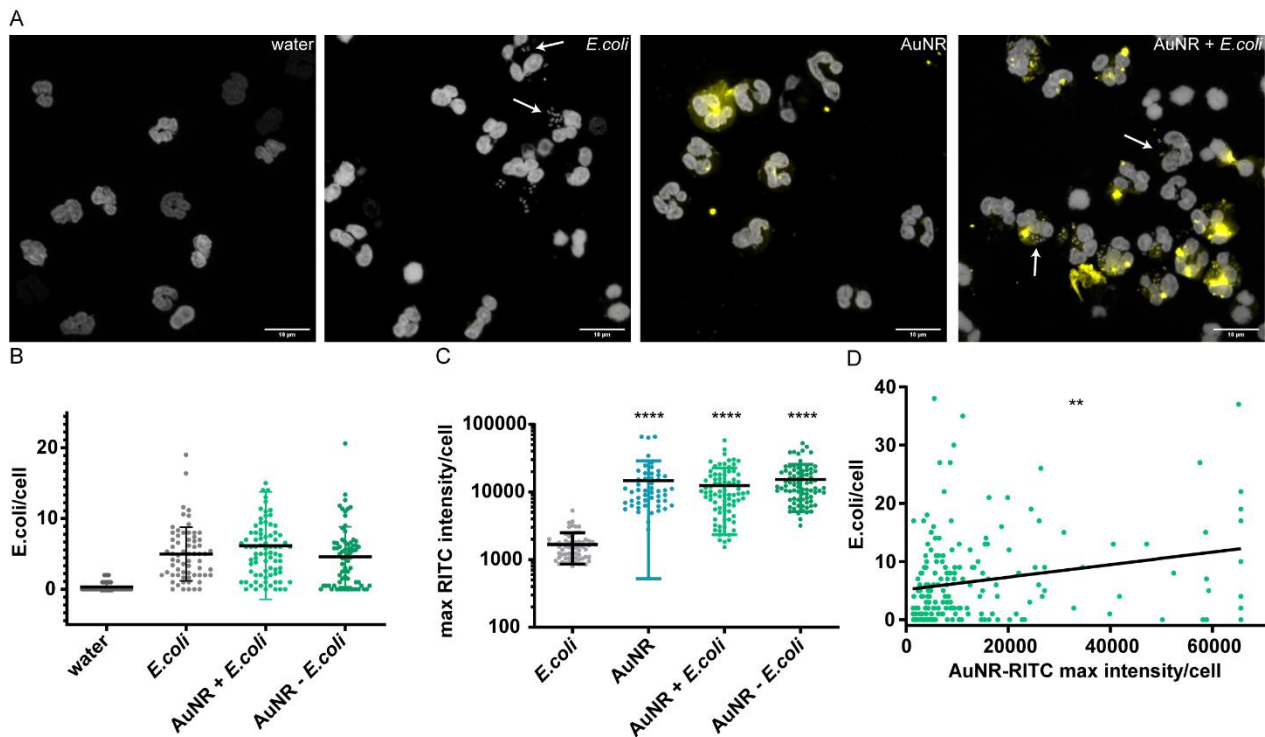


Figure 31: AuNR do not impede phagocytosis of *E. coli* by PMN.

Isolated PMN were treated with water (grey), 5000 AuNR-RITC / PMN (blue), or *E. coli* (50:1 *E. coli*: PMN) for 30 min, as well as AuNR in combination with *E. coli* for 30 min (AuNR + *E. coli*), or AuNR for 30 min, followed by *E. coli* treatment (AuNR - *E. coli*). Nuclei were counterstained with DAPI and confocal microscopy (63x magnification objective) was performed, in order to evaluate the uptake of *E. coli* and AuNR. **(A)** Exemplary pictures of unstimulated water control, *E. coli*, AuNR-RITC (yellow) and combinational treatment of AuNR and *E. coli*. Cell-associated *E. coli* were determined by drawing a 10 μm circle around PMN nuclei and analyzing particles in Fiji ImageJ 1.53c. White Arrows indicate accumulation of *E. coli* in PMN. Scale Bar = 10 μm . **(B)** Quantification of the uptake of *E. coli* ($n=3$, one-way ANOVA, multiple comparisons). **(C)** Quantification of AuNR-RITC uptake measured by maximum intensity per cell ($n=5$, one-way ANOVA, multiple comparisons). **(D)** Data of 5 donors was pooled and uptake of *E. coli* and AuNR was correlated, each dot represents a single cell (Pearson correlation). The statistical significance was defined as **** $p \leq 0.0001$; *** $p \leq 0.001$; ** $p \leq 0.01$; * $p \leq 0.05$. N indicates the number of experimental repetitions, each performed with independent donors.

4.7 AUNR INDUCE FUNCTIONAL CHANGES IN PMN OF CANCER PATIENTS

Certain effects of AuNR (induction of ER stress, LOX1 expression) on PMN are reminiscent of cell biological changes observed in PMN from cancer patients. To evaluate, whether AuNR treatment induces comparable pro-inflammatory effects in PMN from cancer patients, which are already altered by a malignant disease, we analyzed the expression of CD11b, CD182 and LOX1, as well as the production of ROS and IL8 secretion upon AuNR treatment. Detailed information about tumor location and stage is described in Supplementary Table 1. Similar to healthy donors (HD), PMN from cancer patients responded to AuNR by a reduction in CD182 and a higher expression of CD11b and LOX1 (Figure 32A-D). Furthermore, PMN of patients produced more

ROS and secreted more IL8 after AuNR challenge (Figure 32E). These data show that PMN from cancer patients and healthy donors show a similar cell biological response to AuNR.

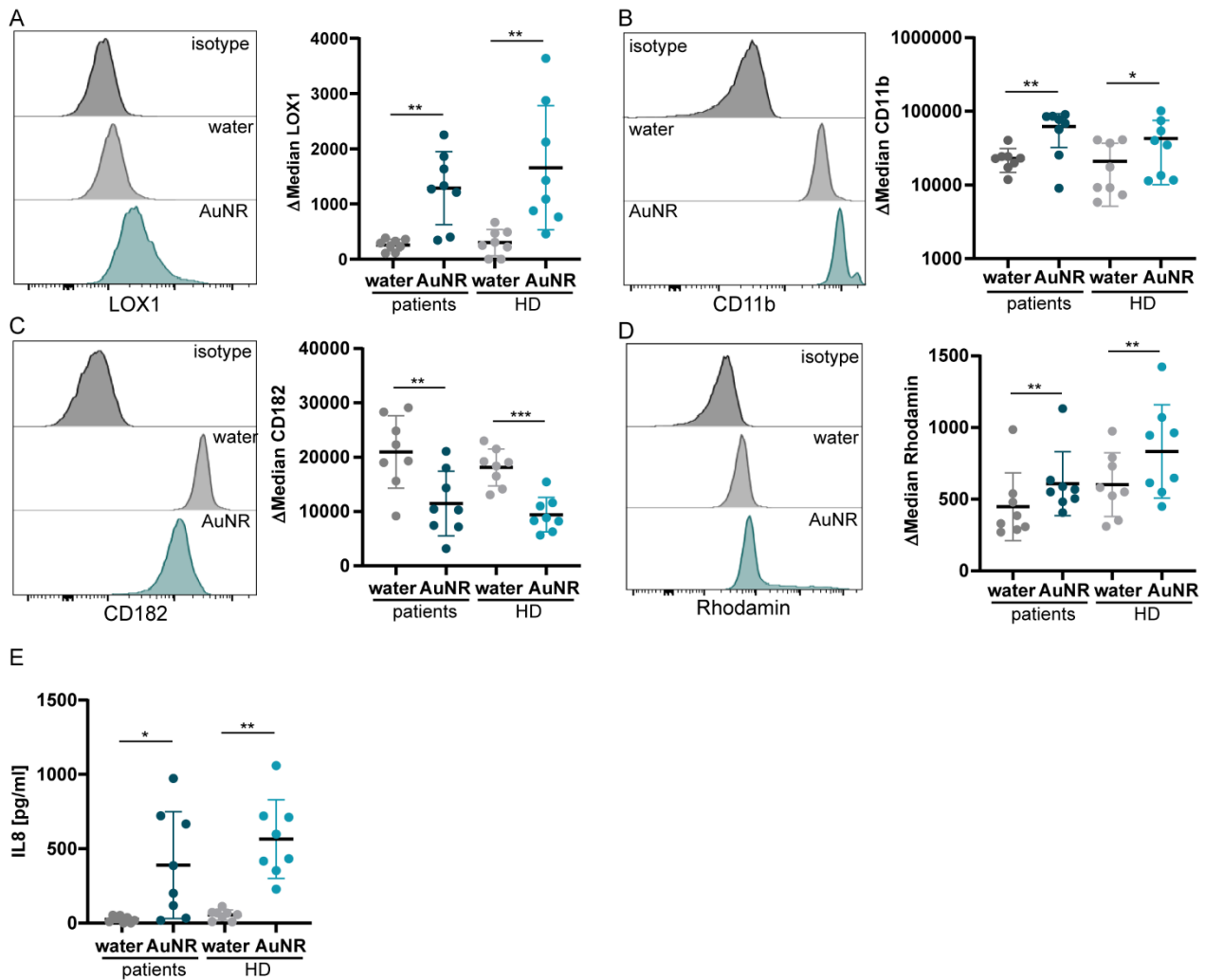


Figure 32: PMN of cancer patients react comparable to AuNR as healthy donor PMN.

Whole blood of head and neck cancer patients (patients) or healthy donors (HD) was treated with water (grey) or 5000 AuNR / PMN (blue) for 2 h. Subsequently, samples were divided for the staining of surface markers and staining for ROS production with DiRhodamin using flow cytometry and IL8 ELISA of the serum to determine secretion of IL8. Left panel shows an exemplary histogram of patient PMN, right panel the quantification of cancer patients and HD. Data of **(A)** LOX1, **(B)** CD11b and **(C)** CD182 expression as well as **(D)** ROS production is shown. **(E)** Serum was isolated to evaluate the level of secreted IL8. Significant regulation between water and AuNR treatment was analyzed using a paired-t test (n=8). Details of tumor localization, t and N staging can be found in Supplementary Table 1. The gating strategy is shown in Supplementary Figure 2. The statistical significance was defined as ****p \leq 0.0001; ***p \leq 0.001; **p \leq 0.01; *p \leq 0.05. N indicates the number of experimental repetitions, each performed with independent donors.

4.8 AUNR AS PHOTOSENSITIZERS FOR SPECIFIC PTT

Absolute requirement for the development of efficient PTT is the precise targeting of photosensitizers to the desired cells. Many groups investigated PTT on murine tumor models showing promising results with respect to tumor shrinkage, biocompatibility and overall survival (M. R. Ali *et al.* 2016; M. R. Ali *et al.* 2017a; M. R. K. Ali *et al.* 2017b; Almeida *et al.* 2014; Camerin *et al.* 2005; Dreaden *et al.* 2011; X. Huang *et al.* 2006; Z. Li *et al.* 2016; Yin *et al.* 2017; L. Zhang *et al.* 2019; Zheng *et al.* 2020). However, the transition from murine to human studies is still lacking. At least in part, this is caused by a lack of understanding on the molecular interplay between AuNP and human immune cells, especially phagocytic immune cells with their intrinsic ability to eliminate AuNP from circulation and tissue. However another cause is the targeting efficiency of nanotherapeutics on a cellular level. Therefore, the second part of this thesis focuses on efficient targeting of immune cells with special focus on reducing the unspecific (non-targeted) phagocytosis by PMN or monocytes.

4.8.1 TARGETING IMMUNE CELLS WITH ANTIBODY COATED AUNR

In order to enable cell-type specific AuNR-targeting, our cooperation partners from AG Schlücker (Department of Chemistry, University of Duisburg-Essen) covalently bound monoclonal antibodies against population markers of PMN, monocytes or T cells and their respective isotype antibodies (anti- (α)CD11b, α IgG2b, α CD3, α mIgG2a) to the surface of AuNR. Successful binding was analyzed by IgG test stripes by members of AG Schlücker (data not shown). To validate the specific binding of AuNR to target cells, we isolated PBMC and PMN and subsequently mixed PBMC and PMN in a 1:1 ratio. Following this, the mixed immune cell culture was treated with AuNR-antibody (AuNR-AB) conjugates. To ensure specific binding of AuNR-AB we removed the excess of AuNR-AB and stained all samples with a secondary antibody (Table 9). T cells, monocytes and PMN were identified by their morphology, with PMN showing higher SSC than monocytes and T cells and the difference in cell size (FSC-A) as shown in Supplementary Figure 3. Experiments show that T cells were specifically recognized by α CD3 antibody alone and α CD3 antibody conjugated AuNR (AuNR- α CD3), while isotope controls showed no binding (Figure 33A). Surprisingly, this difference between isotope and cell-specific AuNR-AB was not observed for the binding of AuNR- α CD11b compared to its isotype AuNR- α IgG2b to monocytes (Figure 33B), or PMN (Figure 33C). Unexpectedly, the isotype-coupled AuNR (AuNR- α IgG2b) showed an even more pronounced fluorescence intensity than AuNR- α CD11b (Figure 33D). To understand what caused this unspecific targeting, we performed confocal microscopy and found

that AuNR-AB were located within PMN. This intracellular location shows that AuNR-AB were randomly phagocytosed, irrespective of the specificity of the antibody (Figure 33E-I). Contrary to that, T cells showed a membranous staining of AuNR- α CD3, without penetration of the cellular membrane (Figure 33G). These data suggest that targeting of non-phagocytic (T) cells by AuNR-AB is feasible, while phagocytic human immune cells show strong non-antibody-mediated binding and uptake of AuNR-AB conjugates. Furthermore, these data emphasize the need for the development of functionalized AuNR that are not phagocytosed by PMN or monocytes. Especially considering the immunopathological effects of AuNR to PMN, described in the first part of this thesis.

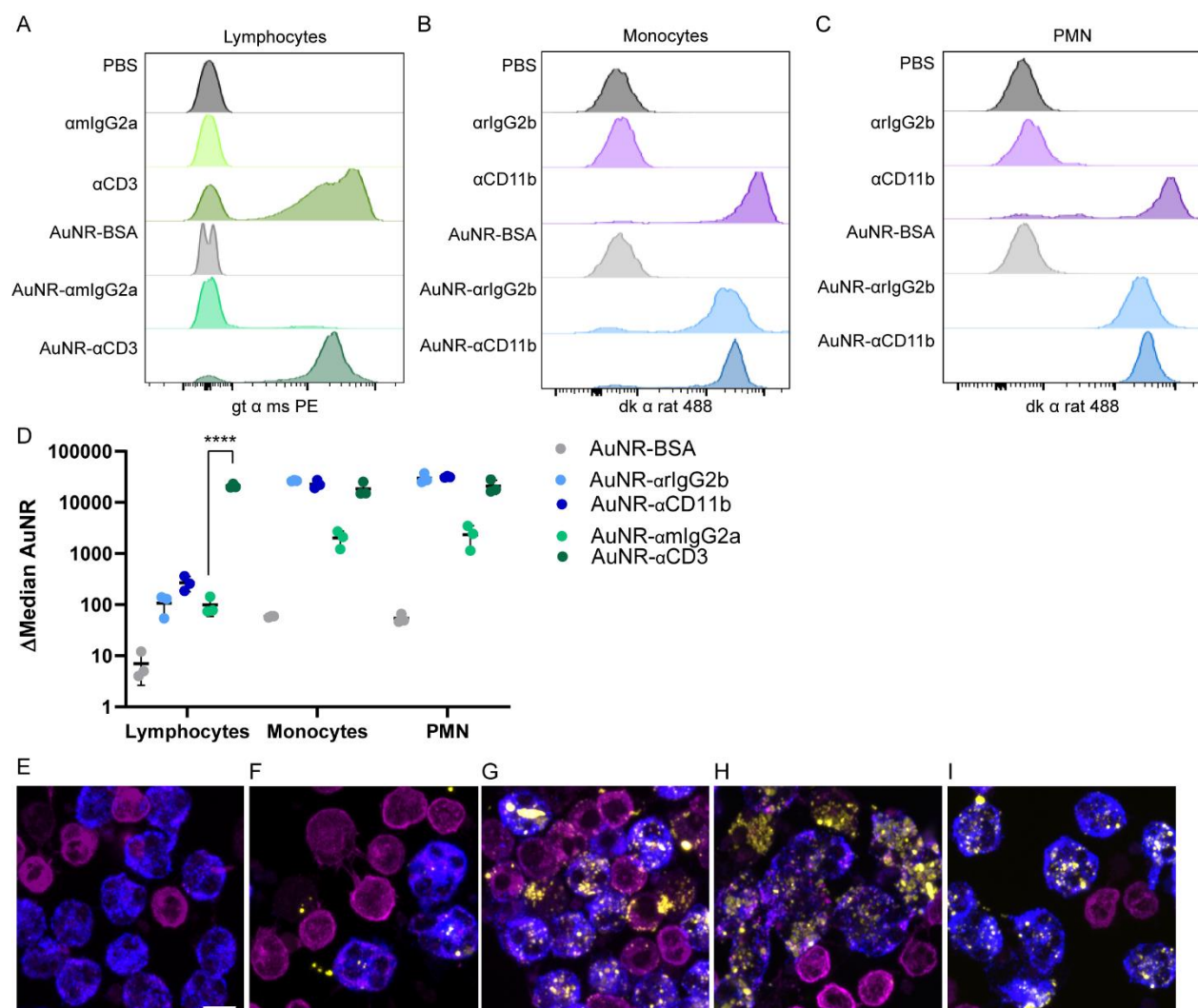


Figure 33: Phagocytic immune cells impede antibody-mediated binding of AuNR.

(A-D) Flow cytometry experiments were performed by Kim Lamers. (A-C) isolated PBMC or isolated PMN were mixed in a 1:1 ratio. In the following, the multicellular culture was either stained with single antibodies (arlG2b, α CD11b, amlgG2a, α CD3), treated with PBS, or with 5000 AuNR / cell, coated with respective antibodies or BSA for 30 min. After washing with PBS, cells were stained with a secondary antibody (Table 9) for 30 min at 37 °C. Subsequently, cells were gated according to their morphology (Supplementary Figure 3) and analyzed via flow cytometry. Exemplary histogram for (A) lymphocytes, (B) monocytes and (C)

isolated PMN. **(D)** Quantification of the fluorescence intensity of differentially coated AuNR (-BSA, -αIlgG2b, -αCD11b, -αIlgG2a, -αCD3) of all 3 populations analyzed by flow cytometry (n=3, two-way ANOVA, Tukey's multiple comparisons test). **(E)** Isolated PMN and PBMCs were mixed in a 1:1 ratio and treated with PBS, or 5000 fluorescently labelled **(F)** αIlgG2a-, **(G)** αCD-3-, **(H)** αIlgG2a-, or **(I)** αCD11b-AuNR / cell for 30 min. Confocal microscopy revealed unspecific uptake of AuNR (yellow) by PMN (blue), whereas T cells (pink) were targeted with AuNR-αCD3. Scale bar = 5 μm. The statistical significance was defined as ****p ≤ 0.0001; ***p ≤ 0.001; **p ≤ 0.01; *p ≤ 0.05. N indicates the number of experimental repetitions, each performed with independent donors.

4.8.2 BINDING OF ANTIBODY-COUPLED AUNR TO NON-PHAGOCYtic T CELLS

Earlier studies performed by other groups spotlighted that the physico-chemical properties and size of particulate materials, such as nanoparticles, influence their uptake by phagocytes (Gustafson *et al.* 2015, Bisso *et al.* 2018). In order to gain further insight into the parameters that influence uptake of AuNP by PMN and to develop more efficient AuNR targeting of specific antigens, evading phagocytosis by immune cells, we modulated AuNP properties. To this end, we compared the binding efficiency of antibody coupled gold nanorods (AuNR) and gold nanospheres (AuNSPH) of 15 nm, 30 nm or 60 nm diameter in whole blood assays. Whole blood represents a competitive multi-cellular environment with a mixture of non-phagocytic (T cells) and phagocytic cells (PMN). This provides answers to two questions: Do phagocytes impede specific binding of AuNR-AB to target cells? And does size and shape affect the non-targeted “unspecific” phagocytosis of AuNP by PMN?

In our experiments, non-phagocytic T cells were specifically targeted by AuNP-αCD3, irrespective of AuNP size or shape and also in the presence of co-cultured phagocytic immune cells. Absolute levels of fluorescence intensity vary between AuNR and AuNSPH of different sizes, because larger size AuNP bind more fluorophores per particle. The same applies for the shape dependent difference in fluorescence intensity. The bigger the AuNP, the more antibodies and fluorochromes bound to the surface. As illustrated in figure 34, αCD3 antibody, coupled to AuNP of different shapes and sizes, specifically bound to T cells, while no binding was observed for unspecific isotope controls or for AuNP-αCD11b conjugates, not targeting T cells. Considering the initial research questions, we can conclude that phagocytes do not impede specific binding of AuNP-αCD3 to T cells. Furthermore, binding of AuNP does not depend on AuNP shape.

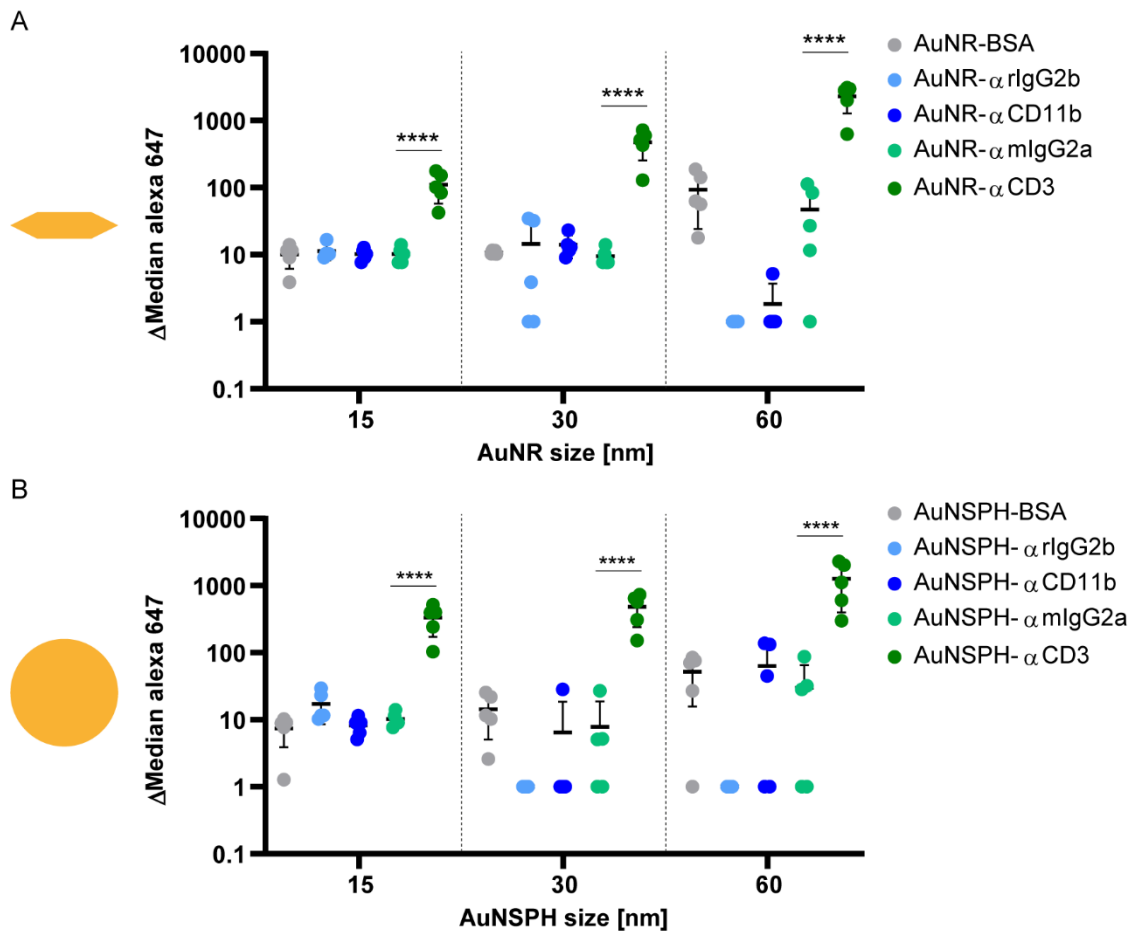


Figure 34: AuNR size and shape does not affect AuNP- α CD3 targeting of T cells.

Whole blood was treated with fluorescently labeled gold nanospheres (AuNSPH) and AuNR of three different sizes (15 nm, 30 nm and 60 nm) with different coatings (BSA and antibodies: α IgG2b, α CD11b, α IgG2a, or α CD3) for 30 min at 37°C in rotation. Gating of T cells is shown in Supplementary Figure 4. **(A)** T cell-associated AuNR or **(B)** AuNSPH fluorescence was analyzed in flow cytometry (n=5, two-way ANOVA, Sidak's multiple comparisons test). Fluorescence intensity of AuNR and AuNSPH as well as between AuNP sizes differs due to varying surface area and therefore varying coating area for antibodies and fluorochromes. Dashed lines separate these different properties. Exemplary histograms are shown in Supplementary Figure 10 A+B. The statistical significance was defined as ****p \leq 0.0001; ***p \leq 0.001; **p \leq 0.01; *p \leq 0.05. N indicates the number of experimental repetitions, each performed with independent donors.

4.8.3 UPTAKE OF ANTIBODY-COUPLED AUNR BY PHAGOCYTES

In the next series of experiments, conjugates used in figure 34 for T cells, were applied to target phagocytic PMN in whole blood. In contrast to earlier experiments with isolated PMN and 24 nm AuNR-AB (Figure 33), here, we found selective targeting of PMN with 15 nm and 30 nm AuNR- α CD11b compared to AuNR- α IgG2b. 60 nm sized AuNR were phagocytosed irrespective of the antibody-targeting (Figure 35A). AuNSPH on the other hand showed no specific antibody-targeting of PMN with spheres of 30nm and 60 nm sizes (Figure 35B). A tendency for improved targeting by AuNSPH- α CD11b was observed for spheres of 15 nm size. This clearly demonstrates

a size and shape dependency of phagocytosis. As shown in figure 6, AuNR were taken up in an actin-dependent manner. We observed an additional contribution of clathrin-mediated uptake when using small AuNR (20 nm) (Figure 7). Studies investigating the shape effect of AuNP uptake controversially discuss, whether a spherical or a rod shape is beneficial for phagocytosis. In a recent study, authors found rod-shaped NP preferentially phagocytosed by PMN compared to spherical NP (Safari *et al.* 2020). Simulation studies support our results by indicating an easier wrapping, thus faster phagocytosis of spherical NP compared to rod-shaped NP (Li *et al.* 2015). The authors pointed out that this information offers the opportunity to produce NP that are not phagocytosed by immune cells, to overcome the unspecific phagocyte problem, impeding efficient targeting of NP. Our results show a clear difference in phagocytosis of spherical and rod-shaped AuNP (Figure 35). Additionally, we identified a size window of 30 nm in diameter and smaller showing reduced unspecific phagocytosis by PMN.

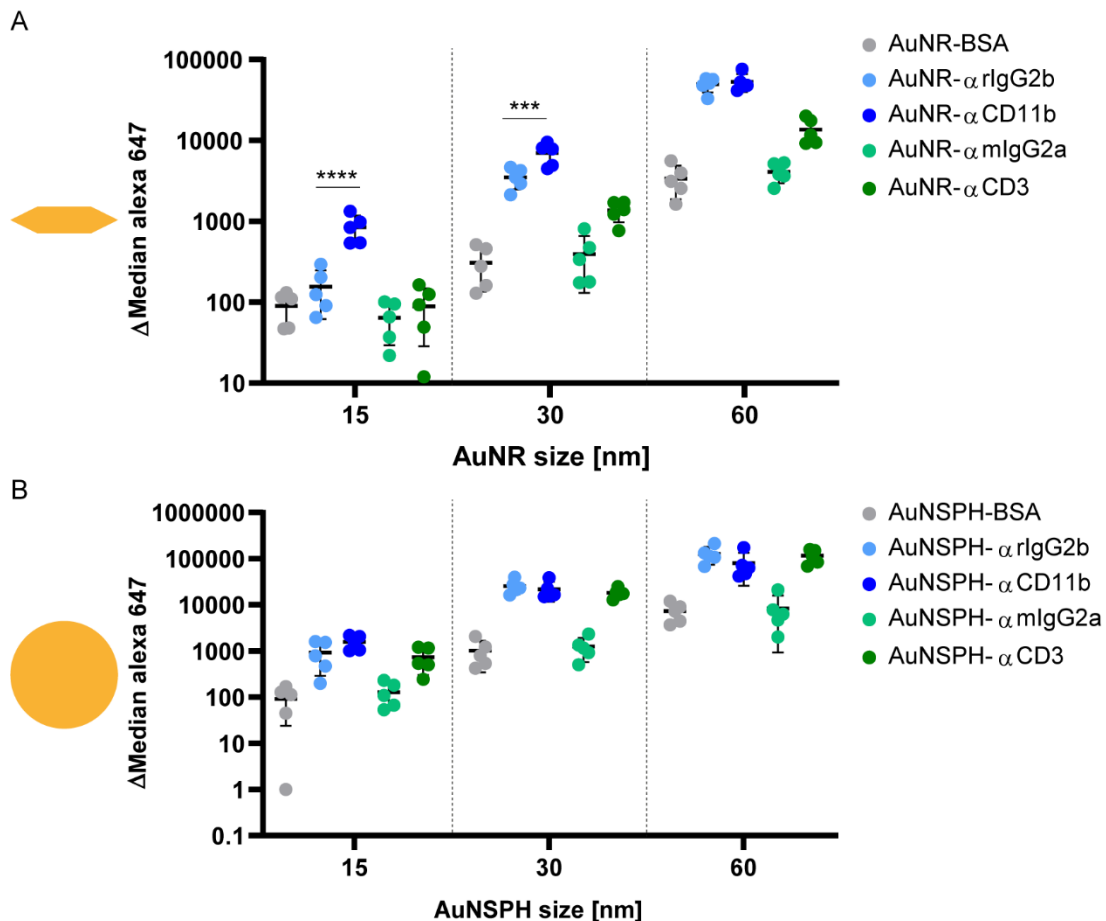


Figure 35: AuNR size and shape massively affect antibody-mediated targeting of PMN in whole blood assays.

Whole blood was treated with fluorescently labeled gold nanospheres (AuNSPH) and AuNR of three different sizes (15 nm, 30 nm and 60 nm) with different coatings (BSA and antibodies: α rlgG2b, α CD11b, α mIgG2a, or α CD3) for 30 min at 37°C in rotation. Gating of PMN is shown in Supplementary Figure 4.

PMN-associated **(A)** AuNSPH or **(B)** AuNR fluorescence was analyzed in flow cytometry (n=5, two-way ANOVA, Sidak's multiple comparisons test). Fluorescence intensity of AuNR and AuNSPH as well as different sizes differs due to varying surface area and therefore varying coating area for antibodies and fluorochromes. Dashed lines separate these different properties. All histograms are shown in Supplementary Figure 10 C+D. The statistical significance was defined as ****p ≤ 0.0001; ***p ≤ 0.001; **p ≤ 0.01; *p ≤ 0.05. N indicates the number of experimental repetitions, each performed with independent donors.

4.8.4 PHAGOCYTOSIS OF AUNR DEPENDS ON THE ISOLATION METHOD OF TARGET CELLS

Experiments in figure 33 and figure 35 showed discrepancies in target-antigen specificity of AuNR-AB conjugates to PMN in whole blood assays *versus* experiments performed with isolated PMN. Since the isolation method may affect cell biological properties and the activation status of PMN, we directly compared AuNR-AB targeting in whole blood *versus* isolated PMN. Thus, we performed uptake experiments and compared the efficiency of AuNR- α CD11b binding with or without prior isolation of PMN. Additional to 15 nm, 30 nm and 60 nm sized AuNR, we tested 24 nm AuNR for their antibody mediated binding to PMN, since this size was used in all experiments of the first section of this thesis. Confirming our experiments detailed in figure 35, we found significantly enhanced PMN-associated fluorescence with 15 nm sized AuNR- α CD11b over isotype in whole blood (Figure 36A). Similarly, also 24 and 30 nm sized AuNR- α CD11b showed higher capacity to bind to PMN in whole blood than the respective AuNR- α IgG2b, but did not reach statistical significance with n = 5 donors. Surprisingly, when using isolated PMN of the same blood donors, solely 15 nm AuNR showed significant AuNR- α CD11b targeting compared to isotype (1.8 fold), but 24, 30 and 60 nm AuNR- α CD11b showed equal or even significantly lower PMN-associated fluorescence intensity than the respective AuNR-isotype, indicating an unspecific phagocytosis that overshadows antigen-specific binding (Figure 36B). These data indicate that the phagocytosis of antibody-coupled AuNR depends on prior isolation methods and the culture conditions of phagocytes. The isolation of PMN *via* density gradient centrifugation resulted in higher unspecific phagocytosis compared to not isolated PMN from whole blood.

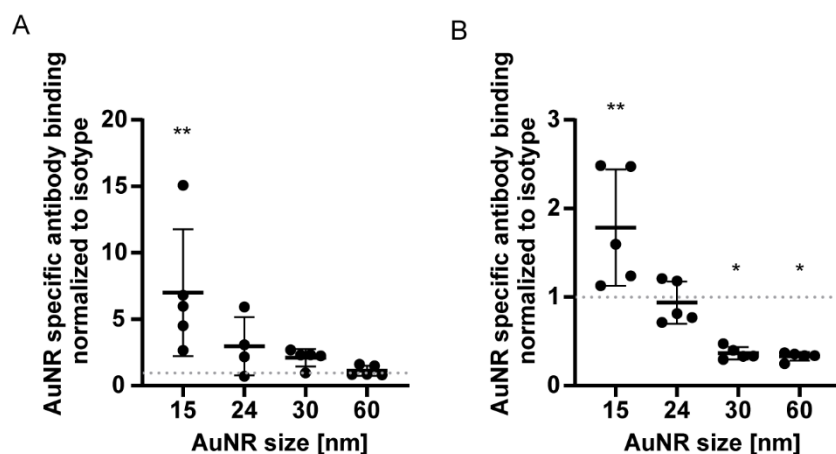


Figure 36: Targeting of AuNR-αCD11b depends on AuNR size and on culture conditions.

AuNR of four different sizes (15 nm, 24 nm, 30 nm and 60 nm) were fluorescently labeled and coated with arlgG2b, or αCD11b. **(A)** Whole blood was treated with 5000 AuNR / PMN for 30 min at 37°C in rotation. PMN-associated AuNR fluorescence was analyzed in flow cytometry. Gating of PMN is shown in Supplementary Figure 4. Fluorescence intensity of AuNR-αCD11b was normalized to fluorescence intensity of AuNR-αIlgG2b (=1, indicated by grey dashed line) (n=5, one-way ANOVA, Dunnett's multiple comparisons test). **(B)** Experiments in panel B were performed by Kim Lamers. Isolated PMN were treated with AuNR (concentration described above) for 30 min at 37°C. PMN-associated AuNR fluorescence was analyzed in flow cytometry. Fluorescence intensity of AuNR-αCD11b was normalized to fluorescence intensity of AuNR-αIlgG2b (=1, indicated by grey dashed line) (n=5, one-way ANOVA, Dunnett's multiple comparisons test). The statistical significance was defined as ****p ≤ 0.0001; ***p ≤ 0.001; **p ≤ 0.01; *p ≤ 0.05. N indicates the number of experimental repetitions, each performed with independent donors.

4.9 KILLING OF IMMUNE CELLS BY PHOTOTHERMAL THERAPY (PTT)

AuNP can be used either as vehicle for site-specific drug delivery (Yu *et al.* 2020), or as therapeutic agents themselves, e.g. in PTT (Dreaden *et al.* 2012, Emami *et al.* 2021). When AuNP absorb light, surface electrons transition from ground to the excited state. This excitation energy subsequently relaxes through non-radiative decay, resulting in overheating of the local environment (Abadeer *et al.* 2016). The local administration of PTT leads to irreversible cell destruction through protein denaturation and coagulation, as well as cell membrane destruction (Zharov *et al.* 2005, Ali *et al.* 2016, Aioub *et al.* 2017). AuNR are especially promising due to their split LSPR with a stronger absorption in the near infrared region (NIR ~650 – 950 nm, longitudinal oscillation) and a weaker absorption (transverse oscillation) around 520 nm, allowing the excitation within the first biological “water window” (Link *et al.* 1999) (Figure 4).

4.9.1 PTT OF MULTI-IMMUNE CELL CULTURES

In a first approach, we measured the NIR-induced temperature shift in a multicellular 96-well format assay. In order to investigate the specificity of antibody-coupled AuNR, we performed all experiments with isolated PBMC and PMN, mixed in a 1:1 ratio and treated 24 nm AuNR-AB for 30 min. Afterwards, we removed the excess of not bound AuNR by washing with PBS. The

irradiation was performed in a fully automated way, using a 5 W, 808 nm laser beam, centered above each well, irradiating every sample for 5 min. Making use of an infrared camera, we found that the irradiation without photosensitizer (PBS) elevated the temperature around 7.6 °C, whereas AuNR-AB reached a maximum change in temperature between 10 and 21.61 °C, dependent on the antibody, coupled to AuNR, and blood donor. The increase in temperature was very transient, returning to starting temperature ($\Delta\text{temperature} = 0$) within 5 min after the end of irradiation. Surprisingly, AuNR- αIgG2b ($\Delta\text{temperature maximum} = 21.61$ °C) and AuNR- αCD3 ($\Delta\text{temperature maximum} = 21.61$ °C) showed the strongest increase in temperature, while AuNR- αCD11b , targeting monocytes and PMN, therefore a big proportion within the multicellular culture, solely reached a maximum change in temperature of 14.69 °C (Figure 37A). We further analyzed the frequency of living cells 1 hour after laser therapy and found cell death in phagocytes when using AuNR- αIgG2b and AuNR- αCD3 (Figure 37B). We classified this cell death as “non-targeted”, as both constructs are not directed against a target antigen on monocytes and PMN. Considering the unspecific phagocytosis observed in prior experiments, when using isolated PMN and 24 nm AuNR- αCD11b (Figure 33B), the PTT results in multicellular culture emphasize the importance of specific targeting prior to irradiation. Furthermore, AuNR- αCD3 showing specific binding to T cells in isolated and whole blood conditions (Figure 33 and Figure 34), did not induce killing of T cells within the one hour experimental time window (Figure 37B). This indicates that targeting of AuNR does not necessarily result in heat induced cell death within 1 h post laser treatment. We analyzed AuNR- αCD3 mediated T cell killing in the next chapter (4.9.2).

Interestingly, we found significantly more living PMN and monocytes after PTT with AuNR- αmIgG2a compared to AuNR- αrIgG2b (Figure 33B). Our collaboration partners (AG Schlücker), producing the AuNR-AB, performed several quality control experiments showing that antibodies coupled to AuNR to a similar extent (data not shown). Surprisingly, coupling of αmIgG2a or αrIgG2b , both irrelevant isotype control antibodies with 150 kDa, resulted in dramatically different hydrodynamic radii (HR; AuNR- $\alpha\text{mIgG2a} = 43.4$ nm; AuNR- $\alpha\text{rIgG2b} = 111.8$ nm) (Supplementary Table 2). When plotting living PMN, monocytes and T cells of this differently sized AuNR-AB, 1h after irradiation, we identified the HR of the resulting AuNR-AB as a key parameter impacting the uptake and PTT of antibody-AuNR conjugates by phagocytes. These data suggest that AuNR-antibody conjugates must not exceed a certain HR threshold of around 50 nm, in order to enable antigen-specific targeting of phagocytes (Figure 37C). Unfortunately, we were not able to repeat experiments with AuNR-AB with a smaller HR than 50 nm, since their

production turned out to be challenging. Therefore, the observation of size-dependent PTT killing efficiency remains a hypothesis that needs to be validated in future studies obtained by our lab.

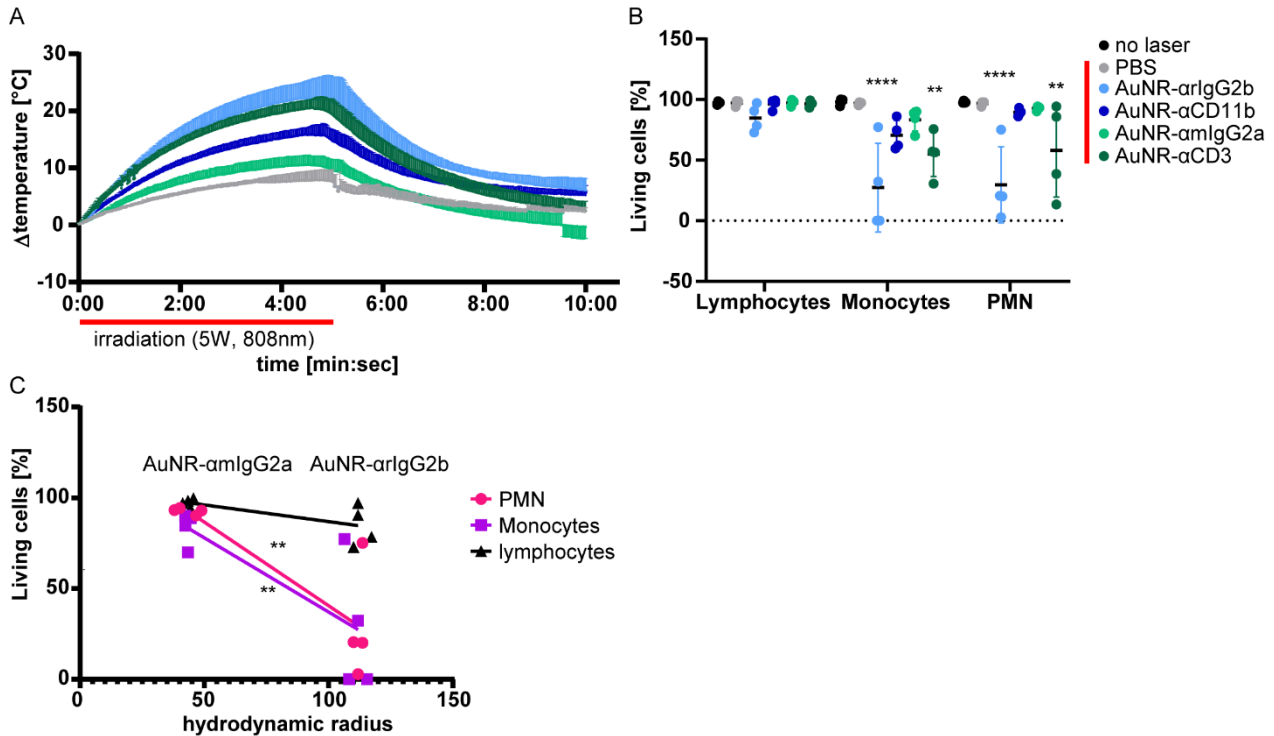


Figure 37: Phagocytosis impedes AuNR targeting resulting in unspecific PTT.

The experiments shown in this figure were performed by Kim Lamers. **(A)** Isolated PMN and PBMC were mixed in a 1:1 ratio and treated for 30 min with PBS (grey), or 10000 AuNR with different antibody coating (α rlgG2b (light blue), α CD11b (dark blue), α mlgG2a (light green), α CD3 (dark green)) / cell. After removing the excess of AuNR washing with PBS, cells were irradiated for 5 min using a 5 W laser at 808 nm and temperature was measured with an infrared camera (Optris Pix connect) for up to 10 min. Δ temperature was calculated by subtracting the temperature before starting the irradiation ($n = 4$). **(B)** After irradiation cells were rested for 1 h at 37°C. Thereafter, apoptosis-related changes in cell membrane topology were assessed by Annexin V Apoptosis Detection Kit in flow cytometry. Gating of PMN, monocytes and lymphocytes is shown in Supplementary Figure 3 ($n=4$, two-way ANOVA, Dunnett's multiple comparisons test). **(C)** Comparison of living PMN, monocytes and lymphocytes (from B) to hydrodynamic radius of AuNR-mlgG2a and -rlgG2b ($n=4$, two-way ANOVA, Sidak's multiple comparisons test). The statistical significance was defined as **** $p \leq 0.0001$; *** $p \leq 0.001$; ** $p \leq 0.01$; * $p \leq 0.05$. N indicates the number of experimental repetitions, each performed with independent donors.

4.9.2 PTT OF NON-PHAGOCYtic T CELLS

While targeting of phagocytes turned out to be very challenging, targeting of non-phagocytic T cells with AuNR- α CD3 showed promising results (Figure 34) so we further tested, whether this specific binding translated into antigen-specific laser-induced PTT. PTT resulted in a very efficient heat induction in AuNR- α CD3 treated T cell cultures (Figure 38A). Nevertheless, we found no specific killing following 1 hour post laser therapy. However, when we cultured T cells for 24 h post laser therapy we found significant cell death (Figure 38B). We did not observe this slow induction of apoptosis when irradiating phagocytes (Figure 37B). This indicates a different PTT-

induced killing mechanism operative in phagocytes versus T cells that need to be validated in future experiments.

In conclusion, these experiments establish important parameters that influence AuNR-induced PTT of human immune cells and demonstrate the feasibility of antigen-specific PTT-induced killing of T cells in simplified mono-cell cultures.

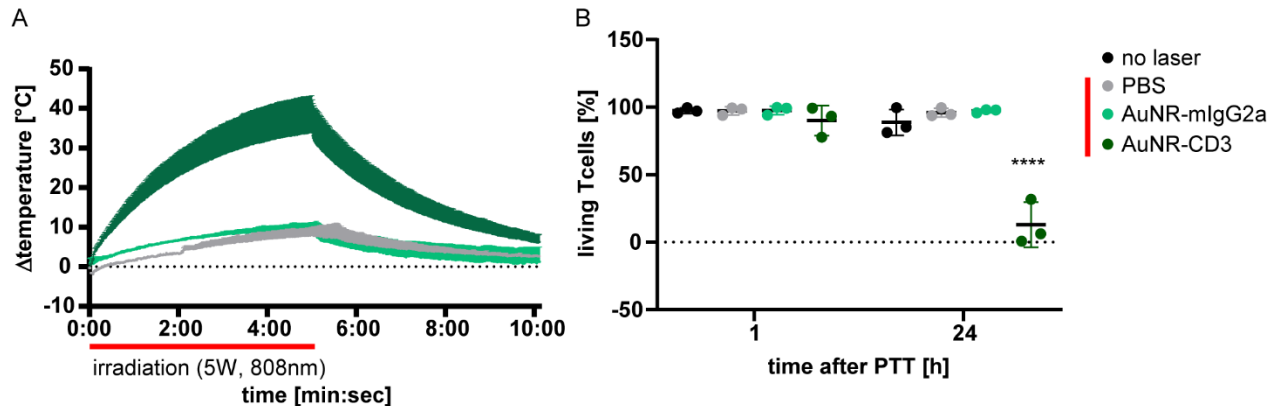


Figure 38: T cells can be specifically killed in PTT using AuNR- α CD3.

The experiments shown in this figure were performed by Kim Lamers. **(A)** Isolated T cells were treated for 30 min with PBS (grey), or 10000 AuNR with different antibody coating (- α mIgG2a (light green), - α CD3 (dark green)) / T cell. After removing the excess of AuNR by washing with PBS, T cells were irradiated for 5 min, using a 5 W laser at 808 nm and temperature was measured with an infrared camera (Optris Pix connect) for up to 10 min. Δ temperature was calculated by subtracting the temperature before starting the irradiation. **(B)** After irradiation, cells were rested for 1 h or 24 h at 37 °C. Apoptosis-related changes in cell membrane topology were assessed by Annexin V Apoptosis Detection Kit (BD Bioscience) in flow cytometry (n=3, two-way ANOVA, Tukey's multiple comparisons test). The statistical significance was defined as **** $p \leq 0.0001$; *** $p \leq 0.001$; ** $p \leq 0.01$; * $p \leq 0.05$. N indicates the number of experimental repetitions, each performed with independent donors.

5 DISCUSSION

This study investigated the interaction of gold nanoparticles, especially gold nanorods, with polymorphonuclear neutrophils (PMN) and T cells. Within this thesis, the following questions were addressed:

1. Do PMN take up AuNP *ex vivo*?

Yes, using confocal microscopy, structured illumination microscopy and flow cytometry, we showed the uptake of fluorescently labelled AuNR by PMN. In order to ensure that the fluorescence corresponds to AuNR uptake we further performed transmission electron microscopy validating the uptake of AuNR with 24 nm length.

2. Does the uptake of AuNP have an impact on the survival of PMN *ex vivo*?

We found no change in Annexin-V dependent apoptosis or the amount of 7AAD using negatively charged AuNR. However, we found reduced survival of PMN after adding high doses of positively charged AuNR.

3. How (molecular mechanism) are AuNP taken up by PMN *ex vivo*?

Using fluorescently labelled AuNR in combination with inhibitors of actin-, clathrin- and caveolin-dependent uptake mechanism we showed a size-dependent uptake of AuNR with actin-dependent (phagocytosis or macropinocytosis) uptake mechanisms, being the major pathway for various sizes including 24 nm AuNR. Depending on the size of AuNR, other mechanisms, like clathrin-dependent endocytosis for smaller AuNR of up to 20 nm size might contribute to the uptake.

4. Does the uptake of AuNP affect the activation level of PMN *ex vivo*?

Yes, we found a higher expression of the surface markers CD11b and LOX1 and downregulation of CD62L and CD182, CD181. Furthermore, AuNR-primed PMN secreted higher levels of IL8 and active MMP9 indicating a pro-inflammatory phenotype.

5. What are the molecular mechanisms behind a potential activation of PMN *ex vivo*?

First, AuNR uptake activates the xenobiotic metabolism, a cell biological response designed to cope with non-biological foreign material; AhR and SHP were major transcription factors involved in the induction of the xenobiotic metabolism. The high

demand for secretory proteins, associated with this xenobiotic response, led to induction of ER stress and UPR via IRE α and PERK, subsequently leading to PMN activation. This initial PMN activation was further accelerated by an autocrine activation loop triggered by induction of LOX1 activation and sustained by IL8 secretion.

6. Can immune cells be targeted by AuNP, functionalized with cell-type specific antibodies?

Yes, non-phagocytic T cells can be targeted with α CD3-coupled AuNR, independent of AuNP shape (spherical- or rod-shaped) and size (15 – 60 nm). Furthermore, AuNR- α CD3 targeting induced specific T cell death in PTT. In contrast, human phagocytes have a high intrinsic propensity for AuNR uptake that may lead to unwanted inflammatory activation and immunopathology. Antibody-mediated targeting of phagocytic immune cells with AuNR requires small rod-shaped AuNP, smaller than 30 nm (gold core) and smaller than 50 nm hydrodynamic radius, to circumvent unspecific phagocytic uptake.

Concluding, specific targeting of immune cells and subsequent PTT using antibody-coated AuNP is feasible as cancer therapy, but has to be designed very carefully to avoid phagocytic clearance of AuNR and ensure antigen-specific binding of AuNR-AB conjugates to target cells.

In the following sections, major findings shall be discussed in the context of existing literature.

5.1 GOLD NANOPARTICLE MODIFICATION AND THEIR BIOMEDICAL APPLICATION

AuNP are synthesized using different protocols, producing various sizes and shapes. AuNP shapes range from stars to cubes, spheres (AuNSPH), rods (AuNR) and clusters (Alaqad *et al.* 2016). Furthermore, AuNP can be functionalized with DNA, proteins and polymers, resulting in multiple biomedical applications, but also affecting biochemical properties of AuNP as for example the surface charge. In the present study, we used AuNR as well as AuNSPH, synthesized by a modified seeded growth method by our collaboration partner at the Department of Chemistry (University of Duisburg-Essen) (Xia *et al.* 2010, Jia *et al.* 2015). The manifold sizes, charges, surface modifications and shapes of AuNP offer diverse applications in the biomedical field but also impede a generalized comparison of different studies. Furthermore, there are discrepancies in the description of size and concentration of AuNP applied to a biological system. For example, most studies describe size and optical density of AuNP and some give the Au concentration measured

by ICP-MS in $\mu\text{g} / \text{mL}$. The applied particle amount heavily depends on the nanoparticle size. In conclusion, the particle-to-cell ratio varies massively between studies, ranging from 0.1 to 10 pg / cell *in vitro* (Bartneck *et al.* 2012, Plan Sangnier *et al.* 2020, Ye *et al.* 2020), impeding the universality of stated AuNP-induced effects. For this reason it is necessary to agree on uniform synthesis and defined AuNP concentration units. To facilitate the comparison of the present study with other studies, we decided to use all common descriptions of applied AuNP concentrations additional to AuNP per cell ratio. Furthermore, AuNP properties, like size, shape and surface modifications, as well as the nanoparticle to protein ratio in a biological fluid alter the formation of a protein corona. The protein corona forms spontaneously upon nanoparticle contact with biological material such as blood serum or cell culture medium, thereby providing a biological finger print that can be detected by the host immune system (Barbero *et al.* 2017). This emphasizes the importance to work in a human system in order to develop efficient cancer therapy. Most studies use either mouse models or cancer cell lines to investigate the molecular interaction of AuNP with cells (discussed below). Nevertheless, the murine and the human immune system exhibit multiple differences (Mestas *et al.* 2004), so a detailed understanding of the interaction of AuNP with human immune cells in human serum is absolutely required in order to develop safe and efficient drugs. Until now, it is not entirely clear, how the protein corona contributes to the binding or uptake of AuNP by cells or their stimulatory intracellular effects. The present study, unraveled the molecular interaction of human immune cells and AuNP in blood as well as in cell culture medium. We did not observe AuNP induced toxicity in PMN *ex vivo*. In contrast to silver nanoparticles, AuNP attract through their chemical inertness, showing no oxidation *in vitro* or *in vivo* (Yaqoob *et al.* 2020). However, it has been shown that colloidal gold could have an anti-arthritis activity *in vivo* (Brown *et al.* 2008). AuNP biocompatibility was analyzed extensively in the last few years, showing contradictory results for AuNP toxicity, probably due to the aforementioned variability in synthesis and application of AuNP (Alkilany *et al.* 2010, Khlebtsov *et al.* 2011, Dykman *et al.* 2017). Furthermore, toxicity of AuNP is heavily affected by surface modification and sterile working conditions during the synthesis, which is influencing endotoxicity. Indeed, we found CTAB- and PSS-coated AuNR being extremely toxic for PMN, whereas PEG-coated AuNR showed no toxicity over time (data not shown). Especially considering the fast and substantial phagocytosis of AuNR by PMN, our results underline the inertness of Au and the influence of surface modifications *in vitro*.

5.2 AUNR SIZE AS THE MAJOR CAUSE OF AUNR CLEARANCE BY PHAGOCYTES?

We showed in this thesis that AuNR uptake and potential clearance heavily depends on the shape and size of AuNP. In this respect, AuNR trigger less unspecific phagocytosis than spherical nanoparticles. For AuNR application in PTT an aspect ratio (length / width) of 4 and absorption maximum at 808 nm is necessary (Jia *et al.* 2015). Reducing the size below 20 nm longitudinal and 5 nm transversal makes AuNR synthesis and stability technically more challenging. However, AuNR do not only consist of the Au itself, but also the coating, which changes the size of AuNR non-uniformly. Thus, another possibility of reducing size is reducing the PEG chain length or reducing the bio-conjugation for example by using aptamers instead of full antibodies. In our study, we used 3.5 kDa PEG, since it provided good stabilization of AuNR. Nevertheless, shorter chain length might reduce the hydrodynamic radius of the overall particle considerably. As this thesis shows, an increased HR of AuNR-antibody conjugates was associated with increased unspecific phagocytosis and killing in PTT. We hypothesize that reducing the HR would lower the unspecific heat induction of untargeted AuNR-AB (α IgG2a and α IgG2b) during PTT. The HR of AuNR-AB mostly depends on the tertiary structure of the antibody (Zheng *et al.* 2016). Therefore it is plausible that the differences in hydrodynamic radii of α IgG2a and α IgG2b occur due to varying PEG-binding as well as differences in the amino acid composition resulting in different charges and therefore varying HR. Furthermore, it has been shown that the antibody orientation on the nanoparticle surface affects the size of hydrodynamic radius (Ruiz *et al.* 2019). Considering the importance of NP size, Bisso and colleagues put a lot of effort in unraveling the parameters affecting PMN phagocytosis. They found 20-200 nm sized nanoparticles (NP) to be particularly suitable for PMN targeting (Bisso *et al.* 2018). Uptake of poly (styrene) nanoparticles, liposomes, and poly lactic-co-glycolic acid (PLGA) was affected by human blood serum, whereas AuNP uptake remained minor, independent of the serum concentration within the culture medium. One has to mention though, that the authors solely tested the uptake of small, 5 to 20 nm sized AuNP contrary to other NP, where they tested 50 to 200 nm sized and found substantial uptake by PMN. It therefore remains unclear, whether the poor uptake of AuNP by PMN is due to the material, surface modification, and protein corona formation or simply by size. As already pointed out in the introduction, PMN are specialists in pathogen clearance (see chapter 1.1.2.2). This comprises the clearance of viruses, bacteria, fungi and cell debris. Human viruses represent the smallest group being phagocytosed by PMN, ranging from 20 nm (Picornaviruses) to 200 nm (herpesviruses) in diameter, with a typical size of approximately 100 nm. Exceptions like the poxviruses approach up to 400 nm, or ebola virus (up to 1000 nm) in length. In comparison, bacteria generally range

between 2 to 3 μm in size and human cells around 10 to 30 μm (Louten 2016). Therefore, it appears to be logical that reducing the size of AuNR below the phagocytosis window, ranging from 20 to 3000 nm, reduces the unspecific phagocytosis of AuNR by PMN. Comparing antibody-mediated targeting of isolated immune cells with PMN and T cells directly from whole blood, we found superior targeting in whole blood. This could be, due to the manipulation during the isolation, activating PMN, but also due to the culture conditions. Isolated PMN were cultured in 10 % autologous serum supplemented medium which is, compared to 100 % serum in whole blood, nutrient deprivation that has been shown to promote phagocytosis (Martinet *et al.* 2009). To test, whether the improved targeting capacity also reflects on PTT efficiency, we performed uptake experiments in whole blood with subsequent laser treatment (data not shown). However, when applying the NIR laser with 5 W for 5 min to whole blood, we found massive absorption of the NIR, already after less than one minute, resulting in cooking of the blood. This might be caused by the high oxygenation of hemoglobin (Hb) during the sample preparation (Murkin *et al.* 2009). This finding is of certain relevance, since it shows the limitations of NIR based therapies. In *in vivo* applications, laser power and the location of the tumor in relation to vasculature would need to be considered prior to application. In order to reduce the number of erythrocytes we used lysis buffers after AuNR treatment, but PMN were especially fragile to this kind of lysis. Further work needs to be done to technically improve this test system.

5.3 AUNP DELIVERY SYSTEMS

During the past years, different approaches for nanoparticle delivery have been developed. They can be divided in passive and active delivery and will be discussed in the following sections.

5.3.1 PASSIVE DELIVERY OF NANOPARTICLES

Most studies investigating AuNP delivery *in vivo* in the past, referred to the enhanced permeability and retention effect (EPR) (Maeda 2001), allowing the passage of AuNP through “leaky” intratumoral vasculature. Since tumors require a lot of oxygen and nutrients to survive and proliferate, they are, especially in fast growing tumors, heavily vascularized (Lugano *et al.* 2020), so it was assumed that AuNP could passively accumulate intratumoral. In 2018, Dai and colleagues pointed out the inefficient delivery of only 0.0014 % of AuNP reaching the targeted cancer cells after intravenous injection of actively targeting AuNP (Trastuzumab) (Dai *et al.* 2018), questioning the existence of the EPR effect in passively targeting systems. Based on our study and related published studies (Gustafson *et al.* 2015), it is likely that large numbers of systemically injected AuNP will be rapidly phagocytosed by myeloid immune cells. Our study underscores this finding

by showing massive uptake of AuNR by PMN within 5 min of exposure. Despite their “problematic” feature of clearing AuNP from the target, phagocytes may be employed as cellular vehicles for targeted therapeutics. In fact, recent studies in preclinical models showed that PMN efficiently take up AuNP and shuttle their cargo through the vasculature and in various organs (Durocher *et al.* 2017, Ye *et al.* 2020). This presumes a careful titration of AuNP, to minimize their immunopathological effects described in the first part of the present study, but also guarantee efficient heat induction or drug release at the target site.

5.3.2 CAMOUFLAGING TECHNIQUES TO AVOID NANOPARTICLE PHAGOCYTOSIS

5.3.2.1 Polymer Coating

Previously, PEGylation was used to increase NP circulation time, by stabilizing NP shape and reducing the formation of a protein corona. PEGylation describes the covalent binding of polyethylene glycol to the surface of drugs, to mask the agent from the immune system. It reduces the immunogenicity and prolongs the retention in the blood circulation (Damodaran *et al.* 2010). Nevertheless, it has been shown that PEG enhances PMN phagocytosis in serum, due to the accumulation of human complement proteins in the protein corona (Tenzer *et al.* 2013, Kelley *et al.* 2018). The composition of the protein corona depends, among other factors discussed above, on the density of PEG on the nanoparticle surface (Walkey *et al.* 2012). We observed that PEGylation reduces the phagocytosis compared to further modification with fluorochromes (data not shown). Indeed, PMN cultured in different media, supplemented with either fetal calf serum or human serum did not show comparable induction of enhanced surface expression of e.g. LOX1 compared to whole blood treatment (data not shown). We did not quantify the uptake of AuNR in different culture conditions, thus we cannot exclude the possibility that these functional changes correlated with the amount of phagocytosed AuNR. In order to mimic the *in vivo* system, experiments described in this study were performed either in autologous serum supplemented medium or in whole blood. Our results implicate that PEG generally reduces phagocytosis, which is modulated by the formation of a protein corona consisting of host immune complement proteins. On the other hand, PEG is included in various cosmetics and it has been shown that the efficiency of PEGylated drugs is reduced, due to anti-PEG immunity (Zhang *et al.* 2016). Therefore, it is probable that PEGylation induces opsonization with antibodies, facilitating immunogenic clearance by phagocytes. Recent studies showed beneficial delivery of anticancer drugs for therapy, but especially for tumor imaging, using additional protein coatings with bovine serum albumin (BSA) and high density lipoprotein (Li *et al.* 2021). The data in the present study supports this. We

did not observe high uptake of AuNP-BSA by phagocytes, neither AuNSPH nor AuNR. It was one major aim of this study to test the possibility to specifically target AuNR-AB conjugates to different immune cells. Although we found substantial accumulation of AuNR- α CD3 at T cells, this study clearly shows an unspecific, non-antigen specific phagocytosis of AuNP with a HR bigger than \sim 50 nm. Contrarily, we hypothesized that there is a thin line between antibody-mediated targeting and unspecific phagocytosis of AuNR due to the enlarging hydrodynamic radius by antibody coating. The AuNR-AB conjugates used in this study were synthesized by covalently binding antibodies to the PEG carboxy group *via* 1-Ethyl-3-(3-(dimethylamino) propyl) carbodiimide (EDC) conjugating to N-hydroxysulfosuccinimide (sNHS) (AG Schlücker). This bioconjugation is used in various medical research projects, however the efficiency of antibody-conjugation to nanoparticles is not entirely understood (Totaro *et al.* 2016).

5.3.2.2 Biologically Active Proteins

As an alternative to active targeting using targeting antibodies, strategies of NP immune escape have been developed. Biologically active proteins like CD47 have shown promising reduction of phagocytic NP clearance (Tsai *et al.* 2008, Belhadj *et al.* 2020). CD47 is a heavily glycosylated, ubiquitously expressed transmembrane protein, modulating various cellular functions as proliferation, adhesion, migration, apoptosis and phagocytosis. The expression of CD47 supports phagocytes to distinguish between “self” or “non-self” cells. The binding of CD47, expressed on the cell surface of non-malignant cells, to SIRP α transmembrane protein, expressed on myeloid cells, leads to the formation of the CD47-SIRP α signaling complex. Subsequently, this inhibits the accumulation of myosin IIA in phagocytic synapses and facilitates the release of “don't eat me” signals. Finally, CD47-SIRP α inhibits phagocytosis and normally protects normal cells from being phagocytosed by the immune system. Some types of cancer have been shown to adapt to take on a CD47 expression, thereby escaping the immune response (Russ *et al.* 2018). Unfortunately, coupling of CD47 potentially enlarges the HR of NP and, since it also needs to be coupled to the nanoparticle surface, it reduces the number of coupling sites on the NP surface for specific targeting antibodies. Besides using active “don't eat me” signals (CD47), a hot topic in nanodrug delivery systems in the past 5 years has been the camouflaging of NP with cell membranes. Especially cancer cell membrane-, red blood cell membrane- and leukocyte membrane-based nanocarriers showed promising results considering specific targeted delivery, high cargo loading and increased drug half-life of anticancer drugs in the body (Li *et al.* 2021). It has been shown that a coating with cancer cell membranes can reduce, but not abolish phagocytosis of nanoparticles by RAW 264.7

macrophages. One major drawback might be the incomplete coating of nanoparticles with membranes, since state of the art techniques solely result in around 6 % of nanoparticles being fully coated (Liu *et al.* 2021). Furthermore, these membrane-coated biomimetic nanocarriers increase in size, which might reduce the efficiency of additional antibody-mediated targeting as shown in the present study when applying antibodies on the AuNR surface.

5.4 INTERACTION OF AUNP WITH IMMUNE CELLS

The application of AuNR for PTT has shown promising anti-tumor effects in multiple murine tumor models (Huang *et al.* 2006, Almeida *et al.* 2014, Ali *et al.* 2016, Yin *et al.* 2017, Zhang *et al.* 2019). Many studies focused on the accumulation of AuNP within the tumor (Zhang *et al.* 2019, Yu *et al.* 2020, Emami *et al.* 2021). However, as already pointed out in prior sections, phagocytic immune cells potentially remove intratumorally injected AuNR prior to laser therapy, or clear intravenously injected AuNR, before they reach their target and induce off-target effects due to immune activation. Most studies investigating phagocytes in the context of AuNP uptake, focused on macrophages (Gustafson *et al.* 2015, Dey *et al.* 2021). Dey and colleagues showed no cytotoxic effect of AuNP to macrophages and dendritic cells, but a pro-inflammatory activation. AuNP uptake resulted in the secretion of inflammatory molecules, as well as ROS in murine macrophages and dendritic cells. Furthermore, AuNP uptake affected the mitochondrial respiration and glycolysis of murine macrophages (Gustafson *et al.* 2015, Dey *et al.* 2021). We found comparable pro-inflammatory activation of PMN upon AuNR uptake. The activation comprised IL8 secretion, higher ROS production and modulation of LOX1, CD11b, CD182 and CD62L expression when treating with AuNR and AuNSPH. Additionally, the present study unraveled the molecular pathway by which AuNR induced PMN activation.

5.4.1 INTERACTION OF AUNR WITH PMN

PMN represent the most abundant (40-75%) type of white blood cells with phagocytic capacity in humans, hence their interaction with AuNR is of special interest (Summers *et al.* 2010). Until now, relatively little is known about the AuNP-PMN-interaction. Some studies suggested that PMN do not phagocytose AuNP (Bartneck *et al.* 2010, Bartneck *et al.* 2010, Bisso *et al.* 2018). This thesis is the first study, demonstrating a detailed pathway of AuNR-induced effector functions on human PMN. Our study suggests that AuNR are rapidly phagocytosed by PMN. Especially in the context of cancer therapy this is important, since the accumulation of PMN within the tumor tissue correlates with tumor progression (Jensen *et al.* 2009, Trellakis *et al.* 2011, Ilie *et al.* 2012, Jensen *et al.* 2012, Rao *et al.* 2012, Zhao *et al.* 2012). Intratumoral removal of AuNP by phagocytes would

reduce the efficiency of subsequent NIR laser treatment in PTT. This is of particular relevance, because PMN can be used as a prognostic factor for patients, showing poor survival of patients with high PMN infiltrates (Gentles *et al.* 2015, Si *et al.* 2019). On the other hand, this high infiltration of PMN offers the opportunity of accumulating intratumoral AuNR. Smart timing of AuNR administration and NIR laser treatment could be a beneficial treatment of especially patients with poor prognosis. Furthermore, we show that AuNR uptake results in the activation of the xenobiotic metabolism in PMN. The xenobiotic metabolism comprises a wide range of processes polarizing chemical substances that are foreign to animal life to facilitate their excretion. Several *in vitro* and *in vivo* studies showed either an inhibitory or stimulatory effect of silver or gold nanoparticles on cytochrome P450 (CYP) enzymes, especially CYP1A1, at the transcriptional and protein level. Since detoxification and excretion is taking place in the liver, these studies focused on the organ itself, or hepatic cell lines (Balasubramanian *et al.* 2010, Cho *et al.* 2010). Choi and colleagues suggested a dependency of uptake and activation of phase I xenobiotic metabolism on the functionalization and formation of protein corona. They found reduced ROS production and transcription of CYP isoforms when using human plasma protein coated AuNP (Choi *et al.* 2017). We did not investigate the effect of surface modifications on CYP1A1 activation, nevertheless, all the aforementioned studies used different AuNP preparations, target cells or organs, indicating that the activation of the xenobiotic metabolism by AuNP is a universal effect.

5.4.2 ER STRESS IN PMN

Our data shows AuNR-induced upregulation of Ero1L α and PDI, which principally impairs the formation of protein disulfide bonds and potentially results in the accumulation of not properly folded proteins. Using different ER stress inhibitors, we identified IRE α – XBP1s as main unfolded protein response (UPR) pathway of AuNR-induced ER stress. Noël *et al.* found ER stress induction in PMN after treatment with AuNR resulting in caspase mediated cell death (Noël *et al.* 2016). Our results confirm this and provide even more detailed information about the pathway of AuNR-induced ER stress. The ER orchestrates various intracellular functions like proper folding of secretory proteins, their trafficking and degradation, as well as calcium homeostasis and lipid metabolism. Effects of ER stress have been investigated and reviewed extensively, especially in the context of inflammation and cancer development (Wang *et al.* 2014, Li *et al.* 2019). It has been shown that ER stress can induce immune responses and, depending on ER stress intensity and duration, even induce immunogenic cell death or immunosuppressive properties (Salminen *et al.* 2020). Long-term induction of ER stress has been shown to promote cancer development by the

generation of granulocytic (Ly6G⁺CD11b⁺) myeloid-derived suppressor cell (MDSCs) *in vivo* (Lee, B. R. *et al.* 2014). In this thesis we focused on short-term effects of AuNR-PMN interaction, mainly within the first 2 h of incubation. Remarkably, already during this short time we found a higher expression of LOX1 that has been proposed as marker for MDSC (Condamine *et al.* 2016). Long-term, *in vivo*, this is of certain relevance, since AuNR cannot be digested by cells. Considering AuNP' longevity *in vivo* this could even mean a more severe outcome during therapeutic application. Of note, our findings show that short-term application of AuNR does not promote a suppressive phenotype of PMN *ex vivo*. However, this does not necessarily apply for long-term application of AuNR *in vivo*. An accelerated generation of MDSC, would worsen the immunosuppressive milieu in human cancer patients. We show that AuNR treatment turns PMN pro-inflammatory. By elucidating the mechanism behind this phenotype we identified important mediators of accelerating the pro-inflammatory activation, we propose combinational therapies circumventing this activation. As our results show, additional administration of neutralizing antibodies or pharmacologic inhibitors successfully reduced the AuNR-induced autocrine inflammation *via* LOX1 and IL8 or CD182.

5.5 THERAPEUTIC IMPLICATIONS

Photothermal therapy was developed in order to provide a two-step security to the specific target, (1) the accumulation of the photosensitizer at the target and (2) local application of the NIR laser. Attempts to develop and optimize PTT mostly focus on the efficient induction of heat, and so far, little attention has been paid to the potential immunopathological effect of excessive photosensitizer dosage, due to ineffective targeting. In this study, we show the immunopathological effects of AuNR caused by activation of PMN from healthy donors and cancer patients. Our data emphasize the need for specific targeting, thereby reducing the AuNR dosage. *In vitro* studies and preclinical models suggest that once injected, phagocytic immune cells may interfere with efficient AuNP therapy (Gustafson *et al.* 2015). Phagocytes potentially remove intratumorally injected AuNR prior to laser therapy, remove intravenously injected AuNR, before they reach their target and induce off-target effects due to unwanted immune activation as shown in this study. We further show that the coupling of antibodies to randomly shaped and sized AuNP does not guarantee efficient targeting. Besides providing detailed information about potential immunopathological effects of AuNR in human PMN, we further propose a list of AuNP properties, circumventing unspecific phagocytosis. We found rod-shaped AuNP being more suitable for specific antibody-mediated targeting. Furthermore we found AuNR hydrodynamic radius and culture conditions to

clearly affect targeting efficiency. However, we were not able to transfer the information, gained during targeting experiments, to functional PTT of phagocytic immune cells or non-phagocytic T cells in a multicellular environment. In order to investigate cell-specific killing in a multicellular environment a new system defined by reduced heat conduction needs to be developed. This test system should resemble the heat conduction of tissue, rather than that of an aqueous solution as the presented test system with immune cells in medium. The combination of reduced unspecific phagocytosis by reduction of the HR of AuNR-AB in combination with this advanced test system would offer the opportunity to develop a cell-type-specific PTT, resulting in a specific cancer therapy with minor side effects.

5.6 CONCLUSIONS

Collectively, these data demonstrate that AuNR induce metabolic changes in PMN that result in a pro-inflammatory autocrine activation loop that involves LOX1 expression and IL8 secretion. This study provides detailed insight in AuNR-immune cell interaction that is crucial for further immunological clinical studies. In order to overcome this immunopathological effects we herein offer targets to overcome pro-inflammatory activation and provide beneficial AuNP properties lowering unspecific phagocytosis. Our study also uncovers AuNR parameters that influence target specificity of AuNR-antibody conjugates and provides further insight into the behavior of functionalized AuNR in complex mixed cellular systems of immune cells.

6 SUMMARY

Gold nanoparticles (AuNP) represent promising agents for various biomedical applications, including drug and gene delivery, bioimaging and cancer treatment. Previous studies identified the massive phagocytosis by cells of the innate immune system as a major challenge for *in vivo* applications of AuNP. Polymorphonuclear neutrophils (PMN) represent the most abundant phagocytic immune cells in the human system. Therefore, understanding the interaction of AuNR with PMN and exploring the role of phagocytes during antibody-mediated AuNP targeting is key for the development of safe and efficient therapeutic applications.

In this study we investigated the cell biological response of PMN to PEGylated and antibody-coupled (-AB) gold nanorods (AuNR) and gold nanospheres (AuNSPH). Antibody-mediated targeting of AuNR and AuNSPH to phagocytes occurs as a competition of non-antigen specific phagocytosis of AuNP *versus* binding of the conjugated antibody to its cellular target. The ratio between both mechanisms is influenced by AuNP size and shape. We found that antigen-specific binding of AuNR-AB conjugates to T cells and PMN can be best achieved with AuNR of small size (15 nm) and rod-shape. Furthermore, we show that AuNR-AB are suitable tools for photothermal therapy (PTT), efficiently killing non-phagocytic T cells upon near-infrared radiation. In a series of experiments analyzing the interaction of non-targeting AuNR with PMN we showed that AuNR are taken up mainly in an actin-dependent manner within 5 min of incubation. Uptake of AuNR induced endoplasmic reticulum (ER) stress and resulted in an unfolded protein response (UPR) in PMN. Associated with this response were changes in the xenobiotic metabolism and an autocrine activation that involved a higher expression of lectin-type oxidized LDL receptor 1 (LOX1) on the cell surface as well as increased secretion of interleukin 8 (IL8) and reactive oxygen species (ROS) production within 2 hours. Collectively, this study provides a mechanistic insight into the interaction of PMN and AuNP and further supplies information on basic parameters that influence the efficiency of AuNP-AB targeting in multi-cellular culture systems of immune cells.

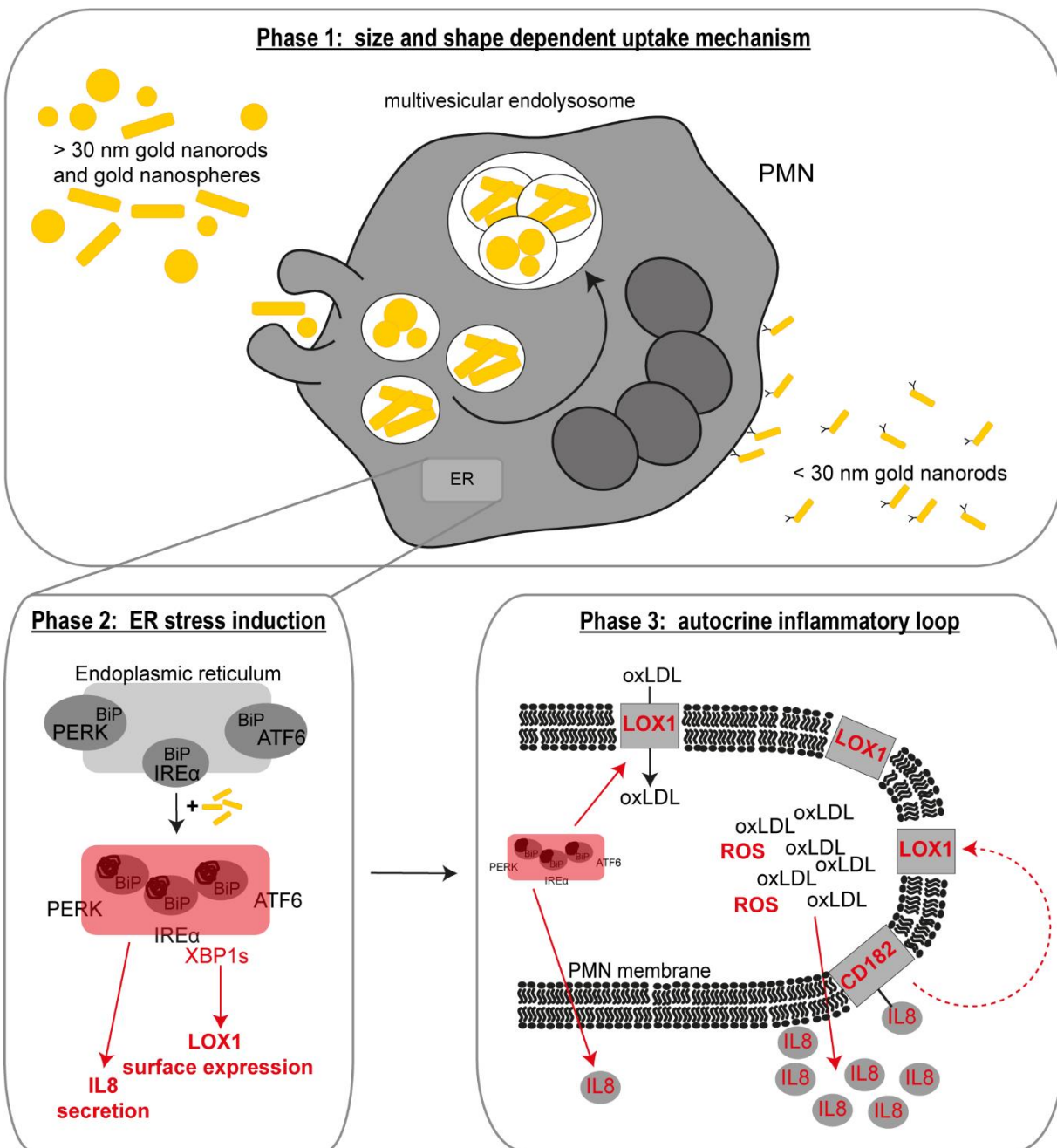


Figure 39: Graphical Abstract

When PMN are exposed to gold nanoparticles, PMN rapidly phagocytose spherical and bigger rod-shaped nanoparticles. Once phagocytosed, AuNP enter multi-vesicular endolysosomes. Conversely, gold nanorods smaller than 30 nm display lower unspecific phagocytosis and can be therefore used for specific targeting via antibody-coupling (Phase 1: size and shape dependent uptake mechanism). This phase is followed by an induction of ER stress mediated by binding of misfolded proteins to BiP, which activates IRE α signaling, XBP1 splicing and a higher expression of LOX1 on the cell surface of PMN (Phase 2: ER stress induction). In the third phase, the increased LOX1 expression accelerates the ER stress induced IL8 secretion via autocrine signaling. Furthermore CD182 signaling promotes higher expression of LOX1 creating a vicious cycle of pro-inflammatory activation (Phase 3: autocrine inflammatory loop).

7 ZUSAMMENFASSUNG

Goldnanopartikel (AuNP), insbesondere Goldnanostäbchen (AuNR), und deren Verwendung in der Biomedizin wurden in den letzten zwanzig Jahren intensiv erforscht. Dies führte zu verschiedenen, vielversprechenden Anwendungen der AuNR, zum Beispiel in der Bildgebung und Krebstherapie, sowie als Vehikel in der Gen- und Arzneimittel-Therapie. Vorangegangene Studien identifizierten die intrinsische und vor allem unspezifische Aufnahme körperfremder Stoffe durch phagozytierende Immunzellen als größtes Hindernis in der medizinischen Anwendung von Nanopartikeln. Polymorphonukleäre Neutrophile (PMN) stellen den größten Anteil innerhalb der phagozytischen Immunzellen im menschlichen Immunsystem dar. Daher ist ein allumfassendes Verständnis der Interaktion zwischen AuNR und PMN entscheidend für die Entwicklung sicherer und vor allem effizienter Krebstherapien.

Die vorgelegte Studie untersuchte die zellbiologische Antwort Polymorphonukleärer Neutrophile nach Exposition von PEGylierten und Antikörper-konjugierten stäbchenförmigen sowie sphärischen AuNP. Hierbei zeigte sich, dass Nanopartikeleigenschaften, wie Größe und Form, die selektive Bindung von Antikörper-konjugierten Nanopartikeln an Phagozyten beeinflussen. Der Vergleich verschiedener Größen und Formen von Goldnanopartikeln zeigte, dass unspezifische Phagozytose durch die Verwendung von 15 nm kleinen stäbchenförmigen AuNR umgangen werden kann. Mittels verschiedener Experimente wurde die Interaktion zwischen PMN und AuNR analysiert. PMN nahmen AuNR bereits innerhalb der ersten 5 Minuten über Phagozytose oder Makropinozytose auf. Die Aufnahme führte zu Endoplasmatischem Retikulum (ER) Stress und vermittelte eine „unfolded protein response“ (UPR) in PMN, welche sich durch die Aktivierung des xenobiotischen Metabolismus und einer Aktivierung der PMN auszeichnete. Diese resultierte in einer erhöhten Expression von lectin-type oxidized LDL receptor 1 (LOX1) auf der Zelloberfläche, sowie in einer verstärkten Sekretion von Interleukin 8 und der Produktion von reaktive Sauerstoffspezies (ROS) aus, welche sich in einem autokrin gegenseitig verstärkten. All diese potenziell immunpathologischen Effekte manifestierten sich innerhalb von 2 Stunden nach Exposition.

Zusammenfassend beschreibt diese Studie die molekulare Interaktion von Goldnanopartikeln und PMN. Ein Verständnis für potenzielle immunpathologischer Effekte ist insbesondere wichtig, da phagozytische Immunzellen, wie PMN, AuNR in hohem Maße und unspezifisch aufnehmen. Dies kann nicht durch die Konjugation spezifischer Antikörper, jedoch durch die Modulation der AuNR-Eigenschaften unterbunden werden. Des Weiteren wird deutlich, dass eine nähere Untersuchung

des Immunsystems, speziell der phagozytischen Immunzellen, von zentraler Bedeutung für die Entwicklung von sicheren und effizienten AuNR-vermittelten Therapien ist.

REFERENCES

- Abadeer, N. S. & Murphy, C. J. Recent Progress in Cancer Thermal Therapy Using Gold Nanoparticles. *J Phys Chem C* **120**, 4691-4716, doi:10.1021/acs.jpcc.5b11232 (2016).
- Abrahamse, H. & Hamblin, M. R. New Photosensitizers for Photodynamic Therapy. *Biochem J* **473**, 347-364, doi:10.1042/BJ20150942 (2016).
- Aioub, M., Panikkanvalappil, S. R. & El-Sayed, M. A. Platinum-Coated Gold Nanorods: Efficient Reactive Oxygen Scavengers That Prevent Oxidative Damage toward Healthy, Untreated Cells During Plasmonic Photothermal Therapy. *ACS Nano* **11**, 579-586, doi:10.1021/acs.nano.6b06651 (2017).
- Alaqad, K. & Saleh, T. A. Gold and Silver Nanoparticles: Synthesis Methods, Characterization Routes and Applications Towards Drugs. *Journal of Environmental & Analytical Toxicology* **6**, doi:10.4172/2161-0525.1000384 (2016).
- Albregues, J., Shields, M. A., Ng, D., Park, C. G., Ambrico, A., Poindexter, M. E., Upadhyay, P., Uyeminami, D. L., Pommier, A., Kuttner, V. *et al.* Neutrophil Extracellular Traps Produced During Inflammation Awaken Dormant Cancer Cells in Mice. *Science* **361**, doi:10.1126/science.aao4227 (2018).
- Ali, M. R., Ali, H. R., Rankin, C. R. & El-Sayed, M. A. Targeting Heat Shock Protein 70 Using Gold Nanorods Enhances Cancer Cell Apoptosis in Low Dose Plasmonic Photothermal Therapy. *Biomaterials* **102**, 1-8, doi:10.1016/j.biomaterials.2016.06.017 (2016).
- Ali, M. R., Rahman, M. A., Wu, Y., Han, T., Peng, X., Mackey, M. A., Wang, D., Shin, H. J., Chen, Z. G., Xiao, H. *et al.* Efficacy, Long-Term Toxicity, and Mechanistic Studies of Gold Nanorods Photothermal Therapy of Cancer in Xenograft Mice. *Proc Natl Acad Sci U S A* **114**, E3110-e3118, doi:10.1073/pnas.1619302114 (2017).
- Alkilany, A. M. & Murphy, C. J. Toxicity and Cellular Uptake of Gold Nanoparticles: What We Have Learned So Far? *J Nanopart Res* **12**, 2313-2333, doi:10.1007/s11051-010-9911-8 (2010).
- Almeida, J. P., Figueroa, E. R. & Drezek, R. A. Gold Nanoparticle Mediated Cancer Immunotherapy. *Nanomedicine* **10**, 503-514, doi:10.1016/j.nano.2013.09.011 (2014).
- Baek, S. K., Makkouk, A. R., Krasieva, T., Sun, C. H., Madsen, S. J. & Hirschberg, H. Photothermal Treatment of Glioma; an in Vitro Study of Macrophage-Mediated Delivery of Gold Nanoshells. *J Neurooncol* **104**, 439-448, doi:10.1007/s11060-010-0511-3 (2011).
- Balasubramanian, S. K., Jittiwat, J., Manikandan, J., Ong, C. N., Yu, L. E. & Ong, W. Y. Biodistribution of Gold Nanoparticles and Gene Expression Changes in the Liver and Spleen after Intravenous Administration in Rats. *Biomaterials* **31**, 2034-2042, doi:10.1016/j.biomaterials.2009.11.079 (2010).
- Barbero, F., Russo, L., Vitali, M., Piella, J., Salvo, I., Borrajo, M. L., Busquets-Fite, M., Grandori, R., Bastus, N. G., Casals, E. *et al.* Formation of the Protein Corona: The Interface between Nanoparticles and the Immune System. *Semin Immunol* **34**, 52-60, doi:10.1016/j.smim.2017.10.001 (2017).
- Bartneck, M., Keul, H. A., Singh, S., Czaja, K., Bornemann, J., Bockstaller, M., Moeller, M., Zwadlo-Klarwasser, G. & Groll, J. Rapid Uptake of Gold Nanorods by Primary Human Blood Phagocytes and Immunomodulatory Effects of Surface Chemistry. *ACS Nano* **4**, 3073-3086, doi:10.1021/nn100262h (2010).
- Bartneck, M., Keul, H. A., Wambach, M., Bornemann, J., Gbureck, U., Chatain, N., Neuss, S., Tacke, F., Groll, J. & Zwadlo-Klarwasser, G. Effects of Nanoparticle Surface-Coupled Peptides, Functional Endgroups, and Charge on Intracellular Distribution and Functionality

- of Human Primary Reticuloendothelial Cells. *Nanomedicine* **8**, 1282-1292, doi:10.1016/j.nano.2012.02.012 (2012).
- Bartneck, M., Keul, H. A., Zwadlo-Klarwasser, G. & Groll, J. Phagocytosis Independent Extracellular Nanoparticle Clearance by Human Immune Cells. *Nano letters* **10**, 59-63, doi:10.1021/nl902830x (2010).
- Belhadj, Z., He, B., Deng, H., Song, S., Zhang, H., Wang, X., Dai, W. & Zhang, Q. A Combined "Eat Me/Don't Eat Me" Strategy Based on Extracellular Vesicles for Anticancer Nanomedicine. *J Extracell Vesicles* **9**, 1806444, doi:10.1080/20013078.2020.1806444 (2020).
- Binnewies, M., Roberts, E. W., Kersten, K., Chan, V., Fearon, D. F., Merad, M., Coussens, L. M., Gabrilovich, D. I., Ostrand-Rosenberg, S., Hedrick, C. C. *et al.* Understanding the Tumor Immune Microenvironment (Time) for Effective Therapy. *Nat Med* **24**, 541-550, doi:10.1038/s41591-018-0014-x (2018).
- Bisso, P. W., Gaglione, S., Guimaraes, P. P. G., Mitchell, M. J. & Langer, R. Nanomaterial Interactions with Human Neutrophils. *Acs Biomaterials Science & Engineering* **4**, 4255-4265, doi:10.1021/acsbiomaterials.8b01062 (2018).
- Bjerregaard, M. D., Jurlander, J., Klausen, P., Borregaard, N. & Cowland, J. B. The in Vivo Profile of Transcription Factors During Neutrophil Differentiation in Human Bone Marrow. *Blood* **101**, 4322-4332, doi:10.1182/blood-2002-03-0835 (2003).
- Bogdan Allemann, I. & Kaufman, J. Laser Principles. *Curr Probl Dermatol* **42**, 7-23, doi:10.1159/000328236 (2011).
- Borregaard, N. Neutrophils, from Marrow to Microbes. *Immunity* **33**, 657-670, doi:10.1016/j.immuni.2010.11.011 (2010).
- Borregaard, N., Sorensen, O. E. & Theilgaard-Monch, K. Neutrophil Granules: A Library of Innate Immunity Proteins. *Trends Immunol* **28**, 340-345, doi:10.1016/j.it.2007.06.002 (2007).
- Brandau, S., Trellakis, S., Bruderek, K., Schmaltz, D., Steller, G., Elian, M., Suttman, H., Schenck, M., Welling, J., Zabel, P. *et al.* Myeloid-Derived Suppressor Cells in the Peripheral Blood of Cancer Patients Contain a Subset of Immature Neutrophils with Impaired Migratory Properties. *J Leukoc Biol* **89**, 311-317, doi:10.1189/jlb.0310162 (2011).
- Breasted, J. H. *The Edwin Smith Surgical Papyrus, Volume 1: Hieroglyphic Transliteration, Translation, and Commentary*. Vol. vol.1 (1930).
- Brinkmann, V., Reichard, U., Goosmann, C., Fauler, B., Uhlemann, Y., Weiss, D. S., Weinrauch, Y. & Zychlinsky, A. Neutrophil Extracellular Traps Kill Bacteria. *Science* **303**, 1532-1535, doi:10.1126/science.1092385 (2004).
- Bronte, V., Brandau, S., Chen, S. H., Colombo, M. P., Frey, A. B., Greten, T. F., Mandruzzato, S., Murray, P. J., Ochoa, A., Ostrand-Rosenberg, S. *et al.* Recommendations for Myeloid-Derived Suppressor Cell Nomenclature and Characterization Standards. *Nature communications* **7**, 12150, doi:10.1038/ncomms12150 (2016).
- Brown, C. L., Whitehouse, M. W., Tiekink, E. R. & Bushell, G. R. Colloidal Metallic Gold Is Not Bio-Inert. *Inflammopharmacology* **16**, 133-137, doi:10.1007/s10787-007-0017-6 (2008).
- Bruderek, K., Schirrmann, R. & Brandau, S. Immunophenotyping of Circulating Myeloid-Derived Suppressor Cells (Mdsc) in the Peripheral Blood of Cancer Patients. *Methods Mol Biol* **2236**, 1-7, doi:10.1007/978-1-0716-1060-2_1 (2021).
- Bruderek, K., Schirrmann, R. & Brandau, S. Isolation of Human Circulating Myeloid-Derived Suppressor Cells and Analysis of Their Immunosuppressive Activity. *Methods Mol Biol* **2236**, 43-56, doi:10.1007/978-1-0716-1060-2_5 (2021).

- Brzezinski, M. R., Abraham, T. L., Stone, C. L., Dean, R. A. & Bosron, W. F. Purification and Characterization of a Human Liver Cocaine Carboxylesterase That Catalyzes the Production of Benzoyllecgonine and the Formation of Cocaethylene from Alcohol and Cocaine. *Biochemical Pharmacology* **48**, 1747-1755, doi:10.1016/0006-2952(94)90461-8 (1994).
- Calandra, T. & Roger, T. Macrophage Migration Inhibitory Factor: A Regulator of Innate Immunity. *Nat Rev Immunol* **3**, 791-800, doi:10.1038/nri1200 (2003).
- Camerin, M., Jori, G., Della Ciana, L., Fabbri, S., Bonacchi, S., Montalti, M. & Prodi, L. Photothermal Sensitisation and Therapeutic Properties of a Novel Far-Red Absorbing Cyanine. *Photochem Photobiol Sci* **8**, 1422-1431, doi:10.1039/b908495a (2009).
- Camerin, M., Rello, S., Villanueva, A., Ping, X., Kenney, M. E., Rodgers, M. A. & Jori, G. Photothermal Sensitisation as a Novel Therapeutic Approach for Tumours: Studies at the Cellular and Animal Level. *Eur J Cancer* **41**, 1203-1212, doi:10.1016/j.ejca.2005.02.021 (2005).
- Cao, Y., Long, J., Liu, L., He, T., Jiang, L., Zhao, C. & Li, Z. A Review of Endoplasmic Reticulum (Er) Stress and Nanoparticle (Np) Exposure. *Life Sci* **186**, 33-42, doi:10.1016/j.lfs.2017.08.003 (2017).
- Cashman, J. R. Human Flavin-Containing Monooxygenase: Substrate Specificity and Role in Drug Metabolism. *Curr Drug Metab* **1**, 181-191, doi:10.2174/1389200003339135 (2000).
- Chekeni, F. B. & Ravichandran, K. S. The Role of Nucleotides in Apoptotic Cell Clearance: Implications for Disease Pathogenesis. *J Mol Med (Berl)* **89**, 13-22, doi:10.1007/s00109-010-0673-7 (2011).
- Chen, T. H., Chiang, Y. H., Hou, J. N., Cheng, C. C., Sofiyatun, E., Chiu, C. H. & Chen, W. J. Xbp1-Mediated Bip/Grp78 Upregulation Copes with Oxidative Stress in Mosquito Cells During Dengue 2 Virus Infection. *Biomed Res Int* **2017**, 3519158, doi:10.1155/2017/3519158 (2017).
- Cheng, H., Zheng, Z. & Cheng, T. New Paradigms on Hematopoietic Stem Cell Differentiation. *Protein Cell* **11**, 34-44, doi:10.1007/s13238-019-0633-0 (2020).
- Cho, W. S., Cho, M., Jeong, J., Choi, M., Han, B. S., Shin, H. S., Hong, J., Chung, B. H., Jeong, J. & Cho, M. H. Size-Dependent Tissue Kinetics of Peg-Coated Gold Nanoparticles. *Toxicol Appl Pharmacol* **245**, 116-123, doi:10.1016/j.taap.2010.02.013 (2010).
- Choi, K., Riviere, J. E. & Monteiro-Riviere, N. A. Protein Corona Modulation of Hepatocyte Uptake and Molecular Mechanisms of Gold Nanoparticle Toxicity. *Nanotoxicology* **11**, 64-75, doi:10.1080/17435390.2016.1264638 (2017).
- Choudhury, D., Xavier, P. L., Chaudhari, K., John, R., Dasgupta, A. K., Pradeep, T. & Chakrabarti, G. Unprecedented Inhibition of Tubulin Polymerization Directed by Gold Nanoparticles Inducing Cell Cycle Arrest and Apoptosis. *Nanoscale* **5**, 4476-4489, doi:10.1039/c3nr33891f (2013).
- Clift, M. J. D., Brandenberger, C., Rothen-Rutishauser, B., Brown, D. M. & Stone, V. The Uptake and Intracellular Fate of a Series of Different Surface Coated Quantum Dots in Vitro. *Toxicology* **286**, 58-68, doi:10.1016/j.tox.2011.05.006 (2011).
- Condamine, T., Dominguez, G. A., Youn, J. I., Kossenkov, A. V., Mony, S., Alicea-Torres, K., Tcyganov, E., Hashimoto, A., Nefedova, Y., Lin, C. *et al.* Lectin-Type Oxidized Ldl Receptor-1 Distinguishes Population of Human Polymorphonuclear Myeloid-Derived Suppressor Cells in Cancer Patients. *Science immunology* **1**, doi:10.1126/sciimmunol.aaf8943 (2016).
- Cortez-Retamozo, V., Lauwereys, M., Hassanzadeh Gh, G., Gobert, M., Conrath, K., Muyltermans, S., De Baetselier, P. & Revets, H. Efficient Tumor Targeting by Single-

- Domain Antibody Fragments of Camels. *Int J Cancer* **98**, 456-462, doi:10.1002/ijc.10212 (2002).
- Dai, Q., Wilhelm, S., Ding, D., Syed, A. M., Sindhvani, S., Zhang, Y. W., Chen, Y. Y., Macmillan, P. & Chan, W. C. W. Quantifying the Ligand-Coated Nanoparticle Delivery to Cancer Cells in Solid Tumors. *Acs Nano* **12**, 8423-8435, doi:10.1021/acsnano.8b03900 (2018).
- Dale, D. C., Boxer, L. & Liles, W. C. The Phagocytes: Neutrophils and Monocytes. *Blood* **112**, 935-945, doi:10.1182/blood-2007-12-077917 (2008).
- Damodaran, V. B. & Fee, C. Protein Pegylation: An Overview of Chemistry and Process Considerations. *Eur Pharm Rev* **15**, 18-26 (2010).
- Datta, N. R., Ordonez, S. G., Gaipal, U. S., Paulides, M. M., Crezee, H., Gellermann, J., Marder, D., Puric, E. & Bodis, S. Local Hyperthermia Combined with Radiotherapy and/or Chemotherapy: Recent Advances and Promises for the Future. *Cancer Treat Rev* **41**, 742-753, doi:10.1016/j.ctrv.2015.05.009 (2015).
- Deinhardt, K., Salinas, S., Verastegui, C., Watson, R., Worth, D., Hanrahan, S., Bucci, C. & Schiavo, G. Rab5 and Rab7 Control Endocytic Sorting Along the Axonal Retrograde Transport Pathway. *Neuron* **52**, 293-305, doi:10.1016/j.neuron.2006.08.018 (2006).
- Devasagayam, T. P., Tilak, J. C., Bloor, K. K., Sane, K. S., Ghaskadbi, S. S. & Lele, R. D. Free Radicals and Antioxidants in Human Health: Current Status and Future Prospects. *J Assoc Physicians India* **52**, 794-804 (2004).
- Dey, A. K., Gonon, A., Pecheur, E. I., Pezet, M., Villiers, C. & Marche, P. N. Impact of Gold Nanoparticles on the Functions of Macrophages and Dendritic Cells. *Cells* **10**, doi:10.3390/cells10010096 (2021).
- Di Bucchianico, S., Fabbri, M. R., Cirillo, S., Ubaldi, C., Gilliland, D., Valsami-Jones, E. & Migliore, L. Aneuploidogenic Effects and DNA Oxidation Induced in Vitro by Differently Sized Gold Nanoparticles. *Int J Nanomedicine* **9**, 2191-2204, doi:10.2147/IJN.S58397 (2014).
- Dinarello, C. A. Blocking Il-1 in Systemic Inflammation. *The Journal of experimental medicine* **201**, 1355-1359, doi:10.1084/jem.20050640 (2005).
- Dixit, N. & Simon, S. I. Chemokines, Selectins and Intracellular Calcium Flux: Temporal and Spatial Cues for Leukocyte Arrest. *Front Immunol* **3**, 188, doi:10.3389/fimmu.2012.00188 (2012).
- Dixit, N., Yamayoshi, I., Nazarian, A. & Simon, S. I. Migrational Guidance of Neutrophils Is Mechanotransduced Via High-Affinity Lfa-1 and Calcium Flux. *J Immunol* **187**, 472-481, doi:10.4049/jimmunol.1004197 (2011).
- Dreaden, E. C., Alkilany, A. M., Huang, X., Murphy, C. J. & El-Sayed, M. A. The Golden Age: Gold Nanoparticles for Biomedicine. *Chem Soc Rev* **41**, 2740-2779, doi:10.1039/c1cs15237h (2012).
- Dumitru, C. A., Moses, K., Trellakis, S., Lang, S. & Brandau, S. Neutrophils and Granulocytic Myeloid-Derived Suppressor Cells: Immunophenotyping, Cell Biology and Clinical Relevance in Human Oncology. *Cancer Immunol Immunother* **61**, 1155-1167, doi:10.1007/s00262-012-1294-5 (2012).
- Dunn, G. P., Old, L. J. & Schreiber, R. D. The Three Es of Cancer Immunoediting. *Annu Rev Immunol* **22**, 329-360, doi:10.1146/annurev.immunol.22.012703.104803 (2004).
- Durocher, I., Noel, C., Lavastre, V. & Girard, D. Evaluation of the in Vitro and in Vivo Proinflammatory Activities of Gold (+) and Gold (-) Nanoparticles. *Inflamm Res* **66**, 981-992, doi:10.1007/s00011-017-1078-7 (2017).
- Dykman, L. A. & Khlebtsov, N. G. Uptake of Engineered Gold Nanoparticles into Mammalian Cells. *Chem Rev* **114**, 1258-1288, doi:10.1021/cr300441a (2014).

- Dykman, L. A. & Khlebtsov, N. G. Immunological Properties of Gold Nanoparticles. *Chem Sci* **8**, 1719-1735, doi:10.1039/c6sc03631g (2017).
- Eash, K. J., Greenbaum, A. M., Gopalan, P. K. & Link, D. C. Cxcr2 and Cxcr4 Antagonistically Regulate Neutrophil Trafficking from Murine Bone Marrow. *J Clin Invest* **120**, 2423-2431, doi:10.1172/jci41649 (2010).
- El-Sayed, I. H., Huang, X. & El-Sayed, M. A. Surface Plasmon Resonance Scattering and Absorption of Anti-Egfr Antibody Conjugated Gold Nanoparticles in Cancer Diagnostics: Applications in Oral Cancer. *Nano letters* **5**, 829-834, doi:10.1021/nl050074e (2005).
- El-Sayed, I. H., Huang, X. & El-Sayed, M. A. Selective Laser Photo-Thermal Therapy of Epithelial Carcinoma Using Anti-Egfr Antibody Conjugated Gold Nanoparticles. *Cancer Lett* **239**, 129-135, doi:10.1016/j.canlet.2005.07.035 (2006).
- Emami, F., Pathak, S., Nguyen, T. T., Shrestha, P., Maharjan, S., Kim, J. O., Jeong, J. H. & Yook, S. Photoimmunotherapy with Cetuximab-Conjugated Gold Nanorods Reduces Drug Resistance in Triple Negative Breast Cancer Spheroids with Enhanced Infiltration of Tumor-Associated Macrophages. *J Control Release* **329**, 645-664, doi:10.1016/j.jconrel.2020.10.001 (2021).
- Enyedi, B., Varnai, P. & Geiszt, M. Redox State of the Endoplasmic Reticulum Is Controlled by Ero1 α and Intraluminal Calcium. *Antioxid Redox Signal* **13**, 721-729, doi:10.1089/ars.2009.2880 (2010).
- Faraday, M. X. The Bakerian Lecture. —Experimental Relations of Gold (and Other Metals) to Light. *Philosophical Transactions of the Royal Society of London* **147**, 145-181, doi:10.1098/rstl.1857.0011 (1887).
- Faurschou, M. & Borregaard, N. Neutrophil Granules and Secretory Vesicles in Inflammation. *Microbes Infect* **5**, 1317-1327, doi:10.1016/j.micinf.2003.09.008 (2003).
- Feynman, R. There's Plenty of Room at the Bottom. *Engineering and Science* **23**, 22-36, doi:10.1007/s12045-011-0109-x (1960).
- Filippi, M. D. Neutrophil Transendothelial Migration: Updates and New Perspectives. *Blood* **133**, 2149-2158, doi:10.1182/blood-2018-12-844605 (2019).
- Flannagan, R. S., Jaumouille, V. & Grinstein, S. The Cell Biology of Phagocytosis. *Annu Rev Pathol* **7**, 61-98, doi:10.1146/annurev-pathol-011811-132445 (2012).
- Fujimoto, H., Sakata, T., Hamaguchi, Y., Shiga, S., Tohyama, K., Ichiyama, S., Wang, F. S. & Houwen, B. Flow Cytometric Method for Enumeration and Classification of Reactive Immature Granulocyte Populations. *Cytometry* **42**, 371-378 (2000).
- Galli, F., Aguilera, J. V., Palermo, B., Markovic, S. N., Nistico, P. & Signore, A. Relevance of Immune Cell and Tumor Microenvironment Imaging in the New Era of Immunotherapy. *Journal of experimental & clinical cancer research : CR* **39**, 89, doi:10.1186/s13046-020-01586-y (2020).
- Galluzzi, L., Vitale, I., Aaronson, S. A., Abrams, J. M., Adam, D., Agostinis, P., Alnemri, E. S., Altucci, L., Amelio, I., Andrews, D. W. *et al.* Molecular Mechanisms of Cell Death: Recommendations of the Nomenclature Committee on Cell Death 2018. *Cell Death Differ* **25**, 486-541, doi:10.1038/s41418-017-0012-4 (2018).
- Gazelle, G. S., Goldberg, S. N., Solbiati, L. & Livraghi, T. Tumor Ablation with Radio-Frequency Energy. *Radiology* **217**, 633-646, doi:10.1148/radiology.217.3.r00dc26633 (2000).
- Gentles, A. J., Newman, A. M., Liu, C. L., Bratman, S. V., Feng, W., Kim, D., Nair, V. S., Xu, Y., Khuong, A., Hoang, C. D. *et al.* The Prognostic Landscape of Genes and Infiltrating Immune Cells across Human Cancers. *Nat Med* **21**, 938-945, doi:10.1038/nm.3909 (2015).

- Gery, S., Gombart, A. F., Fung, Y. K. & Koeffler, H. P. C/EBPε Interacts with Retinoblastoma and E2f1 During Granulopoiesis. *Blood* **103**, 828-835, doi:10.1182/blood-2003-01-0159 (2004).
- Gold, M. H. Introduction to Photodynamic Therapy: Early Experience. *Dermatol Clin* **25**, 1-4, doi:10.1016/j.det.2006.09.004 (2007).
- Goldmann, L. *Biomedical Aspects of the Laser*. (Springer, New York, 1967).
- Gombart, A. F., Shiohara, M., Kwok, S. H., Agematsu, K., Komiyama, A. & Koeffler, H. P. Neutrophil-Specific Granule Deficiency: Homozygous Recessive Inheritance of a Frameshift Mutation in the Gene Encoding Transcription Factor Ccaat/Enhancer Binding Protein--Epsilon. *Blood* **97**, 2561-2567, doi:10.1182/blood.v97.9.2561 (2001).
- Gordon, S. Phagocytosis: An Immunobiologic Process. *Immunity* **44**, 463-475 (2016).
- Gref, R., Minamitake, Y., Peracchia, M. T., Trubetskoy, V., Torchilin, V. & Langer, R. Biodegradable Long-Circulating Polymeric Nanospheres. *Science* **263**, 1600-1603, doi:10.1126/science.8128245 (1994).
- Greten, F. R. & Grivnenikov, S. I. Inflammation and Cancer: Triggers, Mechanisms, and Consequences. *Immunity* **51**, 27-41, doi:10.1016/j.immuni.2019.06.025 (2019).
- Gustafson, H. H., Holt-Casper, D., Grainger, D. W. & Ghandehari, H. Nanoparticle Uptake: The Phagocyte Problem. *Nano Today* **10**, 487-510, doi:10.1016/j.nantod.2015.06.006 (2015).
- Guthrie, G. J., Charles, K. A., Roxburgh, C. S., Horgan, P. G., Mcmillan, D. C. & Clarke, S. J. The Systemic Inflammation-Based Neutrophil-Lymphocyte Ratio: Experience in Patients with Cancer. *Crit Rev Oncol Hematol* **88**, 218-230, doi:10.1016/j.critrevonc.2013.03.010 (2013).
- Han, D., Zhu, G., Wu, C., Zhu, Z., Chen, T., Zhang, X. & Tan, W. Engineering a Cell-Surface Aptamer Circuit for Targeted and Amplified Photodynamic Cancer Therapy. *ACS Nano* **7**, 2312-2319, doi:10.1021/nn305484p (2013).
- Hanahan, D. & Weinberg, R. A. Hallmarks of Cancer: The Next Generation. *Cell* **144**, 646-674, doi:10.1016/j.cell.2011.02.013 (2011).
- Handel, T. M., Johnson, Z., Crown, S. E., Lau, E. K. & Proudfoot, A. E. Regulation of Protein Function by Glycosaminoglycans--as Exemplified by Chemokines. *Annu Rev Biochem* **74**, 385-410, doi:10.1146/annurev.biochem.72.121801.161747 (2005).
- Harada, A., Sekido, N., Akahoshi, T., Wada, T., Mukaida, N. & Matsushima, K. Essential Involvement of Interleukin-8 (IL8) in Acute Inflammation. *Journal of Leukocyte Biology* **56**, 559-564, doi:10.1002/jlb.56.5.559 (1994).
- Hedrick, C. C. & Malanchi, I. Neutrophils in Cancer: Heterogeneous and Multifaceted. *Nat Rev Immunol*, doi:10.1038/s41577-021-00571-6 (2021).
- Heit, B., Robbins, S. M., Downey, C. M., Guan, Z., Colarusso, P., Miller, B. J., Jirik, F. R. & Kubes, P. Pten Functions to 'Prioritize' Chemotactic Cues and Prevent 'Distraction' in Migrating Neutrophils. *Nature immunology* **9**, 743-752, doi:10.1038/ni.1623 (2008).
- Hendel, T., Wuithschick, M., Kettemann, F., Birnbaum, A., Rademann, K. & Polte, J. In Situ Determination of Colloidal Gold Concentrations with Uv-Vis Spectroscopy: Limitations and Perspectives. *Anal Chem* **86**, 11115-11124, doi:10.1021/ac502053s (2014).
- Herb, M. & Schramm, M. Functions of Ros in Macrophages and Antimicrobial Immunity. *Antioxidants (Basel)* **10**, doi:10.3390/antiox10020313 (2021).
- Hirai, H., Zhang, P., Dayaram, T., Hetherington, C. J., Mizuno, S., Imanishi, J., Akashi, K. & Tenen, D. G. C/EBPβ Is Required for 'Emergency' Granulopoiesis. *Nature immunology* **7**, 732-739, doi:10.1038/ni1354 (2006).
- Huang, K., Ma, H., Liu, J., Huo, S., Kumar, A., Wei, T., Zhang, X., Jin, S., Gan, Y., Wang, P. C. *et al.* Size-Dependent Localization and Penetration of Ultrasmall Gold Nanoparticles in

- Cancer Cells, Multicellular Spheroids, and Tumors in Vivo. *ACS Nano* **6**, 4483-4493, doi:10.1021/nn301282m (2012).
- Huang, X., El-Sayed, I. H., Qian, W. & El-Sayed, M. A. Cancer Cell Imaging and Photothermal Therapy in the near-Infrared Region by Using Gold Nanorods. *Journal of the American Chemical Society* **128**, 2115-2120, doi:10.1021/ja057254a (2006).
- Huang, X., Jain, P. K., El-Sayed, I. H. & El-Sayed, M. A. Plasmonic Photothermal Therapy (PpTT) Using Gold Nanoparticles. *Lasers Med Sci* **23**, 217-228, doi:10.1007/s10103-007-0470-x (2008).
- Hwang, S., Nam, J., Jung, S., Song, J., Doh, H. & Kim, S. Gold Nanoparticle-Mediated Photothermal Therapy: Current Status and Future Perspective. *Nanomedicine (Lond)* **9**, 2003-2022, doi:10.2217/nmm.14.147 (2014).
- Iglesias, P. A. & Devreotes, P. N. Navigating through Models of Chemotaxis. *Curr Opin Cell Biol* **20**, 35-40, doi:10.1016/j.ceb.2007.11.011 (2008).
- Ilie, M., Hofman, V., Ortholan, C., Bonnetaud, C., Coelle, C., Mouroux, J. & Hofman, P. Predictive Clinical Outcome of the Intratumoral Cd66b-Positive Neutrophil-to-Cd8-Positive T-Cell Ratio in Patients with Resectable Non-small Cell Lung Cancer. *Cancer* **118**, 1726-1737, doi:10.1002/cncr.26456 (2012).
- Jana, N. R., Gearheart, L. & Murphy, C. J. Seed-Mediated Growth Approach for Shape-Controlled Synthesis of Spheroidal and Rod-Like Gold Nanoparticles Using a Surfactant Template. *Advanced Materials* **13**, 1389-1393, doi:10.1002/1521-4095(200109)13:18<1389::Aid-adma1389>3.0.Co;2-f (2001).
- Jana, N. R., Gearheart, L. & Murphy, C. J. Wet Chemical Synthesis of High Aspect Ratio Cylindrical Gold Nanorods. *J Phys Chem B* **105**, 4065-4067, doi:DOI 10.1021/jp0107964 (2001).
- Jensen, H. K., Donskov, F., Marcussen, N., Nordmark, M., Lundbeck, F. & Von Der Maase, H. Presence of Intratumoral Neutrophils Is an Independent Prognostic Factor in Localized Renal Cell Carcinoma. *J Clin Oncol* **27**, 4709-4717, doi:10.1200/JCO.2008.18.9498 (2009).
- Jensen, T. O., Schmidt, H., Moller, H. J., Donskov, F., Hoyer, M., Sjoegren, P., Christensen, I. J. & Steiniche, T. Intratumoral Neutrophils and Plasmacytoid Dendritic Cells Indicate Poor Prognosis and Are Associated with Pstat3 Expression in Ajcc Stage I/II Melanoma. *Cancer* **118**, 2476-2485, doi:10.1002/cncr.26511 (2012).
- Jeyaraj, M., Arun, R., Sathishkumar, G., Mubarakali, D., Rajesh, M., Sivanandhan, G., Kapildev, G., Manickavasagam, M., Thajuddin, N. & Ganapathi, A. An Evidence on G2/M Arrest, DNA Damage and Caspase Mediated Apoptotic Effect of Biosynthesized Gold Nanoparticles on Human Cervical Carcinoma Cells (Hela). *Materials Research Bulletin* **52**, 15-24, doi:10.1016/j.materresbull.2013.12.060 (2014).
- Jia, H., Fang, C., Zhu, X. M., Ruan, Q., Wang, Y. X. & Wang, J. Synthesis of Absorption-Dominant Small Gold Nanorods and Their Plasmonic Properties. *Langmuir* **31**, 7418-7426, doi:10.1021/acs.langmuir.5b01444 (2015).
- Jia, H., Fang, C., Zhu, X. M., Ruan, Q., Wang, Y. X. & Wang, J. Synthesis of Absorption-Dominant Small Gold Nanorods and Their Plasmonic Properties. *Langmuir* **31**, 7418-7426, doi:10.1021/acs.langmuir.5b01444 (2015).
- Kam, N. W. S., O'Connell, M., Wisdom, J. A. & Dai, H. J. Carbon Nanotubes as Multifunctional Biological Transporters and near-Infrared Agents for Selective Cancer Cell Destruction. *P Natl Acad Sci USA* **102**, 11600-11605, doi:10.1073/pnas.0502680102 (2005).
- Kapany, N. S., Peppers, N. A., Zweng, H. C. & Flocks, M. Retinal Photocoagulation by Lasers. *Nature* **199**, 146-149, doi:10.1038/199146a0 (1963).

- Kardosova, M., Zjablovskaja, P., Danek, P., Angelisova, P., De Figueiredo-Pontes, L. L., Welner, R. S., Brdicka, T., Lee, S., Tenen, D. G. & Alberich-Jorda, M. C/Ebpgamma Is Dispensable for Steady-State and Emergency Granulopoiesis. *Haematologica* **103**, e331-e335, doi:10.3324/haematol.2017.173781 (2018).
- Kelley, W. J., Fromen, C. A., Lopez-Cazares, G. & Eniola-Adefeso, O. Pegylation of Model Drug Carriers Enhances Phagocytosis by Primary Human Neutrophils. *Acta Biomater* **79**, 283-293, doi:10.1016/j.actbio.2018.09.001 (2018).
- Khlebtsov, B., Zharov, V., Melnikov, A., Tuchin, V. & Khlebtsov, N. Optical Amplification of Photothermal Therapy with Gold Nanoparticles and Nanoclusters. *Nanotechnology* **17**, 5167-5179, doi:10.1088/0957-4484/17/20/022 (2006).
- Khlebtsov, N. & Dykman, L. Biodistribution and Toxicity of Engineered Gold Nanoparticles: A Review of in Vitro and in Vivo Studies. *Chem Soc Rev* **40**, 1647-1671, doi:10.1039/c0cs00018c (2011).
- Kinnear, C., Dietsch, H., Clift, M. J., Endes, C., Rothen-Rutishauser, B. & Petri-Fink, A. Gold Nanorods: Controlling Their Surface Chemistry and Complete Detoxification by a Two-Step Place Exchange. *Angew Chem Int Ed Engl* **52**, 1934-1938, doi:10.1002/anie.201208568 (2013).
- Kishimoto, T. K., Jutila, M. A., Berg, E. L. & Butcher, E. C. Neutrophil Mac-1 and Mel-14 Adhesion Proteins Inversely Regulated by Chemotactic Factors. *Science* **245**, 1238-1241, doi:10.1126/science.2551036 (1989).
- Klebanoff, S. J. Myeloperoxidase: Friend and Foe. *Journal of Leukocyte Biology* **77**, 598-625 (2005).
- Kohler, G. & Milstein, C. Continuous Cultures of Fused Cells Secreting Antibody of Predefined Specificity. *Nature* **256**, 495-497, doi:10.1038/256495a0 (1975).
- Kolaczowska, E. & Kubes, P. Neutrophil Recruitment and Function in Health and Inflammation. *Nat Rev Immunol* **13**, 159-175, doi:10.1038/nri3399 (2013).
- Krebs, J., Groenendyk, J. & Michalak, M. Ca²⁺-Signaling, Alternative Splicing and Endoplasmic Reticulum Stress Responses. *Neurochem Res* **36**, 1198-1211, doi:10.1007/s11064-011-0431-4 (2011).
- Kuhn, D. A., Vanhecke, D., Michen, B., Blank, F., Gehr, P., Petri-Fink, A. & Rothen-Rutishauser, B. Different Endocytotic Uptake Mechanisms for Nanoparticles in Epithelial Cells and Macrophages. *Beilstein J Nanotechnol* **5**, 1625-1636, doi:10.3762/bjnano.5.174 (2014).
- Kunitomi, C., Harada, M., Kusamoto, A., Azhary, J. M., Nose, E., Koike, H., Xu, Z., Urata, Y., Takahashi, N., Wada-Hiraike, O. *et al.* Induction of Aryl Hydrocarbon Receptor in Granulosa Cells by Endoplasmic Reticulum Stress Contributes to Pathology of Polycystic Ovary Syndrome. *Mol Hum Reprod* **27**, 1-13, doi:10.1093/molehr/gaab003 (2021).
- Lang, S., Bruderek, K., Kaspar, C., Hoing, B., Kanaan, O., Dominas, N., Hussain, T., Droege, F., Eyth, C., Hadaschik, B. *et al.* Clinical Relevance and Suppressive Capacity of Human Myeloid-Derived Suppressor Cell Subsets. *Clinical cancer research : an official journal of the American Association for Cancer Research* **24**, 4834-4844, doi:10.1158/1078-0432.Ccr-17-3726 (2018).
- Lapinet, J. A., Scapini, P., Calzetti, F., Perez, O. & Cassatella, M. A. Gene Expression and Production of Tumor Necrosis Factor Alpha, Interleukin-1beta (Il-1beta), IL8, Macrophage Inflammatory Protein 1alpha (Mip-1alpha), Mip-1beta, and Gamma Interferon-Inducible Protein 10 by Human Neutrophils Stimulated with Group B Meningococcal Outer Membrane Vesicles. *Infect Immun* **68**, 6917-6923, doi:10.1128/IAI.68.12.6917-6923.2000 (2000).

- Lecot, P., Sarabi, M., Pereira Abrantes, M., Mussard, J., Koenderman, L., Caux, C., Bendriss-Vermare, N. & Michallet, M. C. Neutrophil Heterogeneity in Cancer: From Biology to Therapies. *Front Immunol* **10**, 2155, doi:10.3389/fimmu.2019.02155 (2019).
- Lee, B. R., Chang, S. Y., Hong, E. H., Kwon, B. E., Kim, H. M., Kim, Y. J., Lee, J., Cho, H. J., Cheon, J. H. & Ko, H. J. Elevated Endoplasmic Reticulum Stress Reinforced Immunosuppression in the Tumor Microenvironment Via Myeloid-Derived Suppressor Cells. *Oncotarget* **5**, 12331-12345, doi:10.18632/oncotarget.2589 (2014).
- Lee, C. H., Syu, S. H., Chen, Y. S., Hussain, S. M., Aleksandrovich Onischuk, A., Chen, W. L. & Steven Huang, G. Gold Nanoparticles Regulate the Blimp1/Pax5 Pathway and Enhance Antibody Secretion in B-Cells. *Nanotechnology* **25**, 125103, doi:10.1088/0957-4484/25/12/125103 (2014).
- Leto, T. L. & Geiszt, M. Role of Nox Family Nadph Oxidases in Host Defense. *Antioxid Redox Signal* **8**, 1549-1561, doi:10.1089/ars.2006.8.1549 (2006).
- Li, A., Song, N. J., Riesenberger, B. P. & Li, Z. The Emerging Roles of Endoplasmic Reticulum Stress in Balancing Immunity and Tolerance in Health and Diseases: Mechanisms and Opportunities. *Front Immunol* **10**, 3154, doi:10.3389/fimmu.2019.03154 (2019).
- Li, A., Zhao, J., Fu, J., Cai, J. & Zhang, P. Recent Advances of Biomimetic Nano-Systems in the Diagnosis and Treatment of Tumor. *Asian J Pharm Sci* **16**, 161-174, doi:10.1016/j.ajps.2019.08.001 (2021).
- Li, P., Li, M., Lindberg, M. R., Kennett, M. J., Xiong, N. & Wang, Y. Pad4 Is Essential for Antibacterial Innate Immunity Mediated by Neutrophil Extracellular Traps. *The Journal of experimental medicine* **207**, 1853-1862, doi:10.1084/jem.20100239 (2010).
- Li, Y., Kroger, M. & Liu, W. K. Shape Effect in Cellular Uptake of Pegylated Nanoparticles: Comparison between Sphere, Rod, Cube and Disk. *Nanoscale* **7**, 16631-16646, doi:10.1039/c5nr02970h (2015).
- Li, Z., Huang, H., Tang, S., Li, Y., Yu, X. F., Wang, H., Li, P., Sun, Z., Zhang, H., Liu, C. *et al.* Small Gold Nanorods Laden Macrophages for Enhanced Tumor Coverage in Photothermal Therapy. *Biomaterials* **74**, 144-154, doi:10.1016/j.biomaterials.2015.09.038 (2016).
- Link, S. & El-Sayed, M. A. Spectral Properties and Relaxation Dynamics of Surface Plasmon Electronic Oscillations in Gold and Silver Nanodots and Nanorods. *J Phys Chem B* **103**, 8410-8426, doi:DOI 10.1021/jp9917648 (1999).
- Link, S. & El-Sayed, M. A. Shape and Size Dependence of Radiative, Non-Radiative and Photothermal Properties of Gold Nanocrystals. *International Reviews in Physical Chemistry* **19**, 409-453, doi:Doi 10.1080/01442350050034180 (2000).
- Liu, L., Bai, X., Martikainen, M. V., Karlund, A., Roponen, M., Xu, W., Hu, G., Tasciotti, E. & Lehto, V. P. Cell Membrane Coating Integrity Affects the Internalization Mechanism of Biomimetic Nanoparticles. *Nature communications* **12**, 5726, doi:10.1038/s41467-021-26052-x (2021).
- Livak, K. J. & Schmittgen, T. D. Analysis of Relative Gene Expression Data Using Real-Time Quantitative Pcr and the 2(-Delta Delta C(T)) Method. *Methods* **25**, 402-408, doi:10.1006/meth.2001.1262 (2001).
- Lloyd, A. R. & Oppenheim, J. J. Poly's Lament: The Neglected Role of the Polymorphonuclear Neutrophil in the Afferent Limb of the Immune Response. *Immunology Today* **13**, 169-172, doi:10.1016/0167-5699(92)90121-m (1992).
- Loo, C., Lowery, A., Halas, N., West, J. & Drezek, R. Immunotargeted Nanoshells for Integrated Cancer Imaging and Therapy. *Nano letters* **5**, 709-711, doi:10.1021/nl050127s (2005).
- Louten, J. in *Essential Human Virology* 19-29 (2016).

- Lu, R. M., Hwang, Y. C., Liu, I. J., Lee, C. C., Tsai, H. Z., Li, H. J. & Wu, H. C. Development of Therapeutic Antibodies for the Treatment of Diseases. *J Biomed Sci* **27**, 1, doi:10.1186/s12929-019-0592-z (2020).
- Lugano, R., Ramachandran, M. & Dimberg, A. Tumor Angiogenesis: Causes, Consequences, Challenges and Opportunities. *Cell Mol Life Sci* **77**, 1745-1770, doi:10.1007/s00018-019-03351-7 (2020).
- Maeda, H. The Enhanced Permeability and Retention (Epr) Effect in Tumor Vasculature: The Key Role of Tumor-Selective Macromolecular Drug Targeting. *Advances in Enzyme Regulation* **41**, 189-207, doi:10.1016/s0065-2571(00)00013-3 (2001).
- Maiman, T. H. Stimulated Optical Radiation in Ruby. *Nature* **187**, 493-494, doi:DOI 10.1038/187493a0 (1960).
- Mandruzzato, S., Brandau, S., Britten, C. M., Bronte, V., Damuzzo, V., Gouttefangeas, C., Maurer, D., Ottensmeier, C., Van Der Burg, S. H., Welters, M. J. *et al.* Toward Harmonized Phenotyping of Human Myeloid-Derived Suppressor Cells by Flow Cytometry: Results from an Interim Study. *Cancer Immunol Immunother* **65**, 161-169, doi:10.1007/s00262-015-1782-5 (2016).
- Martin, C., Burdon, P. C. E., Bridger, G., Gutierrez-Ramos, J. C., Williams, T. J. & Rankin, S. M. Chemokines Acting Via Cxcr2 and Cxcr4 Control the Release of Neutrophils from the Bone Marrow and Their Return Following Senescence. *Immunity* **19**, 583-593, doi:Doi 10.1016/S1074-7613(03)00263-2 (2003).
- Martinet, W., Schrijvers, D. M., Timmermans, J. P., Herman, A. G. & De Meyer, G. R. Phagocytosis of Bacteria Is Enhanced in Macrophages Undergoing Nutrient Deprivation. *FEBS J* **276**, 2227-2240, doi:10.1111/j.1742-4658.2009.06951.x (2009).
- Masters, A., Steger, A. C., Lees, W. R., Walmsley, K. M. & Bown, S. G. Interstitial Laser Hyperthermia: A New Approach for Treating Liver Metastases. *British journal of cancer* **66**, 518-522, doi:10.1038/bjc.1992.305 (1992).
- Mcdonald, B. & Kubes, P. Cellular and Molecular Choreography of Neutrophil Recruitment to Sites of Sterile Inflammation. *Journal of Molecular Medicine-Imm* **89**, 1079-1088, doi:10.1007/s00109-011-0784-9 (2011).
- Mcdonald, B., Pittman, K., Menezes, G. B., Hirota, S. A., Slaba, I., Waterhouse, C. C., Beck, P. L., Muruve, D. A. & Kubes, P. Intravascular Danger Signals Guide Neutrophils to Sites of Sterile Inflammation. *Science* **330**, 362-366, doi:10.1126/science.1195491 (2010).
- Mestas, J. & Hughes, C. C. Of Mice and Not Men: Differences between Mouse and Human Immunology. *J Immunol* **172**, 2731-2738, doi:10.4049/jimmunol.172.5.2731 (2004).
- Metzemaekers, M., Gouwy, M. & Proost, P. Neutrophil Chemoattractant Receptors in Health and Disease: Double-Edged Swords. *Cell Mol Immunol* **17**, 433-450, doi:10.1038/s41423-020-0412-0 (2020).
- Metzler, K. D., Goosmann, C., Lubojemska, A., Zychlinsky, A. & Papayannopoulos, V. A Myeloperoxidase-Containing Complex Regulates Neutrophil Elastase Release and Actin Dynamics During Netosis. *Cell reports* **8**, 883-896, doi:10.1016/j.celrep.2014.06.044 (2014).
- Middleton, J., Patterson, A. M., Gardner, L., Schmutz, C. & Ashton, B. A. Leukocyte Extravasation: Chemokine Transport and Presentation by the Endothelium. *Blood* **100**, 3853-3860, doi:10.1182/blood.V100.12.3853 (2002).
- Mironava, T., Hadjiargyrou, M., Simon, M., Jurukovski, V. & Rafailovich, M. H. Gold Nanoparticles Cellular Toxicity and Recovery: Effect of Size, Concentration and Exposure Time. *Nanotoxicology* **4**, 120-137, doi:10.3109/17435390903471463 (2010).

- Mironava, T., Hadjiargyrou, M., Simon, M. & Rafailovich, M. H. Gold Nanoparticles Cellular Toxicity and Recovery: Adipose Derived Stromal Cells. *Nanotoxicology* **8**, 189-201, doi:10.3109/17435390.2013.769128 (2014).
- Mishra, H. K., Long, C., Bahaie, N. S. & Walcheck, B. Regulation of Cxcr2 Expression and Function by a Disintegrin and Metalloprotease-17 (Adam17). *J Leukoc Biol* **97**, 447-454, doi:10.1189/jlb.3HI0714-340R (2015).
- Mollinedo, F., Nakajima, M., Llorens, A., Barbosa, E., Callejo, S., Gajate, C. & Fabra, A. Major Co-Localization of the Extracellular-Matrix Degradative Enzymes Heparanase and Gelatinase in Tertiary Granules of Human Neutrophils. *Biochem J* **327** (Pt 3), 917-923, doi:10.1042/bj3270917 (1997).
- Momoi, T. Caspases Involved in Er Stress-Mediated Cell Death. *J Chem Neuroanat* **28**, 101-105, doi:10.1016/j.jchemneu.2004.05.008 (2004).
- Mukaida, N., Sasaki, S. I. & Baba, T. Two-Faced Roles of Tumor-Associated Neutrophils in Cancer Development and Progression. *Int J Mol Sci* **21**, doi:10.3390/ijms21103457 (2020).
- Murkin, J. M. & Arango, M. Near-Infrared Spectroscopy as an Index of Brain and Tissue Oxygenation. *Br J Anaesth* **103 Suppl 1**, i3-13, doi:10.1093/bja/aep299 (2009).
- Murphy, K. T. P. W. M. J. C. *Janeway's Immunobiology*. (Garland Science, 2012).
- Nan, J., Xing, Y. F., Hu, B., Tang, J. X., Dong, H. M., He, Y. M., Ruan, D. Y., Ye, Q. J., Cai, J. R., Ma, X. K. *et al.* Endoplasmic Reticulum Stress Induced Lox-1(+) Cd15(+) Polymorphonuclear Myeloid-Derived Suppressor Cells in Hepatocellular Carcinoma. *Immunology* **154**, 144-155, doi:10.1111/imm.12876 (2018).
- Neumann, J. *Immunobiologie*. (2008).
- Noël, C., Simard, J. C. & Girard, D. Gold Nanoparticles Induce Apoptosis, Endoplasmic Reticulum Stress Events and Cleavage of Cytoskeletal Proteins in Human Neutrophils. *Toxicol In Vitro* **31**, 12-22, doi:10.1016/j.tiv.2015.11.003 (2016).
- Ocana, A., Nieto-Jiménez, C., Pandiella, A. & Templeton, A. J. Neutrophils in Cancer: Prognostic Role and Therapeutic Strategies. *Mol Cancer* **16**, 137-137, doi:10.1186/s12943-017-0707-7 (2017).
- Oh, E., Delehanty, J. B., Sapsford, K. E., Susumu, K., Goswami, R., Blanco-Canosa, J. B., Dawson, P. E., Granek, J., Shoff, M., Zhang, Q. *et al.* Cellular Uptake and Fate of Pegylated Gold Nanoparticles Is Dependent on Both Cell-Penetration Peptides and Particle Size. *ACS Nano* **5**, 6434-6448, doi:10.1021/nn201624c (2011).
- Pan, Y., Neuss, S., Leifert, A., Fischler, M., Wen, F., Simon, U., Schmid, G., Brandau, W. & Jähnen-Dechent, W. Size-Dependent Cytotoxicity of Gold Nanoparticles. *Small (Weinheim an der Bergstrasse, Germany)* **3**, 1941-1949, doi:10.1002/sml.200700378 (2007).
- Panariti, A., Miserocchi, G. & Rivolta, I. The Effect of Nanoparticle Uptake on Cellular Behavior: Disrupting or Enabling Functions? *Nanotechnol Sci Appl* **5**, 87-100, doi:10.2147/NSA.S25515 (2012).
- Parks, W. C., Wilson, C. L. & Lopez-Boado, Y. S. Matrix Metalloproteinases as Modulators of Inflammation and Innate Immunity. *Nat Rev Immunol* **4**, 617-629, doi:10.1038/nri1418 (2004).
- Patra, C. R., Bhattacharya, R., Wang, E., Katarya, A., Lau, J. S., Dutta, S., Muders, M., Wang, S., Buhrow, S. A., Safgren, S. L. *et al.* Targeted Delivery of Gemcitabine to Pancreatic Adenocarcinoma Using Cetuximab as a Targeting Agent. *Cancer research* **68**, 1970-1978, doi:10.1158/0008-5472.CAN-07-6102 (2008).
- Petri, B. & Sanz, M. J. Neutrophil Chemotaxis. *Cell Tissue Res* **371**, 425-436, doi:10.1007/s00441-017-2776-8 (2018).

- Pillay, J., Den Braber, I., Vrisekoop, N., Kwast, L. M., De Boer, R. J., Borghans, J. A., Tesselaar, K. & Koenderman, L. In Vivo Labeling with $^2\text{H}_2\text{O}$ Reveals a Human Neutrophil Lifespan of 5.4 Days. *Blood* **116**, 625-627, doi:10.1182/blood-2010-01-259028 (2010).
- Plan Sangnier, A., Van De Walle, A., Aufaure, R., Fradet, M., Motte, L., Guenin, E., Lalatonne, Y. & Wilhelm, C. Endosomal Confinement of Gold Nanospheres, Nanorods, and Nanoraspberries Governs Their Photothermal Identity and Is Beneficial for Cancer Cell Therapy. *Adv Biosyst* **4**, e1900284, doi:10.1002/adbi.201900284 (2020).
- Qiu, Y., Liu, Y., Wang, L., Xu, L., Bai, R., Ji, Y., Wu, X., Zhao, Y., Li, Y. & Chen, C. Surface Chemistry and Aspect Ratio Mediated Cellular Uptake of Au Nanorods. *Biomaterials* **31**, 7606-7619, doi:10.1016/j.biomaterials.2010.06.051 (2010).
- Radomska, H. S., Huettner, C. S., Zhang, P., Cheng, T., Scadden, D. T. & Tenen, D. G. Ccaat/Enhancer Binding Protein Alpha Is a Regulatory Switch Sufficient for Induction of Granulocytic Development from Bipotential Myeloid Progenitors. *Mol Cell Biol* **18**, 4301-4314, doi:10.1128/MCB.18.7.4301 (1998).
- Ramadoss, P., Marcus, C. & Perdew, G. H. Role of the Aryl Hydrocarbon Receptor in Drug Metabolism. *Expert Opin Drug Metab Toxicol* **1**, 9-21, doi:10.1517/17425255.1.1.9 (2005).
- Rao, H. L., Chen, J. W., Li, M., Xiao, Y. B., Fu, J., Zeng, Y. X., Cai, M. Y. & Xie, D. Increased Intratumoral Neutrophil in Colorectal Carcinomas Correlates Closely with Malignant Phenotype and Predicts Patients' Adverse Prognosis. *PLoS One* **7**, e30806, doi:10.1371/journal.pone.0030806 (2012).
- Rao, R. V., Ellerby, H. M. & Bredesen, D. E. Coupling Endoplasmic Reticulum Stress to the Cell Death Program. *Cell Death and Differentiation* **11**, 372-380, doi:10.1038/sj.cdd.4401378 (2004).
- Riveros, A., Dadlani, K., Salas, E., Caballero, L., Melo, F. & Kogan, M. J. Gold Nanoparticle-Membrane Interactions: Implications in Biomedicine. *Journal of Biomaterials and Tissue Engineering* **3**, 4-21, doi:10.1166/jbt.2013.1067 (2013).
- Rocquelin, G., Juaneda, P. & Cluzan, R. Influence of Physical Training on the Effects of Dietary Oils on Cardiac Morphology and Phospholipids in Rats. *Ann Nutr Metab* **25**, 350-361, doi:10.1159/000176516 (1981).
- Rogalla, T., Ehrnsperger, M., Preville, X., Kotlyarov, A., Lutsch, G., Ducasse, C., Paul, C., Wieske, M., Arrigo, A. P., Buchner, J. *et al.* Regulation of Hsp27 Oligomerization, Chaperone Function, and Protective Activity against Oxidative Stress/Tumor Necrosis Factor Alpha by Phosphorylation. *J Biol Chem* **274**, 18947-18956, doi:10.1074/jbc.274.27.18947 (1999).
- Rosmarin, A. G., Yang, Z. & Resendes, K. K. Transcriptional Regulation in Myelopoiesis: Hematopoietic Fate Choice, Myeloid Differentiation, and Leukemogenesis. *Exp Hematol* **33**, 131-143, doi:10.1016/j.exphem.2004.08.015 (2005).
- Ruiz, G., Tripathi, K., Okyem, S. & Driskell, J. D. Ph Impacts the Orientation of Antibody Adsorbed onto Gold Nanoparticles. *Bioconjug Chem* **30**, 1182-1191, doi:10.1021/acs.bioconjchem.9b00123 (2019).
- Russ, A., Hua, A. B., Montfort, W. R., Rahman, B., Riaz, I. B., Khalid, M. U., Carew, J. S., Nawrocki, S. T., Persky, D. & Anwer, F. Blocking "Don't Eat Me" Signal of Cd47-Sirpalpha in Hematological Malignancies, an in-Depth Review. *Blood Rev* **32**, 480-489, doi:10.1016/j.blre.2018.04.005 (2018).
- Safari, H., Kelley, W. J., Saito, E., Kaczorowski, N., Carethers, L., Shea, L. D. & Eniola-Adefeso, O. Neutrophils Preferentially Phagocytose Elongated Particles-an Opportunity for Selective Targeting in Acute Inflammatory Diseases. *Sci Adv* **6**, eaba1474, doi:10.1126/sciadv.aba1474 (2020).

- Salminen, A., Kaarniranta, K. & Kauppinen, A. Er Stress Activates Immunosuppressive Network: Implications for Aging and Alzheimer's Disease. *Journal of Molecular Medicine-Imm* **98**, 633-650, doi:10.1007/s00109-020-01904-z (2020).
- Samanta, A. K., Oppenheim, J. J. & Matsushima, K. Interleukin 8 (Monocyte-Derived Neutrophil Chemotactic Factor) Dynamically Regulates Its Own Receptor Expression on Human Neutrophils. *Journal of Biological Chemistry* **265**, 183-189, doi:10.1016/s0021-9258(19)40213-5 (1990).
- Schirrmann, R., Erkelenz, M., Lamers, K., Sritharan, O., Nachev, M., Sures, B., Schlucker, S. & Brandau, S. Gold Nanorods Induce Endoplasmic Reticulum Stress and Autocrine Inflammatory Activation in Human Neutrophils. *ACS Nano*, doi:10.1021/acsnano.2c03586 (2022).
- Schwarz, D. S. & Blower, M. D. The Endoplasmic Reticulum: Structure, Function and Response to Cellular Signaling. *Cell Mol Life Sci* **73**, 79-94, doi:10.1007/s00018-015-2052-6 (2016).
- Seegenschmiedt, M. H., Brady, L. W. & Sauer, R. Interstitial Thermoradiotherapy - Review on Technical and Clinical Aspects. *Am J Clin Oncol-Canc* **13**, 352-363, doi:10.1097/00000421-199008000-00016 (1990).
- Segal, A. W. How Neutrophils Kill Microbes. *Annual Review Immunology* **23**, 197-223 (2005).
- Seo, J. H., Park, J. H., Lee, E. J., Vo, T. T., Choi, H., Kim, J. Y., Jang, J. K., Wee, H. J., Lee, H. S., Jang, S. H. *et al.* Arid1-Mediated Hsp70 Acetylation Balances Stress-Induced Protein Refolding and Degradation. *Nature communications* **7**, 12882, doi:10.1038/ncomms12882 (2016).
- Seo, S., Baye, L. M., Schulz, N. P., Beck, J. S., Zhang, Q., Slusarski, D. C. & Sheffield, V. C. Bbs6, Bbs10, and Bbs12 Form a Complex with Cct/Tric Family Chaperonins and Mediate Bbsome Assembly. *Proc Natl Acad Sci U S A* **107**, 1488-1493, doi:10.1073/pnas.0910268107 (2010).
- Shaul, M. E. & Fridlender, Z. G. The Dual Role of Neutrophils in Cancer. *Semin Immunol*, 101582, doi:10.1016/j.smim.2021.101582 (2021).
- Si, Y., Merz, S. F., Jansen, P., Wang, B., Bruderek, K., Altenhoff, P., Mattheis, S., Lang, S., Gunzer, M., Klode, J. *et al.* Multidimensional Imaging Provides Evidence for Down-Regulation of T Cell Effector Function by Mds1 in Human Cancer Tissue. *Science immunology* **4**, doi:10.1126/sciimmunol.aaw9159 (2019).
- Simon Brown, I. H., Ewan Ross, Kate Shaw, Chris D. Buckley and John Savill. Apoptosis Disables Cd31-Mediated Cell Detachment from Phagocytes Promoting Binding and Engulfment. *Nature* **418**, 200-203 (2002).
- Skrabalak, S. E., Chen, J., Au, L., Lu, X., Li, X. & Xia, Y. Gold Nanocages for Biomedical Applications. *Adv Mater* **19**, 3177-3184, doi:10.1002/adma.200701972 (2007).
- Smilowitz, H. M., Meyers, A., Rahman, K., Dymont, N. A., Sasso, D., Xue, C., Oliver, D. L., Lichtler, A., Deng, X., Ridwan, S. M. *et al.* Intravenously-Injected Gold Nanoparticles (Aunps) Access Intracerebral F98 Rat Gliomas Better Than Aunps Infused Directly into the Tumor Site by Convection Enhanced Delivery. *Int J Nanomedicine* **13**, 3937-3948, doi:10.2147/IJN.S154555 (2018).
- Smith, A. M., Mancini, M. C. & Nie, S. Bioimaging: Second Window for in Vivo Imaging. *Nat Nanotechnol* **4**, 710-711, doi:10.1038/nnano.2009.326 (2009).
- Soenen, S. J., Manshian, B. B., Abdelmonem, A. M., Montenegro, J.-M., Tan, S., Balcaen, L., Vanhaecke, F., Brisson, A. R., Parak, W. J., De Smedt, S. C. *et al.* The Cellular Interactions of Pegylated Gold Nanoparticles: Effect of Pegylation on Cellular Uptake and Cytotoxicity. *Particle & Particle Systems Characterization* **31**, 794-800, doi:10.1002/ppsc.201300357 (2014).

- Sokolov, K., Follen, M., Aaron, J., Pavlova, I., Malpica, A., Lotan, R. & Richards-Kortum, R. Real-Time Vital Optical Imaging of Precancer Using Anti-Epidermal Growth Factor Receptor Antibodies Conjugated to Gold Nanoparticles. *Cancer research* **63**, 1999-2004 (2003).
- Solovjov, D. A., Pluskota, E. & Plow, E. F. Distinct Roles for the Alpha and Beta Subunits in the Functions of Integrin α 5 β 1. *J Biol Chem* **280**, 1336-1345, doi:10.1074/jbc.M406968200 (2005).
- Stanley, E., Lieschke, G. J., Grail, D., Metcalf, D., Hodgson, G., Gall, J. A., Maher, D. W., Cebon, J., Sinickas, V. & Dunn, A. R. Granulocyte/Macrophage Colony-Stimulating Factor-Deficient Mice Show No Major Perturbation of Hematopoiesis but Develop a Characteristic Pulmonary Pathology. *Proc Natl Acad Sci U S A* **91**, 5592-5596 (1994).
- Stanley, L. A. in *Pharmacognosy* 527-545 (2017).
- Stark, M. A., Huo, Y., Burcin, T. L., Morris, M. A., Olson, T. S. & Ley, K. Phagocytosis of Apoptotic Neutrophils Regulates Granulopoiesis Via Il-23 and Il-17. *Immunity* **22**, 285-294, doi:10.1016/j.immuni.2005.01.011 (2005).
- Steger, A. C., Lees, W. R., Walmsley, K. & Bown, S. G. Interstitial Laser Hyperthermia: A New Approach to Local Destruction of Tumours. *BMJ* **299**, 362-365, doi:10.1136/bmj.299.6695.362 (1989).
- Storhoff, J. J., Elghanian, R., Mucic, R. C., Mirkin, C. A. & Letsinger, R. L. One-Pot Colorimetric Differentiation of Polynucleotides with Single Base Imperfections Using Gold Nanoparticle Probes. *Journal of the American Chemical Society* **120**, 1959-1964, doi:DOI 10.1021/ja972332i (1998).
- Sultan, R. A. Tumour Ablation by Laser in General Surgery. *Lasers in Medical Science* **5**, 185-193, doi:10.1007/bf02031380 (1990).
- Summers, C., Rankin, S. M., Condliffe, A. M., Singh, N., Peters, A. M. & Chilvers, E. R. Neutrophil Kinetics in Health and Disease. *Trends Immunol* **31**, 318-324, doi:10.1016/j.it.2010.05.006 (2010).
- Svaasand, L. O., Gomer, C. J. & Morinelli, E. On the Physical Rationale of Laser Induced Hyperthermia. *Lasers in Medical Science* **5**, 121-128, doi:10.1007/bf02031373 (1990).
- Takahashi, H., Niidome, Y., Niidome, T., Kaneko, K., Kawasaki, H. & Yamada, S. Modification of Gold Nanorods Using Phosphatidylcholine to Reduce Cytotoxicity. *Langmuir* **22**, 2-5, doi:10.1021/la0520029 (2006).
- Takeuchi, O. & Akira, S. Pattern Recognition Receptors and Inflammation. *Cell* **140**, 805-820, doi:10.1016/j.cell.2010.01.022 (2010).
- Taye, A. & El-Sheikh, A. A. Lectin-Like Oxidized Low-Density Lipoprotein Receptor 1 Pathways. *Eur J Clin Invest* **43**, 740-745, doi:10.1111/eci.12092 (2013).
- Templeton, A. J., Mcnamara, M. G., Seruga, B., Vera-Badillo, F. E., Aneja, P., Ocana, A., Leibowitz-Amit, R., Sonpavde, G., Knox, J. J., Tran, B. *et al.* Prognostic Role of Neutrophil-to-Lymphocyte Ratio in Solid Tumors: A Systematic Review and Meta-Analysis. *J Natl Cancer Inst* **106**, dju124, doi:10.1093/jnci/dju124 (2014).
- Tenzer, S., Docter, D., Kuharev, J., Musyanovych, A., Fetz, V., Hecht, R., Schlenk, F., Fischer, D., Kiouptsi, K., Reinhardt, C. *et al.* Rapid Formation of Plasma Protein Corona Critically Affects Nanoparticle Pathophysiology. *Nat Nanotechnol* **8**, 772-781, doi:10.1038/nnano.2013.181 (2013).
- Totaro, K. A., Liao, X., Bhattacharya, K., Finneman, J. I., Sperry, J. B., Massa, M. A., Thorn, J., Ho, S. V. & Pentelute, B. L. Systematic Investigation of Edc/Snhs-Mediated Bioconjugation Reactions for Carboxylated Peptide Substrates. *Bioconjug Chem* **27**, 994-1004, doi:10.1021/acs.bioconjchem.6b00043 (2016).

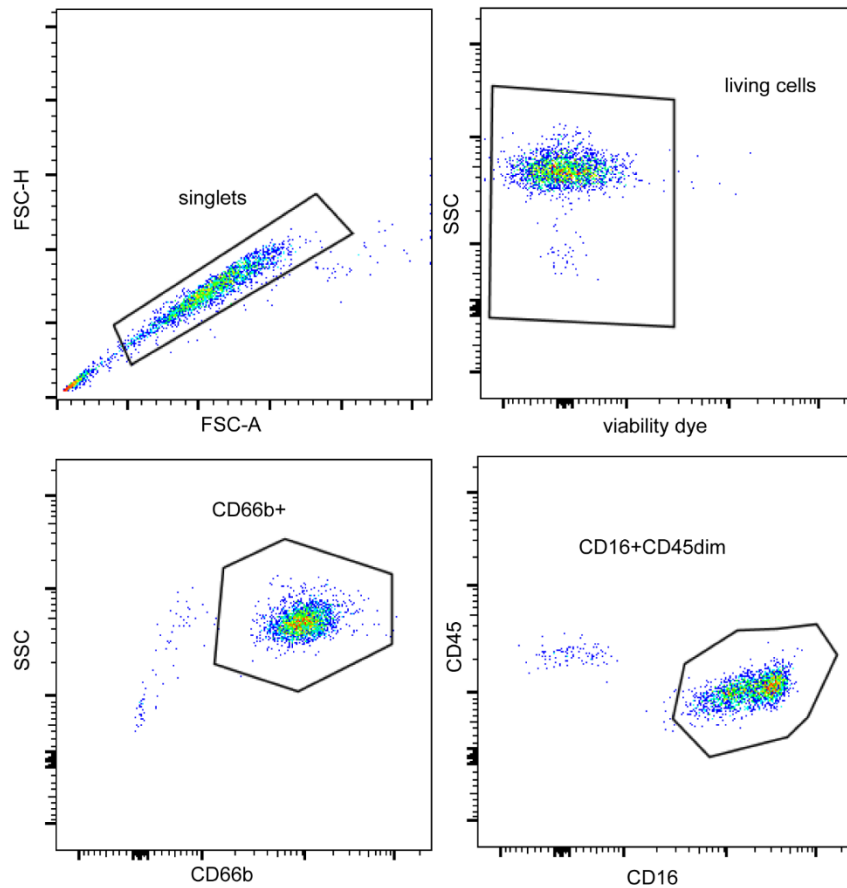
- Trellakis, S., Bruderek, K., Dumitru, C. A., Gholaman, H., Gu, X., Bankfalvi, A., Scherag, A., Hutte, J., Dominas, N., Lehnerdt, G. F. *et al.* Polymorphonuclear Granulocytes in Human Head and Neck Cancer: Enhanced Inflammatory Activity, Modulation by Cancer Cells and Expansion in Advanced Disease. *Int J Cancer* **129**, 2183-2193, doi:10.1002/ijc.25892 (2011).
- Tsai, R. K. & Discher, D. E. Inhibition of "Self" Engulfment through Deactivation of Myosin-II at the Phagocytic Synapse between Human Cells. *J Cell Biol* **180**, 989-1003, doi:10.1083/jcb.200708043 (2008).
- Tsai, Y. Y., Huang, Y. H., Chao, Y. L., Hu, K. Y., Chin, L. T., Chou, S. H., Hour, A. L., Yao, Y. D., Tu, C. S., Liang, Y. J. *et al.* Identification of the Nanogold Particle-Induced Endoplasmic Reticulum Stress by Omic Techniques and Systems Biology Analysis. *ACS Nano* **5**, 9354-9369, doi:10.1021/nn2027775 (2011).
- Tu, B. P. & Weissman, J. S. Oxidative Protein Folding in Eukaryotes: Mechanisms and Consequences. *J Cell Biol* **164**, 341-346, doi:10.1083/jcb.200311055 (2004).
- Tuffin, J. R. & Carruth, J. A. The Carbon Dioxide Surgical Laser. *Br Dent J* **149**, 255-258, doi:10.1038/sj.bdj.4804505 (1980).
- Turkevich, J., Stevenson, P. C. & Hillier, J. A Study of the Nucleation and Growth Processes in the Synthesis of Colloidal Gold. *Discussions of the Faraday Society*, 55-&, doi:DOI 10.1039/df9511100055 (1951).
- Vorobjeva, N. V. & Chernyak, B. V. Netosis: Molecular Mechanisms, Role in Physiology and Pathology. *Biochemistry (Mosc)* **85**, 1178-1190, doi:10.1134/S0006297920100065 (2020).
- Walkey, C. D., Olsen, J. B., Guo, H., Emili, A. & Chan, W. C. Nanoparticle Size and Surface Chemistry Determine Serum Protein Adsorption and Macrophage Uptake. *Journal of the American Chemical Society* **134**, 2139-2147, doi:10.1021/ja2084338 (2012).
- Wang, L., Liu, Y., Li, W., Jiang, X., Ji, Y., Wu, X., Xu, L., Qiu, Y., Zhao, K., Wei, T. *et al.* Selective Targeting of Gold Nanorods at the Mitochondria of Cancer Cells: Implications for Cancer Therapy. *Nano letters* **11**, 772-780, doi:10.1021/nl103992v (2011).
- Wang, M. & Kaufman, R. J. The Impact of the Endoplasmic Reticulum Protein-Folding Environment on Cancer Development. *Nat Rev Cancer* **14**, 581-597, doi:10.1038/nrc3800 (2014).
- Wengner, A. M., Pitchford, S. C., Furze, R. C. & Rankin, S. M. The Coordinated Action of G-CSF and ECR + CXCL1 Chemokines in Neutrophil Mobilization During Acute Inflammation. *Blood* **111**, 42-49, doi:10.1182/blood-2007-07-099648 (2008).
- Wey, K., Schirrmann, R., Diesing, D., Lang, S., Brandau, S., Hansen, S. & Epple, M. Coating of Cochlear Implant Electrodes with Bioactive DNA-Loaded Calcium Phosphate Nanoparticles for the Local Transfection of Stimulatory Proteins. *Biomaterials* **276**, 121009, doi:10.1016/j.biomaterials.2021.121009 (2021).
- Wu, F., Chen, W. Z., Bai, J., Zou, J. Z., Wang, Z. L., Zhu, H. & Wang, Z. B. Pathological Changes in Human Malignant Carcinoma Treated with High-Intensity Focused Ultrasound. *Ultrasound Med Biol* **27**, 1099-1106, doi:Doi 10.1016/S0301-5629(01)00389-1 (2001).
- Xia, H., Bai, S., Hartmann, J. & Wang, D. Synthesis of Monodisperse Quasi-Spherical Gold Nanoparticles in Water Via Silver(I)-Assisted Citrate Reduction. *Langmuir* **26**, 3585-3589, doi:10.1021/la902987w (2010).
- Xia, J., Boxer, L. A. & Link, D. C. ER Stress-Induced Expression of CCAAT/Enhancer Binding Protein Gamma (C/EBPγ) May Contribute to the Block in Granulocytic Differentiation in Severe Congenital Neutropenia. *Blood* **120**, 8-8, doi:DOI 10.1182/blood.V120.21.8.8 (2012).

- Xia, Y. N. & Halas, N. J. Shape-Controlled Synthesis and Surface Plasmonic Properties of Metallic Nanostructures. *Mrs Bull* **30**, 338-344, doi:DOI 10.1557/mrs2005.96 (2005).
- Yaqoob, S. B., Adnan, R., Rameez Khan, R. M. & Rashid, M. Gold, Silver, and Palladium Nanoparticles: A Chemical Tool for Biomedical Applications. *Front Chem* **8**, 376, doi:10.3389/fchem.2020.00376 (2020).
- Ye, B., Zhao, B., Wang, K., Guo, Y., Lu, Q., Zheng, L., Li, A. & Qiao, J. Neutrophils Mediated Multistage Nanoparticle Delivery for Prompting Tumor Photothermal Therapy. *J Nanobiotechnology* **18**, 138, doi:10.1186/s12951-020-00682-7 (2020).
- Yen, H. J., Hsu, S. H. & Tsai, C. L. Cytotoxicity and Immunological Response of Gold and Silver Nanoparticles of Different Sizes. *Small (Weinheim an der Bergstrasse, Germany)* **5**, 1553-1561, doi:10.1002/sml.200900126 (2009).
- Yin, C. & Heit, B. Armed for Destruction: Formation, Function and Trafficking of Neutrophil Granules. *Cell Tissue Res* **371**, 455-471, doi:10.1007/s00441-017-2731-8 (2018).
- Yin, D., Li, X., Ma, Y. & Liu, Z. Targeted Cancer Imaging and Photothermal Therapy Via Monosaccharide-Imprinted Gold Nanorods. *Chem Commun (Camb)* **53**, 6716-6719, doi:10.1039/c7cc02247f (2017).
- Yipp, B. G., Petri, B., Salina, D., Jenne, C. N., Scott, B. N., Zbytnuik, L. D., Pittman, K., Asaduzzaman, M., Wu, K., Meijndert, H. C. *et al.* Infection-Induced Netosis Is a Dynamic Process Involving Neutrophil Multitasking in Vivo. *Nat Med* **18**, 1386-1393, doi:10.1038/nm.2847 (2012).
- Yu, X., Dai, Y., Zhao, Y., Qi, S., Liu, L., Lu, L., Luo, Q. & Zhang, Z. Melittin-Lipid Nanoparticles Target to Lymph Nodes and Elicit a Systemic Anti-Tumor Immune Response. *Nature communications* **11**, 1110, doi:10.1038/s41467-020-14906-9 (2020).
- Yuk, J. M., Jin, H. S. & Jo, E. K. Small Heterodimer Partner and Innate Immune Regulation. *Endocrinol Metab (Seoul)* **31**, 17-24, doi:10.3803/EnM.2016.31.1.17 (2016).
- Zanger, U. M., Raimundo, S. & Eichelbaum, M. Cytochrome P450 2d6: Overview and Update on Pharmacology, Genetics, Biochemistry. *Naunyn Schmiedebergs Arch Pharmacol* **369**, 23-37, doi:10.1007/s00210-003-0832-2 (2004).
- Zeidler, C., Germeshausen, M., Klein, C. & Welte, K. Clinical Implications of Ela2-, Hax1-, and G-Csf-Receptor (Csf3r) Mutations in Severe Congenital Neutropenia. *Br J Haematol* **144**, 459-467, doi:10.1111/j.1365-2141.2008.07425.x (2009).
- Zhang, K. Z. & Kaufman, R. J. From Endoplasmic-Reticulum Stress to the Inflammatory Response. *Nature* **454**, 455-462, doi:10.1038/nature07203 (2008).
- Zhang, L., Zhang, Y., Xue, Y., Wu, Y., Wang, Q., Xue, L., Su, Z. & Zhang, C. Transforming Weakness into Strength: Photothermal-Therapy-Induced Inflammation Enhanced Cytopharmaceutical Chemotherapy as a Combination Anticancer Treatment. *Adv Mater* **31**, e1805936, doi:10.1002/adma.201805936 (2019).
- Zhang, P., Sun, F., Liu, S. & Jiang, S. Anti-Peg Antibodies in the Clinic: Current Issues and Beyond Pegylation. *J Control Release* **244**, 184-193, doi:10.1016/j.jconrel.2016.06.040 (2016).
- Zhao, J. J., Pan, K., Wang, W., Chen, J. G., Wu, Y. H., Lv, L., Li, J. J., Chen, Y. B., Wang, D. D., Pan, Q. Z. *et al.* The Prognostic Value of Tumor-Infiltrating Neutrophils in Gastric Adenocarcinoma after Resection. *PLoS One* **7**, e33655, doi:10.1371/journal.pone.0033655 (2012).
- Zharov, V. P., Galitovskaya, E. N., Johnson, C. & Kelly, T. Synergistic Enhancement of Selective Nanophotothermolysis with Gold Nanoclusters: Potential for Cancer Therapy. *Lasers Surg Med* **37**, 219-226, doi:10.1002/lsm.20223 (2005).
- Zheng, T., Cherubin, P., Cilenti, L., Teter, K. & Huo, Q. A Simple and Fast Method to Study the Hydrodynamic Size Difference of Protein Disulfide Isomerase in Oxidized and Reduced

Form Using Gold Nanoparticles and Dynamic Light Scattering. *Analyst* **141**, 934-938, doi:10.1039/c5an02248g (2016).

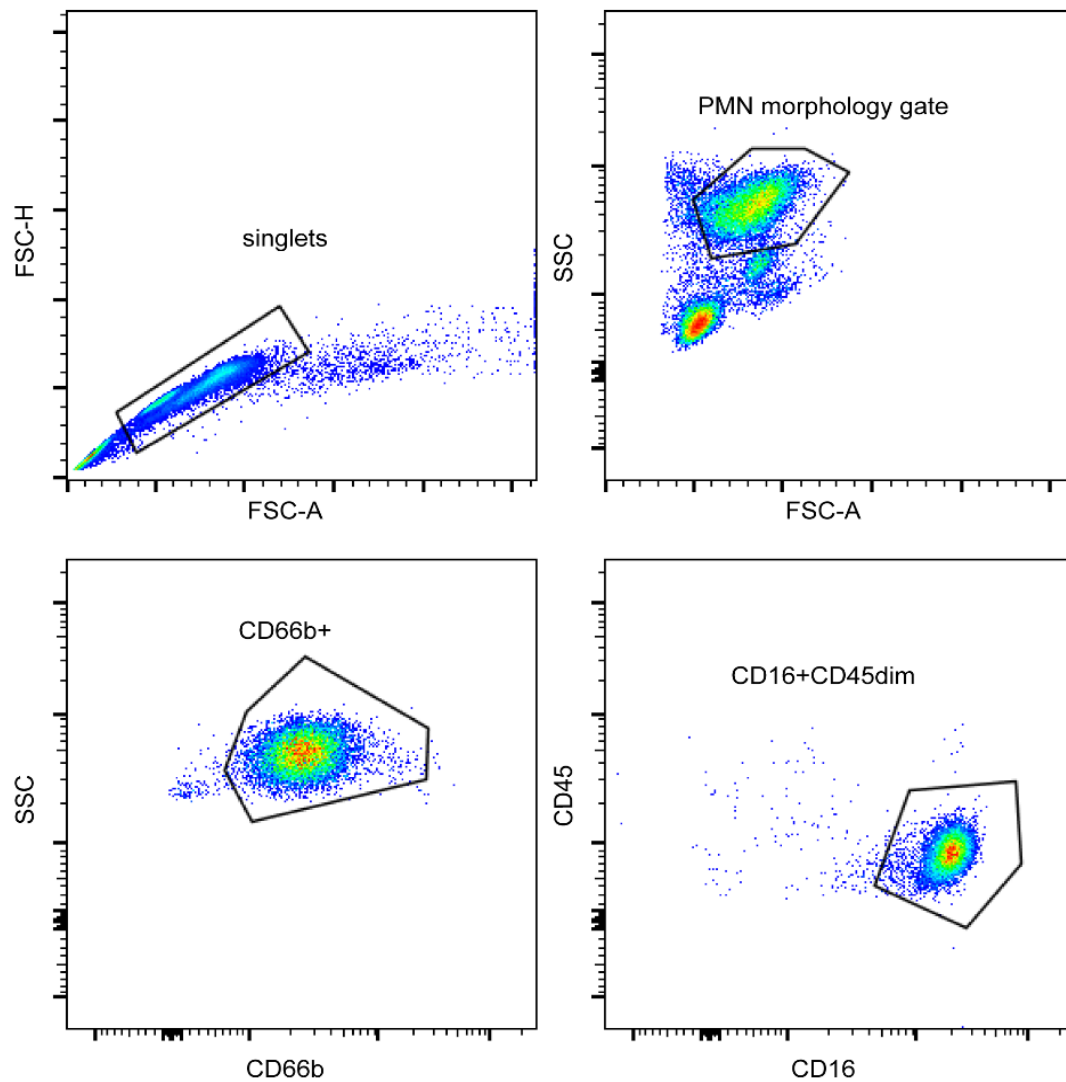
APPENDIX

This section lists supplementary figures and additional information in relation to the presented study.



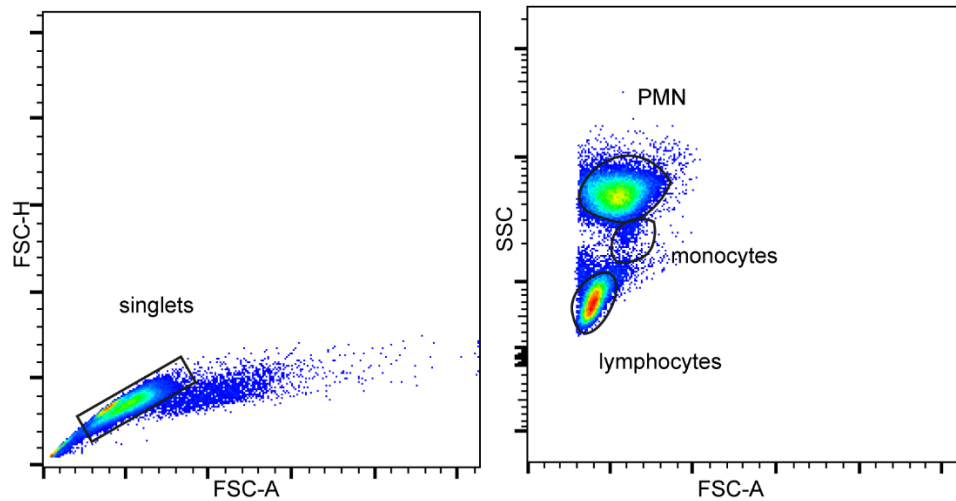
Supplementary Figure 1: Gating strategy for isolated PMN in flow cytometry.

First doublets were removed by FSC-H versus FSC-A (upper left). Living cells were depicted according to their viability dye (upper right). Gating for PMN was then completed by gating on CD66b-positive cells and subsequent exclusion of eosinophils by their higher CD45 staining and absence of CD16 (lower panels).



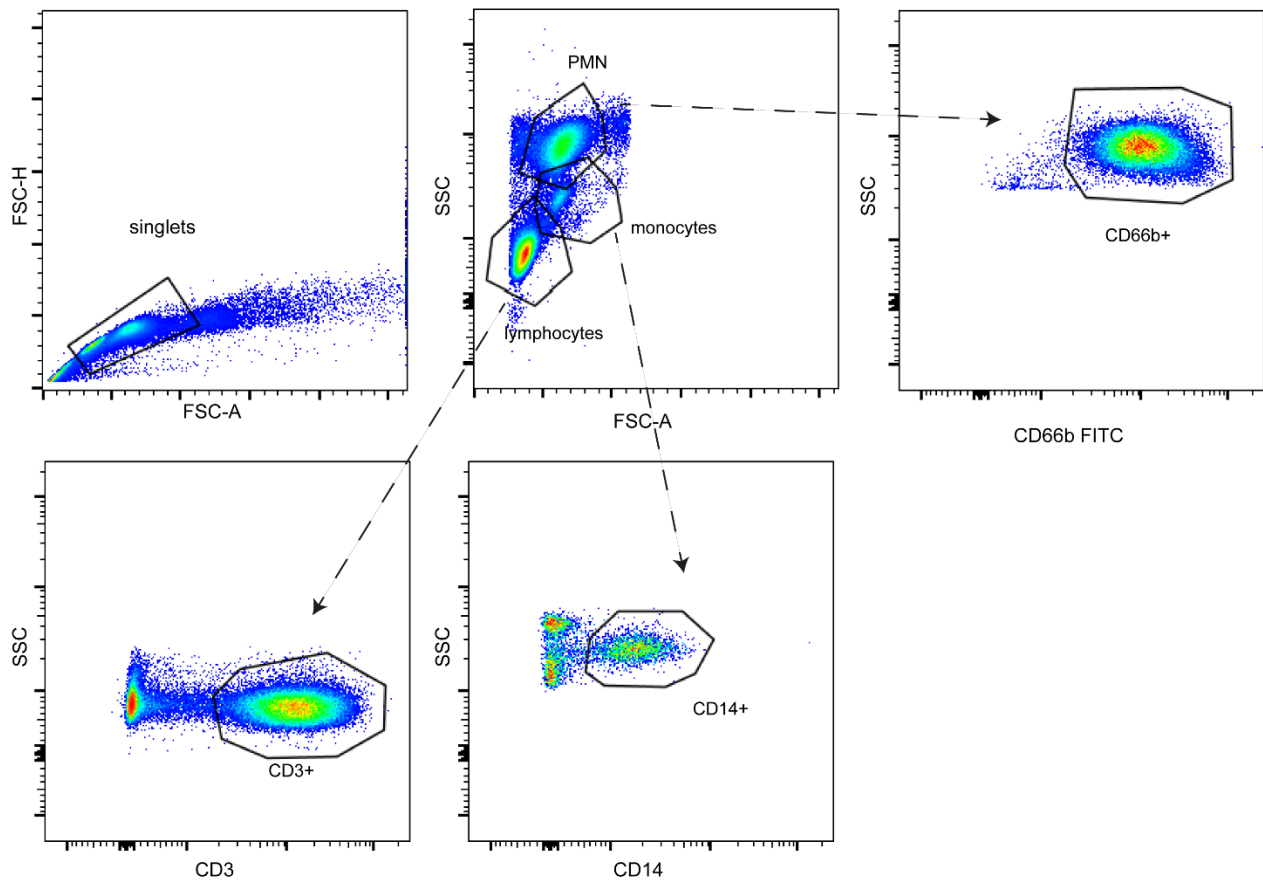
Supplementary Figure 2: Whole blood flow cytometry gating strategy for PMN.

First doublets were removed by FSC-H versus FSC-A (upper left). Then PMN were selected by a morphological gate using SSC versus FSC-A (upper right). Gating for PMN was then completed by gating on CD66b-positive cells and subsequent exclusion of eosinophils by their higher CD45 staining and absence of CD16 (lower panels).



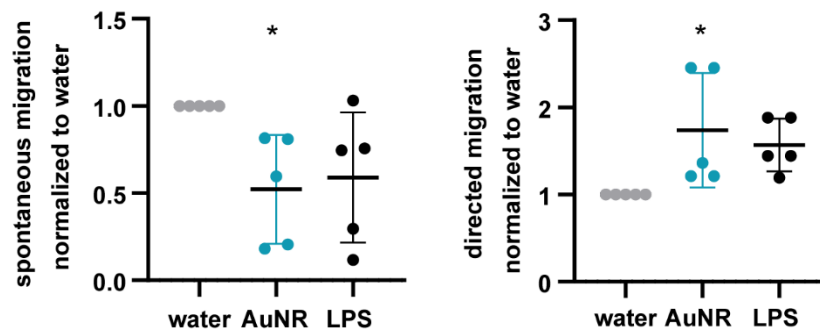
Supplementary Figure 3: Gating of PMN, T cells and Monocytes from mixed PBMC / PMN cultures.

First doublets were removed by FSC-H versus FSC-A (left). Then PMN were selected by a morphological gate using SSC versus FSC-A (right).



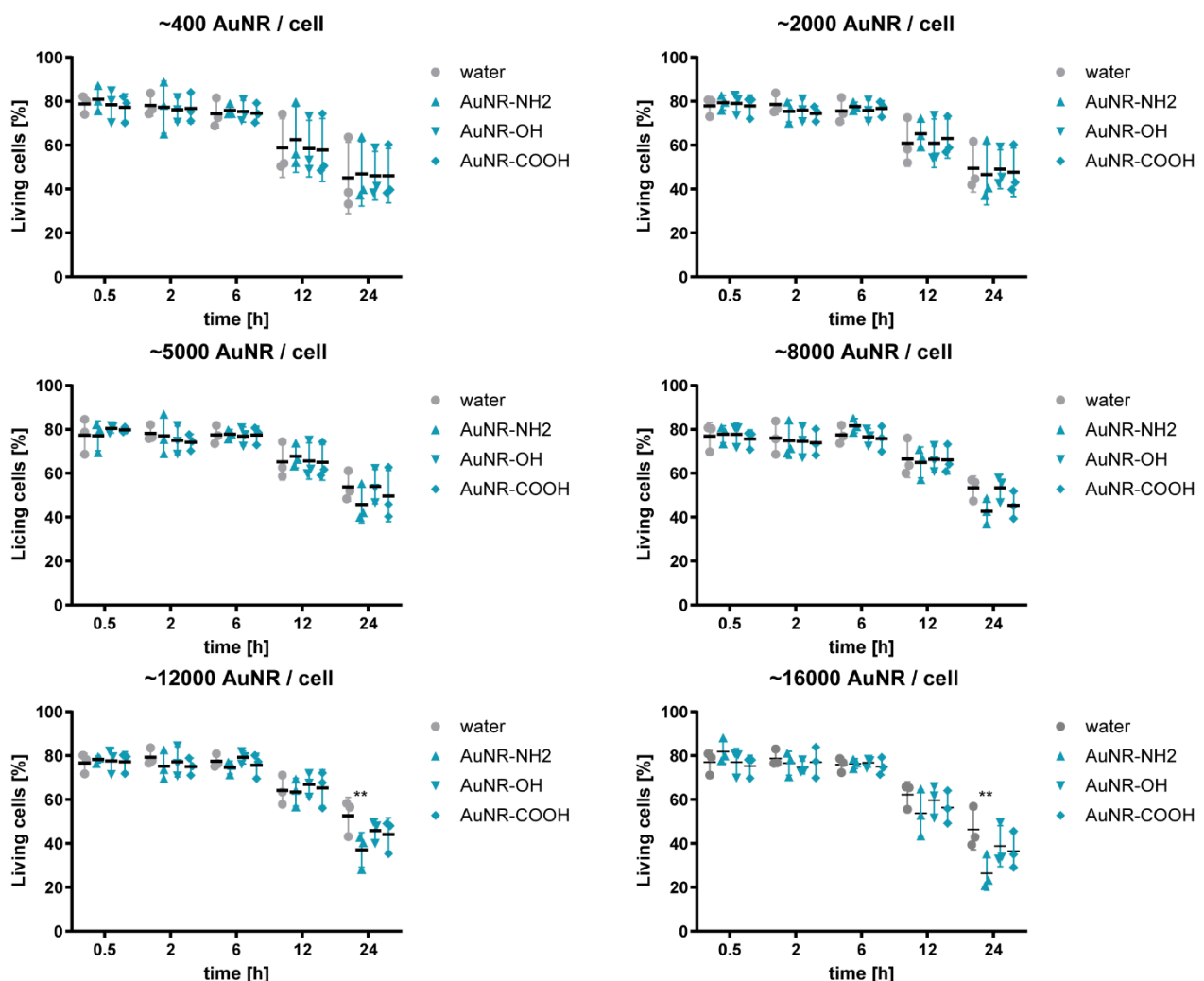
Supplementary Figure 4: Gating of PMN, T cells and Monocytes from whole blood.

First, doublets were removed by FSC-H versus FSC-A (upper left). Then, PMN, monocytes and T cells were identified by their morphology (middle panel) and specific expression of surface markers (PMN = CD66b+, monocytes = CD14+, T cells = CD3+).



Supplementary Figure 5: AuNR pretreatment reduced PMN spontaneous migration and accelerated directed migration towards tumor supernatant.

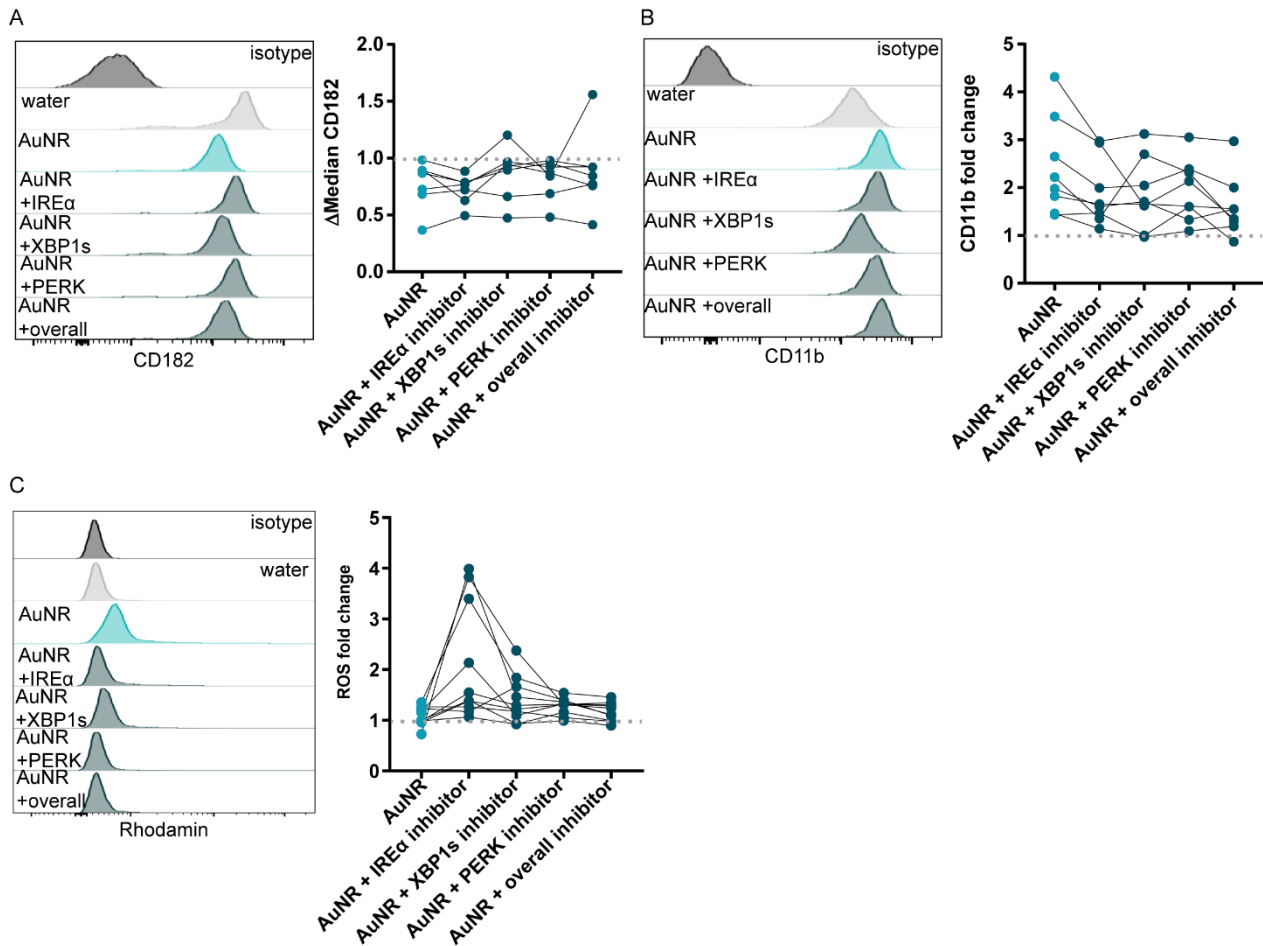
Isolated PMN were treated with water (NC= grey), AuNR (blue) or LPS (black) for 4 h prior to 3 h migration through 3 μ m transwells.



Supplementary Figure 6: Negatively charged AuNR are non-toxic.

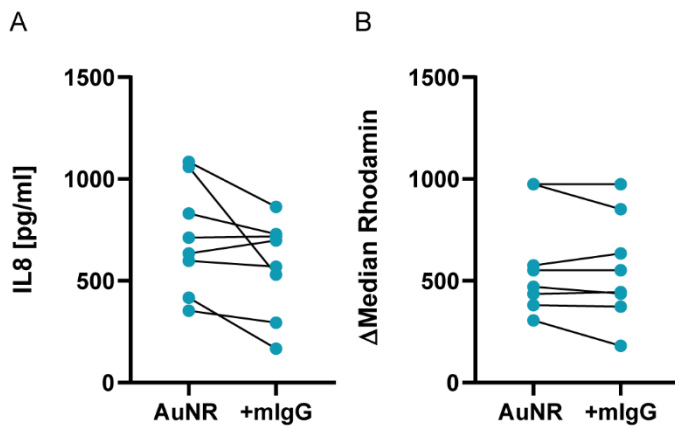
Isolated PMN were incubated with water or indicated amounts of AuNR with positive (-NH₂), neutral (-OH) or negative (COOH) charge over 0.5 h, 2 h, 6 h, 12 h and 24 h. Apoptosis-related changes in cell membrane topology were assessed by Annexin V Apoptosis Detection Kit (BD Bioscience) in flow cytometry (n=3, two-way ANOVA, Dunnett's multiple comparisons). The statistical significance was defined as ****p \leq 0.0001;

*** $p \leq 0.001$; ** $p \leq 0.01$; * $p \leq 0.05$. N indicates number of experimental repetitions, each performed with independent donors.



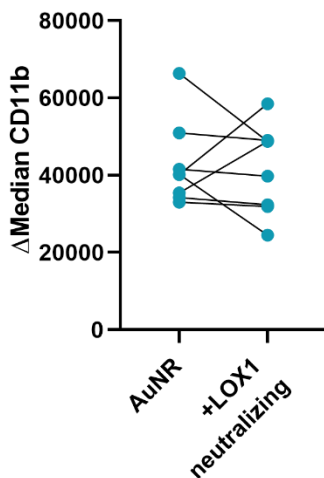
Supplementary Figure 7: ER stress inhibition did not change expression of CD182, CD11b or ROS production.

Whole blood was incubated with ER stress inhibitors (listed in Table 7) for 30 min at 37°C in rotation prior to addition of water or 5000 AuNR / PMN. Whole blood was incubated for another 2 h. Expression of (A) CD182, (A) CD11b and production of (A) ROS was analyzed using flow cytometry. All data was normalized to unstimulated water control with respective inhibitor (=1 indicated by dashed line). (n=8, one-way ANOVA, Dunnett's multiple comparisons test). The statistical significance was defined as **** $p \leq 0.0001$; *** $p \leq 0.001$; ** $p \leq 0.01$; * $p \leq 0.05$. N indicates number of experimental repetitions, each performed with independent donor.



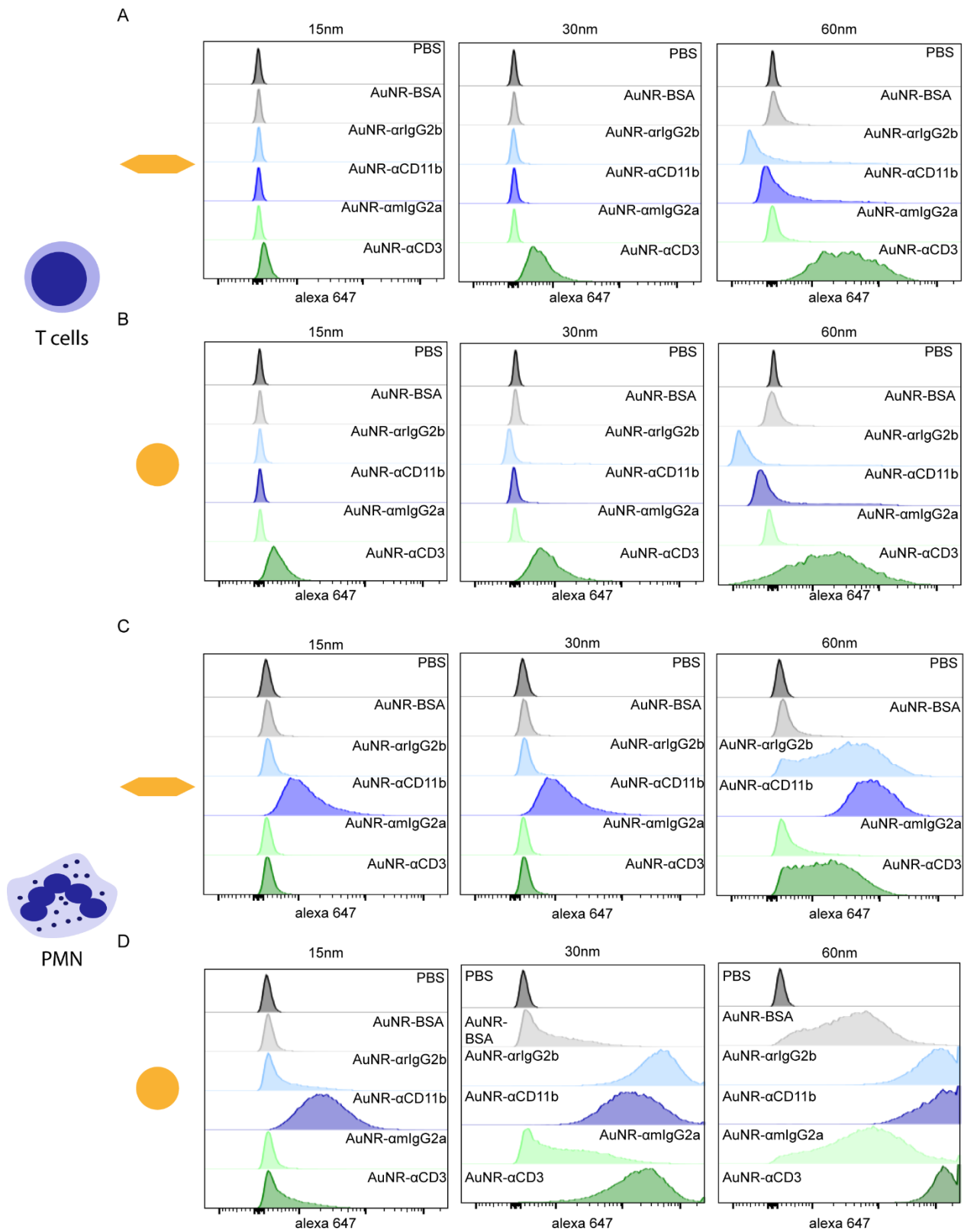
Supplementary Figure 8: IgG antibody does not affect IL8 secretion and ROS production.

Whole blood was incubated with nothing or mIgG (listed in Table 7) for 30 min at 37°C in rotation prior to addition of AuNR. Whole blood was incubated for another 2 h. Serum was isolated to define the level of secreted IL8. ROS production was analyzed in flow cytometry. (n=8, one-way ANOVA, Dunnett's multiple comparisons test). The statistical significance was defined as ****p ≤ 0.0001; ***p ≤ 0.001; **p ≤ 0.01; *p ≤ 0.05. N indicates number of experimental repetitions, each performed with independent donor.



Supplementary Figure 9: LOX1 neutralizing does not affect AuNR-induced CD11b expression.

Whole blood was incubated with nothing or LOX1 neutralizing antibody (listed in Table 7) for 30 min at 37°C in rotation prior to addition of AuNR. Whole blood was incubated for another 2 h. CD11b expression was analyzed in flow cytometry. (n=8, one-way ANOVA, Dunnett's multiple comparisons test). The statistical significance was defined as ****p ≤ 0.0001; ***p ≤ 0.001; **p ≤ 0.01; *p ≤ 0.05. N indicates number of experimental repetitions, each performed with independent donor.



Supplementary Figure 10: Exemplary histograms of cell associated AuNR fluorescence.

Fluorescently labeled gold nanorods (AuNR) and gold nanospheres (AuNSPH) of three different sizes (15nm, 30nm and 60nm) were coated with BSA and different antibodies (rIgG2b (CD11b isotype), CD11b, mlgG2a (CD3 isotype) and CD3). Whole blood was treated with AuNSPH or AuNR of different sizes with

different coating for 30min at 37°C in rotation. Exemplary histograms show the T cell- and PMN-associated AuNSPH /AuNR fluorescence, analyzed in flow cytometry.

Supplementary Table 1: Detailed description of patients used in this thesis.

	n	%
ALL samples	8	100
Sex		
Male	7	87.5
Female	1	12.5
Male mean age	64+/-8	
Female mean age	74	
Tumor localization		
Oropharynx	3	37.5
Oral cavity	1	12.5
Larynx	4	50.0
T category		
T1	2	25.0
T2	0	0.0
T3	3	37.5
T4	3	37.5
Lymph node involvement		
N0	3	37.5
N1	1	12.5
N2abc	4	50.0
N3	0	0.0
Distant metastasis		
M0	0	0
M1	0	0
HPV status		

HPV 16 positive	2	25.0
HPV 16 negative	2	25.0
unknown or not determined	4	50.0

Supplementary Table 2: Dynamic light scattering analysis of AuNR size during protein coupling. Analysis was performed by Oliver Sritharan and Michael Erkelenz (Department of Chemistry, University of Duisburg-Essen).

	Hydrodynamic radius [nm]	SD [nm]	Zetapot. [mV]
AuNR	42,8	8,8	15
AuNR-PEG	60,6	8,1	-31
AuNR-PEG-BSA	66,8	1,2	-15
AuNR-PEG-CD3	128,5	3,9	-9
AuNR-PEG-mIgG2a	43,4	4,7	-8
AuNR-PEG-CD11b	85,6	2,8	-12
AuNR-PEG-rIgG2b	111,8	4,9	-11

8 PUBLICATIONS AND PRESENTATIONS

8.1 PUBLICATIONS

8.1.1 FIRST AUTHOR

Schirrmann, R., Erkelenz, M., Lamers, K., Sritharan, O., Nachev, M., Sures, B., Schlucker, S. & Brandau, S. Gold Nanorods Induce Endoplasmic Reticulum Stress and Autocrine Inflammatory Activation in Human Neutrophils. *ACS Nano*, doi:10.1021/acsnano.2c03586 (2022).(Schirrmann *et al.* 2022)

8.1.2 SHARED FIRST AUTHOR

Wey, K., **Schirrmann, R.**, Diesing, D., Lang, S., Brandau, S., Hansen, S. & Epple, M. Coating of Cochlear Implant Electrodes with Bioactive DNA-Loaded Calcium Phosphate Nanoparticles for the Local Transfection of Stimulatory Proteins. *Biomaterials* **276**, 121009, doi:10.1016/j.biomaterials.2021.121009 (2021).(Wey *et al.* 2021)

8.1.3 CO-AUTHOR

Bruderek, K., **Schirrmann, R.** & Brandau, S. Immunophenotyping of Circulating Myeloid-Derived Suppressor Cells (Mdsc) in the Peripheral Blood of Cancer Patients. *Methods Mol Biol* **2236**, 1-7, doi:10.1007/978-1-0716-1060-2_1 (2021). (Bruderek *et al.* 2021)

Bruderek, K., **Schirrmann, R.** & Brandau, S. Isolation of Human Circulating Myeloid-Derived Suppressor Cells and Analysis of Their Immunosuppressive Activity. *Methods Mol Biol* **2236**, 43-56, doi:10.1007/978-1-0716-1060-2_5 (2021).(Bruderek *et al.* 2021)

8.2 ORAL PRESENTATIONS

Ronja Weller. “Modulation of cellular functions by nanoparticles” in Genetics and cell biology BIOME annual retreat, Bonn, 04.12.2017 – 05.12.2017

Ronja Weller. “Modulation of cellular functions by nanoparticles” in BIOME Graduate Seminar, march 2018

Ronja Schirrmann. “Modulation of cellular functions by nanoparticles” in BIOME Graduate Seminar, November 2018

Ronja Schirrmann. “Modulation of cellular functions by nanoparticles” in BIOME Graduate Seminar, June 2019

Ronja Schirrmann. “Modulation of cellular functions by nanoparticles” in BIOME Graduate Seminar, November 2019

Ronja Schirrmann. “Modulation of cellular functions by nanoparticles” in BIOME Graduate Seminar, may 2020

8.3 POSTER PRESENTATIONS

Tag der Forschung der Medizinischen Fakultät Universität Duisburg –Essen, Essen, 17.12.2018, Ronja Weller, Karolin Wey, Sven Brandau, Matthias Epple, Stephan Lang, Stefan Hansen, „A genetically active coating of cochlear implant electrodes with calcium phosphate nanoparticles“

Cost Mye-Euniter, 5th ECI Workshop, Heraklion, 15.04.2018 – 18.04.2018, Ronja Weller, Michael Erkelenz, Stefan Hansen, Sebastian Schlücker, Sven Brandau “*Modulation of neutrophil functions by gold nanoparticles*”

Ronja Schirrmann. “Modulation of cellular functions by nanoparticles” in Genetics and cell biology BIOME annual retreat, Münster, 03.12.2018 – 04.12.2018

Award: Poster award

1st European symposium on myeloid regulatory cells in health and disease, Essen, 01.11.2018 – 03.11.2018, Ronja Schirrmann, Michael Erkelenz, Stefan Hansen, Sebastian Schlücker, Sven Brandau, “*Modulation of neutrophil functions by gold nanoparticles*”

90. Jahresversammlung der Deutschen Gesellschaft für HNO-Heilkunde, Kopf- und Hals-Chirurgie e.V., Bonn – Digitalisierung in der HNO-Heilkunde, Berlin, 29. – 01.06.2019, Ronja Schirrmann, Karolin Wey, Matthias Epple, Sven Brandau, Stephan Lang, Stefan Hansen, „*Transfection of DNA into Cochlear Cells by Functionalized Calcium Phosphate Nanoparticles*“

Tag der Forschung der Medizinischen Fakultät Universität Duisburg –Essen, Essen, 22.11.2019 Ronja Schirrmann, Michael Erkelenz, Stefan Hansen, Sebastian Schlücker, Sven Brandau „*Modulation of neutrophil functions by gold nanoparticles*“

Ronja Schirrmann. “Modulation of cellular functions by nanoparticles” in Genetics and cell biology BIOME annual retreat, Essen, 25.11.2019

Tag der Forschung der Medizinischen Fakultät Universität Duisburg – Essen, Essen, 27.11.2020 Ronja Schirrmann, Michael Erkelenz, Stefan Hansen, Sebastian Schlücker, Sven Brandau „*Modulation of neutrophil functions by gold nanoparticles*“

Neutrophil 2021, Edinburgh, neutrophil „zoomed in“ online conference, 31.05.2021 – 01.06.2021, Ronja Schirrmann, Michael Erkelenz, Stefan Hansen, Sebastian Schlücker, Sven Brandau, “*Modulation of neutrophil functions by gold nanoparticles*”

Award: Organizing Committee Prizes – Post Docs – Second Place

Tag der Forschung der Medizinischen Fakultät Universität Duisburg – Essen, Essen, 19.11.2021 Ronja Schirrmann, Michael Erkelenz, Sebastian Schlücker, Sven Brandau „*Gold nanorods induce endoplasmic reticulum stress and autocrine inflammatory activation in human neutrophils*“

Award: Presentation award

ACKNOWLEDGMENTS

I always had problems expressing my feelings in a text at the end of such a long journey. Nevertheless, finishing this PhD was not a one-man show, therefore I will try to express my gratitude to all of the persons involved. First, I want to thank my supervisor, Prof. Sven Brandau, for teaching me to always ask questions and not being satisfied with just the “easy” answer. The last 5 years were honestly the hardest I have ever experienced, but I can already see now, how much I learned and how much this time will influence my future career and life! Thank you for making that possible. I would like to express my sincere thanks to our cooperation partner Prof. Sebastian Schlücker. You really taught me that the devil is in the details, raising our publication to another level. In line with him I want to thank Michael Erkelenz for setting the base for this project and always helping out, when problems occurred. I really admire your knowledge about the literature dealing with nanoparticles and their biomedical applications of the past 20 years. How can one always remember the authors’ names, publication titles and little details of all these papers?! Science really lost an outstanding postdoc when you left academia.

I would like to deeply thank my lab mates for accompanying me through this turbulent time. A special thanks goes to Kirsten Bruderek for teaching me all the techniques, proofreading all the material and methods of papers and this thesis, as well as organizing the lab. You and Petra Altenhoff kind of adopted me and provided a smooth and easy start in my PhD. Thanks to Sebastian Vollmer, for endless conversations about the good things in life: wine and food. When I started in 2017, the Brandau lab was really small, giving me the time and space to learn. Back then, Alex Hackel and Yu Si accompanied me. Although we just spent one year together in the lab I am really happy to say that I found a really close friend in Yu. I am glad that we are still in contact and can share these memories together. Thanks to Alex, your insane stories always made me laugh and you really cheered me up (except in the evenings / early mornings when finding a mess in the lab...)! Great thanks to Jagoda Szlachetko (who probably skipped whole thesis to read what I wrote in acknowledgements)! I am really gratefully for our shared time in the office(s). Our personalities couldn’t be more different (you, the grumpy pessimist and me, the naïve optimist), but somehow this atmosphere and our endless discussions about some data point really helped me to survive occasional nightshifts. Thank you for proofreading all my abstracts and manuscripts, as well as training presentations and always helping me out, when I miss an English word. I further want to thank Tanja Hardt-Knechtli and Larissa Loska for organizing everything and especially Larissa for all the coffee breaks in the container. Great thanks to Kim Lamers! Her work can be found everywhere in this thesis. Training you and working together with you in a team was a great pleasure. Although we could not realize all our plans, I still think we did a great job! Thank you for joining me in the final phase of my PhD. I further want to thank Antonio Hrvat, Benedict Antuamwine, Xi Wang, Christian Doreth and Rebeka Bošnjaković for discussions and the general improvement of my project. As Mathias Schmidt would say: “you almost did a good job!” Speaking of Mathias, I thank you for all our coffee rounds, cheering me up and supporting me with the endless production of buffers.

Lastly, I want to thank my friends and especially my family for all the phone calls, as well as zoom, skype and once in a while personal meetings! I dedicate this thesis to my grandpa and my dad, who essentially arouse my curiosity and enthusiasm for science. Although some time past between our dissertations and we work(ed) in completely different fields, you could always relate to what I was going through, celebrating breakthroughs and cheering me up in bumpy times. Thanks to my mom, for being so proud about what I am doing and supporting me, when I didn't see the objective anymore. Thanks to my sister for trying to understand what I am doing, although science is really not her cup of tea. Lastly, I want to thank my husband, Marcel, for supporting my dreams, travelling together with me nearly 200000 km with DB, spending a lot of time, money and frustration on the railway, so that we could see each other. This was by far not the easiest way, but we managed! I am really grateful for all your support and trust.

As my grandma keeps telling: "when one door closes, another opens". Thank you all, for supporting me to reach this door and I am curious what happens behind the next one...

CURRICULUM VITAE

Ronja Larissa Schirrmann (née Weller)

(M. Sc. Biology)

For data protection reasons, the CV is not included in the online version.

For data protection reasons, the CV is not included in the online version.

AFFIDAVIT**Declaration:**

In accordance with § 6 (para. 2, clause g) of the Regulations Governing the Doctoral Proceedings of the Faculty of Biology for awarding the doctoral degree Dr. rer. nat., I hereby declare that I represent the field to which the topic “Modulation of Neutrophil Functions by Gold Nanoparticles” is assigned in research and teaching and that I support the application of Ronja Schirrmann.

Essen, date _____

Prof. Dr. Sven Brandau

Name of the scientific supervisor / member of
the University of Duisburg-Essen

Signature of the scientific supervisor /
member of the University of Duisburg-Essen

Declaration:

In accordance with § 7 (para. 2, clause d and f) of the Regulations Governing the Doctoral Proceedings of the Faculty of Biology for awarding the doctoral degree Dr. rer. nat., I hereby declare that I have written the herewith submitted dissertation independently using only the materials listed, and have cited all sources taken over verbatim or in content as such.

Tübingen, date _____

Signature of the doctoral candidate

Declaration:

In accordance with § 7 (para. 2, clause e and g) of the Regulations Governing the Doctoral Proceedings of the Faculty of Biology for awarding the doctoral degree Dr. rer. nat., I hereby declare that I have undertaken no previous attempts to attain a doctoral degree, that the current work has not been rejected by any other faculty, and that I am submitting the dissertation only in this procedure.

Tübingen, date _____

Signature of the doctoral candidate

DuEPublico

Duisburg-Essen Publications online

UNIVERSITÄT
DUISBURG
ESSEN

Offen im Denken

ub | universitäts
bibliothek

Diese Dissertation wird via DuEPublico, dem Dokumenten- und Publikationsserver der Universität Duisburg-Essen, zur Verfügung gestellt und liegt auch als Print-Version vor.

DOI: 10.17185/duepublico/78412

URN: urn:nbn:de:hbz:465-20240403-085431-3



Dieses Werk kann unter einer Creative Commons Namensnennung - Nicht kommerziell - Keine Bearbeitungen 4.0 Lizenz (CC BY-NC-ND 4.0) genutzt werden.